The Synthesis, Stabilization and Sintering of High Performance Semicrystalline Polymeric Powders

by

Andrew E. Brink

Dissertation submitted to the Faculty of the Virginia Polytechnic Institute and State University in partial fulfillment of the requirements for the degree of

DOCTOR OF PHILOSOPHY

in

Chemistry

Approved by:

Judy S. Riffle, Chair

J. E. McGrath

J. P. Wightman

R. M. Davis

H. Marand

April, 1994

Blacksburg, Virginia

The Synthesis, Stabilization and Sintering of High Performance Semicrystalline Polymeric Powders

Andrew E. Brink

Judy S. Riffle, Chair
Chemistry Department

(Abstract)

Aqueous dispersion prepregging, a relatively new method for forming graphite reinforced, polymer matrix composites, was investigated. This methodology could circumvent many of the environmental and processing problems prominent in the current state of the art. Aqueous dispersion prepregging requires that the matrix resin be in the form of a stable colloidal dispersion, preferably of small uniform particles. Formation of submicron particles from poly(ether ether ketone) (PEEK) for use in aqueous dispersion prepregging was demonstrated. The procedure involved synthesis 4,4'-difluoro (N-benzohydroxylidene aniline) followed by the step polymerization of this monomer and hydroquinone via aromatic nucleophilic substitution to form an amorphous PEEK derivative, poly(ether ether ketimine). This monomer can also be statistically copolymerized with 4,4'-difluorobenzophenone to afford a semicrystalline, soluble PEEK derivative. Acid catalyzed hydrolysis of these derivatives to insoluble PEEK can be used to generate submicron particles.

A high performance stabilizer, which was used for suspending PEEK particles in water, has also been developed. This facilitated the development of processes for aqueous dispersion prepregging. The stabilizer is a poly(arylene

ether) copolymer formed from 4,4'-difluoro- (N-benzohydroxylidene aniline), 2,6-dichloropyridine, and hydroquinone.

Poly(ether ether ketone) has excellent mechanical properties as well as solvent resistance. However, it has been reported that under the recommended high temperature melt processing conditions the material may degrade via branching and crosslinking. An alternative to melt processing PEEK is to apply the powder metallurgy technique of sintering. This involves cold (room temperature) compaction of the polymeric powder, followed by pressure free sintering of the resultant green body. Sintering occurs due to a reduction of surface free energy, and in this regard small particles (large surface area) have a large driving force for sintering. Pressure free sintering of PEEK particles with emphasis on the development of mechanical properties such as stiffness and strength as a function of sintering time, temperature, and particle size was examined. The data was analyzed using the two particle model developed by Frenkel and the crack healing theory developed by Wool. The latter is based on the reptation theory of de Gennes and Doi and Edwards. Sintering conditions were established which allowed for the attainment of comparable mechanical behavior to conventional processes.

Dedicated to

My Wife and Best Friend, Heather.
"She is a Summer Love in The Spring, Fall and Winter"

Acknowledgements

As with many research efforts within the National Science Foundation Center for High Performance Polymeric Adhesives and Composites, this work was conducted with the aid of many other students. Thus, I want to extend my appreciation to all the students involved in the NSF Center and more specifically Dr. Cheryl Heisey, Jack Lesko, Dr. Tim Lin, Vesslin Velikov, Srivatsan Srinivas (Watson), and Alvaro Ibarra-Gonzalez for their invaluable help in my research. I would also like to thank those within Professor Riffle's research group, especially Dr. Qin Liu, Dr. J. R. Babu, John Facenelli, John Bronk, and Kathy Stickney, for their everyday discussions and guidance. There were also several summer interns who played critical parts in this research effort including Stephan Gutzeit, Mona Lin, and Kurt Jordens.

In addition to those who have helped me in this research I would like to acknowledge those faculty who have provided guidance throughout my years at Virginia Tech including Professor Garth Wilkes, Professor S. Desu, Steve McCartney, Tom Glass and particularly my advisory committee, Professor James E. McGrath, Professor Herve Marand, Professor Richey Davis, Professor Ron Kander, and Professor James Wightman.

When I first started research, at the undergraduate level, there were several people who helped guide me, and taught me most of what I needed to successfully complete my graduate research. Therefore, I would like to extend my very sincere thanks to Dr. Guru Sinai - Zingde, Professor Joseph DeSimone and Dr. Qin Liu whose guidance was invaluable. Likewise there are several key people whom I am greatly indebted to for their motivation, inspiration and

guidance. Fist I would like to acknowledge Deborah Fineberg, my high school chemistry professor, who is largely responsible for me pursuing an education in science in the first place. Also, Professor James Glanville, my undergraduate advisor who provided crucial guidance during my freshman year at Virginia Tech. Most of all I would like to thank my advisor and friend Professor Judy Riffle who first took me under her wing as a sophomore and shared with me her enthusiasm and energy in Polymer Science. Judy always provided me encouragement and support when I needed it, and for that I thank her.

Finally I would like to thank my friend, study partner, and loving wife Heather for constant support over the last four years. She was always there, providing encouragement and motivation when everything seemed impossible, and there to laugh with on the better days. Thank you, Heather, for everything.

Table of Contents

List of Figures

List of Tables

Chapter 1 - Scope of Dissertation

The research presented in this dissertation was addressed towards three major goals. The first was to prepare high performance, semicrystalline, submicron powders for use in composite processing and to develop the science base needed for the control of particle size. The composite processing methodology addressed here, aqueous suspension prepregging, requires these particles be in the form of a stable suspension. Thus, the second goal was to develop a correspondingly high performance suspension stabilizer for these particles. The third aspect of this research was to examine potential processing advantages of submicron polymeric powders. These goals covered four inter-related topics including poly(arylene ethers), composite materials, colloid stability and sintering, which will be discussed in the chapter entitled "Literature Review". Following the Literature Review is the Experimental section which describes the origin and purification of materials used as well as the experimental methods utilized in this research. The Results and Discussion chapter describes how each of the three major goals were realized, and the Conclusions section highlights the major contributions of this thesis.

Chapter 2 - Literature Review

2.1 Introduction:

The research in this dissertation as well as this literature review will cover four inter-related topics including poly(arylene ethers), composite materials, colloid stability, and sintering. It is not intended to be comprehensive, but rather to serve as a background for the experimental and results sections that follow. The first section will review poly(arylene ethers) including their general synthesis and properties. Next, a review of composite materials and composite processing will be presented. Colloid stability, and how it relates to composite processing is described in the third section. Sintering and how it relates to polymer processing will be the last topic discussed.

2.2 Poly(Arylene Ethers):

2.2.1 Introduction to Poly(Arylene Ethers):

Poly(arylene ethers) (Figure 2.1)[1] have an attractive combination of chemical, physical and mechanical properties that have made them an important class of engineering thermoplastics.[1-6] There are many commercially available poly(arylene ethers) such as Udel® (polysulfone), Kadel® (Polyketone), and Victrex® (Polyethersulfone and Polyetherketone) which are used in a wide variety of applications including coatings, adhesives, composites, molded components, toughening agents and membranes.[2] Likewise there are several different synthetic methods for preparing poly(arylene ethers) including Friedel-Crafts reactions[3,7-10], oxidative coupling[10], and nucleophilic aromatic substitution[1-6,10]. The first two methods

will be described briefly and nucleophilic aromatic substitution, which is the focus of this research, will be described in greater detail.

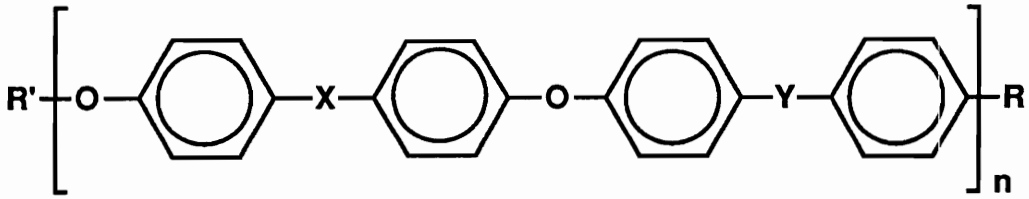

Where X = $C(CH_3)_2$, SO_2, CO, or a chemical bond
Y = SO_2, CO, or a chemical bond
R = Cl, F, OH, or OCH_3
R' = H, CH_3

Figure 2.1: The General Backbone Structure of Poly(Arylene Ethers)[1]

2.2.2 Synthetic Methods to Poly(arylene ethers):

Friedel-Crafts chemistry was used to form the first wholly aromatic polyether-ketone by Bonner[7] as described in Figure 2.2. However, only low molecular weight polymer was formed due to the crystallinity, and therefore insolubility, of the forming polymer. The problem of insolubility was technically solved by researchers at Du Pont by using liquid HF as a solvent. Indeed, Friedel-Crafts chemistry is still used by Du Pont to synthesize their PEKK material.[9]

Oxidative coupling is best described by the synthesis of Poly(2,6-dimethyl 1,4-phenylene ether) (PPO) which is marketed by GE as a blend with toughened polystyrene under the trade name Noryl. PPO is synthesized by the coupling of 2,6 disubstituted phenols (Figure 2.3).[10] It is important that both ortho positions be substituted. Otherwise the coupling reaction can occur at both the ortho and para sites resulting in a branched or even crosslinked

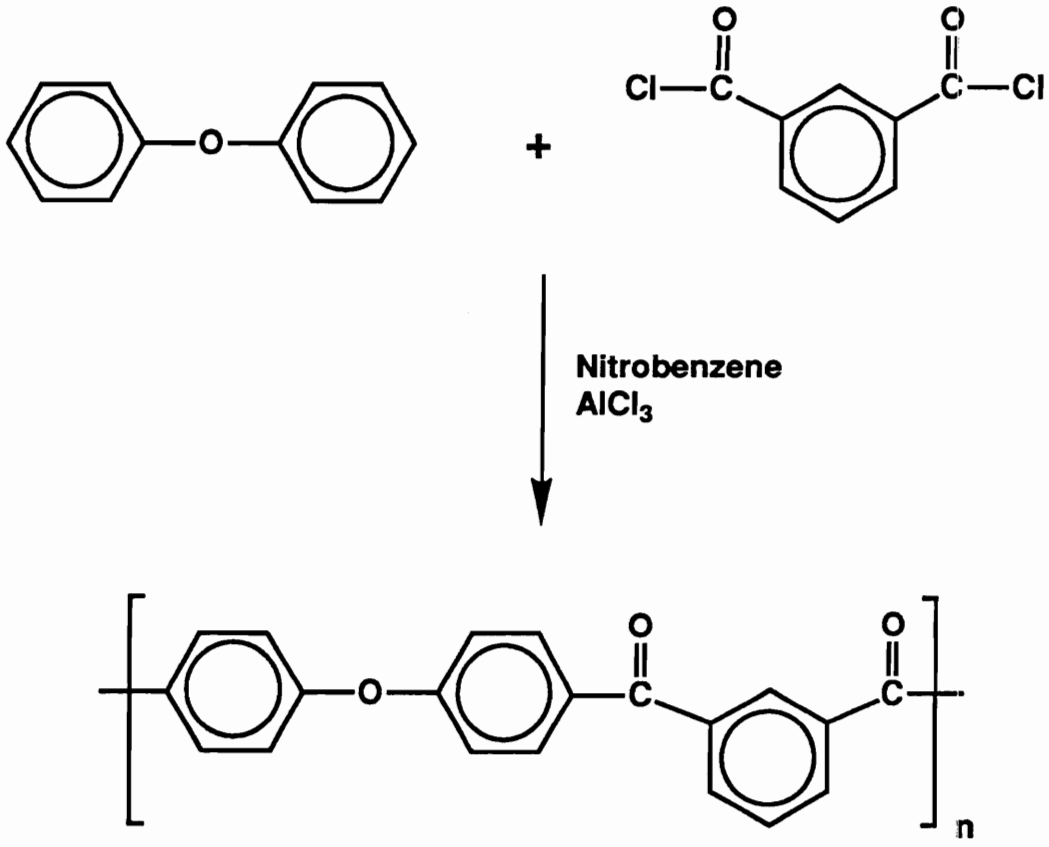

Figure 2.2: First Wholly Aromatic Polyetherketone[7]

topology. 2,6-Dimethylphenol can be polymerized by passing oxygen through a phenol solution containing a copper halide salt and aliphatic amine catalyst system. The reaction temperature is typically 25 - 50°C.[10]

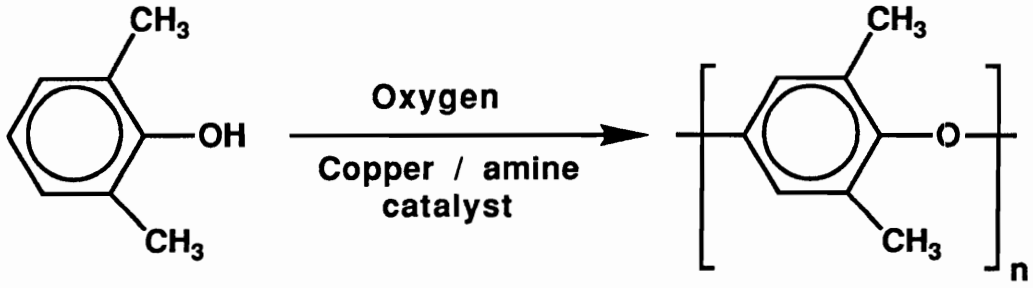

Figure 2.3: Synthesis of Poly(phenylene ether)[15]

Nucleophilic aromatic substitution was first used to synthesize poly(arylene ethers) by Johnson, et al.[4] at the Union Carbide Corporation. Their synthesis involved the solution condensation of a dialkali metal salt of a bisphenol with an activated dihalide in dimethylsulfoxide. Commercially available Udel® Polysulfone, which is marketed by Amoco Chemical, is synthesized in this manner (Figure 2.4). The bisphenoxide is first formed from the bisphenol using a stoichiometric amount of a metal hydroxide. This method has several drawbacks including potential hydrolytic side reactions and bisphenate insolubility. An alternative synthetic method utilizes anhydrous potassium carbonate to form the bisphenoxide. This method has the advantage that an excess of base can be used without causing premature hydrolysis of the activated aromatic halide monomer or the polymer.[11-14]

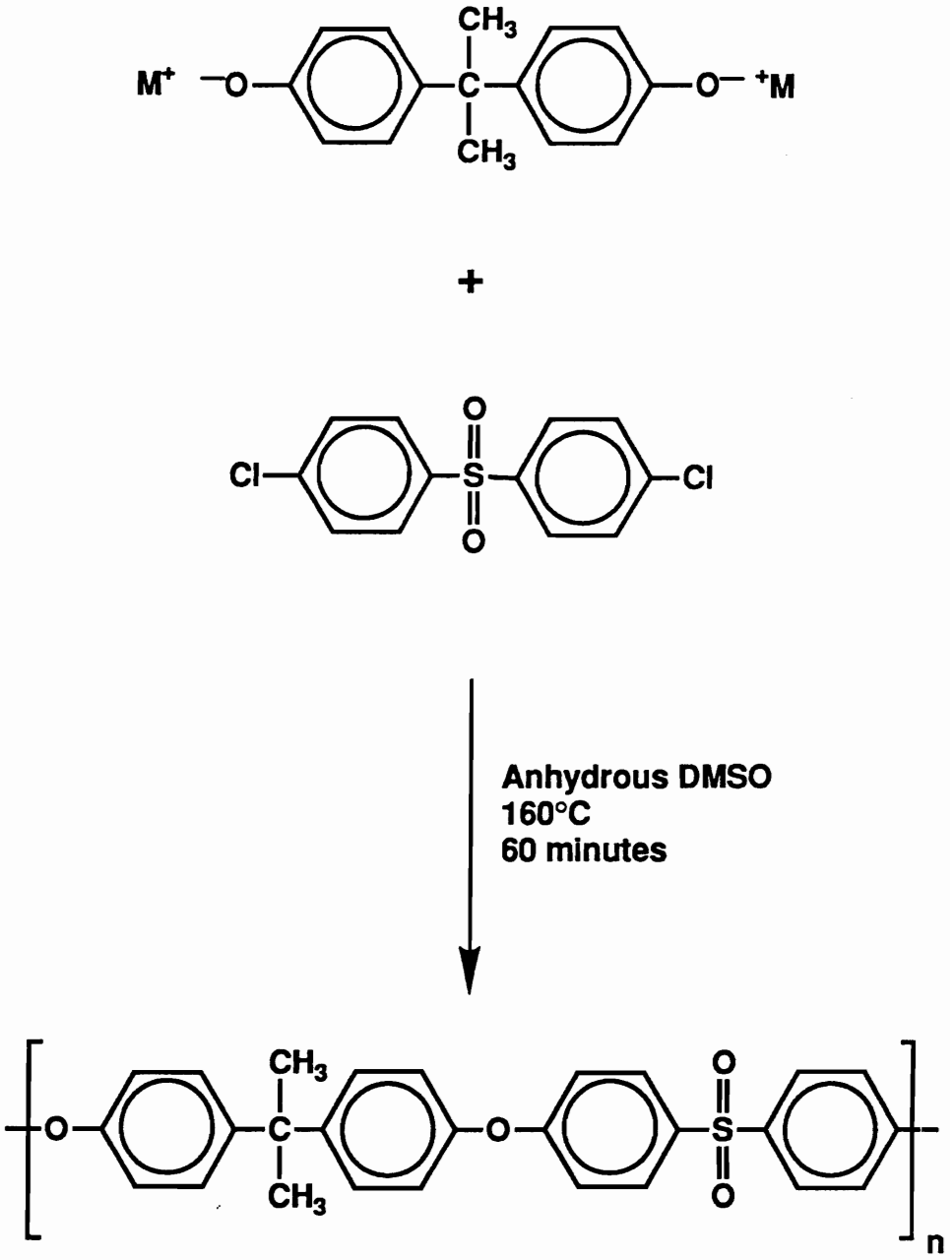

Figure 2.4: Synthesis of Udel® Polysulfone[4]

2.2.3 Nucleophilic Aromatic Substitution:

Nucleophilic aromatic substitution can occur by either the addition-elimination (S_NAr) or elimination-addition (benzyne) mechanisms. These mechanisms are required because the more common S_N2 and S_N1 mechanisms are not possible. The S_N2 type substitution is impossible due to the geometry of the benzene ring, which prevents the required back-side approach of the nucleophile, and the S_N1 mechanism would involve the extremely unstable phenyl cation. The elimination-addition mechanism involves the high energy benzyne intermediate followed by substitution. The attacking nucleophile has two possible sites for substitution, and therefore could not be used to form an exclusively para-linked polymer backbone (Figure 2.5)[15].

The addition-elimination mechanism (Figure 2.6) requires that the nucleophile first attack a vacant π^* orbital on the aromatic ring to be substituted, without displacement of any existing substituents. If the nucleophilic attack occurs at a position that bears a potential leaving group, then net substitution can take place via a second step involving the loss of that leaving group. The addition intermediate, or Meisenheimer complex, is isoelectronic to a pentadienyl anion. This anion is greatly stabilized by an electron withdrawing group ortho or para to the point of substitution. In fact, an electron withdrawing group is required before such a substitution can occur except under extreme conditions. Nitro, cyano, sulfone, and carbonyl groups are examples of such electron withdrawing groups.[15]

The leaving group, often a halide, is also critical to the sucess of this reaction. However, the order of reactivity, F>Cl>Br>I, is the opposite of S_N2

Step 1:

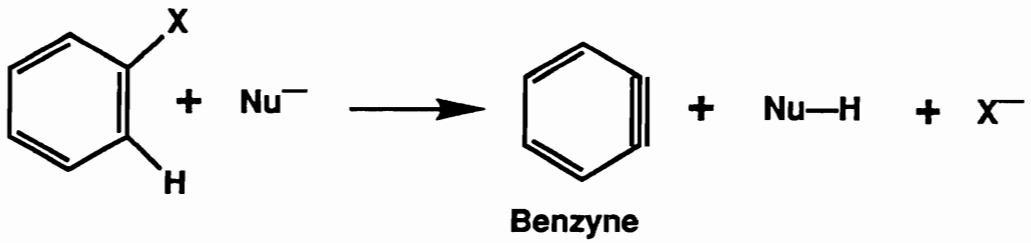

Step 2:

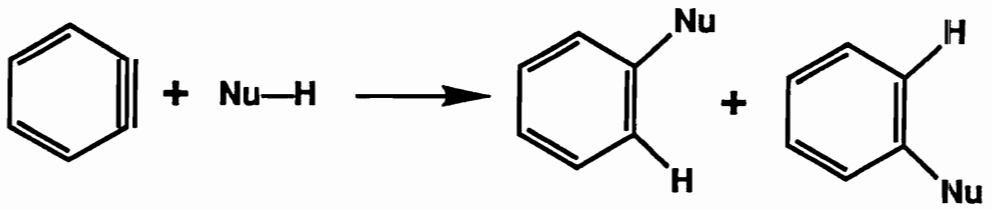

Figure 2.5: Elimination-Addition Mechanism (Benzyne)[15]

Step 1: Rate Determining

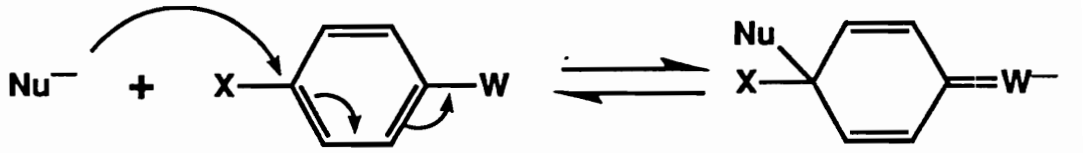

Meisenheimer Complex

Step 2: Fast

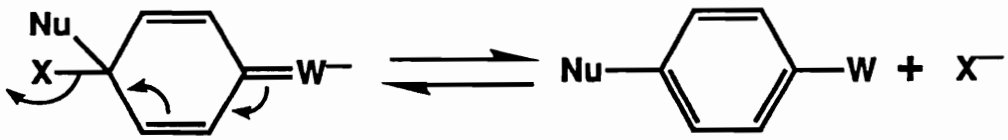

Figure 2.6: Addition - Elimination (S_NAr) Mechanism[15]

reactions where I>Br>Cl>F. This difference in reactivity is due to the fact that the rate determining step is the attack of the nucleophile (which disrupts aromaticity) not the breaking of the carbon-halide bond as it is in the S_N2 mechanism. Therefore the more electron withdrawing the leaving group is, the faster the rate determining step.[15]

With the correct choice of nucleophile, electron withdrawing group, and leaving group the S_NAr mechanism can be carried out to essentially 100% conversion. This makes it possible to utilize this mechanism for the formation of high molecular weight linear polymers.[4-6] Johnson, et al.[4] also found the choice of solvent critical, with dimethylsulfoxide and sulfolane providing the best results, as the solvent not only had to solvate the nucleophile but also solublize the forming polymer. Their method involved first forming the phenolate using aqueous sodium hydroxide. Once the phenolate is formed quantitatively the system is dehydrated using chlorobenzene (Figure 2.7), the activated dihalide is added and high molecular weight polymer is obtained in about 60 minutes as previously described in Figure 2.4.[4] Often, after the dihalide was added, the reaction color was an orange to yellow or deep green which the authors believed to be due to the Meisenheimer type sigma complex (Figure 2.8). After high molecular weight has been achieved the basic endgroups are neutralized by conversion to the methyl ether with methyl chloride. The authors found that the resulting polymer was exclusively para linked, confirming the mechanism to be S_NAr and not the benzyne mechanism. In addition a kinetic study by Attwood, et al.[16] showed this reaction to be S_NAr with a rate equation of

$$-\frac{d[ArO^-]}{dt} = k[ArO^-][ArX]. \qquad (2.1)$$

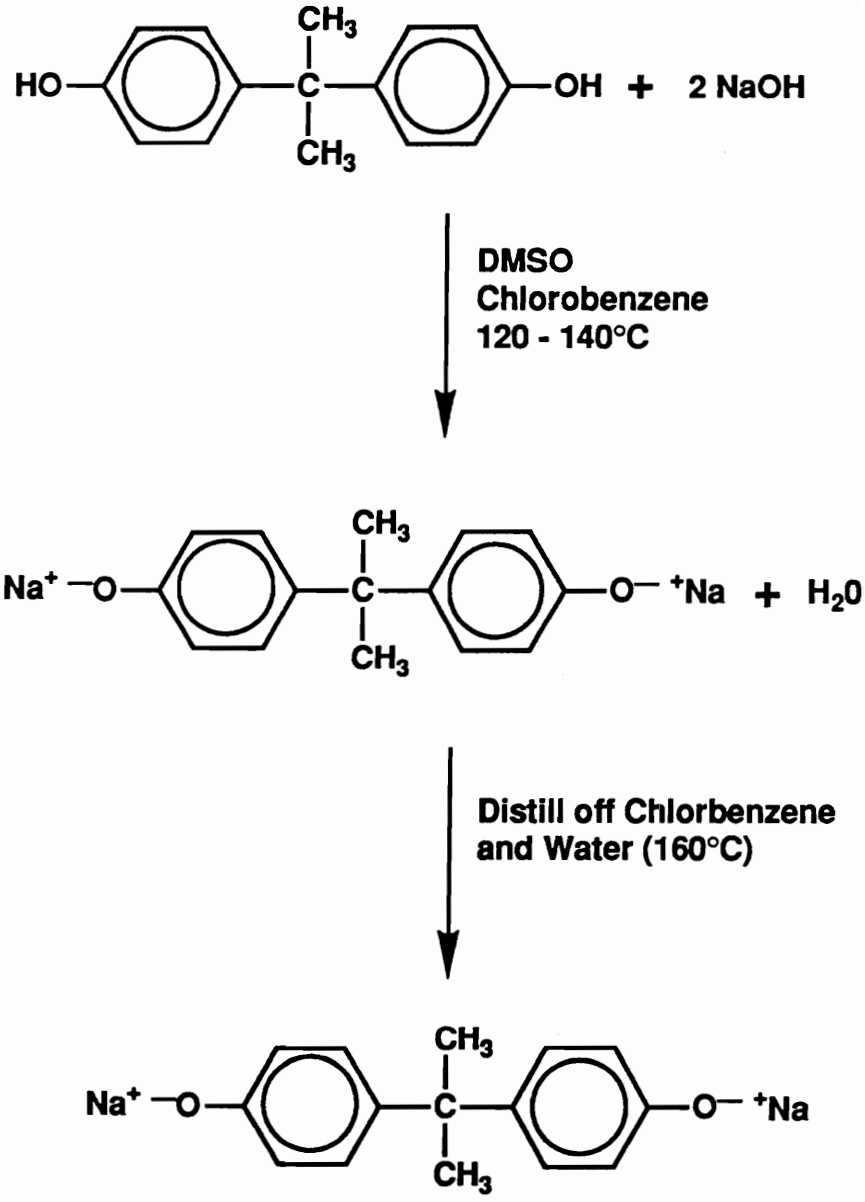

Figure 2.7: Synthesis of Bisphenolate[4]

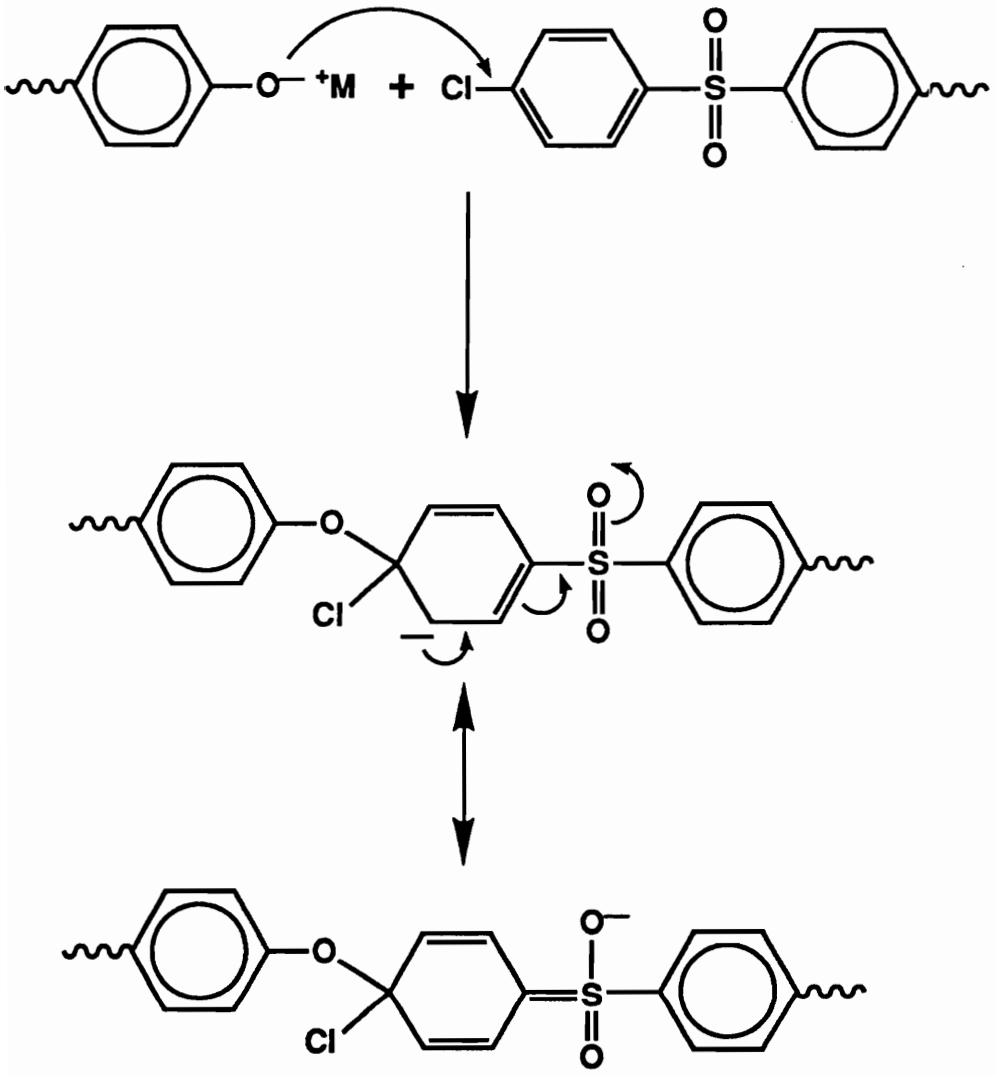

Meisenheimer Complex

Figure 2.8: Sulfone Meisenheimer Complex[16]

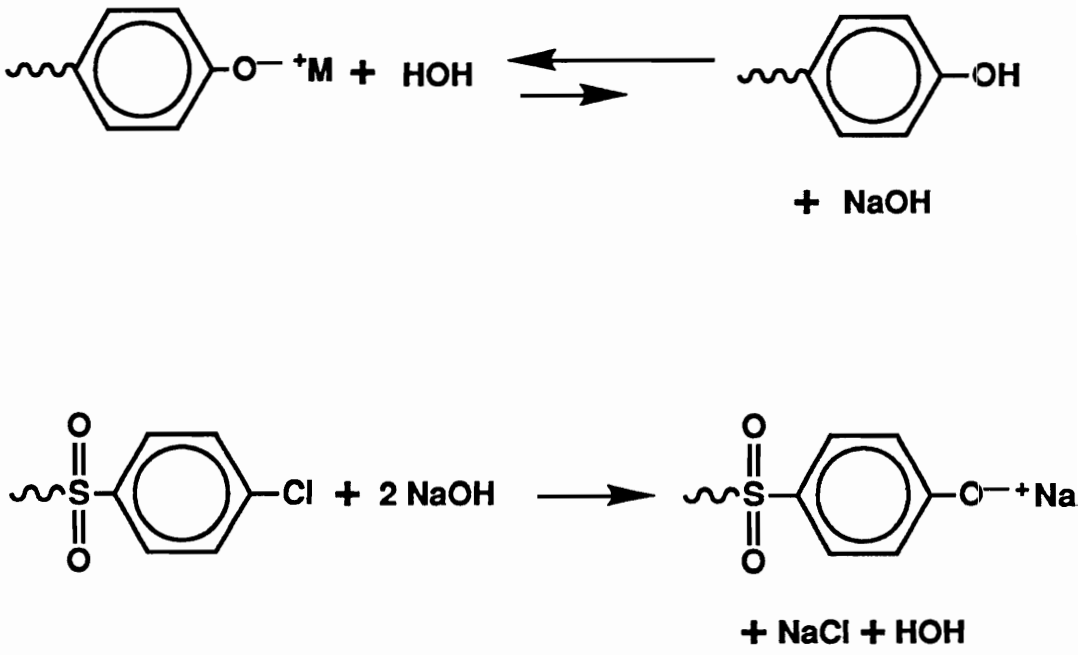

Figure 2.9: Hydrolytic Side Reaction[6]

Their study also indicated the formation of the Meishenhimer complex is indeed the rate determining step.

Johnson et al.[6] also found it critical to completely dehydrate the reaction or a devastating hydrolytic side reaction resulted (Figure 2.9). This side reaction results in upsetting the one to one stoichiometry and thus limits the molecular weight. Besides complete dehydration, an exact stoichiometric amount of sodium hydroxide is also required to obtain high molecular weight. An excess of base would result in essentially the same hydrolysis reaction as shown in Figure 2.9. A deficiency of base would not form the phenolate quantitatively and thus disturb the stoichiometry. In addition to this it has been reported that the unreacted phenol can hydrogen bond to a phenolate moiety and thus decrease its reactivity by one order of magnitude (Figure 2.10).[14] Due to the presence of the hydrolysis side reaction another alternate method was developed which involved utilizing anhydrous potassium carbonate as the base.[11-14] This method has an advantage in that K_2CO_3 can be used in excess without the occurrence of any side reaction.

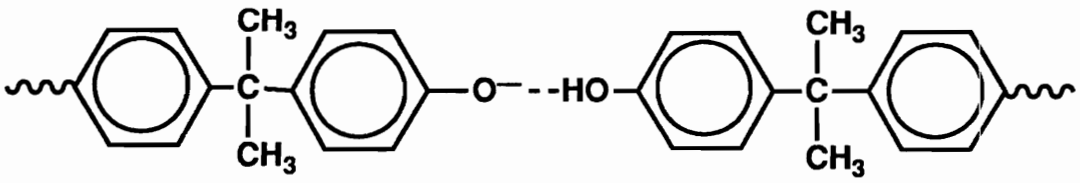

Figure 2.10: Phenolate - Phenol H-bonded complex[14]

McGrath, et al.[14] reported on the synthesis and kinetic observations of poly(arylene ether sulfones) synthesized via this potassium carbonate process using DMAc as a solvent and toluene to azeotrope off the water. The kinetics are considerably more complex than those using a metal hydroxide to form the

phenolate because it is heterogeneous in nature, and governed by a series of equilibria for phenolate formation (Figure 2.11). Once a phenolate is formed it can react with the activated dihalide in exactly the same manner as shown in Figure 2.4. Since its first publication the nucleophilic aromatic substitution route utilizing potassium carbonate has grown in popularity, and it is now even used commercially for the synthesis of poly(arylene ethers) including poly(ether ether ketone) (PEEK).

2.2.4 PEEK- Synthesis and Characterization:

Since the carbonyl moiety is a sufficiently good electron withdrawing group to stabilize the Meisenheimer intermediate, poly(arylene ether ketones) can be made using the synthetic mechanisms described above. However, depending on the bisphenol used, many of these polymers are semicrystalline in nature and require reaction temperatures of 300°C or higher to keep the polymer in solution. These high reaction temperatures preclude the use of DMSO, DMAc, or NMP as solvents and often diphenylsulfone is used.[3] Poly(ether ether ketone) (PEEK) marketed by ICI under the trade name Victrex® is an example of such a poly(arylene ether ketone) and will be the focus of this discussion. PEEK is considered to be a "high performance" engineering thermoplastic with commercial uses including graphite composites, fluid control adapters, piston engine seal washers, and electronic and medical markets.[17] PEEK is a semicrystalline polymer (Tg ≈ 143°C, Tm ≈ 334°C) with 0 - 48 % crystallinity depending on its thermal history.[18-28]

The first reported synthesis of PEEK was conducted at 160°C in DMSO where it crystallized from solution and did not reach high molecular weight.[4]

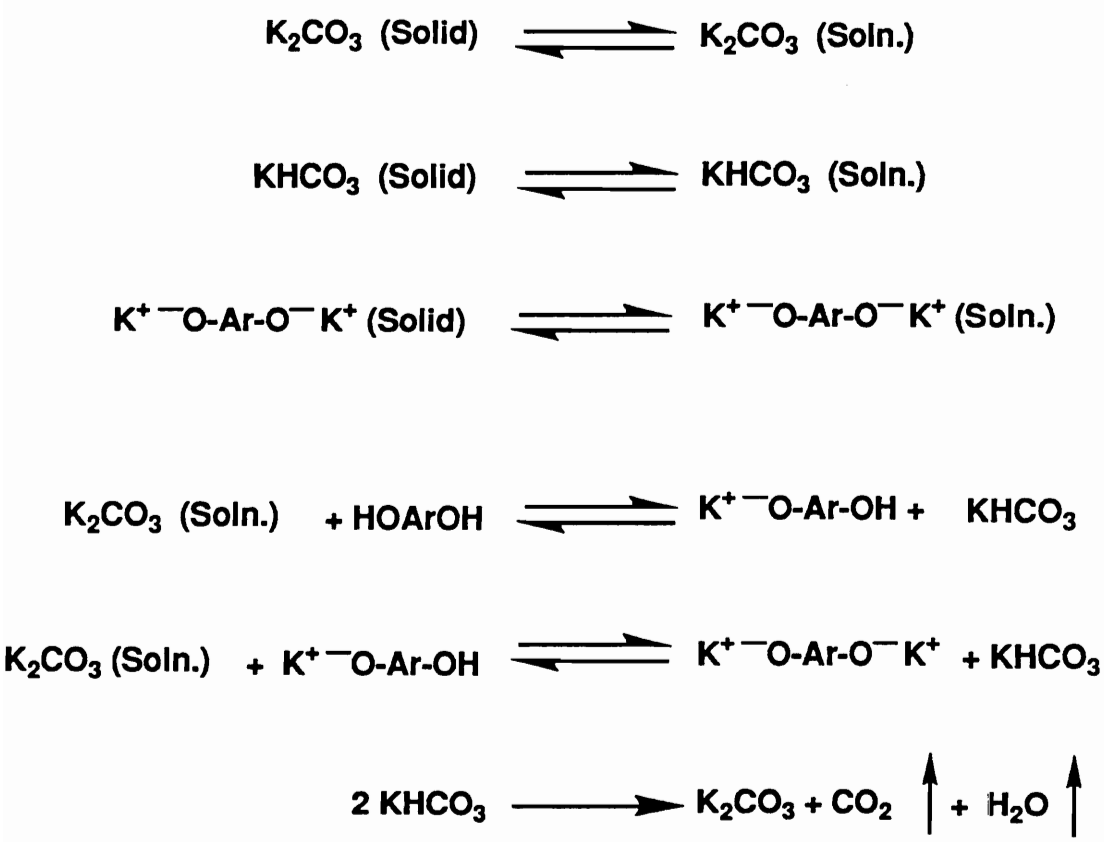

Figure 2.11: Potassium Carbonate - Phenolate Equilibria[14]

The use of a much higher reaction temperature (>300°C) and diphenylsulfone as a solvent prevented crystallization from solution and made it possible to synthesize high molecular weight PEEK.[29,30] The reaction scheme for synthesis of PEEK is shown in Figure 2.12.[10] The drawback to using the high reaction temperature to prevent crystallization is that it also may cause a branching side reaction that is not seen in lower temperature polymerizations.[31] This side reaction has been suggested to involve the basic phenolate abstracting the relatively acidic proton ortho to a halogen (Figure 2.13)[3]. The resulting carbanion can either displace a flourine through nucleophilic aromatic substitution or can attack a carbonyl carbon. Both of these reactions can lead to branching and even some gel formation.[3] The extent to which these side reactions occur in the synthesis of PEEK has been shown to be minimal, and essentially no gel fraction is found.

Due to its relatively insoluble nature, PEEK has been a challenging polymer to characterize, as most conventional techniques require dilute solutions. There have been several acidic solvent systems explored for PEEK including H_2SO_4, HSO_3Cl, HF, and mixtures of phenol and 1,2,4-trichlorobenzene.[32-35] The strong acids protonate the carbonyl oxygen essentially quantitatively and thus induce solubility. Sulfuric acid also sulfonates the PEEK backbone. Sulfonation occurs on the activated aromatic ring which has two para ether links exclusively and quantitatively (Figure 2.14).[32] This has been confirmed by FTIR and titrations, as well as by NMR spectroscopy. The stronger sulfonating agent HSO_3Cl has also been shown to sulfonate PEEK, but not as selectively. Even the deactivated ketone substituted rings are sulfonated with this reagent.[33] The sulfonation of PEEK has enabled

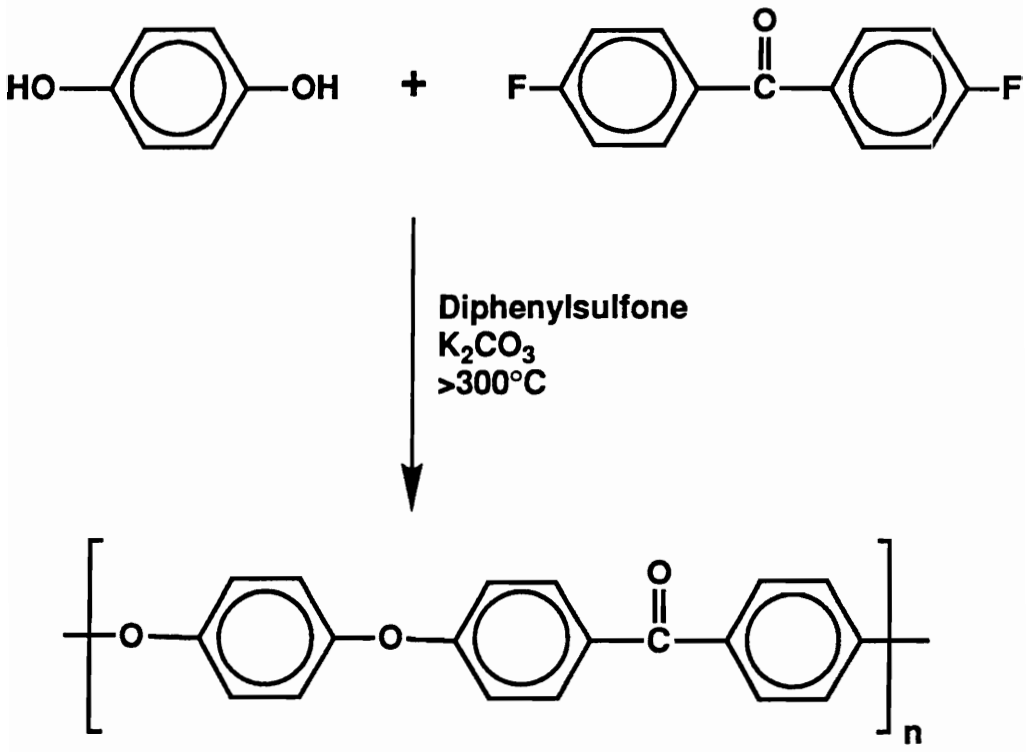

Figure 2.12: Synthesis of Victrex® PEEK[3]

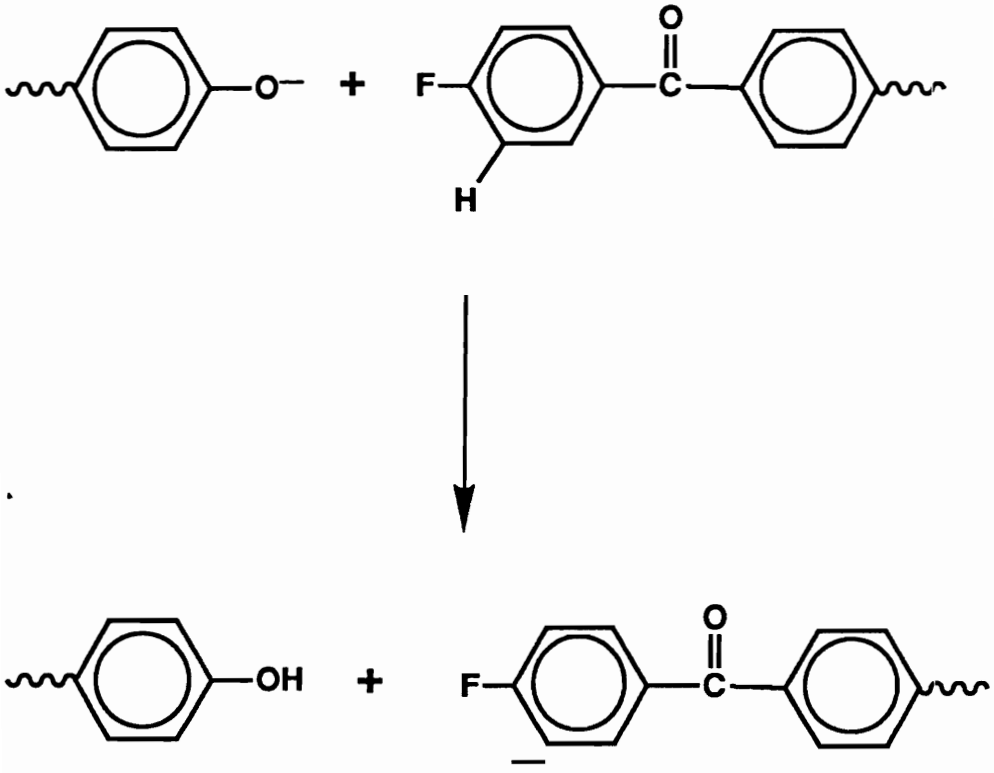

Figure 2.13: Side Reaction Leading to Branching[3]

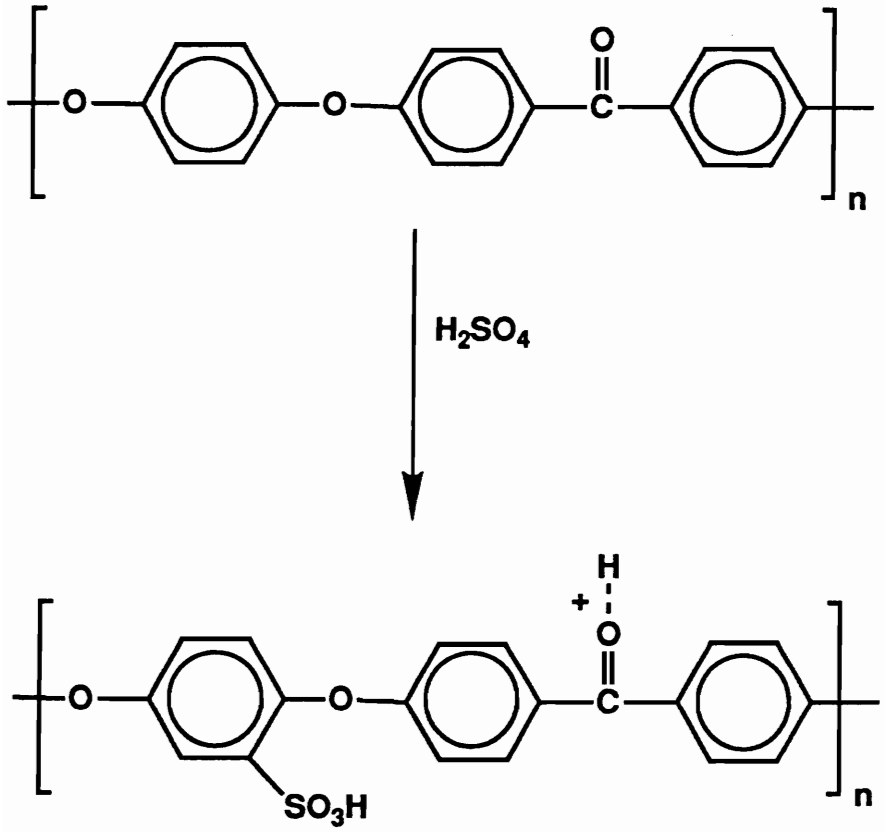

Figure 2.14: Sulfonation of PEEK[32]

molecular weight analysis using GPC, ^{19}F NMR, light scattering, and viscosity studies. Non-sulfonating solvent systems such as a 50:50 mix of phenol and 1,2,4-trichlorobenzene have also been used for characterization of PEEK. Although these systems require relatively high temperatures for solvation to occur (180°C), they have enabled analysis of unsulfonated PEEK.[32,33] These molecular weight analyses combined with melt viscosity measurements have resulted in the following relationship[33];

$$\log_{10}M_v = -15.06 + 3.21\log_{10}\langle Mw\rangle \qquad (2.2)$$

where M_v is given in kiloNewton seconds per meter squared ($kNsm^{-2}$). The Mark-Houwink expressions for PEEK in sulfuric acid (2.3) and phenol-1,2,4-trichlorobenzene (2.4) have also been determined.[32]

$$[\eta_a]_{25°C} = 6.195x10^{-5}(\bar{M}_w)^{0.94}(dl/g) \qquad (2.3)$$

$$[\eta]_{115°C} = 7.588x10^{-4}(\bar{M}_w)^{0.67}(dl/g) \qquad (2.4)$$

It is interesting to note that GPC analysis of PEEK has also shown the existence of low molecular weight oligomers or cyclics which can be extracted out of the insoluble semicrystalline material.[36]

The thermal stability of PEEK is a critical issue since PEEK's targeted commercial uses are for relatively high temperature applications. Also, due to it's relatively high Tm, processing of PEEK has to be at elevated temperatures (≈ 400°C). The melt stability of PEEK was assessed in a study by Jonas and Legras[36]. It was determined that under the recommended processing conditions PEEK undergoes branching and eventually crosslinks. A reaction resulting in branching was identified by examining the changes in molecular weight and molecular weight distributions as a function of time and temperature. At temperatures of 380°C and higher, the <Mn> remains constant but <Mw> and

<Mz> increase significantly. The mechanism proposed by Jonas, et al.[36] was a homolytic random chain scission that produces relatively stable radicals that can attack the polymer backbone to form branches and eventually crosslinks. The activation energy for PEEK degradation was determined to be ≈ 105 kJ/mol. The branches formed decreased the polymer's ability to crystallize in terms of both rate and absolute degree of crystallinity attainable. PEEK degradation was found to be limited by oxygen diffusion, with a higher surface/volume ratio resulting in more degradation.[36] If the temperature was elevated in the absence of oxygen (nitrogen or vacuum), degradation was also minimized.[36]

As discussed, there has been a great deal of characterization performed on PEEK, however its lack of solubility is always a concern. For this reason there have been three alternate methods developed for synthesizing semicrystalline poly(arylene ether ketones) that utilize an amorphous soluble precursor route. The soluble precursors can then be converted to PEEK utilizing an acid hydrolysis procedure. These methods allow one to fully characterize the precursor by conventional solution techniques, and then relate the information obtained to PEEK properties after the hydrolysis reaction is used. Kelsey, et al.[31] converted 4,4'-dihydroxybenzophenone to the corresponding 1,3-dioxolane (Figure 2.15). This could then be polymerized with 4,4'-difluorobenzophenone in a lower temperature polycondensation reaction (Figure 2.16). This method, however, cannot be used to make PEEK specifically because the acetal functionality is not activating for nucleophilic aromatic substitution. However, it has been used to synthesize PEK, and several other semicrystalline poly(arylene ether ketones).[31]

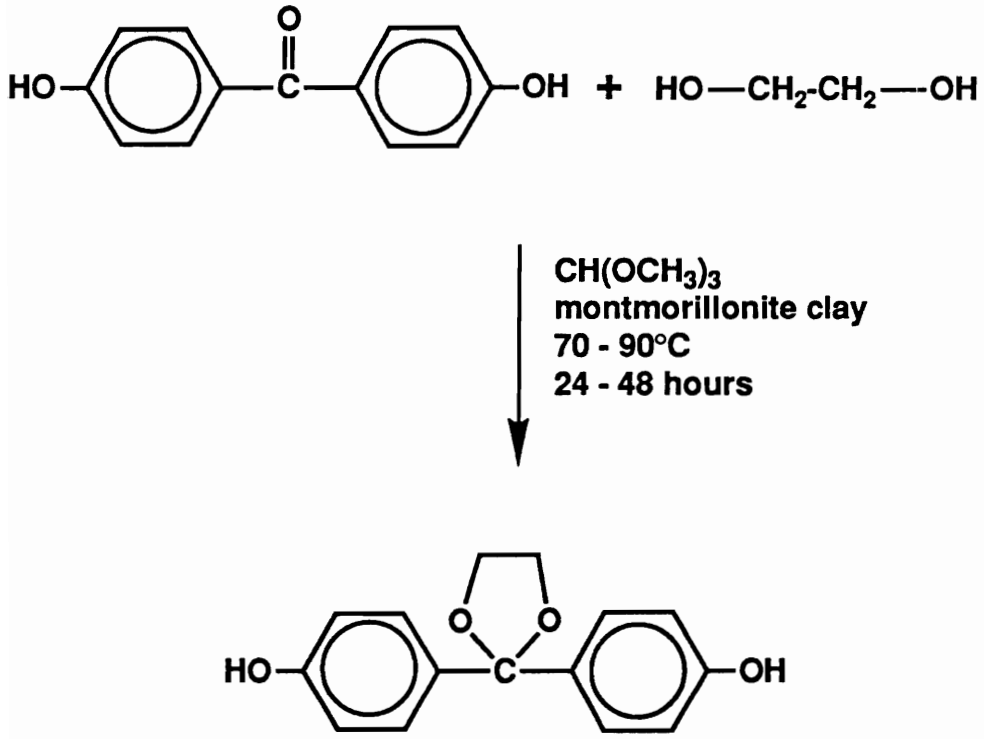

Figure 2.15: Synthesis of Acetal Monomer[31]

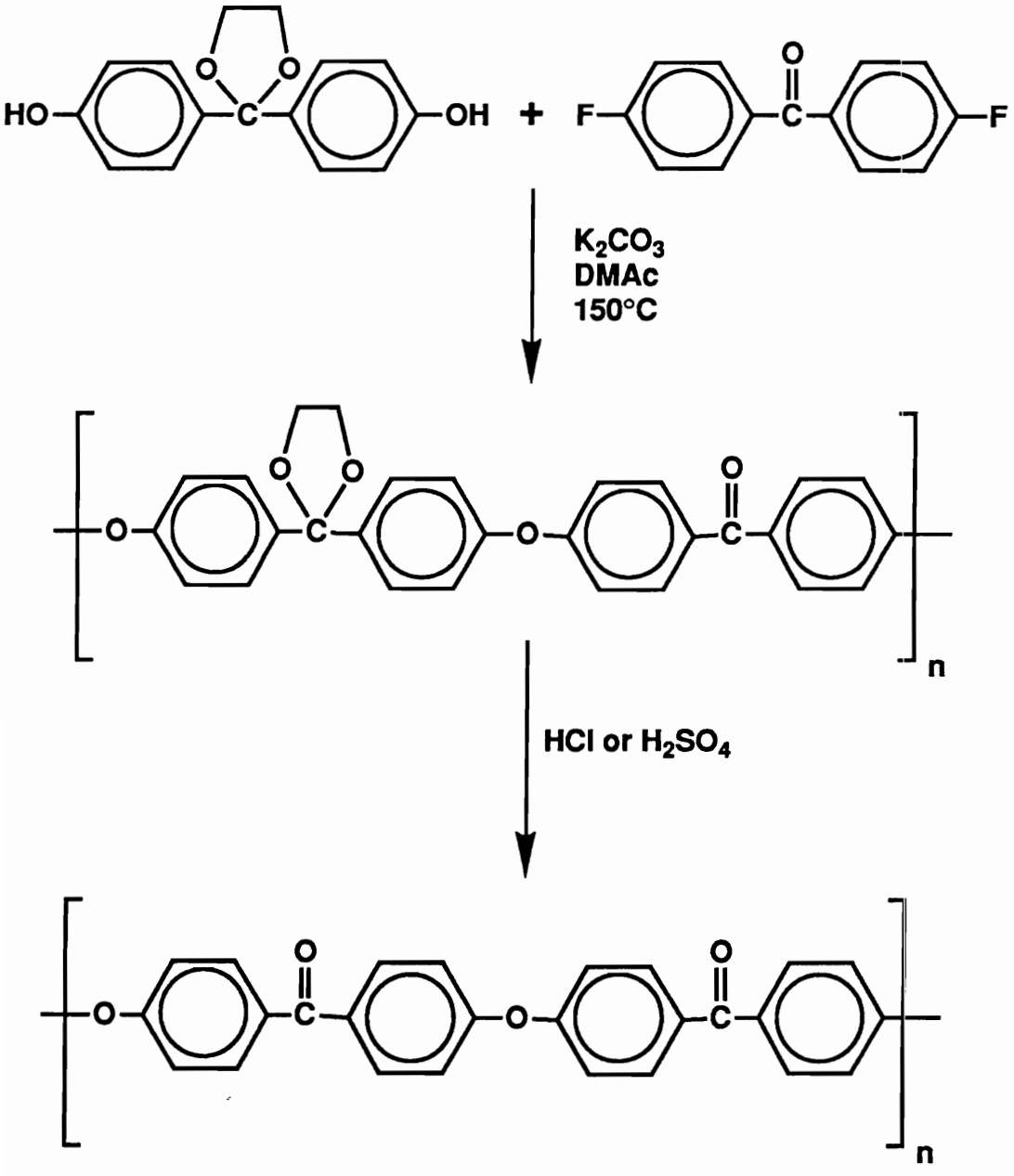

Figure 2.16: Synthesis of PEK via Acetal Monomer[31]

A soluble precursor to PEEK was also synthesized by the incorporation of bulky alkyl groups (e.g., t-butyl) along the polymer backbone.[37] These bulky groups prevent crystallization rendering PEEK soluble. The removal of these groups was achieved using acids such as trifluoromethanesulfonic acid, however long reaction times are required (> 20 hours).[37]

The third route to an amorphous PEEK precursor is through a Schiff base, or ketimine derivative of 4,4'-difluorobenzophenone (Figure 2.17). The ketimine is sufficiently electron withdrawing to enable nucleophilic aromatic substitution (Figure 2.18).[38-40] If hydroquinone is used as the bisphenol the polymer formed after the ketimine hydrolysis is identical to that of PEEK (Figure 2.19). This method has allowed for fractionation of the ketimine precursor, and examination of its solution properties.[41,42] Roovers, et al.[41] found the Mark-Houwink-Sakurada relationship to be

$$[\eta] = 6.3_4 \times 10^{-4} M^{0.617} \qquad (2.5)$$

for PEEKt in THF at 25°C. Another critical discovery, made by McGrath and Lyon et al.[40], was that during hydrolysis of the ketimine to PEEK, the converted polymer precipitated from solution in relatively small particulates. This will be a key issue in this research as it enables the use of aqueous dispersion prepregging to form high performance continuous fiber graphite composites.

2.3 Composite Materials:

2.3.1 Introduction to Composites:

A composite, broadly defined, is the material formed when two or more different components are combined. With this definition, almost everything is a composite including teeth, bones, feathers, and plant leaves. The focus here is

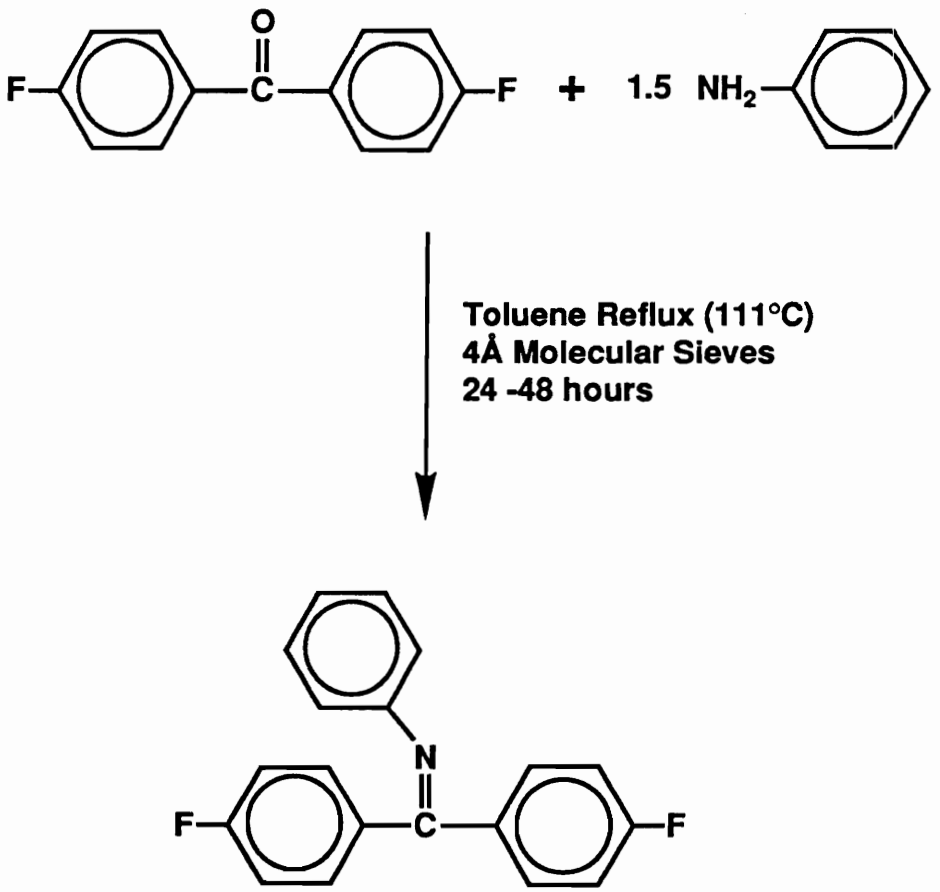

Figure 2.17: Synthesis of Ketimine Monomer[38]

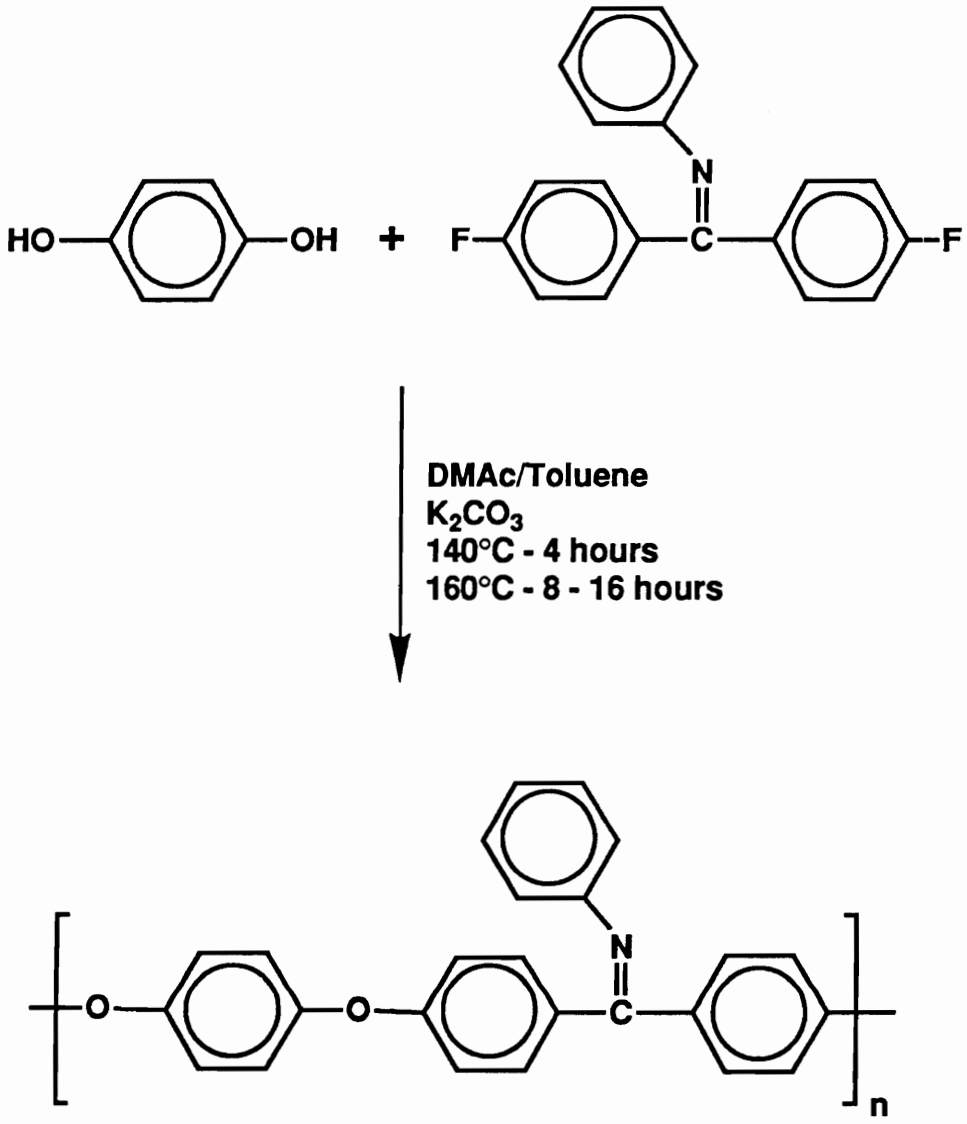

Figure 2.18: Synthesis of Poly(ether ether ketimine) (PEEKt)[38]

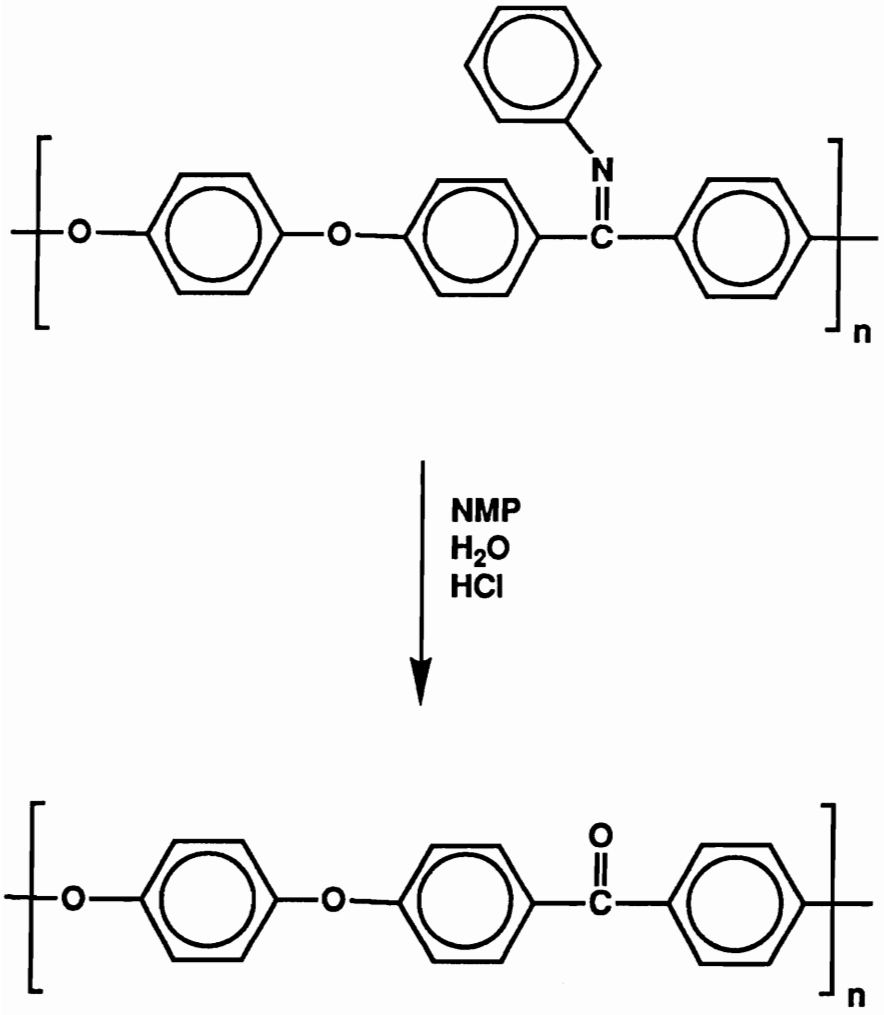

Figure 2.19: Hydrolysis of PEEKt to PEEK[38]

a more restricted definition for composite materials. The combination of an extremely strong, stiff, oriented material (fiber) with a polymer matrix resin.[10] The fibers provide the stiffness and strength, carry most of the load and make up about 60 - 70% of the weight or volume. Typical fibers consist of glass, aramide, and graphite and can be either continuous or chopped. The 'highest performance' of these are continous graphite fibers, which will be the focus of this discussion. The resin is needed to separate and bind the fibers as well as to distribute the stress evenly.[43] The resin must also protect the fibers, which are typically very brittle. The durability, interlaminar toughness, and shear, compressive, and transverse strength of the composite are also partly determined by the matrix resin.[44] Resins are most commonly thermosets such as epoxy resins but can also be thermoplastics such as PEEK. Resins and fibers can be combined to provide a material with high strength, light weight, and mechanical properties that exceed those of most metals (Table 2.1).[44] In fact polymer matrix composites can exceed even the lightest and strongest metals in terms of strength-to-weight (Figure 2.20)[10] and stiffness-to-weight ratios .[44] Because of these features, over the last two decades high performance fiber-reinforced composites have been used increasingly as replacements for metals in the high performance and fuel economy driven applications of the aerospace industry as well as in the automotive, and sporting goods industries.[43,45]

Table 2.1: Potential Benefits of Composites over Metals[44]

Potential Benefits of Composites over Metals
•Potential increased design flexibility
•Better damage tolerance
Increased impact resistance
Increased fracture toughness
Greater scuff resistance
•Better corrosion resistance
•High specific strength and stiffness
•Low thermal coefficient of expansion
•Better fatigue resistance
•Potential lower component costs
Lower fabrication costs
Lower quality assurance costs
Lower scrappage rate
•Integral construction of composite structures
Minimal plies
Fewer joints
Ply dimensions can correspond to load path

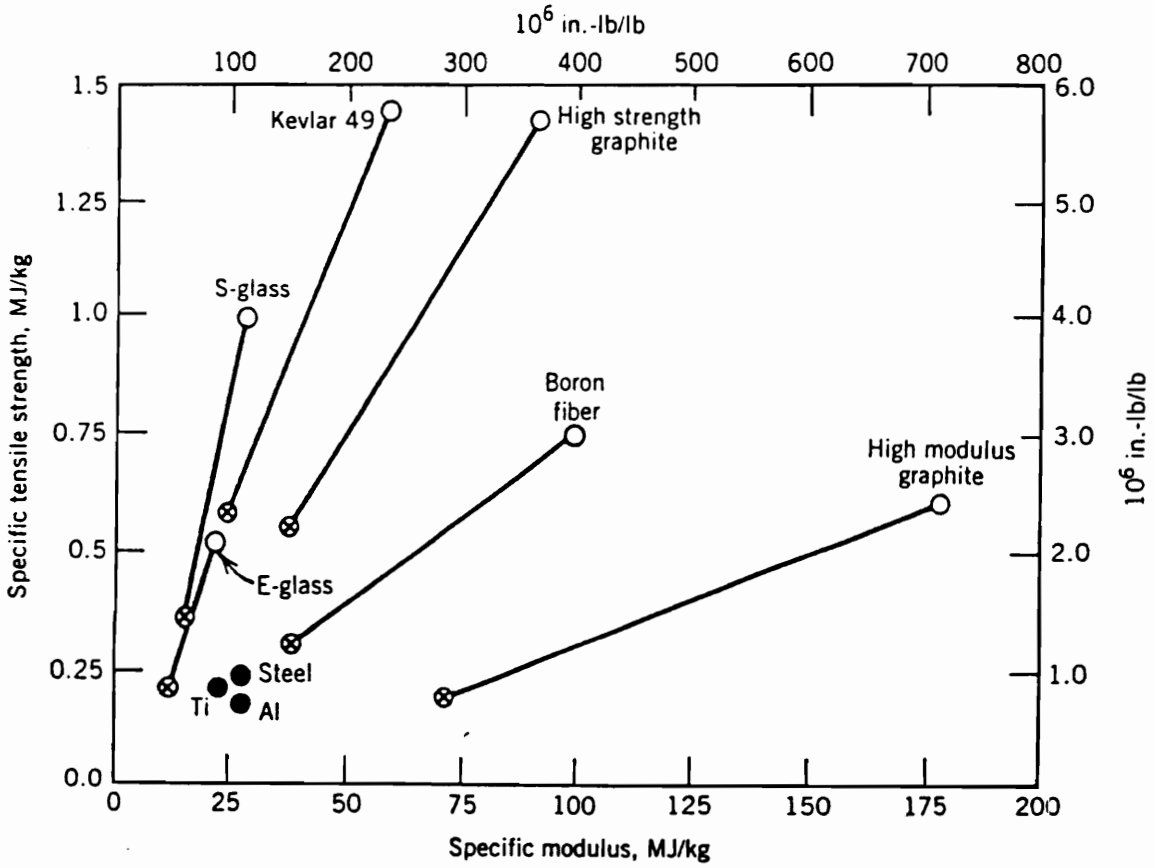

Figure 2.20: Specific Strength vs Specific Modulus of Unidirectional and Quasi-isotropic Materials; Fibers are in an Epoxy Matrix. o, Unidirectional Composite; • Bulk Material; ⊛, Quasi-isotropic Composite[10]

One of the most challenging and promising applications for high performance continuous graphite fiber composites is for the "high speed civil transport" (HSCT) that is being planned by NASA in combination with the aerospace industries. The HSCT will fly at speeds between 2.0 and 2.4 Mach, carry 250 - 300 passengers and may contain about 75,000 lbs of composite material per airplane. The number of requirements for these composite materials is enormous. The composite lifetime will have to exceed 72,000 total flight hours at use temperatures between 177°C and -54°C on each flight. The evaluation of many different material combinations is underway and the composite performance, cost and manufacturability are the three most critical parameters.[46,47] Currently both thermoplastics and thermosets are being considered. The potential advantages and disadvantages of each will be discussed.

2.3.2 Thermoplastic vs. Thermoset Matrix Resins:

Traditionally graphite composites have been made utilizing thermosetting resins. Over 95% of the advanced composite materials sold in 1991 were based on thermosets.[43] Thermoset composites have excellent tensile, shear and compressive strengths, as well as excellent thermal and dimensional stability, high modulus, outstanding adhesive properties, and solvent resistance. However, they have been limited by poor damage tolerance, compressive strength after impact, and hot/wet stability.[48] They also have a relatively high manufacturing cost which is mainly due to the need to cure the composite in an autoclave, which translates into low production per unit time.[49] Also, because the extent of cure greatly affects the final properties,

the cure kinetics must be carefully monitored. This creates an additional processing challenge which has been the focus of much research.[50-55] Further complications arise from the fact that even with the same degree of cure the thermoset can have different concentrations of chain ends, branch points and crosslinks, which translates into different macroscopic properties.[51]

Another concern for thermosetting composites is shelf-life. The first step in composite production is often the formation of a prepreg. A prepreg is the ready to mold material in which the fibers and the resin have already been combined.[43] In the case of a thermoset, it is important that the gelpoint is not reached until the final consolidation process, and therefore reaction in the prepreg stage must be avoided. This requires that most thermosetting prepregs be kept in refrigerated storage.[48]

Thermoplastics are the alternative to thermosets. Thermoplastics have many advantages, such as unlimited shelf life, shorter processing cycles, no cure reaction, reformability, enhanced fracture toughness, better damage tolerance, and potentially reduced manufacturing cost.[43,48] For example Figure 2.21 compares the open hole compressive strain of a thermoplastic PEEK composite vs. that of an epoxy.[48]

Another distinct advantage of thermoplastic matrices over thermosets is improved interlaminar properties. Delamination is one of the most common modes of failure in advanced composite structures.[56] Thermosets require adhesives or mechanical fasteners to join the laminates into the final part. Mechanical fasteners require cutting holes which result in stress concentrators and cut fibers. Adhesives may be a disadvantage in that they add another variable that must be controlled. Thermoplastic composite laminates, however,

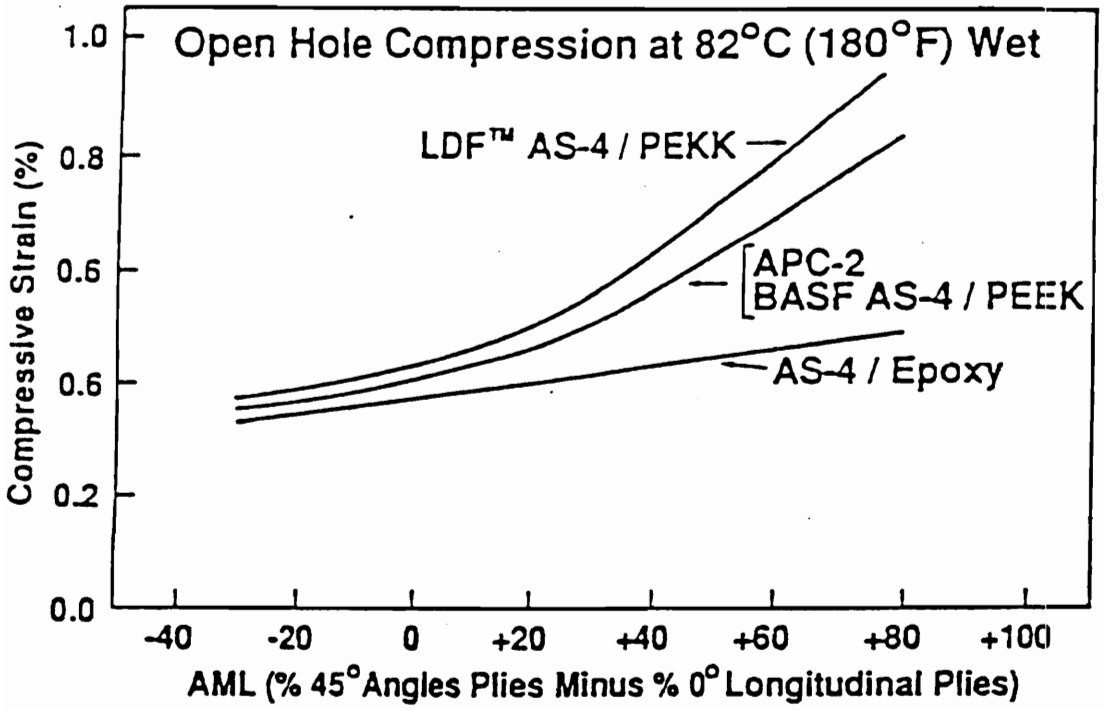

Figure 2.21: Open Hole Compressive Strain of AS-4 Composites[48]

can be joined in a process known as welding. Welding involves fusion and consolidation of the polymer at a common interface. The final result is bond performance identical to the bulk properties.[57-59]

With all of the advantages of thermoplastics why are thermosetting resins still the dominant force in graphite composites? The main reason is that the industry 'grew up' with them, the resins are inexpensive, and most of the current processing equipment is designed for them. Also the most severe problem, poor damage tolerance, has been improved by incorporation of reactive engineering thermoplastics to toughen these systems and therefore improve their compressive strength after impact.[60-66] However, the potential advantages of thermoplastics has led to the development of new processing methods designed specifically for them, as well as studies to examine their processing - property interrelationships.[67-73] The comparison of thermosets to thermoplastics is summarized in Table 2.2.[44]

Current methods for processing thermoplastic composites are really simply adaptations of thermosetting processes that involve dissolving or melting the desired matrix resin. However, high performance thermoplastic polymers are typically insoluble, or soluble only in dipolar aprotic solvents such 1-methyl-2-pyrrolidinone (NMP), which makes large-scale solution prepregging impractical. Melt prepregging of these types of materials is also impractical, owing to both their high thermal transitions (causing degradation at melt temperatures) as well as their high viscosities which cause fiber breakage. The prepregs formed using these methods are boardy with poor drape and tack which makes them difficult to consolidate into the final composite.[43] Relatively new methods of prepreg formation, electrostatic and aqueous suspension

prepregging, have been developed which can potentially circumvent these problems.[43, 74-78]

Table 2.2: Summary of Trade-offs of Thermosets and Thermoplastics as Composite Matrix Resins[44]

Property	Thermosets	Thermoplastics
Formulations	Complex	Simple
Melt Viscosity	Very low	High
Fiber impregnation	Easy	Difficult
Prepreg tack	Good	None
Prepreg drape	Good	None to fair
Prepreg stability	Poor	Excellent
Processing cycle	Long	Short to long
Processing temperature/pressure	Low to moderate	High
Fabrication cost	High	Low (potentially)
Mechanical properties: -54 to 93°·C, hot/wet	Fair to good	Fair to good
Environmental durability	Good	Unknown
Solvent resistance	Excellent	Poor to good
Damage tolerance	Poor to excellent	Fair to good
Database	Very large	Small
Recycling	Probably no	Possibly yes

Electrostatic prepregging involves adding the desired matrix resin to the continous carbon fiber tow as a dry powder. The powder sticks to the tow by an electrostatic attraction that is introduced by putting an electrical current across the fibers. This method involves no solvents, and does not require the matrix resin to be in the form of a low viscosity melt (Figure 2.22).[43] The prepreg formed also has good tack and drape making it easier to handle than traditional

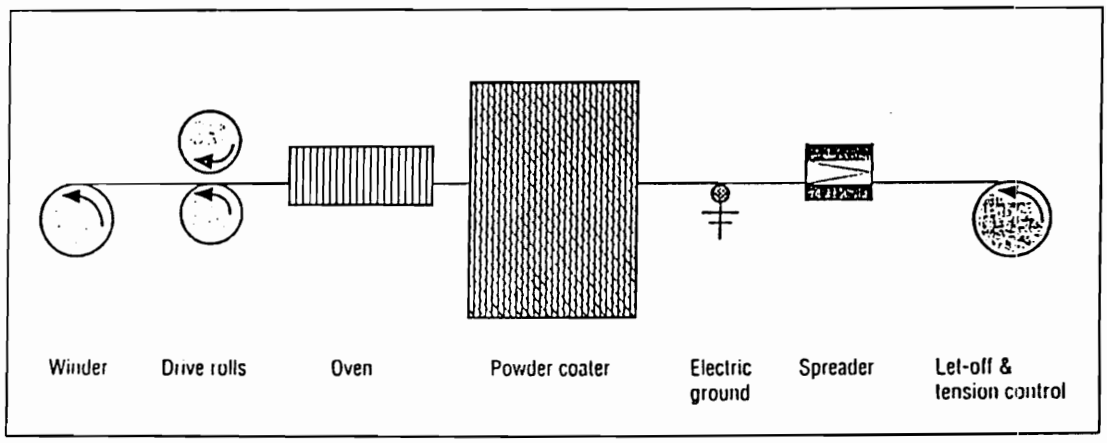

Figure 2.22: Process Diagram for Producing Flexible Powder Coated Towpreg: Electrostatic Prepregger[43]

thermoplastic prepregs. The limitation to this process, however, is that the polymeric resin must be in the form of a uniform dry powder with an optimum particle diameter of 50 - 80 μm. If the powder size is too small then the particles aggregate and if it is too large the particles do not have enough electrostatic attraction to bind to the fiber.[43, 74, 77]

Aqueous dispersion prepregging involves impregnating the carbon fiber tow by passing it through a concentrated suspension of the desired matrix resin. This method does not involve melting the resin, uses water as an alternative to toxic organic solvents, and provides a prepreg with good tack and drape (Figure 2.23)[78]. The limitations of this method are that the desired matrix resin must be in the form of particles in a stable aqueous suspension. This method has an advantage over electrostatic prepregging in that there is no minimum particle size limitation. This could prove to be a great advantage in that, if the particles can be made small enough, they may be processible by a sintering mechanism similar to that used in ceramic processing. Another advantage is that if the particles are small enough (< 1 μm) they could potentially be used to prepreg a pre-woven fabric.[79]

2.4 Colloid Stability:

2.4.1 Introduction to Colloid Stability:

Colloids, first clearly recognized by Graham in 1861[80], are a form of matter that lie in between the solid (bulk) state and the molecularly dispersed (dissolved) state. Dispersed particles with dimensions in the range of 10 Å to 1 μm are typically considered colloidal. They have much higher surface to volume ratios than the solid state, but less than that of a solution. This results in

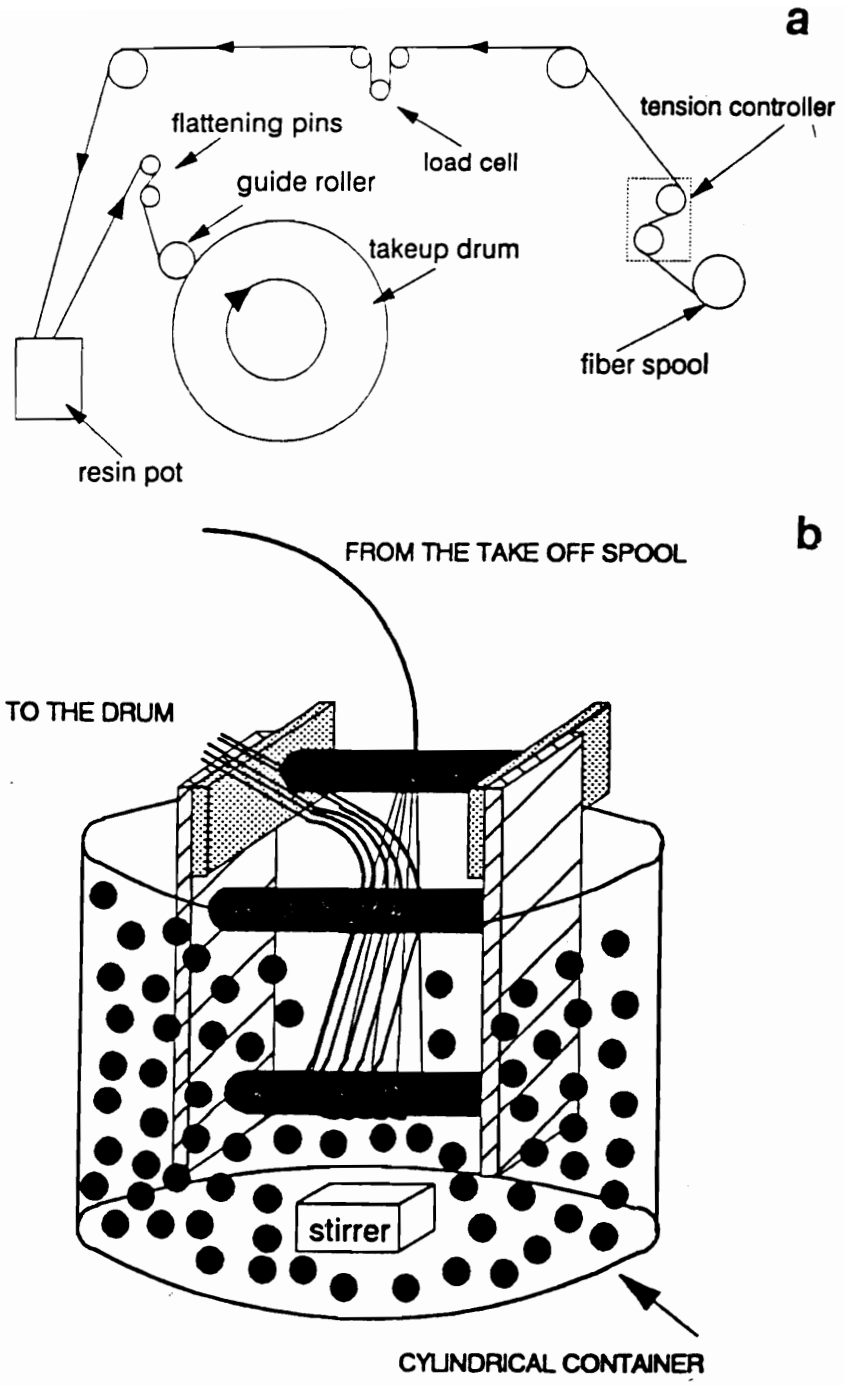

Figure 2.23: Aqueous Dispersion Prepregger: (a) Drumwinder, (b) resin pot[78]

rather unique properties for colloidal suspensions, as surface chemistry is of critical importance. Figure 2.24[81] shows the % of molecules that are at the surface of a particle as a function of particle diameter.

The surface of any material has a higher free energy than that of the bulk state. Dividing a material, a process which increases surface area, requires work (Figure 2.25).[81] This increase in energy (surface excess free energy) is a function of the material's surface tension (σ) and the area (A) created (2.6)[81].

$$\Delta G = \Delta W = 2\sigma^{o}A \qquad (2.6)$$

One fundamental principle of thermodynamics is that a system will tend to change spontaneously to lower its overall free energy. It should therefore be a spontaneous process for the divided material to recombine, lower its surface area and thus reduce its free energy.[82] As mentioned a colloidal system has a very large surface to volume ratio. Thermodynamically this means that a colloidal system is unstable and should spontaneously coagulate to reduce its surface area. This is not always the case because whether a suspension coagulates rapidly, slowly, or not at all depends on the sum of all the forces acting on the particles. In many cases these forces result in an activation energy barrier which must be overcome before coagulation can occur, much like a bimolecular reaction in organic chemistry. The process of coagulation has even been successfully treated as a bimolecular reaction with a rate equation of (2.7)[83]

$$-\frac{dn}{dt} = k_r n^2 \qquad (2.7)$$

where k_r is the rate constant and n is the number of particles. The average energy due to brownian motion of a colloidal particle is about (3/2)kT. Therefore an activation energy barrier of 10kT would make it extremely unlikely

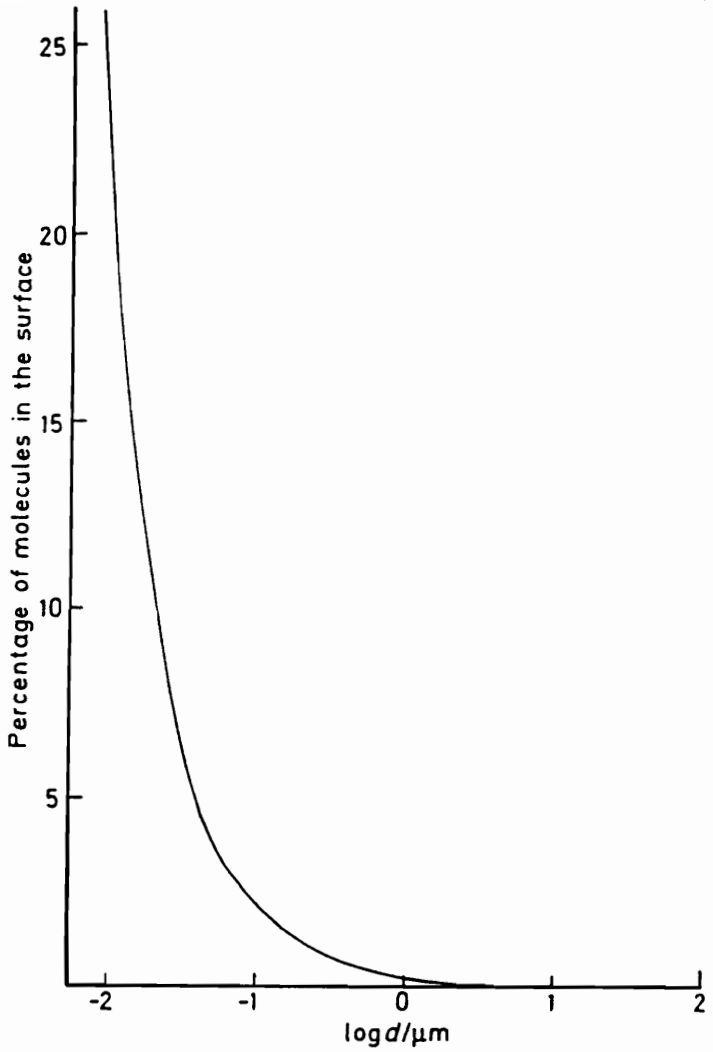

Figure 2.24: The Percentage of Molecules in the Surface as a Function of Particle Size for a Substance with a Molar Volume of 30 cm^3 mol^{-1}.[81]

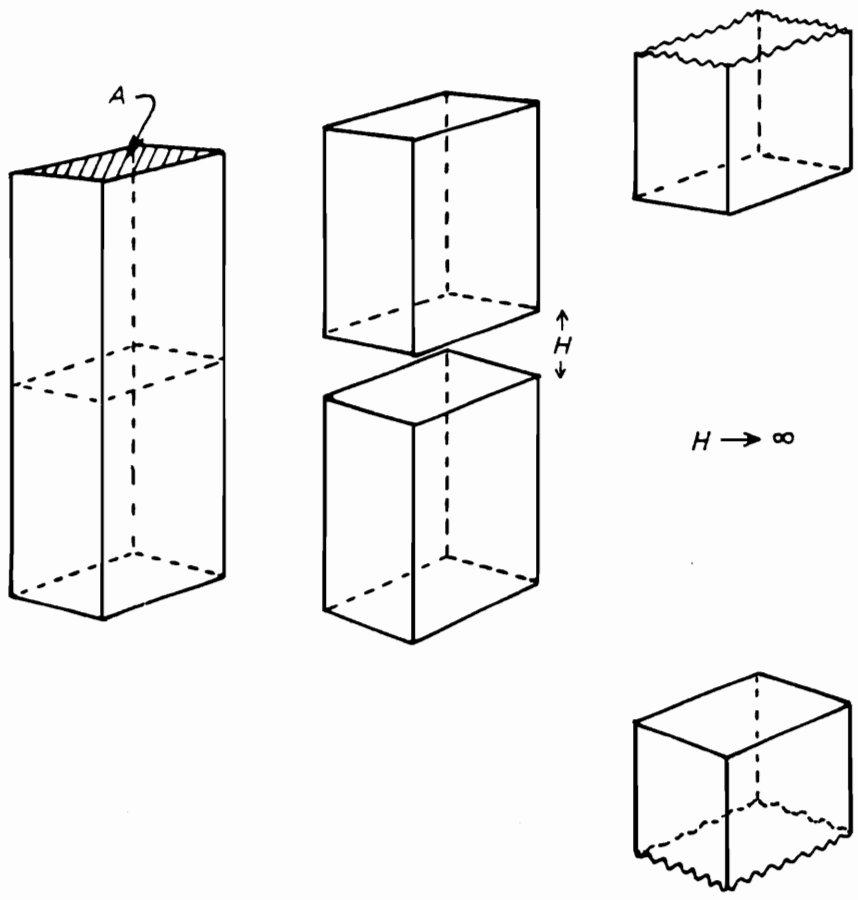

Figure 2.25: The Splitting of a Column of Material with Cross-Sectional Area A to Form Two Surfaces with Total Area 2A, and Separation to Infinity.[81]

for any particles to overcome this barrier and coagulate, i.e. the suspension would be kinetically stable, or metastable.[81] The interparticle forces that relate to this kinetic stability are attractive London - van der Waals dispersion, electrostatic repulsion and the repulsion due to adsorbed macromolecules (steric).[81,84] As mentioned in the previous section, the focus of this research is the application of aqueous dispersion prepregging. One requirement for this processing method is formation of a stable aqueous suspension of the desired matrix resin. The method utilized will be electrostatic repulsion. Steric stabilization, although of great industrial importance and the topic of much research,[84 - 91] will not be discussed further here.

2.4.2 Electrostatic Stabilization:

As mentioned above, the three main forces acting on a colloidal particle that effect stability are London - van der Waals dispersion, electrostatic repulsion and the repulsion due to adsorbed macromolecules. The principal cause of coagulation is the only attractive force of these three, London -van der Waals dispersion forces (V_A).[82] In the absence of any adsorbed polymer, the only force to combat coagulation is electrostatic (V_R). Independently two teams of scientists (Deryagin, Landau, and Verywey, Overbeek) proposed a theory, now named DLVO theory, on colloidal stability that assumed that the simple pairwise addition of these two forces controlled whether or not the dispersion would remain stable, coagulate or flocculate (2.8).[80,83,92] A distinction is made between coagulation and flocculation in that coagulation is irreversible and flocculation is reversible.

$$V_T = V_R + V_A \qquad (2.8)$$

Van der Waals attractive forces between two molecules or atoms include permanent dipole-permanent dipole, permanent dipole - induced dipole and induced dipole - induced dipole interactions. Only the induced dipole - induced dipole interactions (London - van der Waals forces) are of significance in colloidal dispersions.[84] They are due to fluctuations in electron densities, decay with the sixth power of distance, and are therefore significant only over very short distances. For two spherical particles the attractive force (V_A) can be defined by (2.9)[92]

$$V_A = \frac{-A_{1(2)}}{6}\left[\frac{2}{s^2-4}+\frac{2}{s^2}+\ln\frac{s^2-4}{s^2}\right] \qquad (2.9)$$

where s is the reduced distance between particles (R/a), R is the separation between the centers of the particles, a is the particle radius, and $A_{1(2)}$ is the mixed Hamaker constant, which describes the attraction between two identical particles 1 in medium 2. Hamaker's approach to interparticle attractions was to assume the pairwise additivity of interatomic attractions. The repulsive contributions are assumed to be negligible except for those molecules on opposing surfaces. Thus the Hamaker constant is mathematically defined as

$$A_{1(2)} = A_{11} + A_{22} - 2A_{12} \approx \left(\sqrt{A_{11}} - \sqrt{A_{22}}\right)^2 \qquad (2.10)$$

where A_{ij} is defined by

$$A_{ij} = A'_{ij}\,\pi^2 q_i^2 \qquad (2.11)$$

and q_i is the density of atoms in the colloidal particle.[81,84] A' is determined by

$$A'_{ij} = \frac{3}{4}h\left(\frac{\nu_1\nu_2}{\nu_1+\nu_2}\right)\alpha_1\alpha_2 \qquad (2.12)$$

where *h* is Planck's constant, ν is a characteristic frequency identified with that of the first ionization potential, and α is the polarizability.[81,84] Often equation (2.9) is simplified assuming V_A is only applicable at short distances to

$$V_A \approx \frac{-A_{1(2)}}{12} \bullet \frac{a}{H_o} \qquad (2.13)$$

where H_o is now the minimum separation distance between particle surfaces.[92]

The electrostatic repulsion is due to the surface of a particle developing a net charge, either positive or negative. This surface charge can come from several sources: the dissociation of surface groups (e.g. silanol moities on a silica particle), the selective adsorption of charged ions such as Ag^+ adsorbing to the surface of AgI particles, the adsorption of ionized surfactants onto the particle surface, or isomorphic substitution (e.g. Al^{3+} substitutes into a Si^{4+} lattice site resulting in a net negative charge).[92] However, it must be pointed out that electroneutrality requires that the particle and the immediate surroundings bear no net charge. What this means is that the surface charge must be compensated by equal and opposite counter-ions in the dispersion media. The combination of the surface charge and the surrounding ions is referred to as the electric double layer (Figure 2.26)[84]. The double layer, depending on its charge distribution, can result in electrostatic stabilization.[93-95] If the counter-ions are relatively spread out in the disperson medium then as two particles come together the 'clouds' of like ions start to interpenetrate while the particles are still far apart. This causes electrostatic repulsion similar to that observed on the molecular level. When atoms come too close together, their electron clouds overlap resulting in Born repulsion. However, if the counter-ions are collapsed onto the surface, the particles can come quite close together before any repulsion occurs. If they are allowed to approach too closely, then

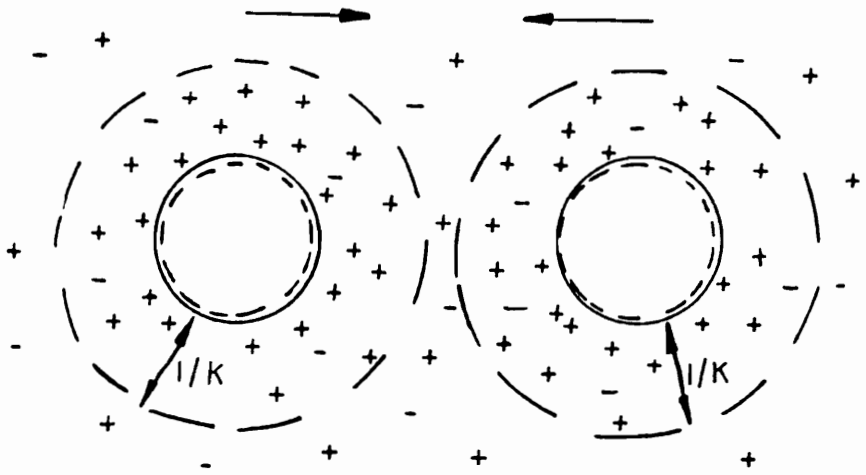

Figure 2.26: Representation of the Electric Double Layer for Negatively Charged Particles.[84]

the van der Waals attraction, discussed above, comes into play and coagulation occurs. Overbeek[83] mathematically defined the repulsive force (V_R), assuming that the ions acted as point charges, as

$$V_R = 2\pi\varepsilon\varepsilon_o a\phi_o^2 \frac{\exp(-\kappa H)}{1 + H/2a} \qquad (2.14)$$

where ε_o is the permittivity of vacuum, ε is the dielectric constant of the medium, ϕ_o is the surface potential, and $1/\kappa$ is the Debye - Huckel length which is defined by equation (2.15).

$$1/\kappa = \left(\varepsilon\varepsilon_o RT / F^2 \sum c_i z_i^2\right)^{1/2} \qquad (2.15)$$

The variables in equation (2.15) include the gas constant (R), absolute temperature (T), Faraday's constant (F), concentration of ions (c_i), and the charge number of the ions (z_i). The value $1/\kappa$, critical to the repulsive force, is defined as the radius of the ionic atmosphere, or the thickness of the electrical double layer. Another point that is of marked importance in colloid science is that this thickness, and therefore the stability, is extremely dependent on the ionic concentration of the dispersion medium. As the ionic concentration rises, $1/\kappa$ decreases rapidly (Table 2.3)[84], and remember that if the counter-ions are collapsed on the surface ($1/\kappa \sim 0$) then coagulation will occur. This makes electrostatically stabilized suspensions extremely sensitive to the purity of the dispersion medium. It also allows for a convenient way to coagulate a suspension if desired, namely adding a salt to the suspension.

Table 2.3: The Effect of a 1:1 electrolyte on the thickness of the electrical double layer ($1/\kappa$)[84]

Concentration (c_I) (M)	($1/\kappa$) (nm)
10^{-5}	100
10^{-4}	30
10^{-3}	10
10^{-2}	3
10^{-1}	1

The direct addition of these two forces (V_R and V_A) according to DLVO theory determines the stability of the suspension. This can best be described graphically as a function of interparticle distance (d) (Figure 2.27).[84] As seen from this figure, a secondary minimum often exists. The secondary minimum is responsible for the phenomenon of flocculation (or reversible coagulation). If a colloidal dispersion flocs, it can usually be re-dispersed with simple agitation.

Colloidal suspensions consist of particles with diameters between 10Å and 1μm. This implies a very high surface to volume ratio, resulting in a free energy excess. Because of this, colloidal suspensions can only be made kinetically stable (metastable). This stability is dependent on the summation of all the forces acting on the particle, namely London - van der Waals dispersion, electrostatic repulsion and steric repulsion. The first two of these are the forces accounted for by the classic DLVO theory. This theory describes the variables that control the electrostatic stabilization of suspensions, and will be utilized to aid in the stabilization of PEEK particles to facilitate aqueous suspension prepregging.

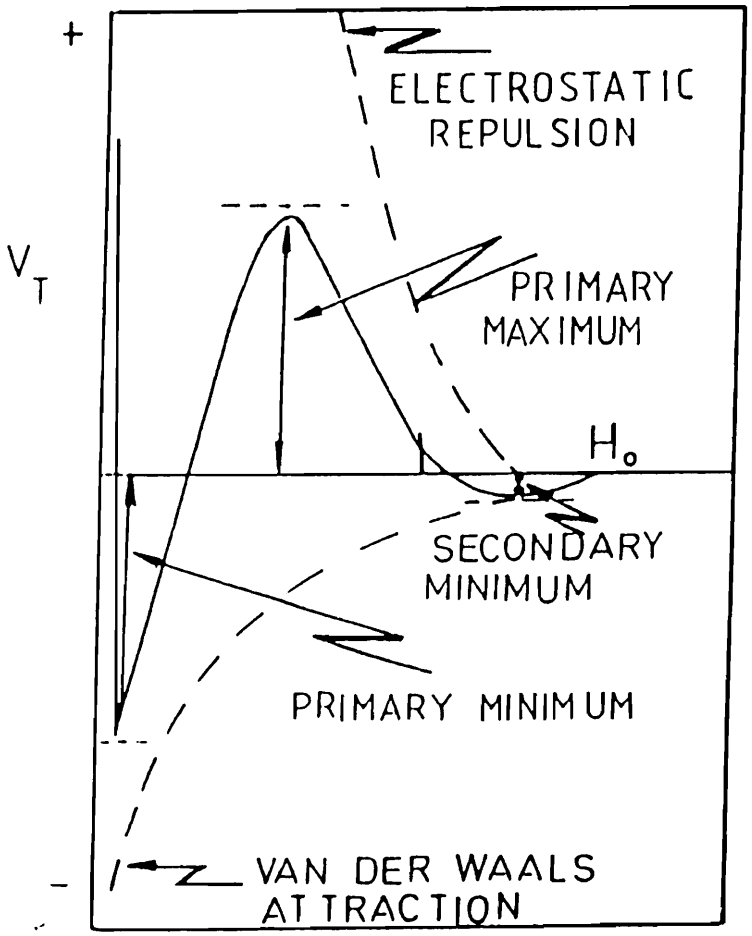

Figure 2.27: Representation of the total potential energy vs distance of separation for a pair of electrostatically stabilized particles. Also shown are the electrostatic repulsion and van der Waals attraction components.[84]

2.5 Sintering:

2.5.1 Introduction to Sintering:

As previously discussed, materials in a particulate form (high surface area) have a thermodynamic driving force to coagulate. If this process is taken out of the context of colloidal suspensions and applied to dry particles, the process is known as sintering. It is well established that packed metal or ceramic powders will bond together and densify (sinter) when they are heated to approximately half of their absolute melting temperatures.[96,97] This densification is also acompanied by significant increases in the strength, and ductility of the material. This technique has been applied to the processing of metals since the beginning of civilization. In fact almost every metal and ceramic material was first processed through a powder precursor.[98]

The driving force for this densification process, exactly the same as for coagulation, is the reduction of surface area, and therefore a reduction in the surface excess free energy. One of the results of the surface free energy is that it gives rise to a pressure difference across a curved surface. This pressure can be viewed as a capillary pressure (P) (Figure 2.28) which is described mathmatically by the LaPlace equation (2.16).[99]

$$P = \gamma\left(\frac{1}{R_1} + \frac{1}{R_2}\right) \qquad (2.16)$$

The surface tension (γ) and the radius of curvature (R) determine the magnitude of this pressure. The smaller the radius, the larger the resulting pressure (Table 2.4).[99] This pressure difference can also be viewed as the driving force to densify, much like if the powder were being compacted due to external applied pressure. The presence of either large particles or large pores (> 100 μm) will make the driving force for sintering (pressure difference) insufficient. However,

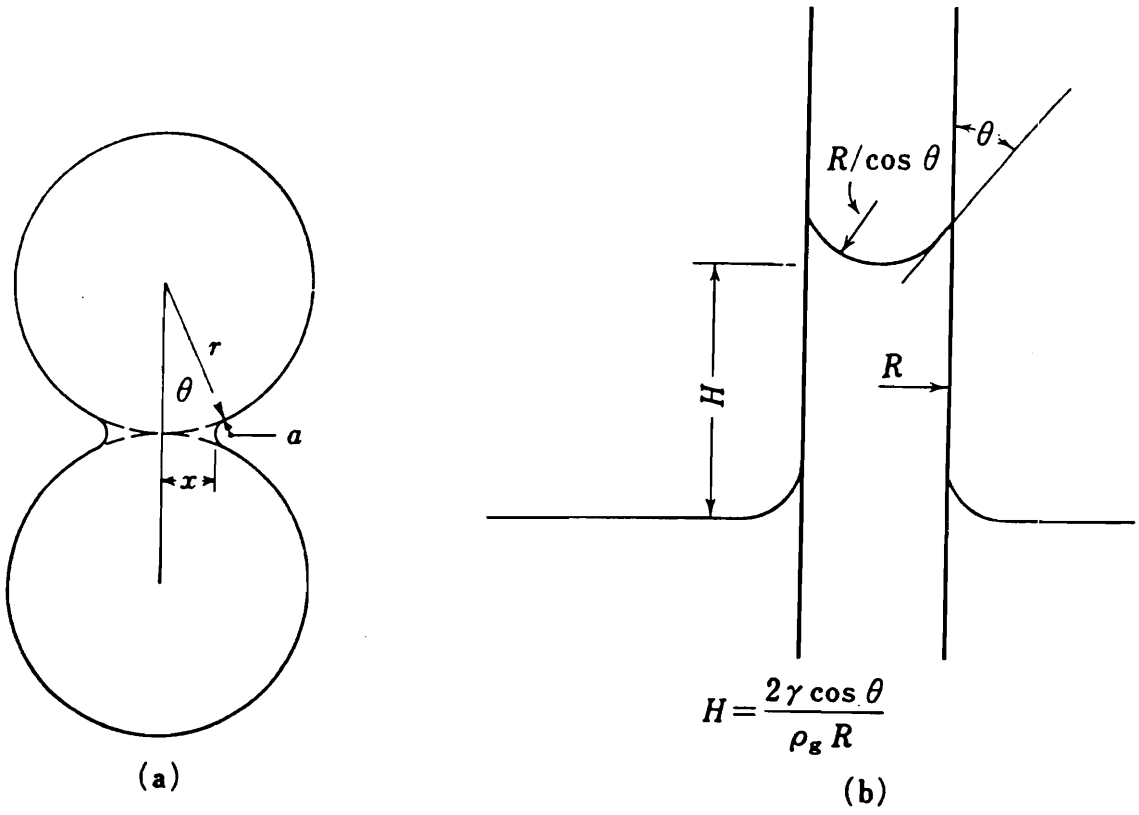

Figure 2.28: Curvature in (a) Capillary Neck Between Particles is Similar to (b) Curvature of Liquid Surface in Ordinary Capillary.[99]

if the particle size is quite small (< 1μm), there is no need to apply an external pressure to the particles to get them to sinter. This pressure can be supplied internally, entirely due to the large surface area and therefore large pressure difference.[97] In fact, theoretically all that is required for this sintering process to occur is that the particles need to be brought close enough for the surface of one particle to interact with the surface of another particle.[100] However, as in colloidal stability, one must consider the kinetics of this process as well.

Table 2.4: Effect of Surface Curvature on Pressure Difference Across a Spherical Surface of Silica Glass at 1700°C[99]

Surface Diameter (μm)	Pressure Difference (PSI)
0.1	1750
1	175
10	17.5
100	1.8
1000	0.18

The actual sintering process requires mass transport from one particle to the other, with the rate determined by the mechanism of this mass transport. There are several different mechanisms available including viscous flow, evaporation - condensation, surface diffusion and volume diffusion.[99,101,102] Since this discussion will focus on sintering of polymeric powders, the mechanism of viscous flow will be further examined. This mechanism was first treated theoretically by Frenkel in 1945.[103]

2.5.2 Frenkel's Two Particle Model

Frenkel derived a model relating the particle radius (a) to the growing neck radius (X) as a function of time for the sintering of two particles by viscous flow (Figure 2.29). This relationship[103] can be written as:

$$\frac{X^2}{a} = \frac{3}{2}\frac{\gamma}{K}t \qquad (2.17)$$

where γ is the surface free energy, t is time, and K is a measure of mobility in a power law fluid (2.18).

$$\sigma = K(\dot{\varepsilon}_s)^n \qquad (2.18)$$

This relationship (2.17) results from equating the rate of surface energy change due to consolidation (dE_s/dt) to the rate of surface energy dissipation by viscous flow (dE/dt).[104]

The derivation of the rate of surface energy change (dE_s/dt) starts with defining E_s as

$$E_s = A\gamma \qquad (2.19)$$

where γ is the surface tension and A is the area between the two particles. From geometry (Figure 2.29) the area can be described as

$$A = 2\pi X^2 \qquad (2.20)$$

therefore,

$$E_s = 2\pi\gamma X^2 \qquad (2.21)$$

and taking the time derivative yields the desired result:

$$\frac{dE_s}{dt} = 4\pi\gamma X\frac{dx}{dt}. \qquad (2.22)$$

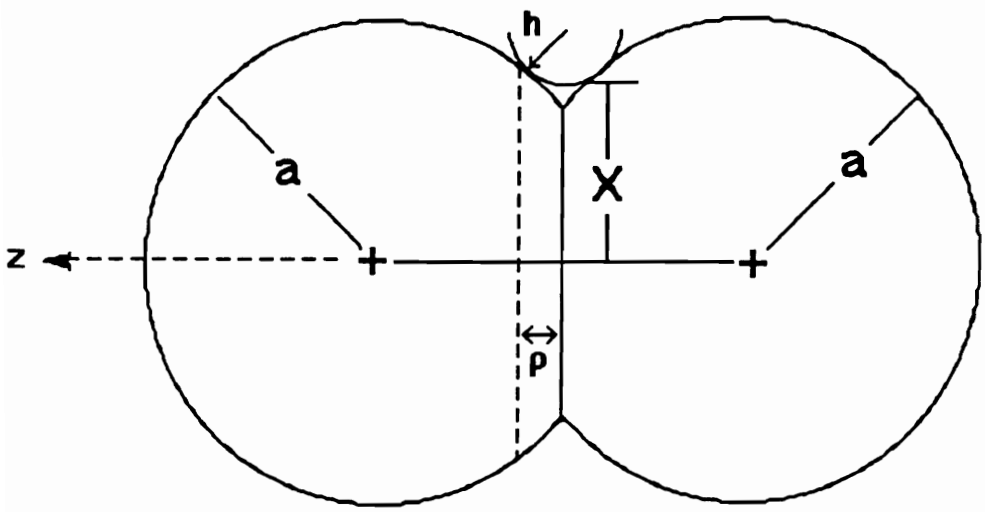

Figure 2.29: Frenkel's Two Particle Model.[104]

The derivation of the rate of surface energy dissipation by viscous flow (dE/dt) starts by examining the shear stress.[104] The energy increase per unit volume due to the shear stress is given by

$$\sigma\dot{\varepsilon}_s \,. \qquad (2.23)$$

Therefore the total energy dissipation rate can be written as

$$\frac{dE}{dt} = 2\int_h^a \sigma\dot{\varepsilon}_s dV \qquad (2.24)$$

where the limits of the integration come from the geometry (Figure 2.29). "h" is the initial particle overlap and "a" is considered the overlap at complete sintering (the particle radius). The Ostwald empirical relation[104] is given by

$$\sigma = K(\dot{\varepsilon}_s)^n \qquad (2.25)$$

and substituting (2.25) into (2.24) gives

$$\frac{dE}{dt} = 2\int_h^a K(\dot{\varepsilon}_s)^n \dot{\varepsilon}_s dV \qquad (2.26)$$

which can be rearranged to

$$\frac{dE}{dt} = 2\int_h^a K(\dot{\varepsilon}_s)^{n+1} dV \,. \qquad (2.27)$$

To use equation (2.27), a relationship for $\dot{\varepsilon}_s$ first needs to be developed. This can be done by first examining the strain rate ($\dot{\varepsilon}$) which is a gradient of the velocity

$$\dot{\varepsilon} = \frac{-d}{dZ}\left(\frac{dz}{dt}\right) \qquad (2.28)$$

and assuming the particles are incompressible

$$\frac{dz}{dt} \Big/ \frac{dh}{dt} = \frac{h}{z} \qquad (2.29)$$

or

$$\frac{dz}{dt} = \frac{h}{z}\frac{dh}{dt} \,. \qquad (2.30)$$

Thus, $\dot{\varepsilon}$ becomes

$$\dot{\varepsilon} = \frac{-d}{dz}\left(\frac{h}{z}\frac{dh}{dt}\right). \qquad (2.31)$$

Assuming that the radius of curvature (ρ) is approximated by the "overlap" (h) of the two particles (this is essentially the same approximation made in calculating capillary pressure), then

$$\dot{\varepsilon} = \frac{-d}{dz}\left(\frac{\rho}{z}\frac{d\rho}{dt}\right) = \frac{-d}{dz}\left(\frac{1}{z}\right)\left(\frac{\rho d\rho}{dt}\right) \qquad (2.32)$$

and since

$$\frac{-d}{dz}\left(\frac{1}{z}\right) = \frac{1}{z^2} \qquad (2.33)$$

then

$$\dot{\varepsilon} = \frac{\rho d\rho}{z^2 dt}. \qquad (2.34)$$

The shear strain rate ($\dot{\varepsilon}_s$) can be related to the strain rate ($\dot{\varepsilon}$) by[104]

$$\dot{\varepsilon}_s = 2\dot{\varepsilon}, \qquad (2.35)$$

thus,

$$\dot{\varepsilon}_s = \frac{2\rho}{z^2}\frac{d\rho}{dt}. \qquad (2.36)$$

Substituting (2.36) back into (2.27) and again making the approximation that $h \approx \rho$, then

$$\frac{dE}{dt} = 2\int_{\rho}^{a} K\left(\frac{2\rho}{z^2}\frac{d\rho}{dt}\right)^{n+1} dV. \qquad (2.37)$$

From the geometry (Figure 2.29)[104]

$$dV = \pi\left(2az - z^2\right)dz \qquad (2.38)$$

and substituting (2.38) into (2.37) gives

$$\frac{dE}{dt} = 2\int_{\rho}^{a} K\left(\frac{2\rho}{z^2}\frac{d\rho}{dt}\right)^{n+1} \pi\left(2az - z^2\right)dz \qquad (2.39)$$

which can be rewritten as

$$\frac{dE}{dt} = 2\int_{\rho}^{a} K(2)^{n+1}(\rho)^{n+1}\left(\frac{d\rho}{dt}\right)^{n+1}\left(\frac{1}{z^2}\right)^{n+1}\pi\left(2az - z^2\right)dz \ . \qquad (2.40)$$

Pulling the constants out of the integral gives

$$\frac{dE}{dt} = \pi K(2)^{n+2}(\rho)^{n+1}\left(\frac{d\rho}{dt}\right)^{n+1}\int_{\rho}^{a}\left(\frac{1}{z^2}\right)^{n+1}\left(2az - z^2\right)dz \qquad (2.41)$$

which can be rearranged to

$$\frac{dE}{dt} = \pi K(2)^{n+2}(\rho)^{n+1}\left(\frac{d\rho}{dt}\right)^{n+1}\int_{\rho}^{a}\left(\frac{2a}{z^{2n+1}} - \frac{1}{z^{2n}}\right)dz \qquad (2.42)$$

which integrates to

$$\frac{dE}{dt} = \pi K(2)^{n+2}(\rho)^{n+1}\left(\frac{d\rho}{dt}\right)^{n+1}\left[\frac{-a}{nz^{2n}} + \frac{1}{(2n-1)z^{2n-1}}\right]_{\rho}^{a} \qquad (2.43)$$

and expansion results in

$$\frac{dE}{dt} = \pi K(2)^{n+2}(\rho)^{n+1}\left(\frac{d\rho}{dt}\right)^{n+1}\left[\begin{array}{l}\left(\dfrac{-a}{na^{2n}} + \dfrac{1}{(2n-1)a^{2n-1}}\right) \\ -\left(\dfrac{-a}{n\rho^{2n}} + \dfrac{1}{(2n-1)\rho^{2n-1}}\right)\end{array}\right] . \qquad (2.44)$$

Because $\rho << a$ only the terms with the highest power of ρ in the denominator will be retained[104], thus

$$\frac{dE}{dt} = \pi K(2)^{n+2}(\rho)^{n+1}\left(\frac{d\rho}{dt}\right)^{n+1}\left[-\left(\frac{-a}{n\rho^{2n}}\right)\right] \qquad (2.45)$$

or

$$\frac{dE}{dt} = \pi K(2)^{n+2}(\rho)^{n+1-2n}\left(\frac{d\rho}{dt}\right)^{n+1}\frac{a}{n} \qquad (2.46)$$

which can be rewritten as

$$\frac{dE}{dt} = \frac{\pi K}{n}a(2)^{n+2}(\rho)^{1-n}\left(\frac{d\rho}{dt}\right)^{n+1} \ . \qquad (2.47)$$

As will be shown in section 2.5.2.1

$$\rho = \frac{X^2}{4a} \quad . \qquad (2.48)$$

Taking the time derivative of (2.48) gives

$$\frac{d\rho}{dt} = \frac{2X}{4a}\frac{dX}{dt} \qquad (2.49)$$

which can be substituted into (2.47) to give

$$\frac{dE}{dt} = \frac{\pi K}{n} a(2)^{n+2} \left(\frac{X^2}{4a}\right)^{1-n} \left(\frac{2X}{4a}\frac{dX}{dt}\right)^{n+1} \quad . \qquad (2.50)$$

Expanding (2.50) results in

$$\frac{dE}{dt} = \frac{\pi K}{n} a(2)^{n+2} \left(\frac{X^{2-2n}}{\left(2^{2-2n}\right)\left(a^{1-n}\right)}\right)\left(\frac{2^{n+1}X^{n+1}}{\left(2^{2+2n}\right)\left(a^{n+1}\right)}\right)\left(\frac{dX}{dt}\right)^{n+1} \quad . \qquad (2.51)$$

Combining terms provides

$$\frac{dE}{dt} = \frac{\pi K}{n}\left(\frac{a}{\left(a^{1-n}\right)\left(a^{n+1}\right)}\right)\left(\frac{\left(2^{n+2}\right)\left(2^{n+1}\right)}{\left(2^{2-2n}\right)\left(2^{2n+2}\right)}\right)\left(\left(X^{2-2n}\right)\left(X^{n+1}\right)\right)\left(\frac{dX}{dt}\right)^{n+1} \qquad (2.52)$$

and simplifying gives

$$\frac{dE}{dt} = \frac{\pi K}{n}\left(\frac{a}{a^2}\right)\left(\frac{\left(2^{2n+3}\right)}{2^4}\right)\left(X^{3-n}\right)\left(\frac{dX}{dt}\right)^{n+1} \quad . \qquad (2.53)$$

Simplifying further yields the desired relationship for the rate of surface energy dissipation by viscous flow as

$$\frac{dE}{dt} = \frac{\pi K}{na} 2^{2n-1} X^{3-n}\left(\frac{dX}{dt}\right)^{n+1} \quad . \qquad (2.54)$$

Then equating (2.54) to (2.22) gives

$$4\pi\gamma X\frac{dx}{dt} = \frac{\pi K}{na} 2^{2n-1} X^{3-n}\left(\frac{dX}{dt}\right)^{n+1} \qquad (2.55)$$

which can be rearranged to

$$\frac{(4\pi\gamma)(na)}{(\pi K)\left(2^{2n-1}\right)} = X^{3-n-1}\left(\frac{dX}{dt}\right)^{n+1-1} \qquad (2.56)$$

which is simplified to

$$\frac{\left(2^{3-2n}\right)(an\gamma)}{K} = X^{2-n}\left(\frac{dX}{dt}\right)^{n} . \qquad (2.57)$$

Taking the n^{th} root results in

$$\left(2^{-2+3/n}\right)\left(\frac{an\gamma}{K}\right)^{1/n} = X^{-1+2/n}\frac{dX}{dt} \qquad (2.58)$$

and integration provides

$$\left(\frac{X^2}{a}\right)^{1/n} = \frac{1}{2n}\left(\frac{8n\gamma}{K}\right)^{1/n} t . \qquad (2.59)$$

Frenkel used n=1 (for a viscous fluid) which gives the desired relation as

$$\frac{X^2}{a} = \frac{4\gamma}{K}t . \qquad (2.60)$$

Frenkel's original derivation yielded equation (2.17) shown again as

$$\frac{X^2}{a} = \frac{3}{2}\frac{\gamma}{K}t . \qquad (2.17)$$

The equation derived here (2.60) is different from (2.17) by a factor of 8/3 and is actually a corrected version of Frenkel's original derivation.[104] Equation (2.60) can be used qualitatively to predict the effect of material parameters such as particle size, surface free energy and melt viscosity on sintering rate (i.e., the time required for X/a = 1). This equation has been verified for sintering glass[105] and poly(methylmethacrylate) spheres[104].

2.5.2.1 The Geometrical Relationship of ρ, X and a in the Two Particle Model

$$\rho = \frac{X^2}{4a} \qquad (2.48)$$

This relationship is derived from the geometry of two sintering particles. From the triangle shown in Figure 2.30, the relationship between a, h and X is

$$(a+h)^2 = (a-h)^2 + (X+h)^2 \ . \qquad (2.61)$$

Expansion gives

$$a^2 + 2ah + h^2 = a^2 - 2ah + h^2 + X^2 + 2Xh + h^2 \qquad (2.62)$$

and simplifying results in

$$4ah = h^2 + X^2 + 2Xh \ . \qquad (2.63)$$

Rearrangement provides

$$h^2 - 4ah + 2Xh + X^2 = 0 \qquad (2.64)$$

and terms can be combined to yield

$$h^2 + (2X - 4a)h + X^2 = 0 \ . \qquad (2.65)$$

Assuming h^2 is very small ($h^2 \approx 0$) simplifies (2.65) to

$$(2X - 4a)h + X^2 = 0 \qquad (2.66)$$

and solving for h gives

$$h = \frac{-X^2}{(2X - 4a)} \ . \qquad (2.67)$$

Assuming that $2X << 4a$ provides

$$h \approx \frac{X^2}{4a} \qquad (2.68)$$

and again making the approximation that $\rho \approx h$ results in the desired equation

$$\rho \approx \frac{X^2}{4a} \ . \qquad (2.69)$$

Equation (2.69) is equation (2.48).

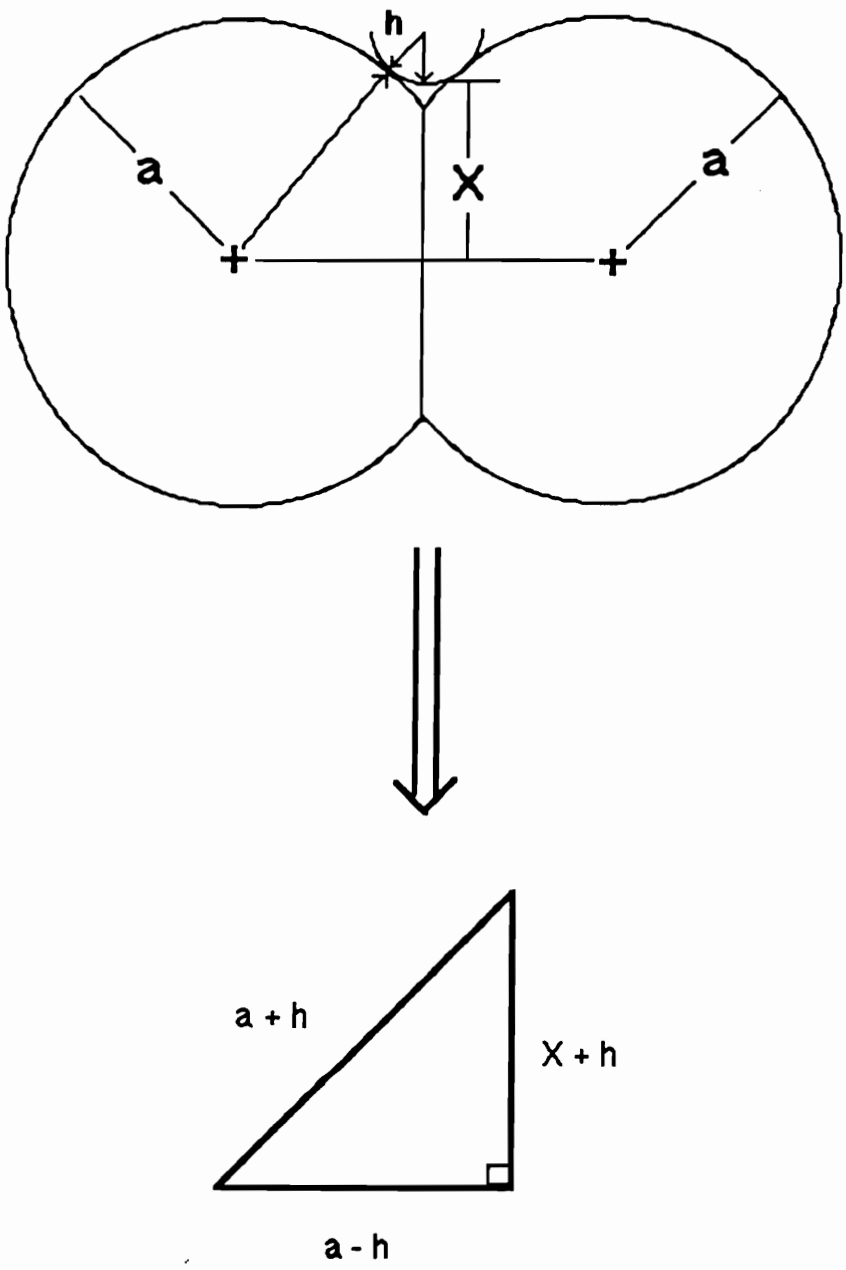

Figure 2.30: Two Particle Model Showing Geometric Relation Between X, h, and a.[104]

2.5.3 Sintering of Polymeric Powders:

As discussed earlier, this research is focused towards the use of high performance semicrystalline thermoplastic matrix resins for graphite composites. Poly(ether ether ketone) (PEEK) is a high performance semi-crystalline thermoplastic with a glass transition temperature of 143°C. The Tm is often quoted as 334°C but the equilibrium melting point is significantly higher (384°C).[106] PEEK has excellent mechanical properties as well as good solvent resistance. However, due to its high thermal transitions it requires high temperatures for processing, at least 370 - 400 °C, where it degrades as previously discussed. An alternative to melt processing PEEK is to apply the powder metallurgy technique of sintering, which is predicted to follow Frenkel's model.

The procedure is not new for polymeric powders and has been applied previously to ultra high molecular weight polyethylene,[107,108] polystyrene,[109] poly(methylmethacrylate),[104] and even polyimides[111-113]. In these studies a particle size of less than 100 μm diameter was required and a free sintering temperature above the polymer glass transition temperature, or the melt temperature for the semicrystalline polyethylenes, was necessary. These polymer sintering temperatures relative to the material transition temperatures are high compared to temperatures normally employed for metal and ceramic sintering. However, one must recall that ceramic sintering is conducted at temperatures less than the absolute melting point of the material. However, particle sizes reported in polymeric powder sintering are large compared to the submicron particles often used for ceramics and metals.[97] Since sintering occurs due to a reduction of surface free energy, smaller particles (larger

surface area) have larger driving forces for sintering. Thus the relatively high temperatures required for polymeric systems could be explained by the large particles used thus far. It should also be noted that organic materials in general have lower surface free energies than metals, and this also lowers the driving force for sintering.

To experimentally follow the process of sintering, the development of mechanical properties, namely yield strength and density, are examined as a function of sintering time, temperature and particle size.[114] When one brings two polymeric particles together into intimate contact through sintering, the initial adhesion between them is due to the lowering of surface energy and the mutual van der Waals interactions. This is the process which was first modeled by Frenkel. However these forces are weak, and therefore the bond between the particles is also weak. If, however, the particles are held in contact long enough and at temperatures that allow for polymer diffusion to occur, then the chains can actually diffuse across the grain boundary. This reptation process "sews" up the interface and allows it to heal.[115] The strength between the particles would then be equivalent to the cohesive strength of the bulk polymer. This process has been modeled by Wool et al.[116-118] as the process often referred to as "crack healing". It is believed that the model proposed by Frenkel combined with that developed by Wool should provide a good basis for interpreting sintering of polymeric powders.

2.5.4 Wool's Theory for Crack Healing

When two pieces of the same (or two miscible) polymer are brought into good contact with each other at a temperature above the glass transition

temperature the interface gradually disappears and the mechanical strength of the bond between them increases. This "crack healing" is due to the diffusion of the polymer chains across the interface.[118]

In the theory developed by Wool, et al.[116-120] the crack healing process has been broken down into five individual steps. These steps include surface rearrangement, surface approach, wetting, diffusion and randomization (Figure 2.31).[120] The barriers to diffusion that are associated with the inhomogeneities of the interface are gone by the end of the third stage (wetting). In other words intimate contact has been reached by this point. These three initial stages are essentially what is described by Frenkel's two particle model. Once intimate contact is reached the polymer chains can move freely across the interface during the stages of diffusion and randomization. These last two steps are the critical ones for the development of mechanical strength, and can be modeled by the reptation theories of de Gennes[121,122] as well as Doi and Edwards[123].

Within a bulk thermoplastic polymeric material, the motion of any one polymer chain is greatly restricted by entanglements with it's neighbors. The reptation model describes these entanglements as a "tube" that confines the polymer chain in question. Due to thermal fluctuations the chain can "wriggle" around in the tube and eventually free itself, although only to confine itself into a new tube (Figure 2.32).[116] The time required for the chain to completely remove itself from the initial tube is defined as T_r (renewal time). The diffusion in the crack healing process can be described using this model (Figures 2.33 and 2.34).[118] Using this reptation theory Wool has developed scaling laws that relate the microscopic polymer chain diffusion to macroscopic measurements such as fracture stress (σ). With the assumption that the first three stages of

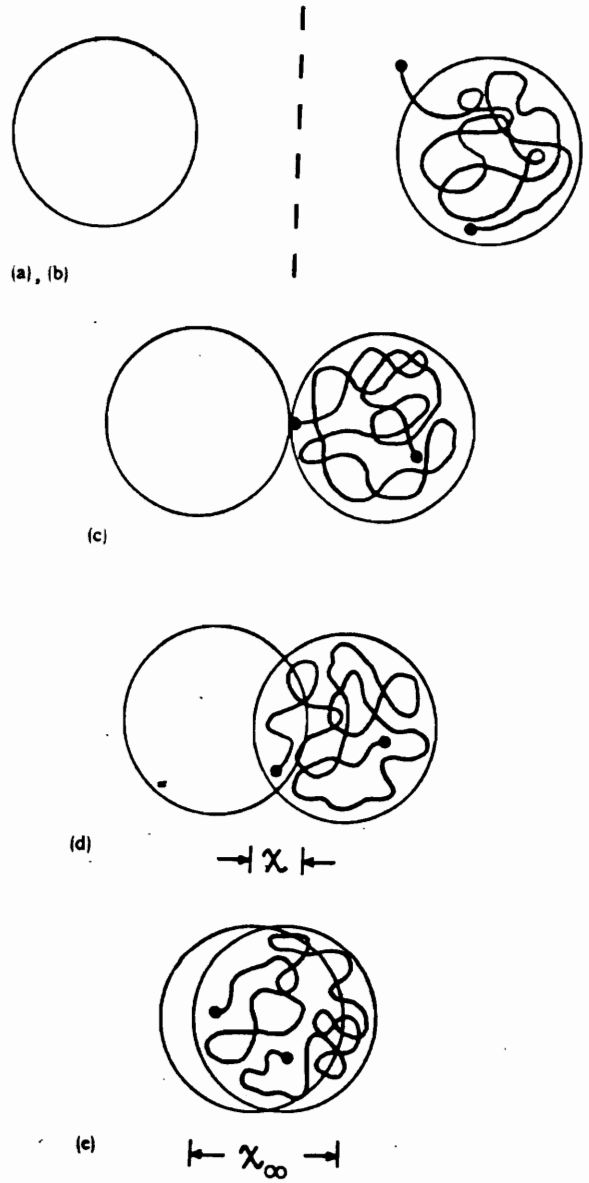

Figure 2.31: The Five Stages of Crack Healing; (a) Rearrangement, (b) Surface Approach, (c) Wetting, (d) Diffusion, and (e) Randomization. The Dashed Line Represents the Original Crack Plane.[120]

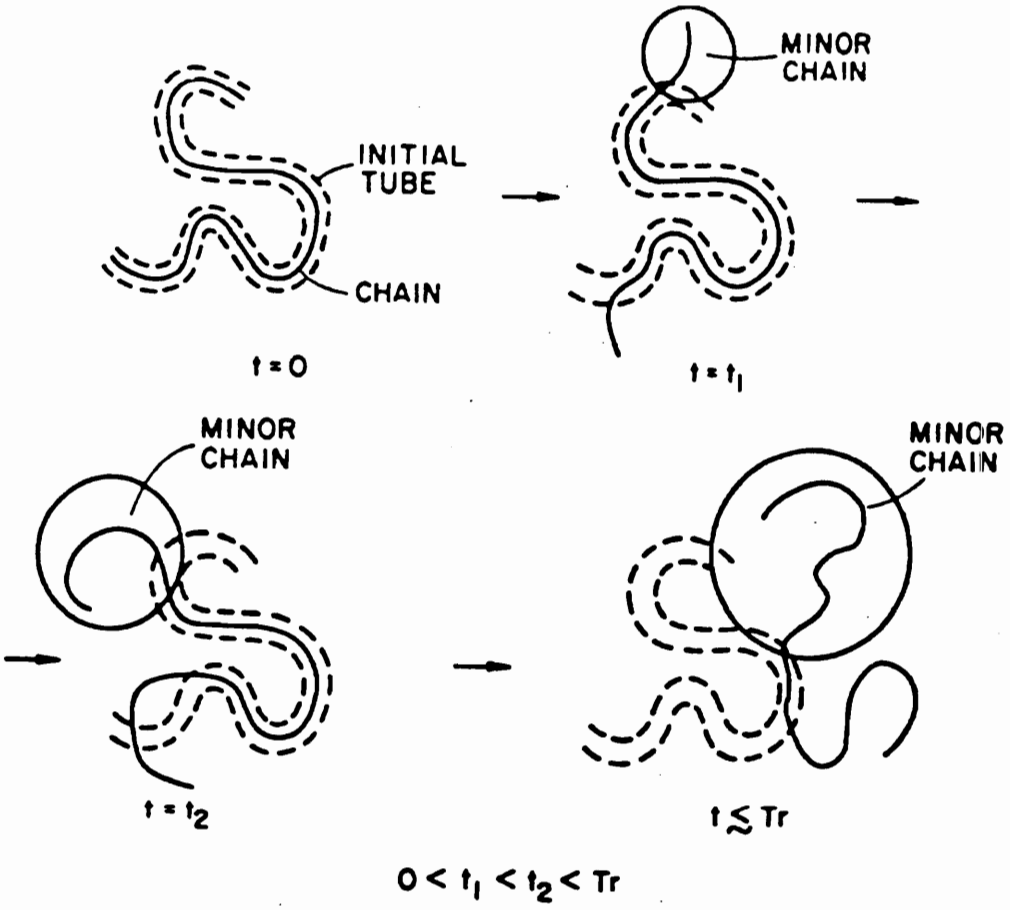

Figure 2.32: The Disentanglement of a Chain From its Initial Tube.[116]

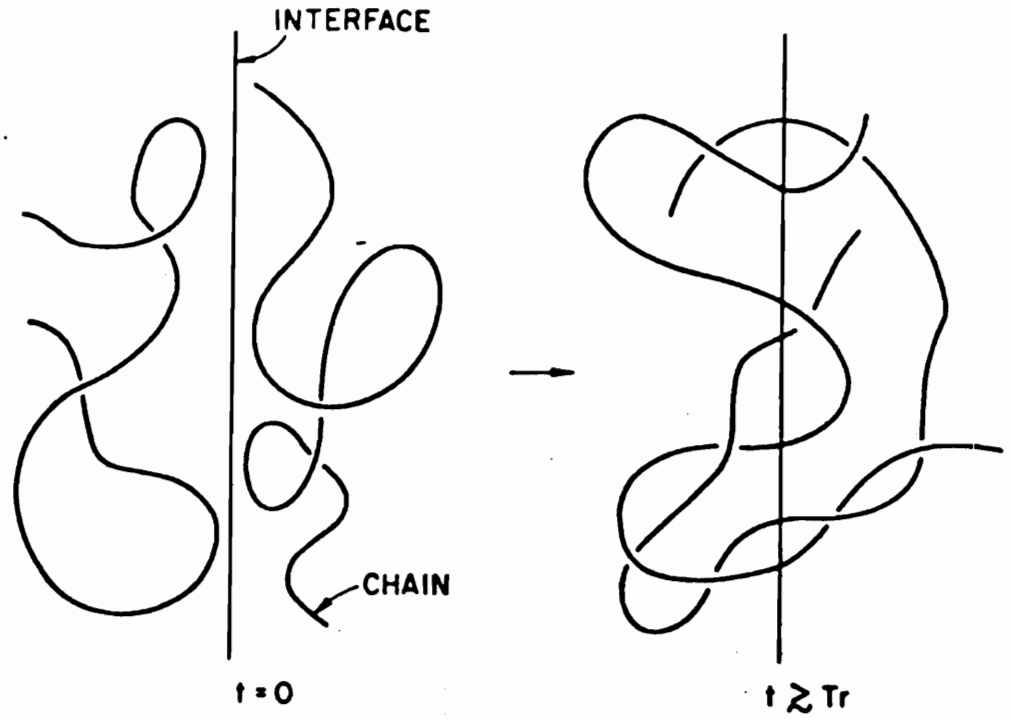

Figure 2.33: Configuration of Two Chains at the Interface Before and After the Stages of Diffusion and Randomization.[118]

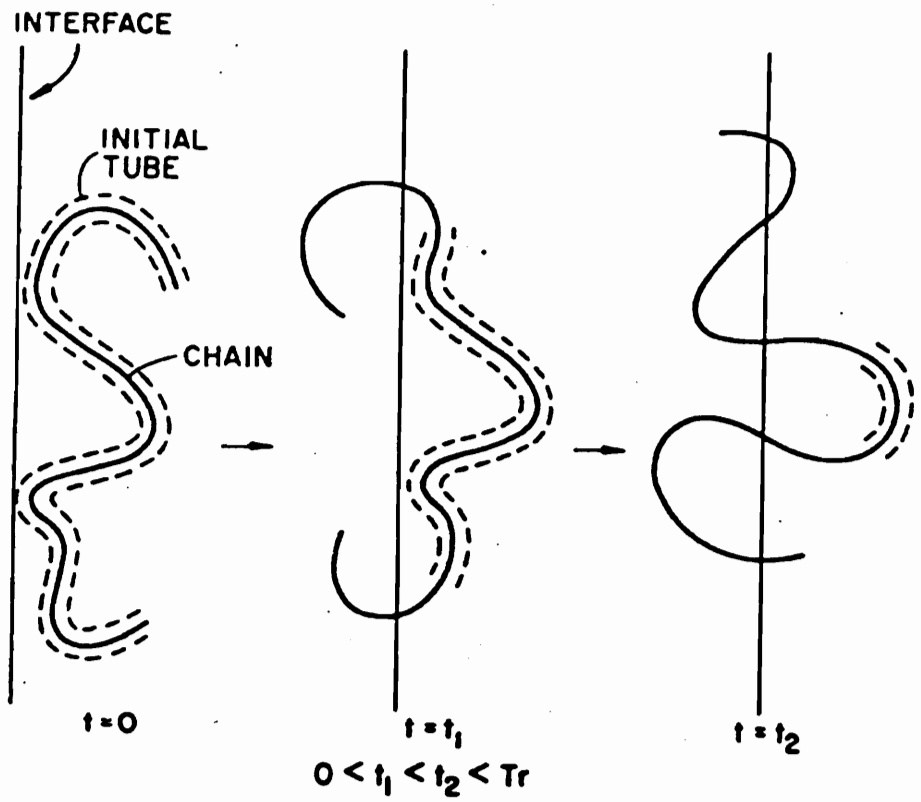

Figure 2.34: Disengagement of a Chain From its Initial Tube Near the Interface.[118]

crack healing are instantaneous, Wool determined that the recovery ratio of fracture stress (σ) with time followed the scaling law[120] of

$$R(\sigma,t) = R_o + \frac{Kt^{1/4}}{\sigma_\infty} \qquad (2.70)$$

where

$$R_o = \frac{\sigma_o}{\sigma_\infty} \qquad (2.71)$$

and

$$R = \frac{\sigma(t)}{\sigma_\infty} \qquad (2.72)$$

the subsripts o and ∞ indicate zero and infinte time respectively. This scaling law also contains K, a constant which is dependent on molecular weight, temperature and pressure. A graphical analysis of this scaling law can be derived by plotting $\log(R-R_0)$ vs. log t. A slope of 1/4 should be obtained. This analysis combined with the two particle model will be utilized to examine the sintering of poly(ether ether ketone particles).

Chapter 3 - Experimental

3.1 Solvents and Their Purification

The purification of all solvents was by distillation, either under reduced pressure or under a nitrogen purge. The distillation apparatus and receiving flasks were flame dried under vacuum. The receiving flask was typically a two-necked flask with one neck sealed with a septum. This allowed transfer of the distilled solvent into a flame dried storage bottle via cannula eliminating exposure to the atmosphere.

3.1.1 Toluene: Toluene, purchased from Aldrich, was purified by washing 800 ml with sulfuric acid (60 ml) twice. The residual sulfuric acid was removed by washing twice with water (100 ml each) followed by saturated sodium bicarbonate until basic (≈ 3 X 50 ml). Water was used for the final washing (100 ml). The toluene was stirred over calcium sulfate in an Erlenmeyer flask (2 - 4 hours) then decanted into another flask containing phosphorous pentoxide and stirred for an additional 8 hours. The dried toluene was distilled from sodium and benzophenone under a nitrogen purge. (b.p. 111°C/760mm)

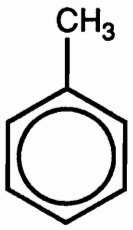

3.1.2 1-Methyl-2-pyrrolidone (NMP): NMP, purchased from Fisher, was dried over P_2O_5 for at least 8 hours and then distilled under reduced pressure (≈ 200 millitorr). (b.p. 205°C/760 mm)

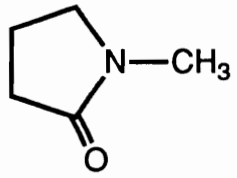

3.1.3 N,N-Dimethylacetamide (DMAc): DMAc, purchased from Fisher, was dried over calcium hydride for at least 8 hours and then distilled under reduced pressure (≈ 200 millitorr). (b.p. 164.5 - 166°C/760mm)

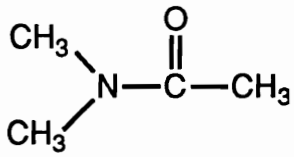

3.1.4 Deuterated Dimethylsulfoxide (d-6 DMSO): d-6 DMSO, purchased from Cambridge Isotope Laboratories, was used as an NMR solvent in most experiments. The d-6 DMSO was used as recieved.

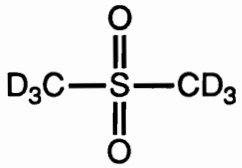

3.1.5 Deuterated Chloroform ($CDCl_3$): $CDCl_3$, purchased from Cambridge Isotope Laboratories, was also used as an NMR solvent. The $CDCl_3$ was used as received, often with 0.05% TMS added as an internal reference.

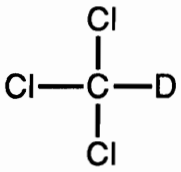

3.1.6 Absolute Ethanol: Ethanol, purchased from Fisher, was used as received for a recrystallization solvent. (b.p. 78 - 79°C)

$$CH_3CH_2—OH$$

3.1.7 Tetrahydrofuran (THF): THF, purchased from Fisher, was used as received to dilute polymer solutions prior to precipitation. (b.p. 67°C)

3.1.8 Water (H_2O): Water was purified using a Barnstead NANOPURE II deionizer until the measured resistance was greater than 17 ohms. This was particularly critical for the electrostatic stabilization experiments.

3.2 Reagent Purification

3.2.1 Aniline: Aniline, purchased from Aldrich, was dried over calcium hydride and tin(II) chloride for at least 8 hours and then distilled under reduced pressure (≈ 200 millitorr). (b. p. 184 °C)

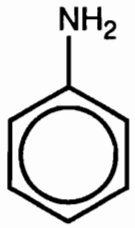

3.2.2 Hydrochloric acid (HCl): 12.1 N aqueous HCl was purchased from Fisher and used as received.

3.2.3 4Å Molecular Sieves: Fisher brand 4Å molecular sieves, used in monomer syntheses, were dried for at least 8 hours at 180°C under vacuum prior to use.

3.2.4 Potassium Carbonate (K_2CO_3): Fisher brand K_2CO_3, used in poly(arylene ether) syntheses, was dried under vacuum at 180°C for at least 8 hours prior to use.

3.2.5 Glacial Acetic Acid (CH_3COOH): Glacial acetic acid, purchased from Fisher, was used as received. (b.p. 116 - 118°C)

3.2.6 Poly(ether ether ketone) particles: PEEK particles were purchased from ICI and then wet sieved to fractions with average particle diameter's of 120, 93.7, 59.7, 42.6, and 34.8 μm. ICI also separately provided particles with an average diameter of 15 μm.

3.2.7 LaRC TPI Polyamic Acid: LaRC TPI in the polyamic acid form was obtained from NASA Langley. The amic acid was converted to the ammonium salt by dissolving 26.5 g of the polymer in 800 ml water with 7.2 ml of ammonium hydroxide. This solution was used as a stabilizer for the PEEK particles.

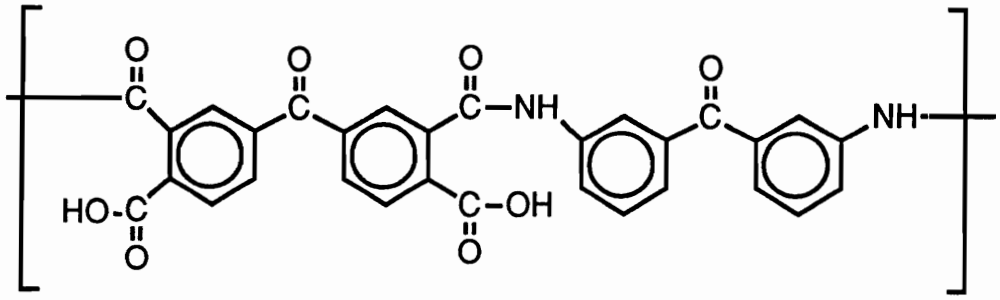

LaRC TPI Polyamic acid

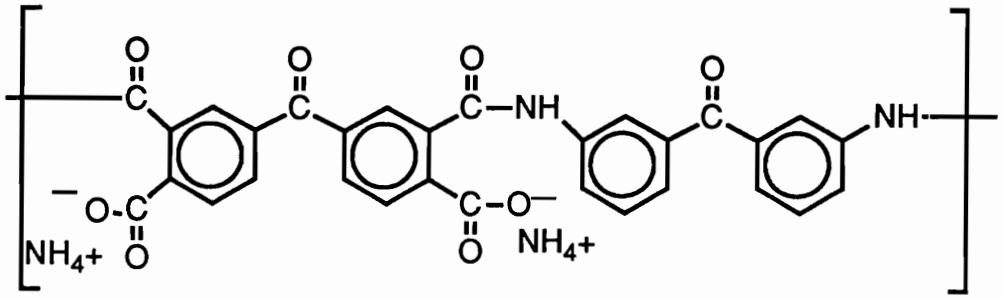

Ammonium Salt of LaRC TPI

3.2.8 Triton X-100: Triton X-100, purchased from Aldrich, was used as a aqueous suspension stabilizer for PEEK particles.

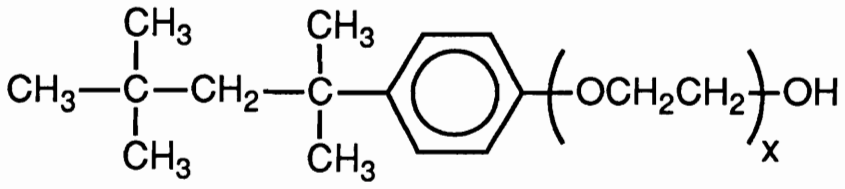

x = 10 (average)

3.3 Monomer Purification

3.3.1 4,4'-Difluorobenzophenone (DFBP): DFBP was kindly supplied by ICI Americas Inc. and purified by recrystallization from ethanol followed by drying in a vacuum oven at ≈ 90°C overnight. (FW = 218.20 amu; m.p. 102 - 105°C)

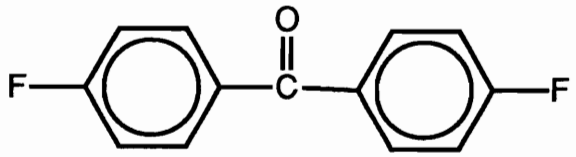

3.3.2 Hydroquinone (HQ): Gold Label hydroquinone was purchased from Aldrich (>99.9% purity) and used as received. (FW = 110.11 amu; m.p. 174.4 - 176.6°C)

3.3.3 2,6-Dichloropyridine: 2,6-Dichloropyridine was purchased from Aldrich, recrystallized from ethanol, and vacuum dried (≈ 50°C) prior to use. (FW = 147.99 amu; m.p. 87 - 88°C)

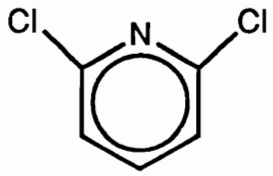

3.3.4 4-*tert*-Butylphenol: 4-*tert*-Butylphenol, purchased from Aldrich, was sublimed prior to use. (FW = 150.22 amu; m. p. 98 - 101°C)

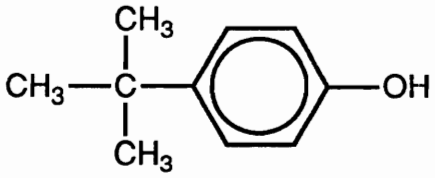

3.4 Monomer and Polymer Synthesis

3.4.1 Synthesis of 4,4'-difluoro (N-benzohydroxylidene aniline) (Ketimine Monomer): First, 120 g (0.55 mol) of 4,4'-difluorobenzophenone (used as received from ICI) and 80 ml (0.88 moles) of aniline were added to a 1000 ml three-necked round-bottomed flask equipped with a nitrogen inlet, overhead stirrer, Dean Stark trap, and a condenser. Then 500 ml of toluene and about 300 g of 4Å molecular sieves were added. This reaction mixture was heated to toluene reflux and held until 100% conversion to the ketimine had occurred (≈ 24 hours) as determined by ^{1}H NMR. The reaction mixture was filtered through Celite™ to remove the molecular sieves. The solvent and excess aniline were

removed by rotary evaporation. The resulting orange product was recrystallized twice from toluene and dried under vacuum at 90°C to provide a pure yellow crystalline material with a melting point of 114-115°C in about 50% yield.

3.4.2 Synthesis of Poly(ether ether ketimine) (PEEKt): The following is a procedure for the synthesis of a poly(ether ether ketimine) via nucleophilic aromatic substitution in a polar aprotic solvent. The molecular weight was controlled to 20,000 g mol^{-1} by offsetting the stoichiometry according to the Carother's equation to provide a hydroquinone terminated polymer. The correct stoichiometry was determined by utilizing a computer program (Appendix 3.1) that solves the Carother's equation.

First, 0.0987 moles (28.936 g) of 4,4'-difluoro (N-benzohydroxylidene aniline), 0.100 moles (11.064 g) of hydroquinone, and 0.15 moles (20 g) of potassium carbonate were dissolved in 200 ml of NMP in a 500 mL three-necked flask equipped with a condenser, Dean Stark trap, overhead stirrer, and nitrogen inlet. Then 60 ml of toluene were added as an azeotroping agent. The reaction mixture was heated to 140°C for three hours and then at 170°C overnight. The solution was then diluted with 200 ml of tetrahydrofuran and neutralized with 10 ml of glacial acetic acid. This solution was then precipitated into methanol/water (80:20), soxhlet extracted with methanol, and dried under vacuum at 60°C for 8 hours followed by 160°C overnight.

3.4.3 Synthesis of Poly((ether ether ketimine) - co - (ether ether ketone)): The following is a procedure for the synthesis of a poly((ether ether ketimine - co - ether ether ketone)) via nucleophilic aromatic substitution in a polar aprotic

solvent. The molecular weight was controlled to 20,000 g mol^{-1} by offsetting the stoichiometry according to the Carother's equation by adding the monofunctional endcapping agent t-butylphenol, again determined by the computer program in Appendix 3.1.

First, 0.0455 moles (13.346 g) of 4,4'-difluoro (N-benzohydroxylidene aniline), 0.0897 moles (9.877 g) of hydroquinone, and 0.103 moles (14.23 g) of potassium carbonate were dissolved in 200 ml NMP in a four-necked 500 ml flask equipped with an overhead stirrer, Dean Stark trap, condenser, and a nitrogen inlet. Then 60 ml of toluene were added as an azeotroping agent. The reaction mixture was heated to 140°C for three hours to dehydrate the system. The temperature was increased to 170°C, and once the reaction temperature equilibrated at 170°C, 0.455 moles (9.928 g) of 4,4'-difluorobenzophenone and 0.0026 moles (0.394 g) of t-butylphenol were added. The reaction was allowed to stir overnight at 170°C under a nitrogen purge. The solution was diluted with 200 ml of tetrahydrofuran and neutralized with 10 mL of glacial acetic acid. This solution was precipitated into methanol/water (80:20), soxhlet extracted for 24 hours with methanol, and dried under vacuum at 60°C for 8 hours followed by 160°C overnight.

3.4.4 Synthesis of Poly((pyridine ether) - co - (ether ether ketimine)): The following is a procedure for the synthesis of a poly((pyridine ether) - co - (ether ether ketimine)) via nucleophilic aromatic substitution in a polar aprotic solvent. The molecular weight was controlled to 20,000 g mol^{-1} by offsetting the stoichiometry according to the Carother's equation by adding the monofunctional endcapping agent t-butylphenol (Appendix 3.1). This example

is for a copolymer containing 10 mole percent 2,6-dichloropyridine and 90 mole percent 4,4'-difluoro(N-benzohydroxylidene aniline) (e.g., the ketimine monomer) for the activated dihalo monomers. Copolymers containing mole ratios of 2,6-dichloropyridine to ketimine of 20/80 and 30/70 were synthesized in a similar manner.

Hydroquinone (0.0628 moles, 6.9164 g), t-butylphenol (0.0026 moles, 0.394 g) and potassium carbonate (0.0942 moles, 13.019 g) were dissolved in 50 ml NMP in a four-necked 250 ml flask equipped with an overhead stirrer, Dean Stark trap, condenser, a nitrogen inlet, and a thermometer. Toluene (50 ml) was added as an azeotroping agent. The reaction mixture was heated to 140°C for three hours to dehydrate the system. The temperature was increased to 165°C, and once the reaction temperature equilibrated at 165°C, 0.0574 moles (16.8413 g) of 4,4'-difluoro(N-benzohydroxylidene aniline) and 0.0064 moles (0.9441 g) of 2,6-dichloropyridine were added with 70 ml of NMP. The reaction was allowed to stir for 17 hours at 165°C. The solution was then cooled to room temperature and diluted with 200 ml of tetrahydrofuran. The polymer was precipitated into methanol/water (80:20), soxhlet extracted for 24 hours with methanol, and dried under vacuum at 60°C for 8 hours followed by 160°C overnight. Upon characterizing these copolymers it was determined that this procedure resulted in only low molecular weight materials. For this reason a modified procedure is described below.

3.4.5 Modified Synthesis of Poly((pyridine ether) - co - (ether ether ketimine)): The following is the modified procedure for the synthesis of a poly((pyridine ether) - co - (ether ether ketimine)) via nucleophilic aromatic substitution in a

polar aprotic solvent. The molecular weight was uncontrolled using a 1:1 stoichiometry of the monomers. This example is for a copolymer containing 20 mole percent 2,6-dichloropyridine and 80 mole percent 4,4'-difluoro(N-benzohydroxylidene aniline) (e.g., the ketimine monomer) for the activated dihalo monomers. N,N-Dimethylacetamide (DMAc) was used instead of NMP for these reactions. Controlled molecular weight polymers (Dp = 66 and 40) of the same composition were made in a similar manner using t-butyl-phenol as the endcapping agent.

Hydroquinone (0.0500 moles, 5.5056 g), 4,4'-difluoro(N-benzohydroxylidene aniline) (0.0400 moles, 11.7326 g) and potassium carbonate (0.0750 moles, 10.3650 g) were dissolved in 90 ml of DMAc in a four-necked 250 ml flask equipped with an overhead stirrer, Dean Stark trap, condenser, a nitrogen inlet, and a thermometer. Toluene (50 ml) was added as an azeotroping agent. The reaction mixture was heated to 140°C for three hours to dehydrate the system. and then increased to 160°C. Once the reaction temperature equilibrated at 160°C, 0.0100 moles (1.4799 g) of 2,6-dichloropyridine were added with 30 ml of DMAc. The reaction was allowed to stir for 35 hours at 160°C. Samples were taken as a function of time, cooled to room temperature, and precipitated into methanol/water (80:20). Gel permeation chromatography analysis was performed on each sample using polystyrene standards to approximate the molecular weight.

3.4.6 Hydrolysis of poly(ether ether ketimine) to poly(ether ether ketone): The following is a procedure for the conversion of the imine functionality to the ketone via acid hydrolysis. These reactions were done at various temperatures

to determine the optimum temperature to obtain the smallest particle size. The composition of the resulting poly(ether ether ketone) was determined by g.c.-pyrolysis-mass spectral analysis, and also thermogravimetric-mass spectral analysis. In all cases there was no imine detected; therefore, the composition of the final polymer was 100% PEEK.

First, 2 g of the purified, dried ketimine containing polymer were dissolved in 38 ml of NMP in a 100 ml single necked round bottomed flask. Then 1.6 ml of water were added to the solution. Once this solution was homogeneous, 3 mL of an HCl/NMP solution (3 ml of 12.1N aqueous HCl in 27 ml NMP) were syringed into the polymer solution while stirring rapidly. The polymer typically precipitated immediately. The precipitate was then filtered and washed with water to remove the solvent and acid. The washed 'particles' were then suspended in water using an aqueous solution of LaRC TPI polyamic acid and ammonium hydroxide (800 ml water, 26.5 g polyamic acid, and 7.2 ml of ammonium hydroxide) as a steric stabilizer. Once the particles were suspended, they were sonicated for 3 minutes at 75 watts to break up any aggregates. The particle size was then measured by a centrifugal particle size analyzer as described in the characterization section. This procedure was also carried out using 3 ml of a more concentrated HCl/NMP solution (taken from a solution of 6 ml of 12.1N aqueous HCl in 24 ml NMP) to study the effect of increased acid concentration on particle size.

3.4.7 Slow and Controlled Hydrolysis of Poly(ether ether ketimine): A slow and controlled hyrdrolysis procedure was desired to synthesize various poly((ether ether ketimine) - co - (ether ether ketone)) copolymers from the same starting

poly(ether ether ketimine) homopolymer. These could then be utilized in a solubility study. This hydrolysis procedure was performed utilizing a 5 wt % solution of poly(ether ether ketimine) in distilled NMP. To this solution exactly 3 wt% water was added, and the temperature was maintained at 23°C. A deficiency of HCl was added while constantly stirring to give a imine to HCl ratio of either 40 or 36. Aliquots were removed as a function of time and the % Hydrolysis (ketimine to ketone) was monitored by ^{1}H NMR.

3.4.8 Hydrolysis of Poly((pyridine ether) - co - (ether ether ketimine)): The following is a procedure for the conversion of the imine functionality to the ketone via acid hydrolysis. These conditions were previously optimized in terms of providing the smallest particle size and for achieving quantitative hydrolysis to the ketone as previously discussed. The acid hydrolysis conditions are such that the pyridine moiety in the backbone is also protonated during this procedure.

The purified, dried poly((pyridine ether) - co - (ether ether ketimine)) (2g) was dissolved in 38 ml of vacuum distilled NMP. Water (1.6 ml) was added to the solution and the mixture was equilibrated in an oil bath at 80°C. Once this solution was homogeneous, 3 ml of an HCl/NMP solution (6 ml of 12.1N aqueous HCl in 24 ml NMP) were syringed into the polymer solution while stirring continously. The polymer typically precipitated immediately. The precipitate was then filtered and washed with water to remove the solvent and acid. The washed "particles" were then suspended in water either without a stabilizer or using an aqueous solution of LaRC TPI polyamic acid and ammonium hydroxide (800 ml water, 26.5 g polyamic acid, and 7.2 ml of

ammonium hydroxide) as a stabilizer. Once the particles were suspended, they were sonicated for 3 minutes at 75 watts to break up any aggregates. The particle size was measured by a centrifugal particle size analyzer as described in the characterization section below.

3.4.9 Stabilization of PEEK particles by Poly((pyridine ether) - co - (ether ether ketimine)): PEEK particles formed from the previously discussed procedure were suspended in NMP with 10 wt% (compared to PEEK) of the poly((pyridine ether) - co - (ether ether ketimine)) copolymer. The copolymer used contained a pyridine to ketimine ratio of 30/70. This suspension was stirred overnight, sonicated for 1 minute at 75 watts, then hydrolyzed as discussed previously. Following hydrolysis, the suspension was precipitated in water, washed exhaustively with deionized water in a blender (3 X 500 ml), and collected as a paste (Figure 3.1). The particles were then measured by the particle size analyzer as described below.

3.5 Characterization

3.5.1 Nuclear Magnetic Resonance (NMR) Spectroscopy: Proton NMR (^{1}H NMR) was utilized to determine reaction conversion, reactivity of monomers, as well as monomer purity. The ^{1}H NMR studies were performed on a Varian Unity NMR spectrometer operating at 400 MHz. Deuterated solvents such as d-6 DMSO and $CDCl_3$ were used with concentrations typically between 1 and 10% solids.

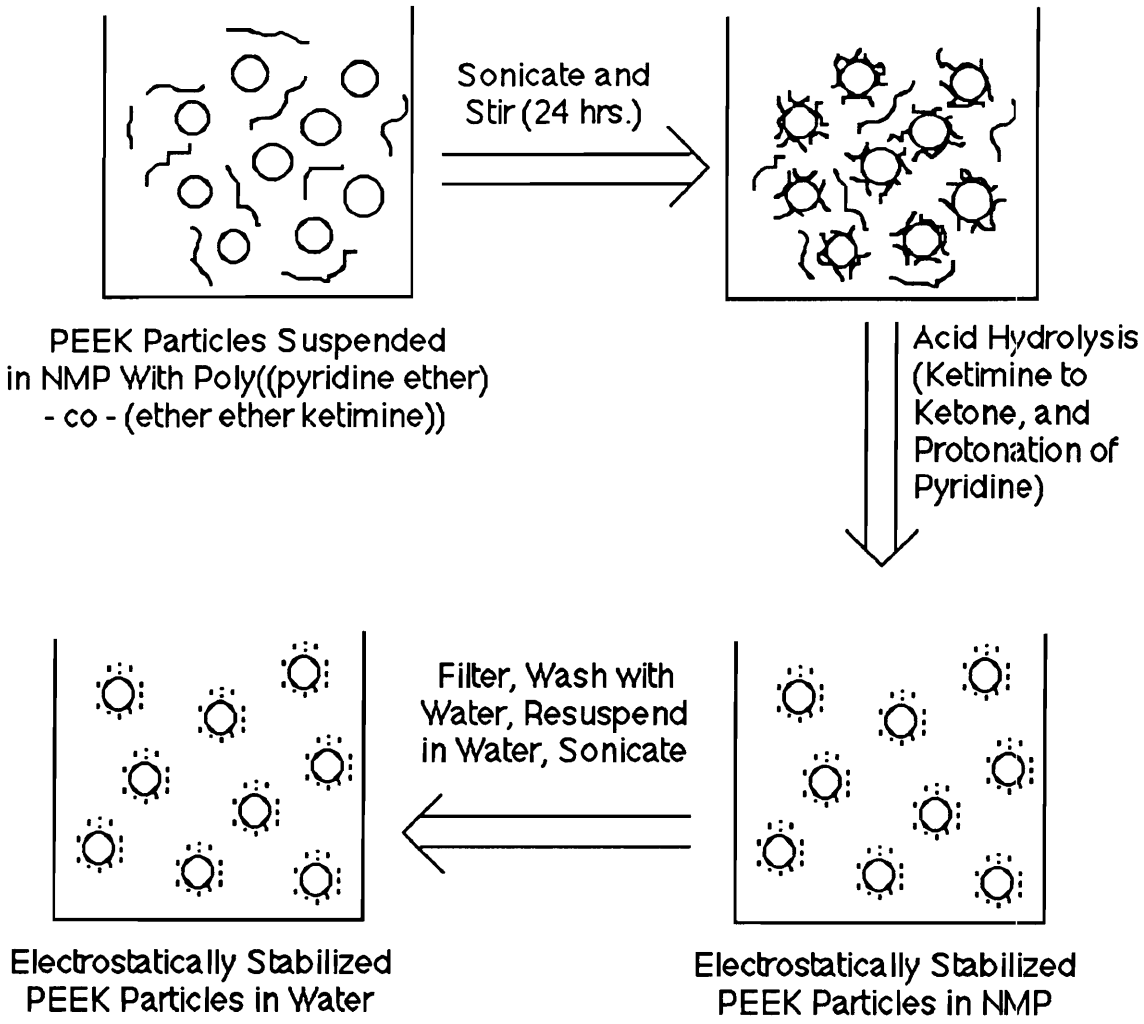

Figure 3.1: Experimental Procedure for the Elecrostatic Stabilization of PEEK Particles

3.5.2 Differential Scanning Calorimetry (DSC): DSC was utilized to determine the glass transition temperature and melting temperature of all polymers synthesized. By evaluating the glass transition temperatures, the miscibility of polymers was determined. DSC was conducted on a Perkin Elmer Series 7 thermal analyzer under a nitrogen purge at a heating rate of 10°C per min. unless otherwise specified.

3.5.3 Thermogravimetric Analysis (TGA): TGA was utilized to examine the thermal and thermo-oxidative stability, as well as solvent contamination of the polymers synthesized. TGA was perfomed on a Perkin-Elmer Series 7 thermal analyzer with an air purge at a heating rate of 10°C per minute. The weight loss of the sample was measured as a function of time and temperature. The temperature corresponding to 5% weight loss was recorded.

3.5.4 Gel Permeation Chromatography (GPC): GPC was performed on a Waters 150-C ALC/GPC chromatograph equipped with a refractive index detector and a Viscotek Model 100 differential viscometer. The mobile phase was NMP with a flow rate of 1 ml/min. at 60°C. The columns were Permagel with pore sizes of 500, 10^3, 10^4, and 10^5 Å. The injection volume was 200 µl with a sample concentration of 3 mg/ml. The Viscotek detector allowed for the determination of Mn and Mw using universal calibration techniques. In a few cases, GPC in chloroform at 30°C using an RI detector with ultrastyragel columns (10^3, 10^4, 10^5 Å), calibrated with polystryene standards was performed. This did not allow for universal calibration, but did give relative molecular weights as a function of reaction time.

3.5.5 Particle Size Analysis: The particle size (median diameter) and particle size distribution were measured by a centrifugal particle size analyzer (model SA-CP3) by Shimadzu. This instrument measures the turbidity of the sedimenting suspension and utilizes Stokes law to correlate the sedimentation rate to particle size. The solvent density and viscosity as well as the density of the particle are required in the calculations.[124] The suspension medium was water (ρ = 0.998 g/mL, η = 0.938 cP). Density of the particles was approximated by that of bulk poly(ether ether ketone) (1.3 g/mL). The particle size was also examined by utilizing scanning electron microscopy. The Shimadzu particle size analyzer was also used as a qualitative tool to examine colloid stability. If the particle size distribution of a specific sample was known, the analyzer could be used to determine if any aggregates were present, indicating a poor suspension.

3.5.6 Scanning Electron Microscopy (SEM): SEM was utilized to qualitatively examine the particle size and distribution of the submicron PEEK particles formed from PEEKt hydrolysis. The samples were placed on a copper strip as a dilute suspension, dried in a vacuum oven, and then gold coated with a high resolution coater. The gold coated sample was then examined using a Philips 420T scanning transmission electron microscope (STEM) with a secondary electron detector, operating at 60 kV in the SEM mode.

3.5.7 Environmental Scanning Electron Microscopy (ESEM): ESEM was utilized for neck growth measurements in samples that were sintered for

specified times and temperatures. It was also used to examine the morphology of these samples in correlation to the mechanical property improvement. An Electro Scan E-3 Environmental SEM operating at 5 torr (water vapor) and 20 kV was utilized for this study. The neck and particle radii were measured directly from the acquired photographs.

3.5.8 Dilatometry: Dilatometry was utilized to examine the sintering rate (densification) of PEEK particles as a function of particle size, temperature, and compact pressure. Green bodies were prepared by cold pressing PEEK particles in a cylindrical die (1.28 cm diameter) on a Carver laboratory press. Each sample contained 3.5 g of particles and was approximately 2.5 cm in length (Figure 3.2). The green bodies had sufficient strength to be handled without addition of a binder. The green bodies were sintered in an Orton 1600c automatic recording dilatometer at a heating rate of 0.5°C per min. and held for 300 min. at variable temperatures. The change in length as a function of temperature and time was recorded, as well as both the green and final densities.

3.5.9 Density Measurements: The densities of dilatometry samples were determined by measuring the diameter (which was constant throughout the length of the sample) and the length of the cylinder, calculating the volume and then dividing by the sample mass. An alternate method was simple water displacement divided by the sample mass. The two methods complimented each other in all cases. A third method for measuring density, utilized only for films, was the ASTM C373-88 procedure. This involved suspending the sample

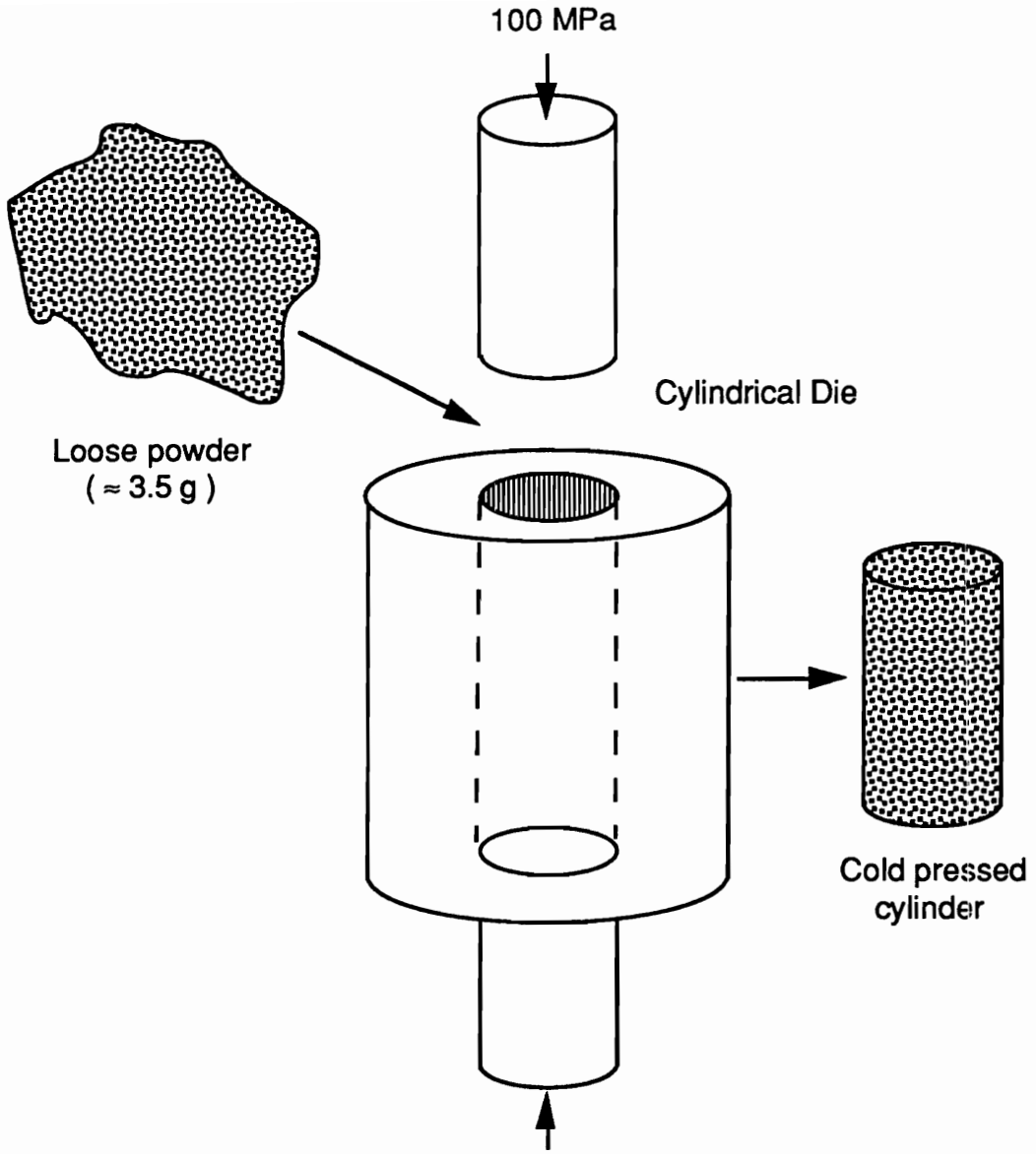

Figure 3.2: Experimental Procedure for the Sample Preparation in Dilatometry Studies

from a balance in air and in ethanol. The density of ethanol is known, and therefore the difference between the measured mass in air and ethanol can be used to determine the sample density.

3.5.10 Tensile Strength Measurements: Tensile strength was determined to evaluate the diffusion across the grain boundary of sintered samples. The data obtained was used to evaluate Wool's scaling laws as described in the literature review. Sample preparation included first cold pressing 0.4 g of PEEK particles in a 2.85 cm diameter die at 100 MPa in a Carver Laboratory press. The resultant disks (≈ 0.5 mm thick) were sintered in a forced air oven under nitrogen for the desired time and temperature. Once sintered, a die was used to prepare dogbone samples for testing on a Polymer Laboratories miniature tensile frame (minimat) with a strain rate of 5 mm/minute (Figure 3.3). The yield strength and percent strain at break were recorded and averaged over a minimum of 3 samples.

3.5.11 Wide Angle X-ray Scattering: WAXS analysis was utilized to compare relative degrees of crystallinity in several PEEK samples. WAXS measurements were made in transmission with a Siemens X-ray diffractometer using Cu K_α radiation (λ=1.54Å). Samples were scanned through 2θ values of 3° to 60° at 0.05° increments with a dwell time of 10 s.

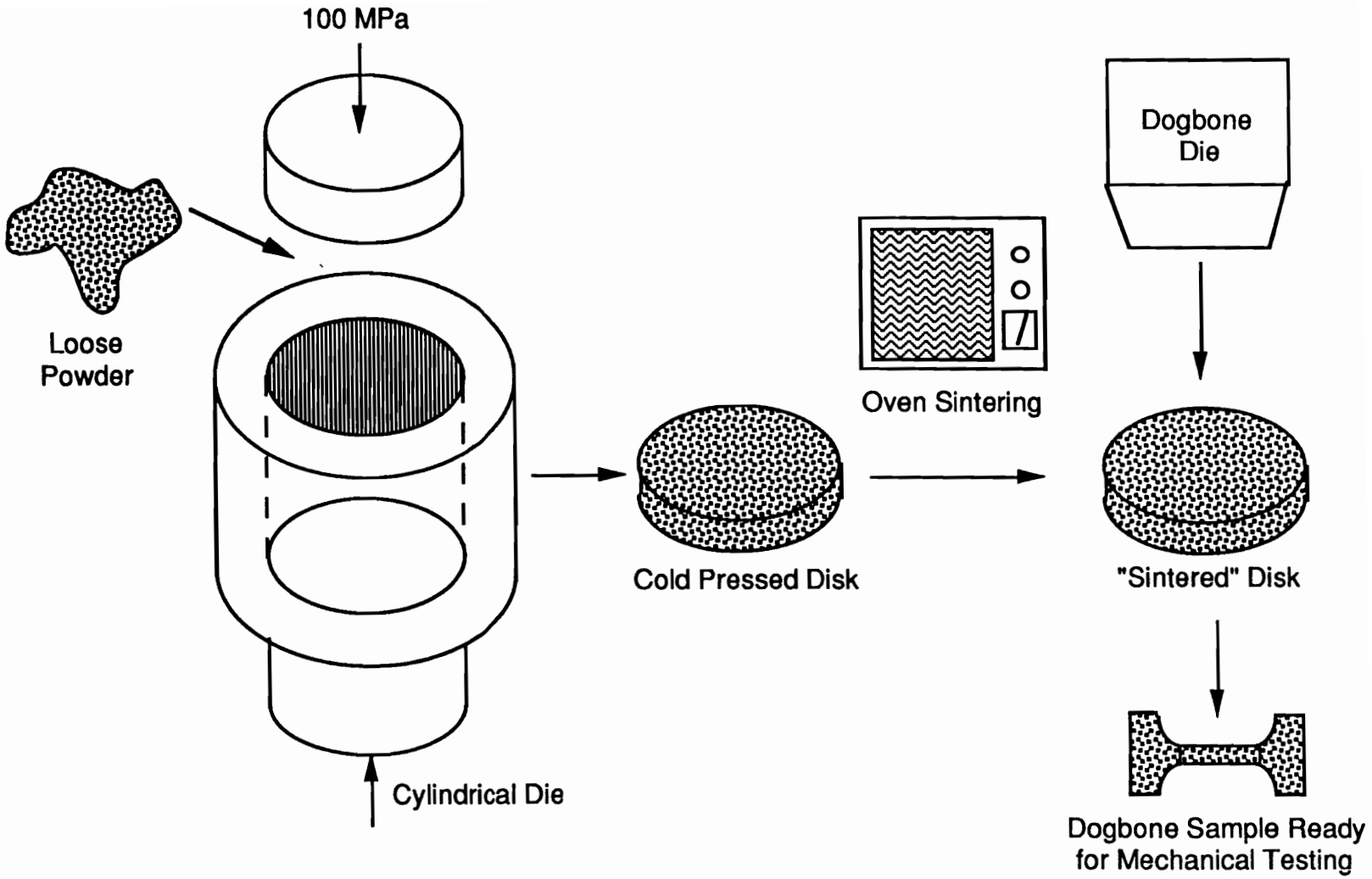

Figure 3.3: Experimental Procedure for the Measurement of Tensile Properties as a Function of Sintered Time, Temperature and Particle Size

3.5.12 Melt Viscosity Determination: Sample preparation included pressing 1 g of polymer powder in a 25 mm diameter steel mold in a oven at 360 °C for 5 minutes followed by a slow cool below the glass transition temperature. The melt viscosity was then determined as a function of frequency at 370°C between flat parallel plates (25 mm diameter) with a gap of 1.8 mm.in a Bohlin VOR Melt Viscometer equiped with a 2,000 g/cm high torque head and a high temperature cell.

3.5.13 Surface Free Energy Measurements: The surface free energy (γ) of PEEK was determined on a melt pressed PEEK film following the procedure described in Owens et al.[125] This involved measuring the contact angle of both water and methylene iodide on a clean PEEK film utilizing a Goniometer. Since the surface energy's of water and methylene iodide are known (Table 3.1), one can calculate that of the film (γ_s) (PEEK) by simultaneously solving equations (3.1) and (3.2) for both liquids.

$$1 + \cos\theta = 2\sqrt{\gamma_s^d}\left(\frac{\sqrt{\gamma_l^d}}{\gamma_{lv}}\right) + 2\sqrt{\gamma_s^h}\left(\frac{\sqrt{\gamma_l^h}}{\gamma_{lv}}\right) \qquad (3.1)$$

$$\gamma_s = \gamma_s^d + \gamma_s^h \qquad (3.2)$$

Table 3.1: Surface Energies for Water and Methylene Iodide

Liquid	γ_l^d (ergs/cm^2)	γ_l^h (ergs/cm^2)	γ_{lv} (ergs/cm^2)
H_2O	21.8	51.0	72.8
CH_2I_2	49.5	1.3	50.8

3.5.14 Pressure Casting: For the submicron PEEK particles, pressure casting was used to prepare the samples for sintering. A 5 wt. % suspension was formed using 5 wt. % stabilizer to particles. Three different stabilizers were used, Triton X - 100, poly((pyridine ether) - co - (ether ether ketimine)), and poly((pyridinium chloride ether) - co - (ether ether ketone)). The Triton X-100 and poly((pyridinium chloride ether) - co - (ether ether ketone)) stabilized suspensions were in water and the poly((pyridine ether) - co - (ether ether ketimine)) stabilized suspension was in toluene. The stable suspension was placed in a high pressure filter containing 0.2 μm teflon filter paper. Air pressure was applied to force the solvent through the filter paper leaving the particles behind in the form of a cake. This cake was dried under vacuum at room temperature for 12 hours, then ramped slowly up to 100°C over an 8 hour period. The sample was held at 100°C for 12 hours. Thermogravimetric analysis confirmed that the samples were thoroughly dried. This dried cake was used for sintering studies.

3.5.15 Meso-Indentation Testing: The method of cutting dogbones and measuring the mechanical properties worked very well, but only if the sample had enough mechanical integrity to withstand the procedure. Since it was desirable to determine relative mechanical properties, before the strength of the sample was well developed an alternate method, meso-indentation, was applied. This utilizies an instrument built by Mr. Jack Lesko in the Engineering Science and Mechanics department at Virginia Tech. This instruments measures the pressure (P) and displacement (h) of a 1/16 inch (D) rounded probe as it is pushed into a flat thin film sample. The sample must be mounted

on a thick (1/2 inch) material with similar properties to the sample being tested. In this case PMMA was used as this material. The instrument actually measures the Meyers Hardness Index (σ_{nl}) which can be described by

$$\sigma_{nl} = \frac{4P}{\pi d^2} \qquad (3.3)$$

where

$$d = \sqrt{2Dh} \qquad (3.4).$$

The Meyers Hardness index (σ_{nl}) can be conveted to an approximate yield stress by dividing by three. Also the percent compression strain ($\%\varepsilon$) can be calculated by

$$\%\varepsilon = \frac{\frac{d}{D}}{5} X100 \qquad (3.5).$$

Typically the same sample preparation utilized in uniaxial tensile measurements was also utilized for the meso-indent tests, with the exception that the dogbones did not have to be cut. The thin disk obtained after sintering could be directly fixed to a PMMA platform and tested. One such disk would be tested five times and an average of the values is reported.

Appendix 3.1: Computer Program (Carother's Equation): The molecular weight and end group control is a crucial factor in the synthesis of condensation polymers, as it affects both processability and thermal stability. The computer program, listed below, was written in Microsoft® Basic on a Macintosh Computer to determine the correct stoichiometry for molecular weight control in a step growth polymerization. The program determines the correct amount, in both moles and grams, of monomers needed for an inputed molecular weight

based on the Carother's equation. The other variables required for this program are the batch size (in grams), and the molecular weight of each monomer used including the monofunctional endcapping reagent if appropriate.

```
10 CLS
11 PRINT "This program will calculate the moles and grams"
12 PRINT "of monomers needed in a step polymerization, as"
13 PRINT "determined by the Carothers equation.  Any number of"
14 PRINT "monomers may be used, including a monofuctional endcapper."
15 PRINT "NOTE: the functionality of the endcapper is designated 'B'"
16 PRINT ""
17 PRINT ""
18  REM ************************************************
19 REM  This section is used to input molecular weights, etc.
20  REM ************************************************
21 INPUT "How many comonomers of functionality A will you be using?",
NMERA
25 INPUT "How many comonomers of functionality B will you be
using?",NMERB
30 INPUT "Will you be using an endcapper (functionality B) ?",ECB$
35 PRINT ""
40 IF ECB$ = "y" GOTO 46
41 IF ECB$ = "n" GOTO 60
45 GOTO 30
46 INPUT "Enter the mol. weight of endcapper",MWEC
60 FOR Z = 1 TO NMERA
65 PRINT "Enter the mol. wt. of monomer (functionality A) ";Z: INPUT MERA(Z)
67 IF NMERA = 1 THEN COMPA(Z) = 1: IF NMERA = 1 GOTO 80
76 PRINT "Enter the mol fraction of functionalilty A desired for monomer ";Z:
INPUT COMPA(Z)
80 NEXT Z
```

```
90 Z = 1
100 FOR Z = 1 TO NMERB
110 PRINT "Enter the mol. wt. of monomer (functionality B) ";Z
115 INPUT MERB(Z)
116 IF NMERB = 1 THEN COMPB(Z) = 1: IF NMERB = 1 GOTO 130
121 PRINT "Enter the mol fraction of functionality B desired for monomer ";Z
122 INPUT COMPB(Z)
130 NEXT Z
140 INPUT "What is your desired molecular weight?", MW
150 INPUT "What is your desired sample size in grams?",SAM
160  REM ****************************************
170 REM This next section calculates the average molecular weight
180 REM of the repeat unit.
190  REM ****************************************
200 Z = 1: RPTA = 0: RPTB = 0
210 FOR Z = 1 TO NMERA
220 RPTA = COMPA(Z)*MERA(Z) + RPTA
230 NEXT Z
240 Z=1
250 FOR Z = 1 TO NMERB
260 RPTB = COMPB(Z)*MERB(Z) + RPTB
270 NEXT Z
271  REM ************************************
272 REM This section will calculate R, and everything else
273  REM ************************************
280 RPT = (RPTA + RPTB)
290 DP = MW/RPT
300 XN = 2*DP
310 R = (XN-1)/(XN+1)
320 NA = .1
325 IF ECB$ = "n" GOTO 1000
330 NB = R/10
340 NBB = (NA/R) - NB
360 Z= 1
```

```
370 FOR Z = 1 TO NMERA
380 MA(Z) = COMPA(Z)*NA
390 GA(Z) = MA(Z)*MERA(Z)
400 NEXT Z
410 Z = 1
420 FOR Z = 1 TO NMERB
430 MB(Z) = COMPB(Z)*NB
440 GB(Z) = MB(Z)*MERB(Z)
450 NEXT Z
460 GEC = NBB*MWEC
470 Z = 1: GTOT = 0
480 FOR Z = 1 TO NMERA
490 GTOT = GA(Z) + GTOT
500 NEXT Z
510 Z = 1
520 FOR Z = 1 TO NMERB
530 GTOT = GB(Z) + GTOT
540 NEXT Z
550 GTOT = GEC + GTOT
560 D = SAM/GTOT
570 Z = 1
580 FOR Z = 1 TO NMERA
590 MA(Z) = MA(Z) * D
600 GA(Z) = MA(Z)*MERA(Z)
700 NEXT Z
710 Z = 1
720 FOR Z = 1 TO NMERB
730 MB(Z) = MB(Z)*D
740 GB(Z) = MB(Z)*MERB(Z)
750 NEXT Z
760 NBB = NBB*D
770 GEC = NBB*MWEC
780 Z = 1
781  CLS
```

```
785 PRINT "FOR FUNCTIONALITY A"
790 FOR Z = 1 TO NMERA
800 PRINT "The number of grams of monomer ";Z;"is ";GA(Z)
810 PRINT "The number of moles of monomer ";Z;"is ";MA(Z)
820 NEXT Z
830 Z = 1
832 PRINT ""
833 PRINT ""
840 PRINT "FOR FUNCTIONALITY B"
850 FOR Z = 1 TO NMERB
860 PRINT "The number of grams of monomer ";Z;"is ";GB(Z)
870 PRINT "The number of moles of monomer ";Z;"is ";MB(Z)
880 NEXT Z
881 PRINT ""
882 PRINT ""
890 PRINT "The number of grams of endcapper is ";GEC
900 PRINT "The number of moles of endcapper is ";NBB
901 PRINT ""
902 PRINT ""
910 PRINT "The ratio r is ";R
920 PRINT "The value Xn is ";XN
925 PRINT "The value Dp is ";DP
926 PRINT ""
930 INPUT "Would you like to calculate another ?",X$
940 IF X$ = "y" GOTO 10
950 IF X$ = "n" THEN END
960 GOTO 930
1000  REM ****************************************
1010 REM This is for calculations with no endcapper
1020  REM ****************************************
1030 NB = NA/R
1040 Z = 1:GTOT = 0
1050 FOR Z = 1 TO NMERA
1060 MA(Z) = COMPA(Z)*NA
```

```
1070 GA(Z) = MA(Z)*MERA(Z)
1075 GTOT = GA(Z) + GTOT
1080 NEXT Z
1090 Z = 1
1100 FOR Z = 1 TO NMERB
1110 MB(Z) = COMPB(Z)*NB
1120 GB(Z) = MB(Z)*MERB(Z)
1125 GTOT = GB(Z) + GTOT
1130 NEXT Z
1140 D = SAM/GTOT
1150 Z = 1
1160 FOR Z = 1 TO NMERA
1170 MA(Z) = MA(Z)*D
1180 GA(Z) = MA(Z)*MERA(Z)
1190 NEXT Z
1200 Z = 1
1210 FOR Z = 1 TO NMERB
1220 MB(Z) = MB(Z)*D
1230 GB(Z) = MB(Z)*MERB(Z)
1240 NEXT Z
1250  CLS
1260 Z = 1
1270 PRINT "FOR FUNCTIONALITY A"
1280 PRINT ""
1290 FOR Z = 1 TO NMERA
1300 PRINT "The number of moles for monomer ";Z;"is ";MA(Z)
1310 PRINT "The number of grams for monomer ";Z;"is ";GA(Z)
1320 PRINT ""
1330 NEXT Z
1340 Z = 1
1345 PRINT "FOR FUNCTIONALITY B"
1350 FOR Z = 1 TO NMERB
1360 PRINT "The number of moles for monomer ";Z;"is ";MB(Z)
1370 PRINT "The number of grams for monomer ";Z;"is ";GB(Z)
```

```
1380 PRINT ""
1390 NEXT Z
1400 PRINT "The ratio r is ";R
1410 PRINT "The value Xn is ";XN
1420 PRINT "The value Dp is ";DP
1425 PRINT ""
1427 PRINT ""
1430 INPUT "Would you like to calculate another (y/n) ?", X$
1440 IF X$ = "y" GOTO 10
1450 IF X$ = "n" THEN END
1460 GOTO 1430
```

Chapter 4 - Results and Discussion

4.1 Introduction:

The research presented in this dissertation was conducted with three major goals. The first was to prepare high performance semicrystalline submicron powders for use in composite processing and to develop the science base needed for control of particle size. The composite processing methodology addressed here, aqueous suspension prepregging, requires these particles be in the form of a stable suspension. Thus, the second goal was to develop a correspondingly high performance suspension stabilizer for these particles. The third aspect of this research was to examine potential processing advantages of submicron polymeric powders. The hypothesis was that the submicron particles, having a very large surface to volume ratio, could be processed in a similar manner to ceramic powders by sintering. This process should have the advantages of lower processing temperatures and shorter consolidation times. The Results and Discussion presented here will address these three major topics. First the synthesis of a high performance semicrystalline polymer, poly(ether ether ketone), in the form of submicron particles will be discussed. Secondly, the development of a high performance electrostatic stabilizer based on pyridine will be explained. Finally the studies examining the feasibility of sintering these poly(ether ether ketone) particles will be discussed.

4.2 Synthesis of Poly(ether ether ketone) Particles:

4.2.1 Introduction:

Current technology for the production of graphite composites typically involves either solution or melt prepregging. High performance amorphous thermoplastic polymers are soluble only in dipolar aprotic solvents such as 1-methyl-2-pyrrolidinone (NMP), which makes large-scale solution prepregging impractical. Melt prepregging these types of materials is also impractical, due to both their high thermal transitions (causing degradation at melt temperatures), as well as their high viscosities. Aqueous dispersion prepregging[74,75], a relatively new method, could potentially circumvent many of the environmental and processing problems as mentioned above. However, aqueous dispersion prepregging requires that the high performance polymer be in the form of a stable colloidal dispersion, preferably of small uniform particles. This section will examine the formation of submicron particles from the high performance thermoplastic polymer, poly(ether ether ketone) (PEEK), for use in aqueous dispersion prepregging. The procedure first involves the synthesis of the monomer 4,4'-difluoro (N-benzohydroxylidene aniline) (Figure 4.1). This monomer and hydroquinone are then polymerized to form the amorphous PEEK derivative poly(ether ether ketimine) (Figure 4.2)[38]. 4,4'-difluoro (N-benzohydroxylidene aniline) can also be copolymerized with 4,4'-difluorobenzophenone and hydroquinone to form a semicrystalline, but soluble, PEEK derivative (Figure 4.3). The subsequent hydrolysis of these derivatives to semicrystalline PEEK under controlled conditions results in the formation of submicron particles. In fact these particles are so small that their surface to

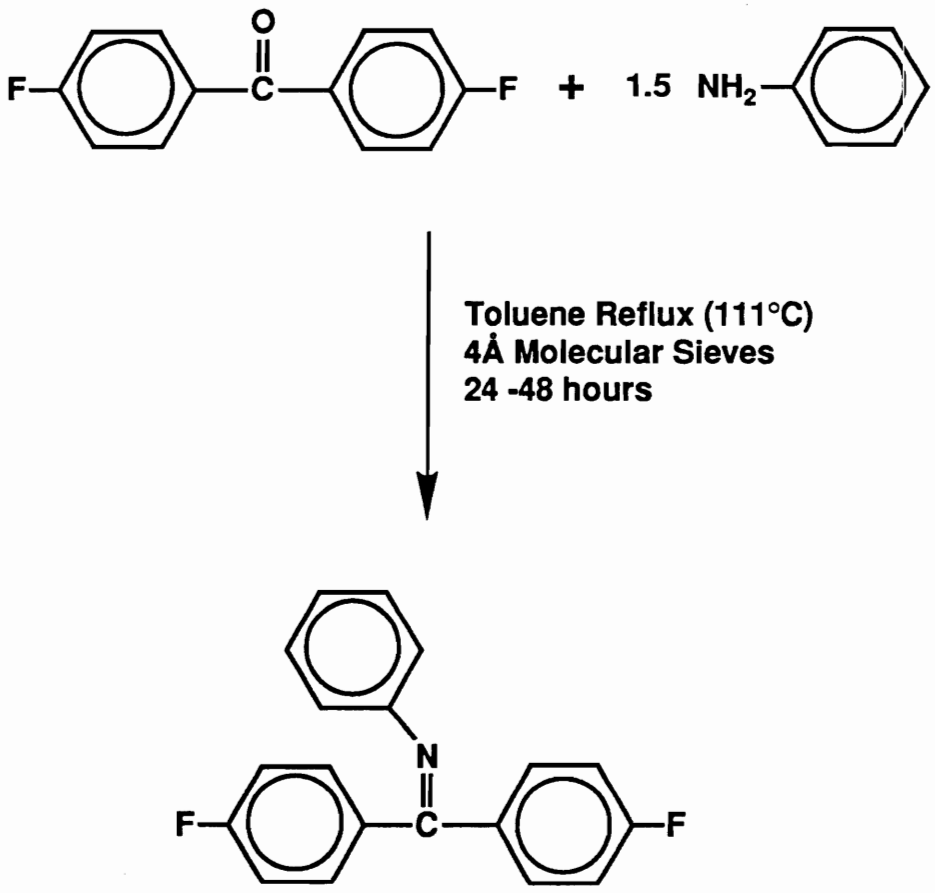

Figure 4.1: Synthesis of 4,4'-difluoro (N-benzohydroxylidene aniline)

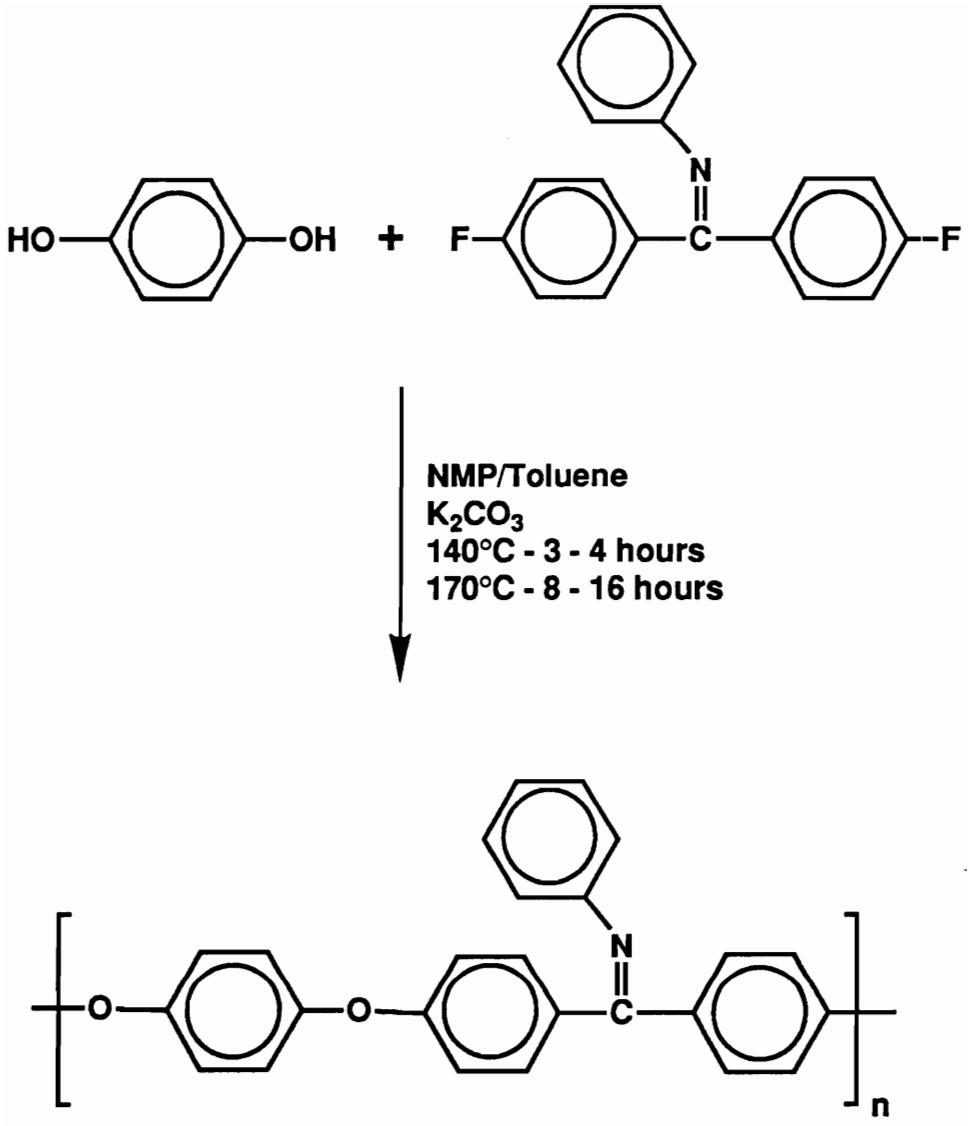

Figure 4.2: Synthesis of Poly(ether ether ketimine) (PEEKt)

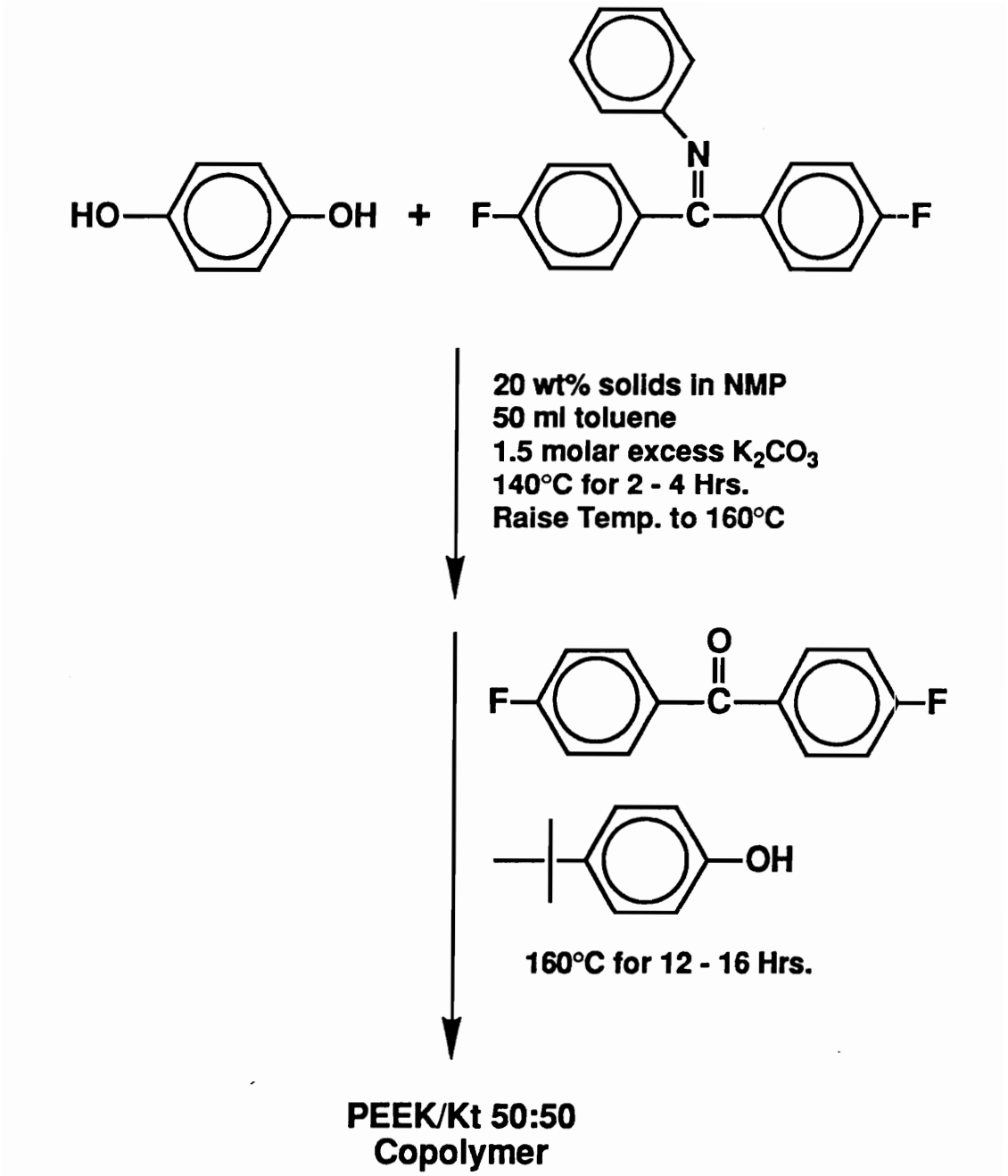

Figure 4.3: Synthesis of Poly((ether ether ketimine) - co - (ether ether ketone))

volume ratio is extremely large. Not only does this make them suitable for aqueous dispersion prepregging it should provide to these particles some unique properties which will be taken advantage of in a processing procedure known as sintering. This process, in the ceramics industry, allows for consolidation of small, well-packed particles at lower temperatures and shorter time cycles relative to more conventional processing methods.

4.2.2 Synthesis of 4,4'-difluoro (N-benzohydroxylidene aniline):

Synthesis of the monomer, 4,4'-difluoro (N-benzohydroxylidene aniline) (Figure 4.1), has been well established.[38,40,41] This synthesis involves the condensation of 4,4'-difluorobenzophenone, the commercial monomer for PEEK, and aniline to form the Schiff base, or ketimine, as discussed in the Experimental Section. Conversion can readily be monitored by ^{1}H NMR. The % conversion can be determined by following the disappearance of the signal at 7.8 ppm due to the four protons ortho to the ketone on 4,4'-difluorobenzophenone, as well as the appearance of the two protons ortho, and trans to the imine bond (7.7 ppm) in d-6 DMSO. An example of the ^{1}H NMR showing almost 100% conversion to the ketimine is displayed in Figure 4.4. Besides % conversion, a few other remarks concerning this ^{1}H NMR should be noted. In 4,4'-difluorobenzophenone, all 4 protons ortho to the ketone are identical because this monomer is symmetrical. However, the ketimine monomer is not symmetrical and therefore the corresponding four ortho protons no longer occur at the same place in the NMR spectrum. The two protons ortho and trans to the imine occur where one would expect, just slightly up-field from those on the ketone at 7.7 ppm. The chemical shift of these ortho protons can

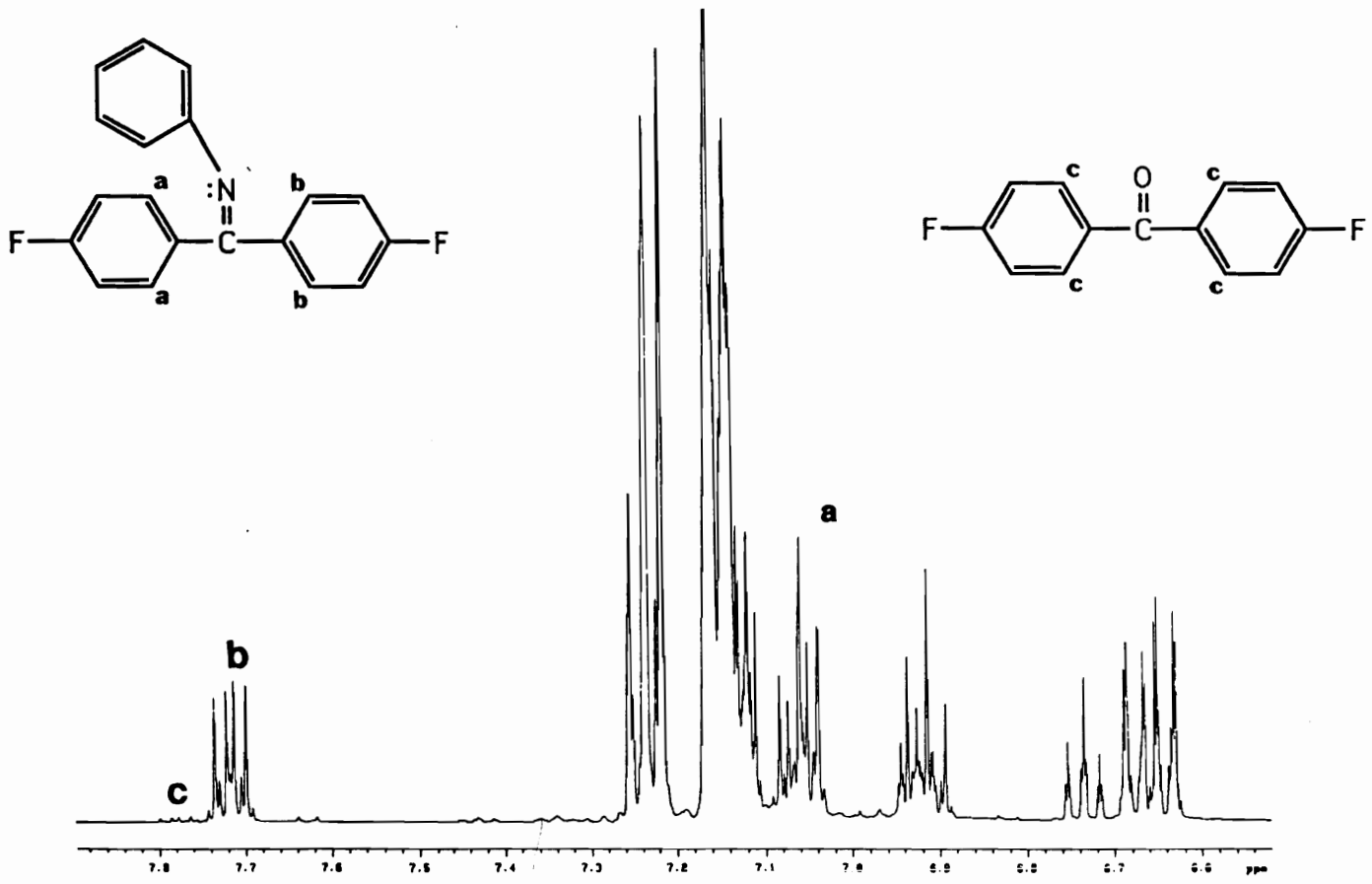

Figure 4.4: ^{1}H NMR of 4,4'-Difluoro (N-benzohydroxylidene aniline) (Ketimine) Synthesis

be used to determine reactivity for nucleophilic aromatic substitution. The further downfield the chemical shift, the more reactive the monomer is. Thus, the ketimine monomer is less reactive than the corresponding ketone.[126,127] The two protons ortho and cis to the imine occur at 6.95 ppm. This indicates that this 'side' of the ketimine monomer should be unreactive towards nucleophilic aromatic substitution. This is because the hindered geometry of the ketimine monomer prohibits both fluorine containing aromatic rings from being in the same plane as the ketimine double bond. Therefore the ring cis to the imine is not coplanar and does not completely feel the electron withdrawing nature of the carbon nitrogen double bond. The determination of which protons were cis to the aniline ring (either δ = 7.7 or 6.95) was determined using molecular modeling and NMR techniques as described below.

The "propeller" like structure of the ketimine monomer from PC Model® is shown in Figure 4.5, which shows that the aromatic ring cis to the former aniline ring is not coplanar with the imine double bond. PC-Model gives only a possible minimum energy confirmation. To confirm the modeling results, a combination of NMR techniques were used. Two dimensional ^{1}H NMR was used to identify all of the chemical shifts on the ketimine monomer (Figure 4.6). However it was still not possible to distinguish which of the protons (E or F) occurred cis to the aniline ring. NOE ^{1}H NMR examines "through-space" interactions of protons. In order for these interactions to occur the protons must be extremely close. By exciting a particular proton, NOE shows which of the other protons are nearby by the sign (positive or negative) of the individual shifts. A positive sign indicates the proton is close enough to the excited proton

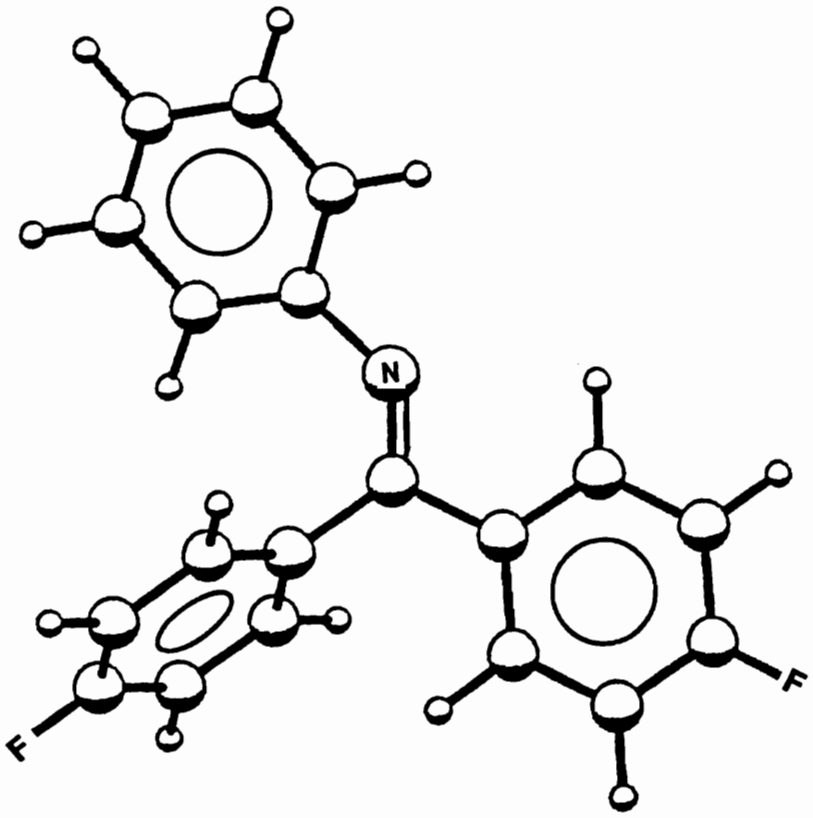

Figure 4.5: 3-D Configuration of 4,4'-Difluoro (N-benzohydroxylidene aniline) (Ketimine) (PC Model®)

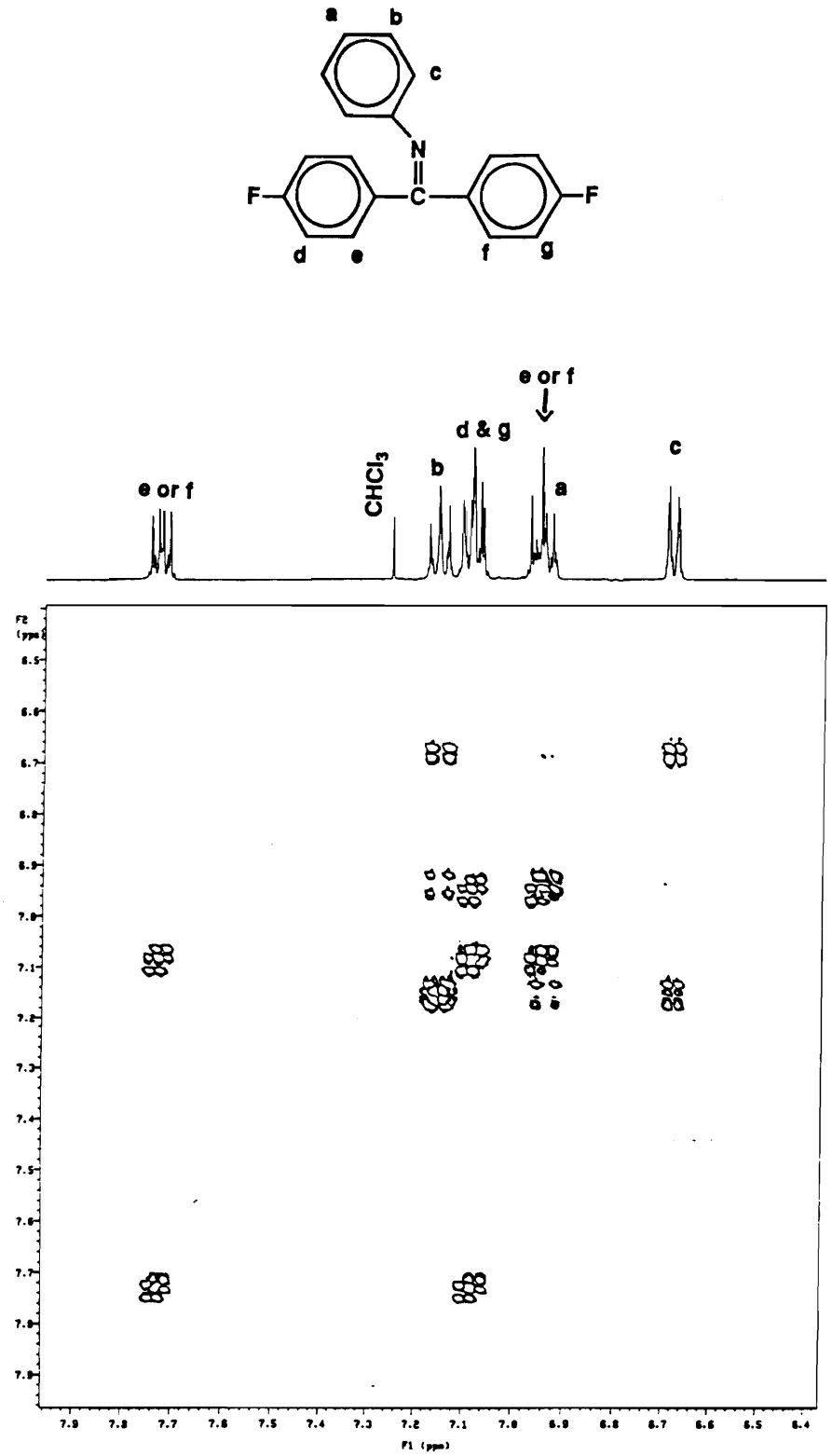

Figure 4.6: Two Dimensional ^{1}H NMR of 4,4'-Difluoro (N-benzohydroxylidene aniline) (Ketimine)

to feel the effect of the NOE, and a negative sign indicates that they are not close enough. The NOE experiment conducted here (Figure 4.7) excited the protons with δ = 6.95 ppm, which consequently show a very intense negative signal. Figure 4.7 shows that the excited protons are coupled with those at 7.7 ppm and 6.7 ppm, as both display positive signals. The chemical shift of 6.7 ppm is known to belong to the ortho protons from the former aniline ring, and the only way these could be close enough to the excited protons is if they were the cis, ortho protons, as the trans ortho protons would be too far away. Figure 4.7 also shows the protons at 7.18 ppm having a positive signal. This is because the excited signal (6.95 ppm) is actually a combination of protons ortho to the imine and para on the former aniline ring. Since the protons meta on the aniline (7.18 ppm) are close enough to the para they also have a low intensity positive signal. The final chemical shift labeling for the ketimine monomer is shown for clarity in Figure 4.8. However, it must be remembered that these studies were performed at 23°C. When variable temperature NMR was used, it was shown that the imine double bond starts to rotate at $\approx$ 100°C in d-6 DMSO (Figure 4.9), which makes the monomer essentially symmetrical and thus providing a difunctional monomer for nucleophilic aromatic substitution. The reaction temperatures for this polymerization are typically 160°C which is well above that required for rotation to occur. Figure 4.10 shows the NMR at 160°C and it can be seen that the two sets of ortho protons have completely merged.

4.2.3 Synthesis of Poly(ether ether ketimine):

The homopolymerization of 4,4'-difluoro (N-benzohydroxylidene aniline) and hydroquinone to form poly(ether ether ketimine) (PEEKt) is well

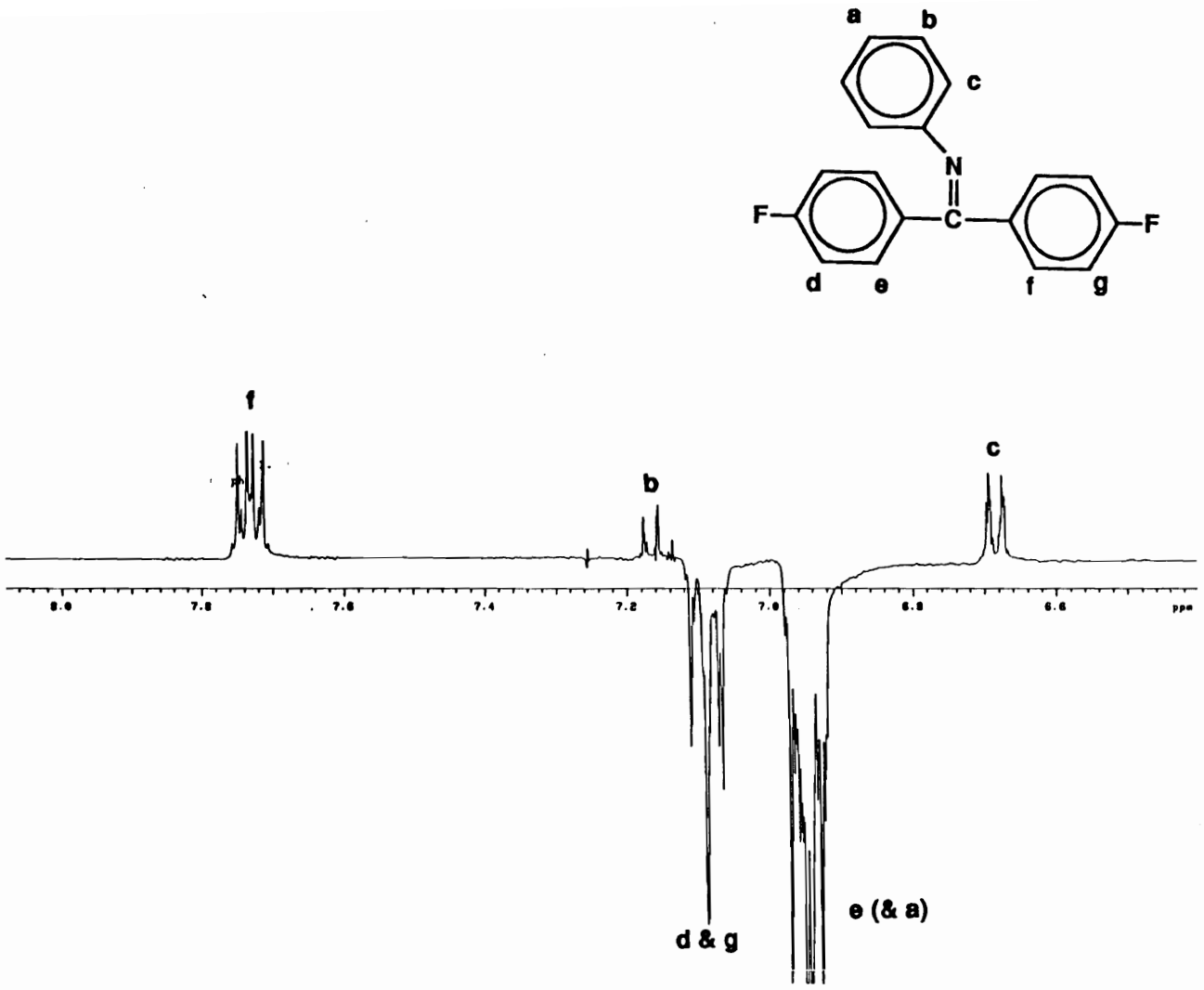

Figure 4.7: NOE NMR of 4,4'-Difluoro (N-benzohydroxylidene aniline) (Ketimine)

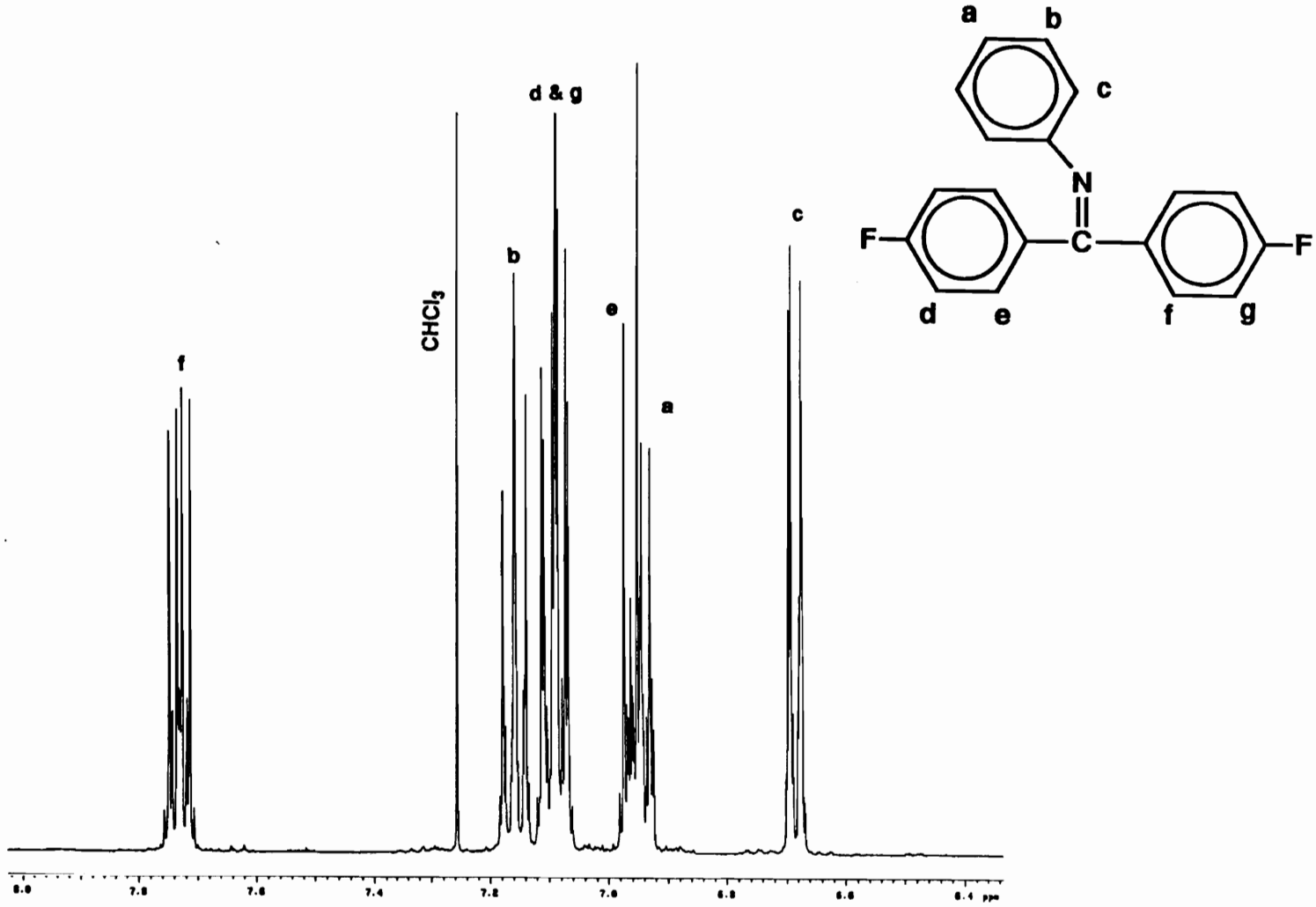

Figure 4.8: ^{1}H NMR of 4,4'-Difluoro (N-benzohydroxylidene aniline) (Ketimine) With all Peaks Labled

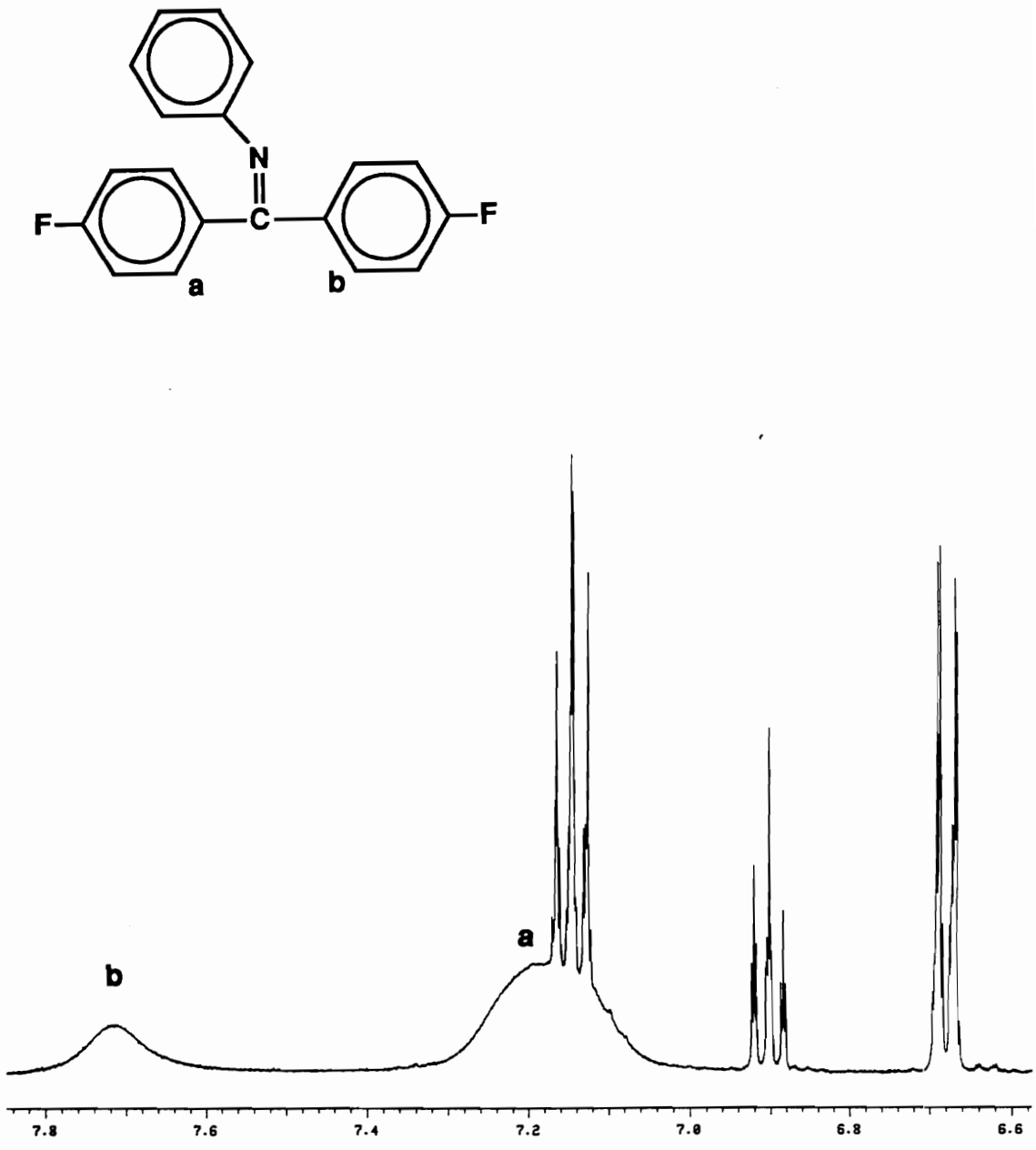

Figure 4.9: ^{1}H NMR of 4,4'-Difluoro (N-benzohydroxylidene aniline) (Ketimine) at 100°C in d-6 DMSO

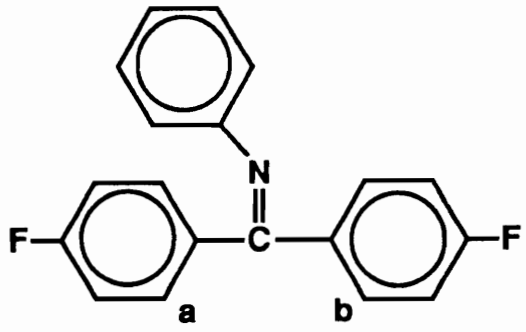

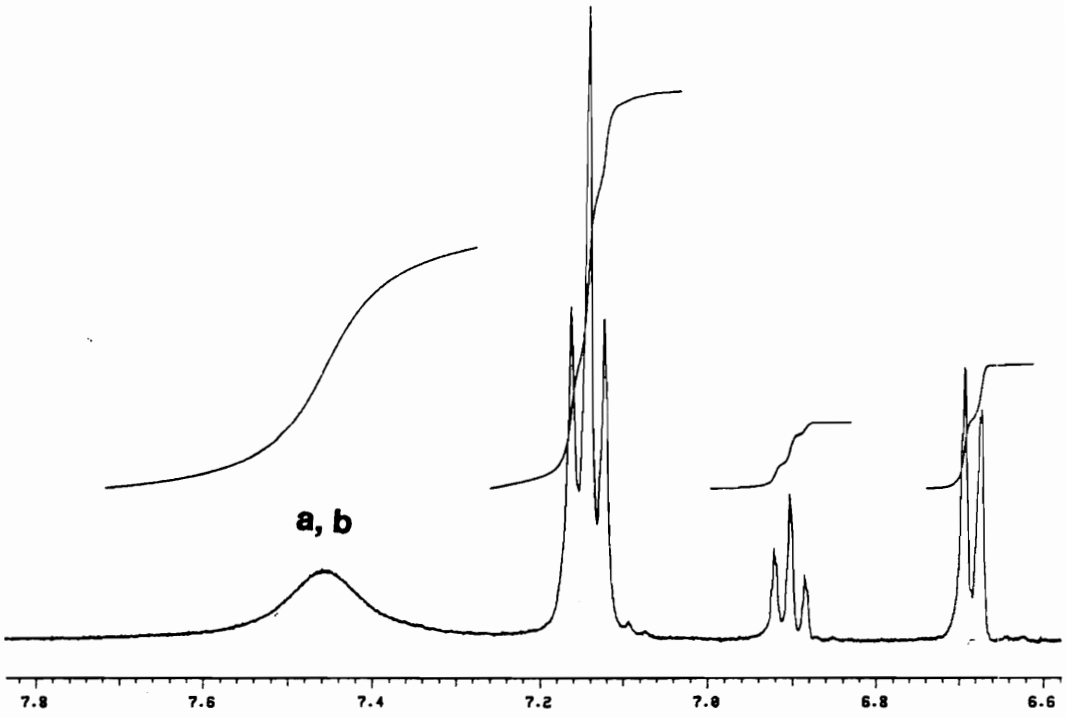

Figure 4.10: ^{1}H NMR of 4,4'-Difluoro (N-benzohydroxylidene aniline) (Ketimine) at 160°C in d-6 DMSO

established[38,40,41]. These monomers form an amorphous polymer with a Tg of 164°C, as determined by DSC.[40] This amorphous polymer is readily soluble in a wide variety of common organic solvents such as THF, toluene, NMP, DMAc, and chloroform. This makes characterization relatively straightforward, and is indeed the original driving force behind it's development as discussed in the Literature Review. The ^1H NMR of PEEKt in $CDCl_3$ is shown in Figure 4.11.

4.2.4 Synthesis of Poly((ether ether ketimine) - co - (ether ether ketone)):

Copolymerization of 4,4'-difluoro- (N-benzohydroxylidene aniline) and 4,4'-difluorobenzophenone (50:50 mole %) with hydroquinone was attempted using the same procedure as for the homopolymer, which involved adding all three of the monomers in the beginning of the polymerization. However, this procedure failed because the polymer precipitated out of solution during reaction. This was believed to be caused by the extremely short lamellar thickness of PEEK (only two repeat units, or 30 Å) required for crystallization (Figure 4.12),[3,128,129] resulting in the oligomer crystallizing out of solution. This problem is enhanced since the 4,4'-difluorobenzophenone is the more reactive monomer and therefore the PEEK oligomers form first. This was avoided by introducing only the ketimine monomer and hydroquinone into the reaction vessel at first, and not adding the ketone monomer until a temperature of 160°C had been reached (Figure 4.3). This alteration in procedure allowed for 'pre-reaction' of the ketimine to prevent initial formation of the PEEK oligomers. Also, since a higher reaction temperature was reached before the ketone monomer was introduced, the oligomers that did form did not crystallize during reaction. This resulted in the polymer remaining in solution until

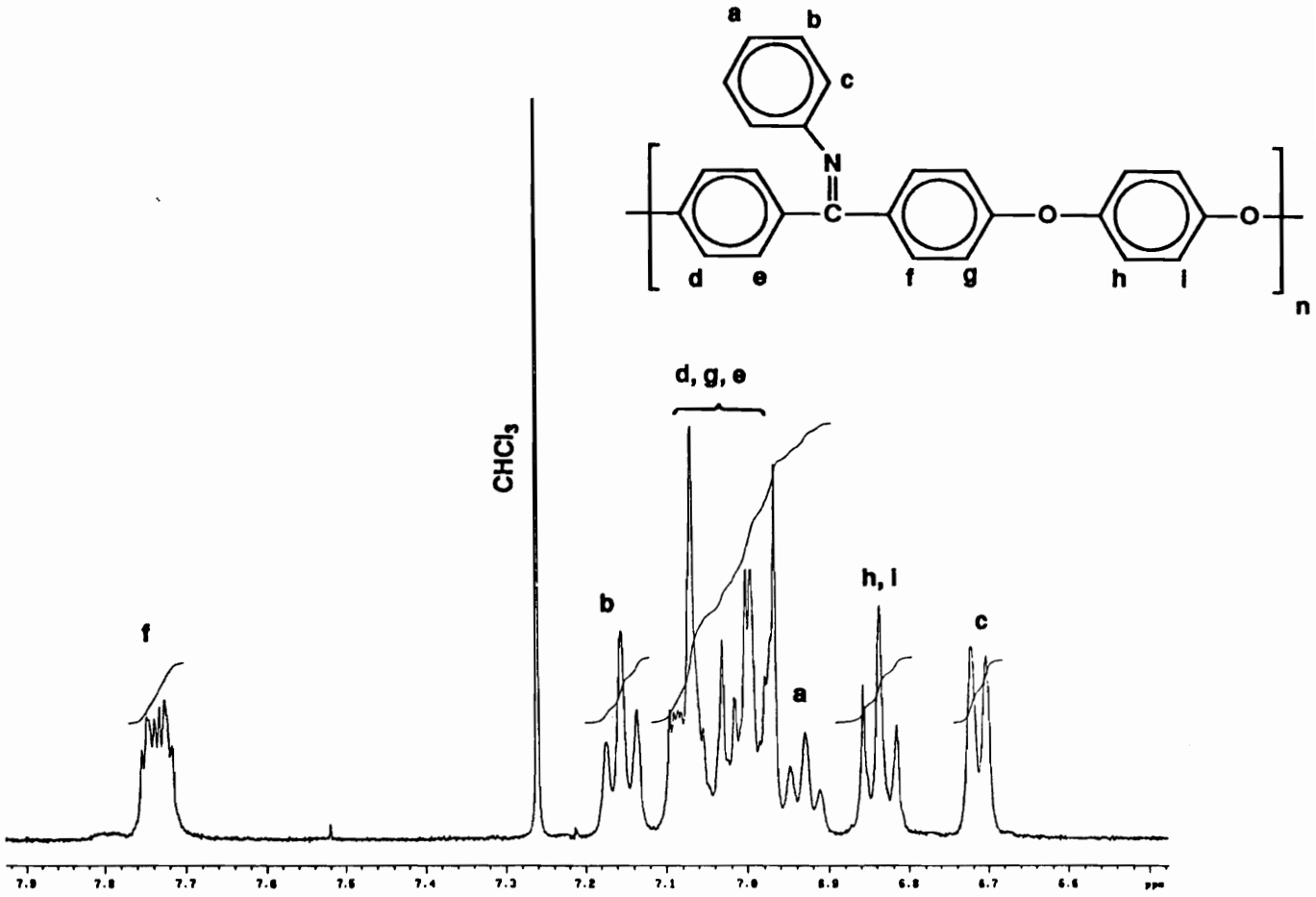

Figure 4.11: ^{1}H NMR of Poly(ether ether ketimine) (PEEKt)

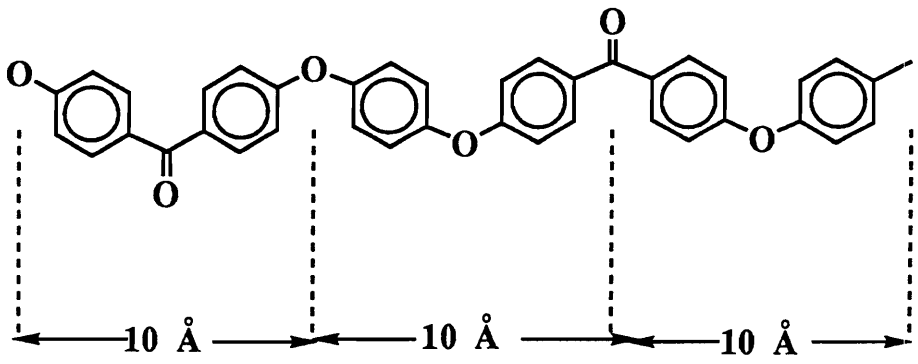

Figure 4.12: The Short Lamellar Thickness of PEEK Required for Crystallization (two repeat units, or 30 Å)[3]

polymerization was complete, and therefore high molecular weight was achieved. The molecular weight was controlled to 20,000 g/mole by using a monofunctional endcapping agent, t-butylphenol, and gel permeation chromatography with a viscosity detector showed an Mn = 20,200 g/mole (Figure 4.13). The 50:50 copolymer (Figure 4.14) was semicrystalline with a Tg = 162°C and a Tm= 228°C (Figure 4.15). This alteration in synthetic method also allowed for the preparation of a 70:30 mole ratio ketone/ketimine copolymer (Table 4.1). However the 70:30 copolymer was insoluble, even at 200°C in NMP, and therefore will not be discussed further.

Table 4.1: DSC Data for Copolymers as a Function of Amount of Ketone

Ketone (%)	Tg (°C)	Tm (°C)
100 (PEEK)	144	335
70	154	302
50	162	228
0 (PEEKt)	164	None

4.2.5 Hydrolysis to Poly(ether ether ketone)

Once the ketimine homopolymer and copolymers were characterized, it was of interest to examine their hydrolysis back to PEEK. This hydrolysis procedure involves first dissolving the derivatized polymer in NMP and then adding known amounts of water and acid. The acid (HCl) first protonates the nitrogen on the imine, allowing for nucleophilic attack of the water on the imine carbon. This is followed by a series of proton transfers providing the ketone (or PEEK) and aniline hydrochloride as a side product (Figure 4.16). As this reaction proceeds the ketimine is converted to the ketone (PEEK) and the

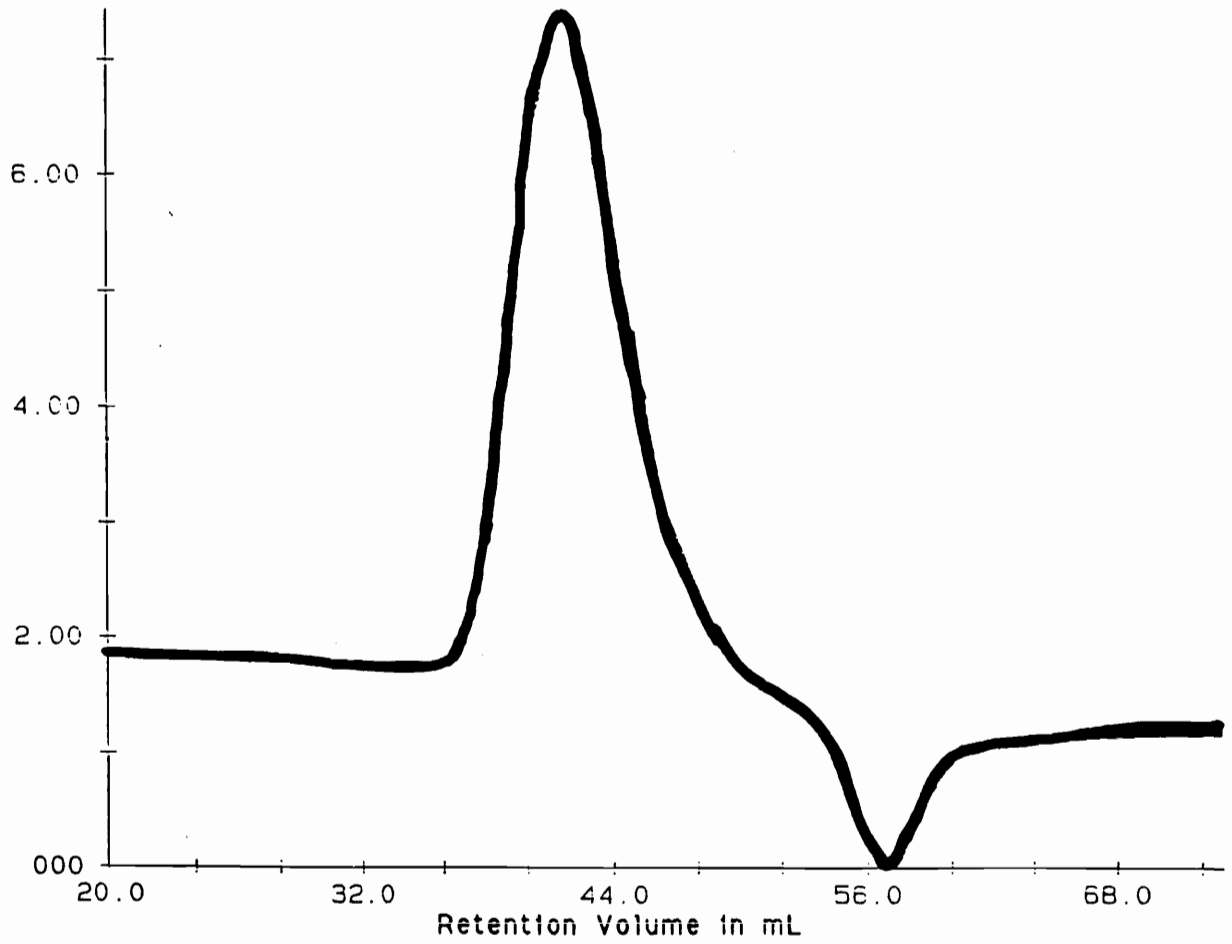

Figure 4.13: Gel Permeation Chromatography of Poly((ether ether ketimne) - co - (ether ether ketone)) (50/50 Copolymer): Solvent = NMP, Flow Rate of 1ml/min. with Universal Calibration

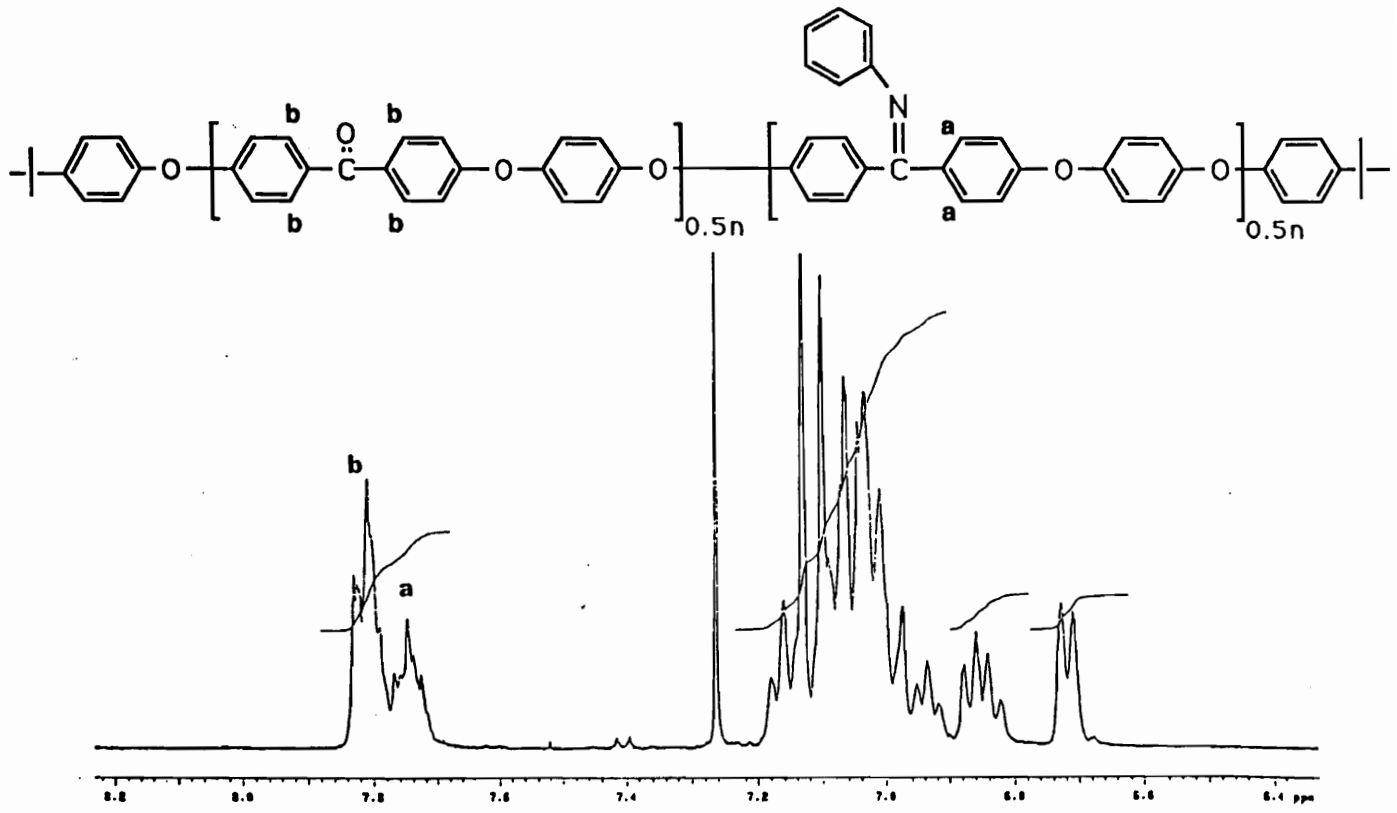

Figure 4.14: ^{1}H NMR of Poly((ether ether ketimine) - co - (ether ether ketone)) (50/50 Copolymer)

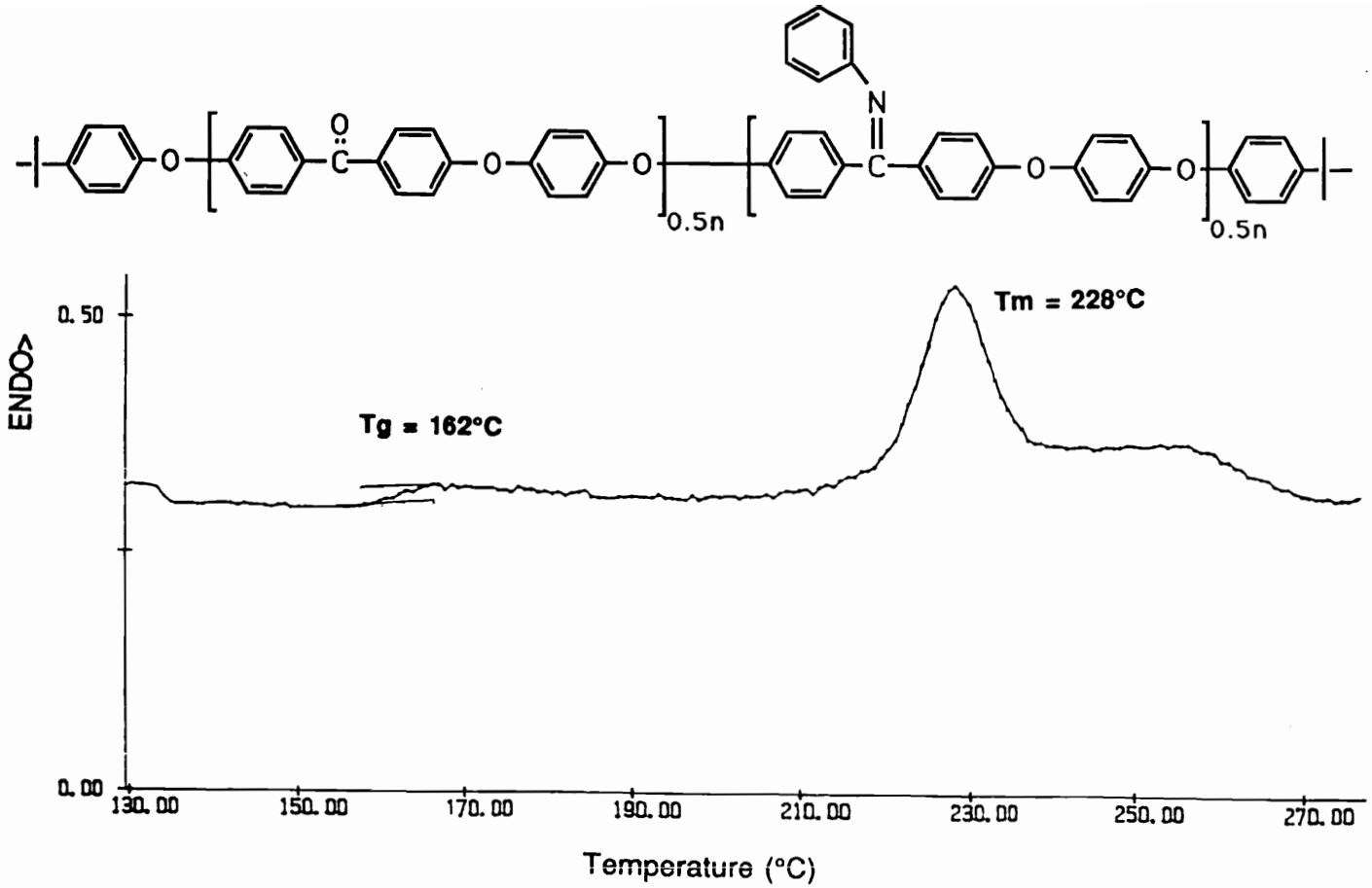

Figure 4.15: Differential Scanning Calorimetry of Poly((ether ether ketimine) - co - (ether ether ketone)) (50/50 Copolymer): Heating Rate of 10°C per minute

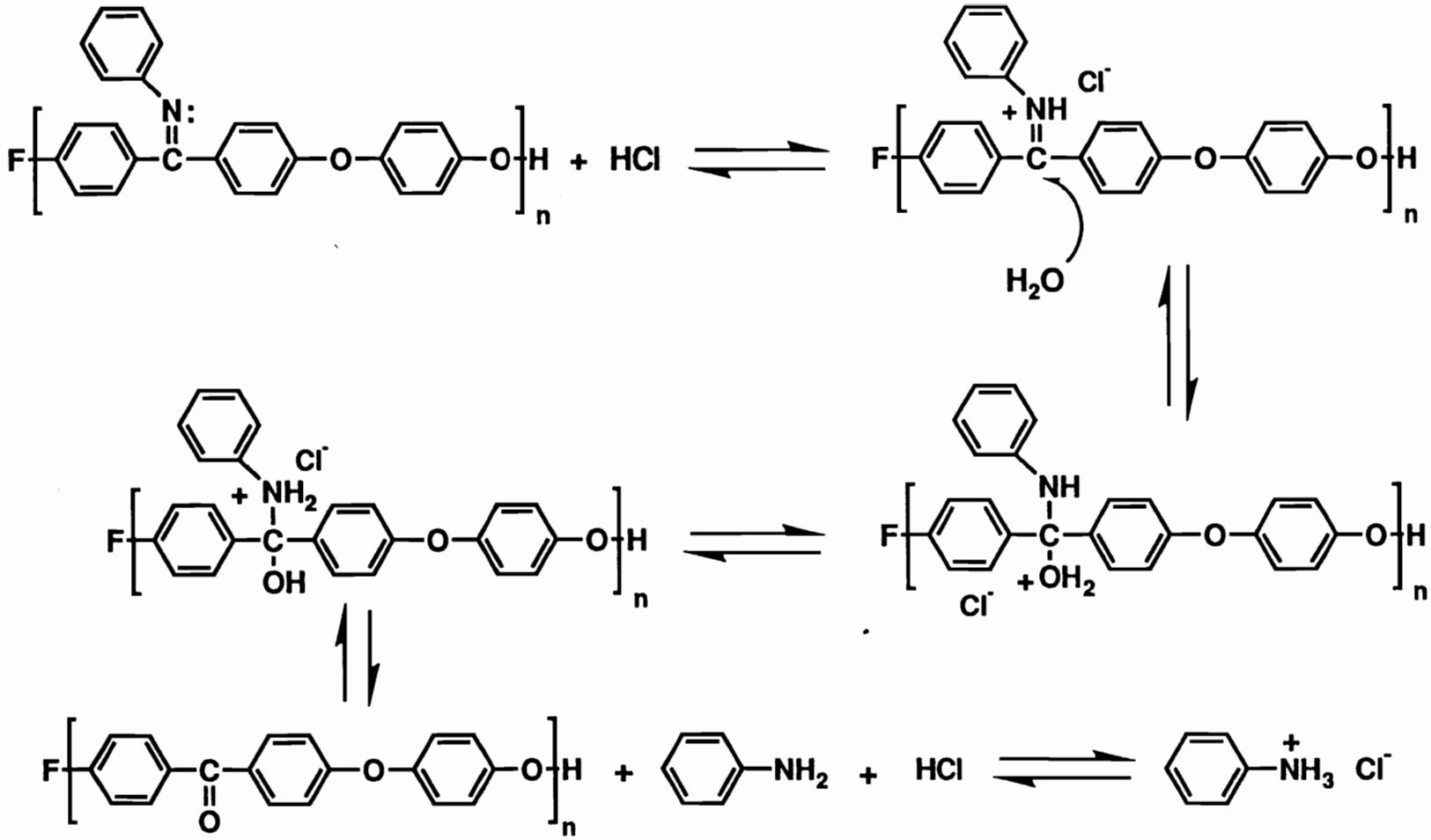

Figure 4.16: The Ketimine to Ketone Hydrolysis Mechanism

polymer precipitates from solution in the form of small particles. The conversion to PEEK is quantitative as determined by Dr. Harvey Grubbs, Philip Morris Corporation, utilizing offline pyrolysis GC mass spectral analysis with a nitrogen/phosphorous selective detector (Figure 4.17). This analysis indicated that there is aniline and NMP present in the particles precipitated by this procedure, but no evidence of the ketimine. This hydrolyzed polymer also has essentially identical thermal and oxidative stability and transition temperatures as commercial PEEK as determined by TGA in helium (Figure 4.18) and DSC (Figure 4.19). The DSC results do indicate that Victrex 450 G (ICI's PEEK) has a slightly higher degree of crystallinity, however this could be do to the addition of nucleating agents in the commercial material

It was of interest to determine the mechanism of phase separation (crystallization or insolubility) of these materials as they were hydrolyzed to PEEK. This was done by examining the solubility of the ketimine polymer as a function of composition. To prepare polymers for this study, a slow and controlled hydrolysis procedure was developed, as described in the experimental section. This has two advantages in that the polymers being compared were all from the same original ketimine derivatized polymer and therefore their molecular weight and molecular weight distributions, which can affect solubility, were identical. This method will also provide polymers with varying amounts of ketone units in the same sequence distribution that would occur during the actual hydrolysis process. This is important because it is unknown whether hydrolysis is a random or blocky process, which could also affect solubility. The conversion of ketimine to ketone was monitored as a function of time using ^{1}H NMR and is displayed graphically in Figure (4.20).

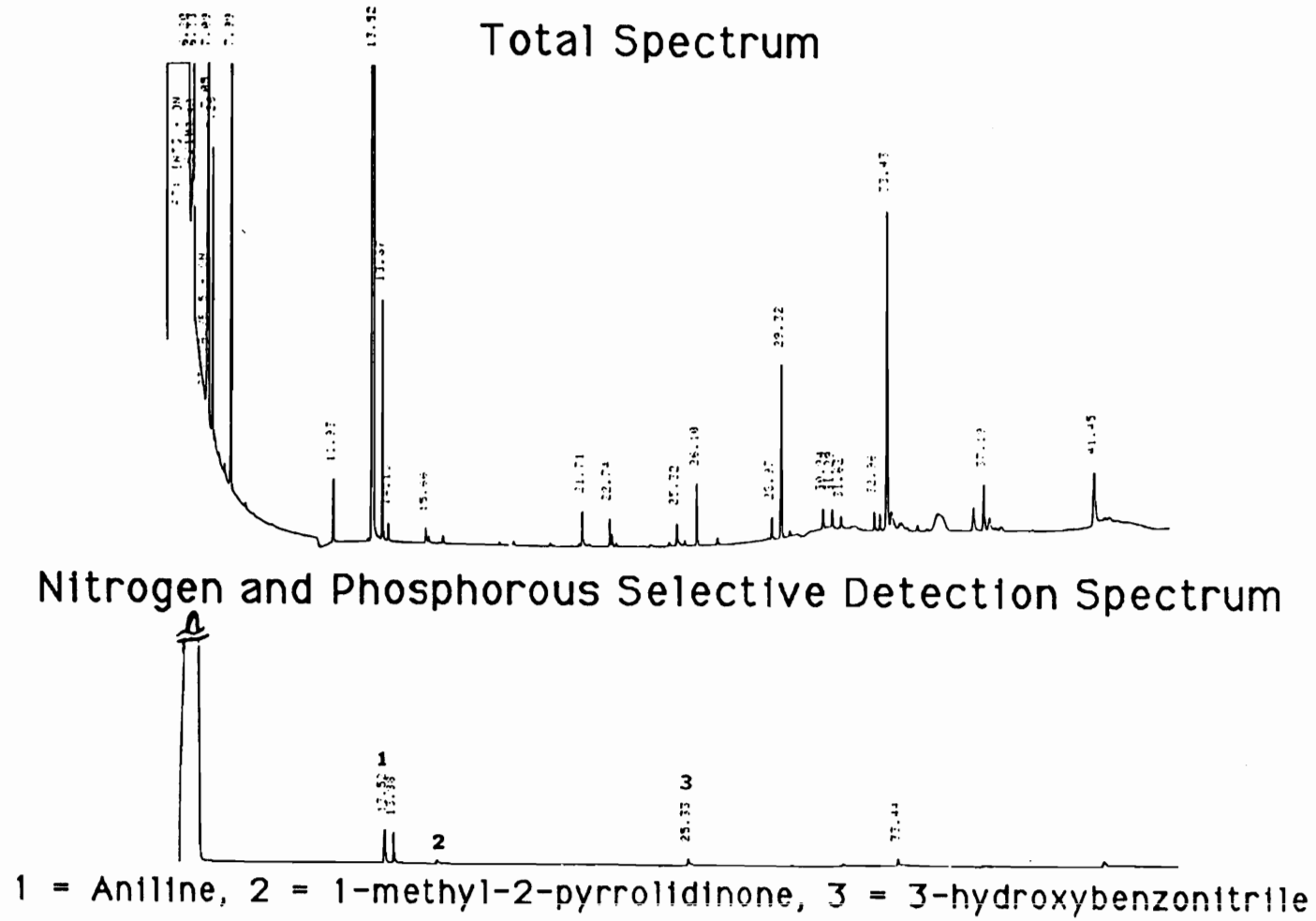

Figure 4.17: Offline Pyrolysis Gas Chromatography Mass Spectra of Acid Hydrolyzed PEEK Particles

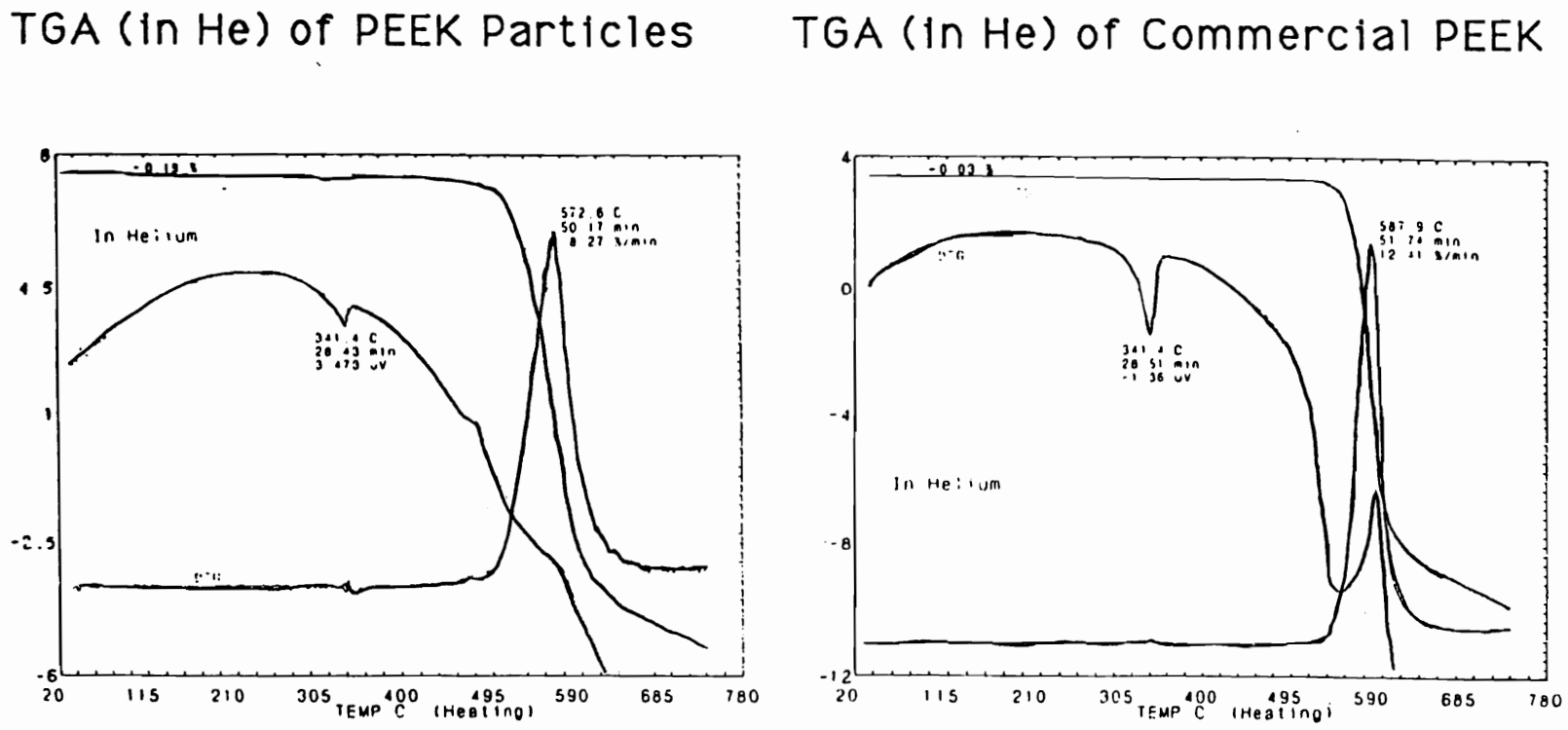

Figure 4.18: Thermal Gravimetric Analysis of Acid Hydrolyzed PEEK Particles vs Commercial PEEK (Victrex 450G): Heating Rate of 20°C per minute in Helium

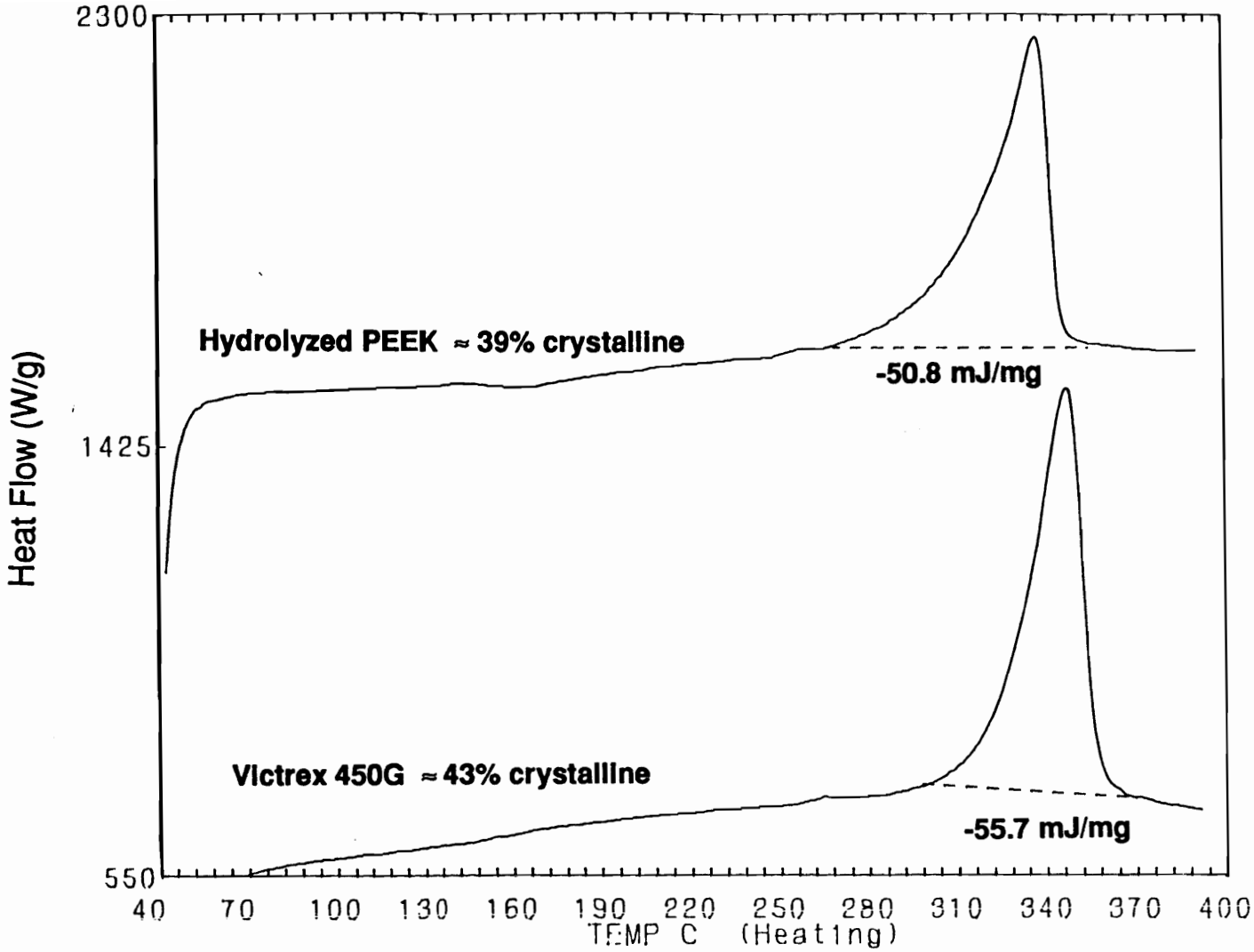

Figure 4.19: Differential Scanning Calorimetry of Acid Hydrolyzed PEEK Particles vs Commercial PEEK (Victrex 450G): Heating Rate of 20°C per minute

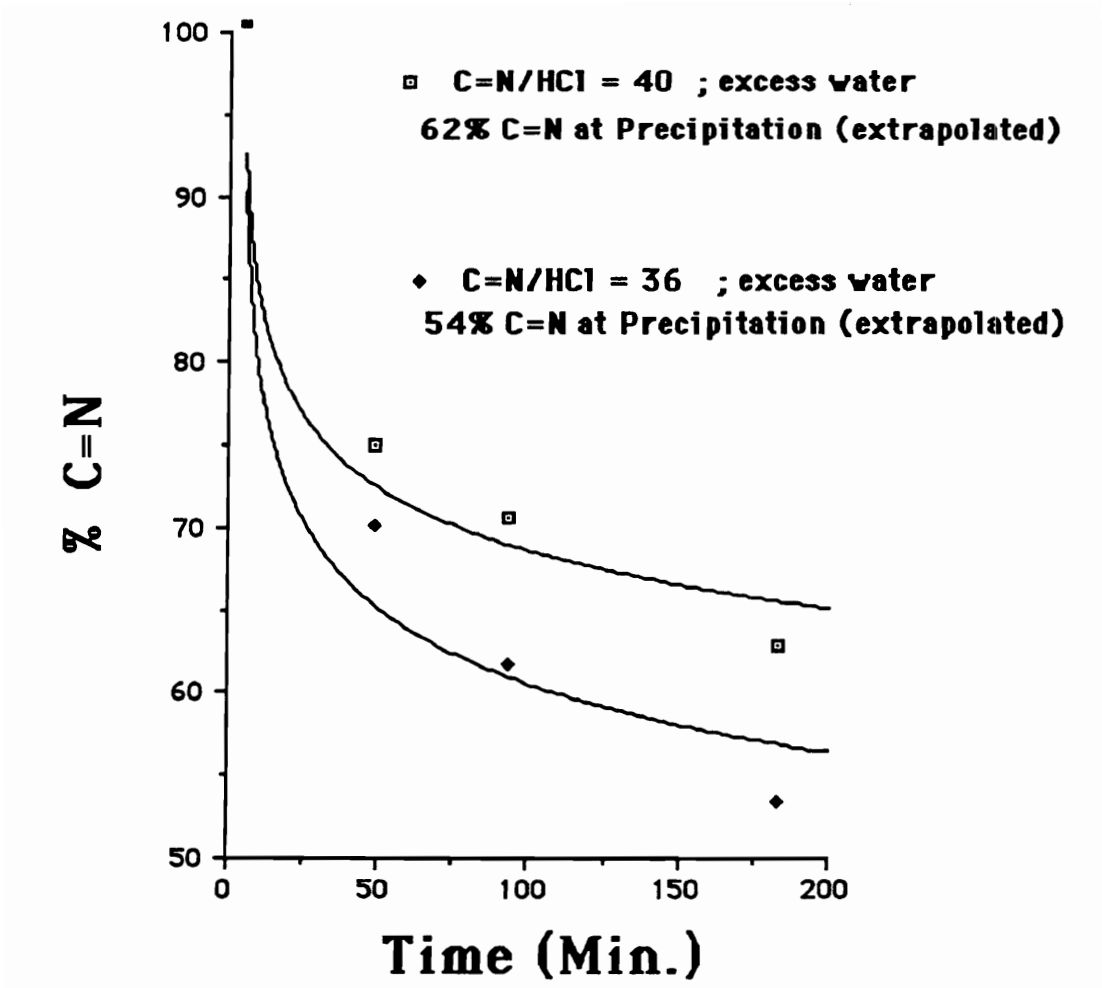

Figure 4.20: % Conversion With Time for the Slow, Controlled Hydrolysis of Poly(ether ether ketimine) to Poly(ether ether ketone)

Utilizing this controlled hydrolysis of the ketimine homopolymer, a series of amorphous copolymers with 0, 15, and 30 mole percent ketone, as confirmed by ^{1}H NMR (Figure 4.21), were synthesized. Their relative solubility was determined by examining cloud points at room temperature in NMP/water solvent compositions as a function of water content.[79] As shown in Table 4.2, all three have identical cloud points, and therefore identical solubility in NMP/water. The similar solubility of PEEK and PEEKt was supported by calculating their respective solubility parameters utilizing group additivity calculations as suggested by Van Krevelen.[130] The values obtained were 25.91 and 25.27 $(\text{cal cm}^{-3})^{1/2}$ for PEEK and PEEKt respectively. From this it was concluded that the polymer must be crystallizing out of solution vs. precipitating as an amorphous polymer, and then crystallizing. This is important in that it shows the polymer is not undergoing a liquid-liquid phase separation, which has both binodal and spinodal phase separation regions, but crystallization from solution, which occurs exclusively by nucleation and growth.

Table 4.2: Copolymer Cloud Points as a Function of Solvent Composition at 23°C

% Ketone	Polymer (wt%)	NMP (wt%)	Water (wt%)
0	2.9	90.0	7.1
15	2.9	90.0	7.1
30	2.9	89.9	7.2

4.2.6 Formation of Poly(ether ether ketone) particles:

When a polymer crystallizes from solution, phase separation occurs by both nucleation and growth. To minimize the diameter of the resulting polymer

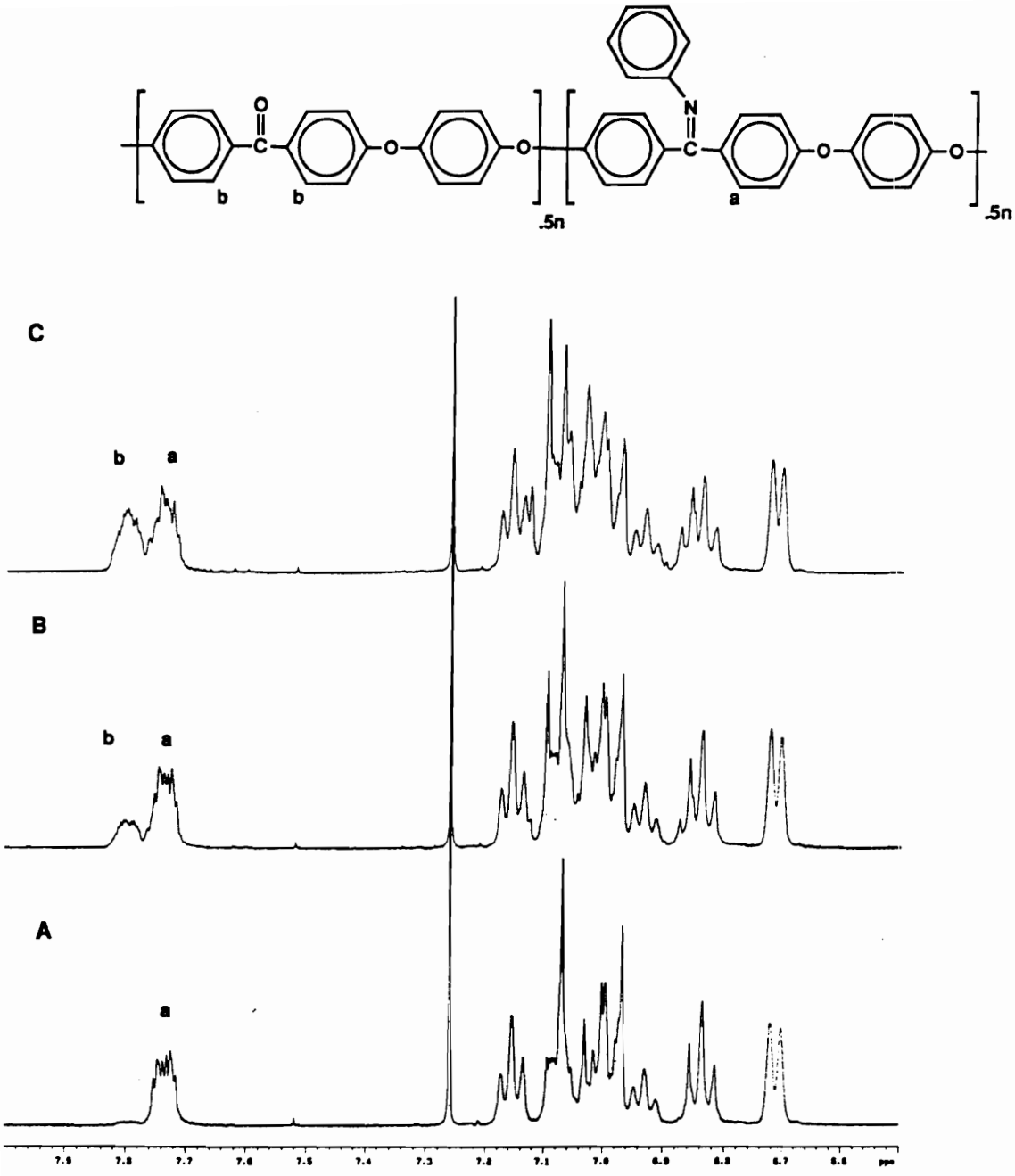

Figure 4.21: ^{1}H NMR Analysis to Determine %Conversion to Ketone Under Slow, Controlled Hydrolysis Conditions: A = 0 minutes, 0% Ketone; B = 1.8 minutes, 15% Ketone; C = 20 minutes, 30% Ketone

particle, nucleation must be maximized and growth minimized. One way to do this is to rapidly extend the system as far into the phase separation region as possible (termed "undercooling" when temperature is the dynamic variable). Unlike most cases, for this system the temperature will be kept constant, and the composition will be changing. Analogous to those cases where temperature is the variable, the ketimine functionalities must be converted to ketones as rapidly as possible. The parameters affecting this conversion, and therefore the particle size, have been determined to be a complex function of variables including the initial copolymer composition, ketimine concentration in solution, acid concentration, water concentration, and hydrolysis temperature (Figure 4.22). Some of the results obtained by varying these parameters are shown in Table 4.3 and Figure 4.23. The median particle size reported is that obtained by centrifugal particle size analysis as described in the experimental section using the ammonium salt of LaRC TPI Polyamic acid as the stabilizing agent. The particles were also viewed by scanning electron microscopy (SEM). Figure 4.24 shows two exemplary photographs taken of particles formed at 65°C with a HCl/repeat unit ratio of 1.30. The first (A) was taken at a magnification of 12,500 times, the second (B) was taken at a magnification of 100,000 times. Both photographs have a scale bar of 0.5 μm. As seen in these photos, there are several large aggregates on the order of 2-3 microns in diameter. However, the large majority of the particles are significantly smaller in size. Photo B indicates that the actual average particle size is significantly lower than 0.3 μm (approximately 0.05 μm , or 50 nm) as measured by the centrifugal particle size analyzer. This is because the particle size analyzer provides a weight

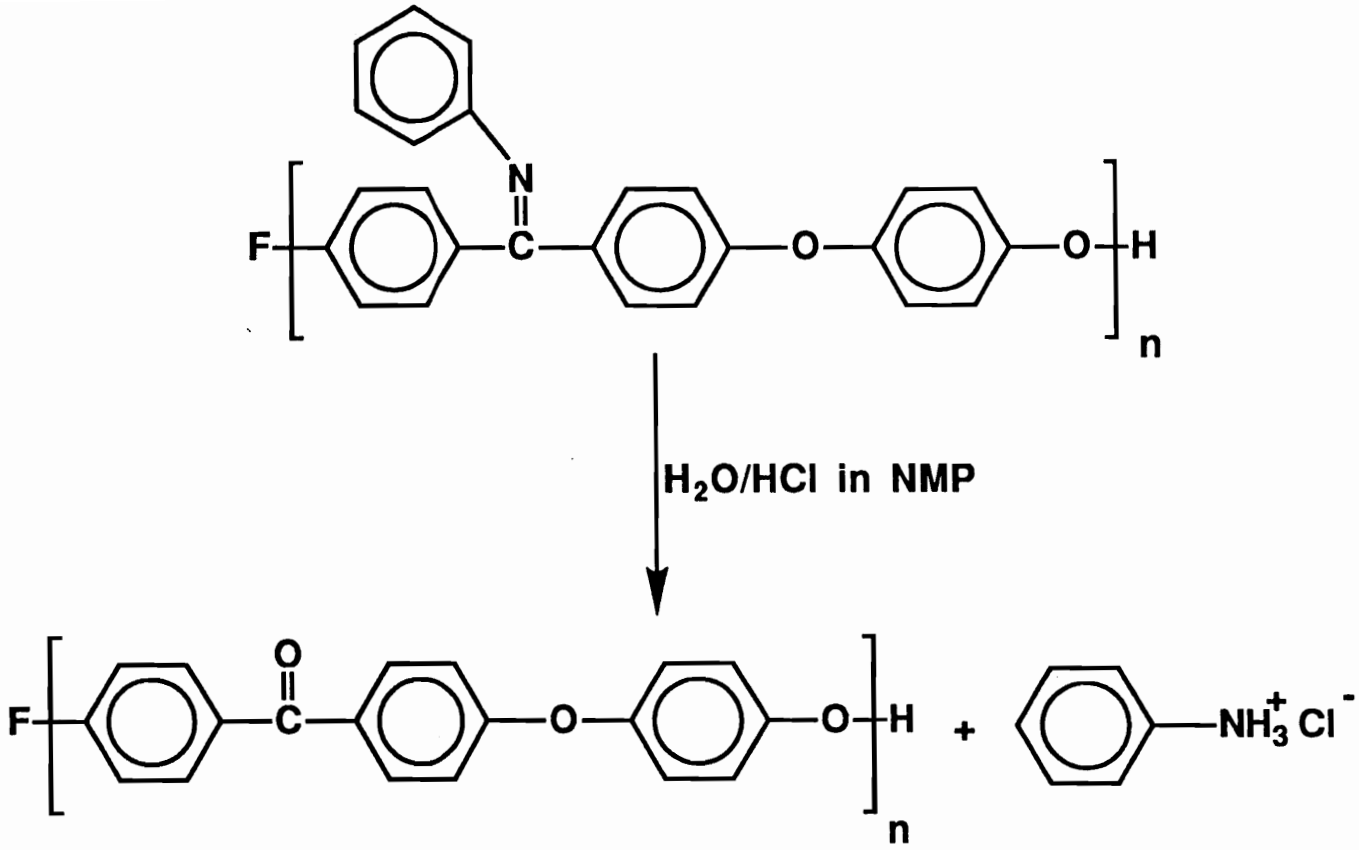

Parameters: Copolymer Composition, HCl Concentration, and Temperature

Figure 4.22: The Most Important Parameters in Controlling the Particle Size in the Hydrolysis of Poly(ether ether ketimine) to Poly(ether ether ketone)

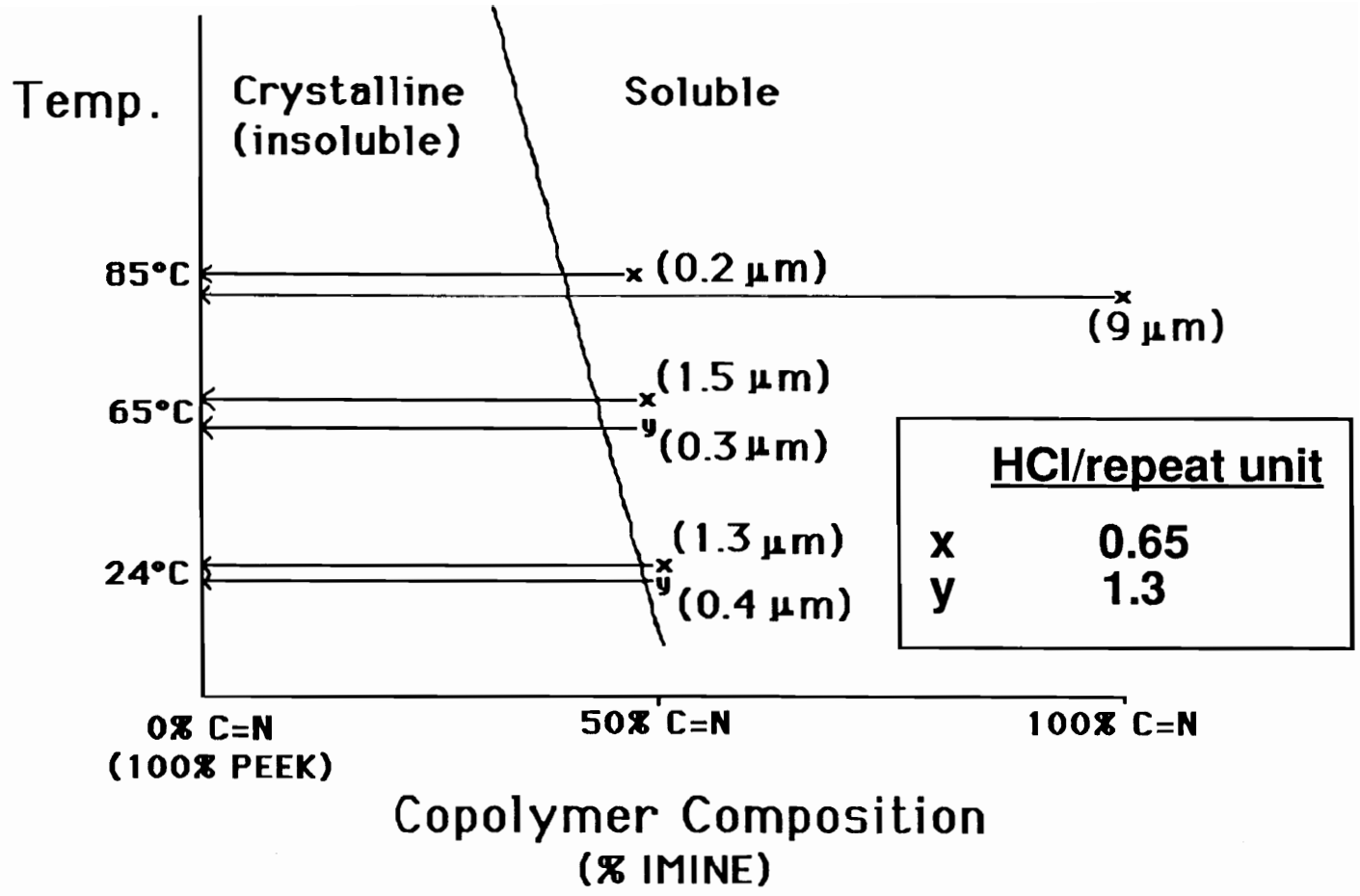

Figure 4.23: PEEK Particle Formation

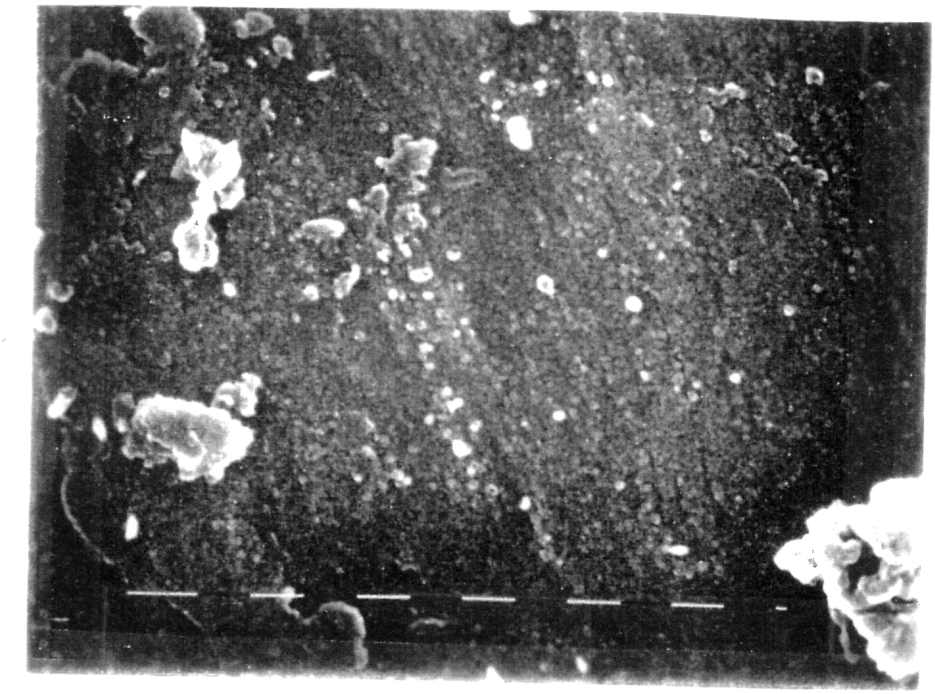

A

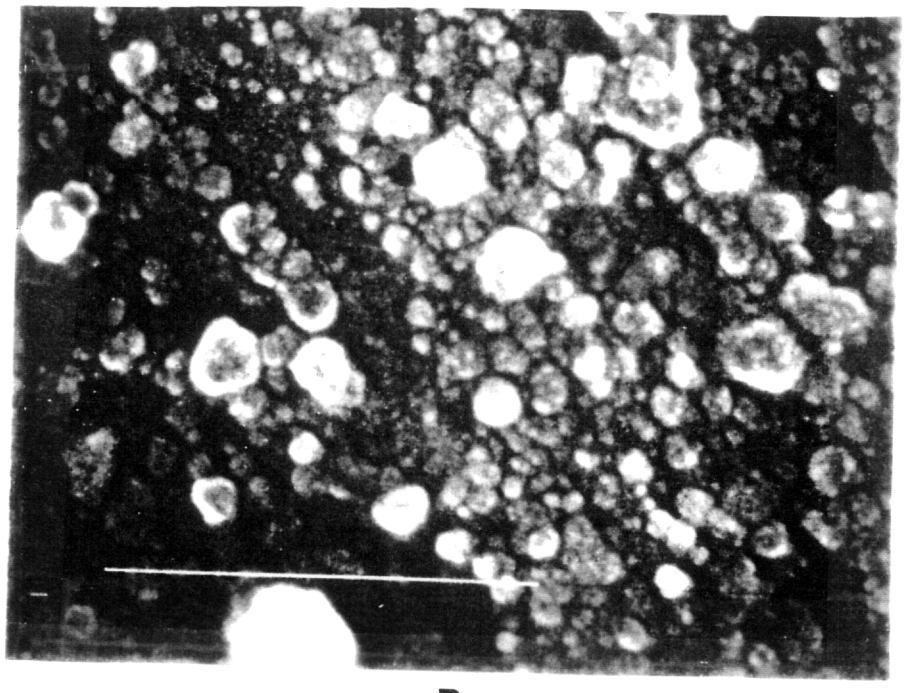

B

Figure 4.24: Scanning electron micrographs of PEEK particles formed at 65°C with a HCl/repeat unit ratio of 1.30: (A) magnification = 12,500, (B) magnification = 100,000; both display a 0.5 μm marker.

averaged particle size, and therefore the few large aggregates present greatly increase the median diameter reported.

Table 4.3: Particle Size as a Function of Hydrolysis Temperature, Acid Ratio, and Initial Copolymer Composition

Temp. (°C)	Initial Mole% Imine	HCl/Repeat Unit	Particle Diameter (μm)
85	100	0.65	9.0
25	50	0.65	1.3
65	50	0.65	1.5
85	50	0.65	0.2
25	50	1.30	0.4
65	50	1.30	0.3

The smallest particle sizes were obtained when the 50:50 ketone to imine copolymer (50% initial mole% imine) was used as the starting material. This can be explained by considering the process occurring during hydrolysis and the corresponding nucleation rate. When the hydrolyzing polymer reaches some critical composition, crystallization by nucleation and growth can occur, which results in insoluble polymer particles[81]. If one starts at 100% ketimine, the polymer is converted toward the ketone and, at any given time, there will be a composition distribution. Within this distribution, some of the copolymer will crystallize out of solution, while some will still be soluble. With further conversion, more mass of polymer will be able to crystallize. However, at this point in the process, there will already be some nuclei present on which polymer can grow. This results in relatively large particles. If one begins the process with a polymer containing only 50% ketimine, a larger concentration of

the polymer reaches the critical composition before nucleation can occur. This results in a larger number of nuclei formed, and therefore a smaller particle size. Likewise, a higher temperature or increased acid concentration results in a faster hydrolysis rate. This also converts a larger portion of the polymer past the critical composition resulting in smaller particles (Figure 4.25).[81] Careful control of the experimental parameters allows the formation of submicron PEEK particles. The particles, with the use of a steric stabilizer, form stable aqueous suspensions for use in aqueous dispersion prepregging. These particles were also used in a study to examine the feasibility of sintering high performance semicrystalline polymeric powders.

4.3 The Synthesis of a High Performance Electrostatic Stabilizer for PEEK Particles

4.3.1 Introduction:

Aqueous dispersion prepregging is a relatively new method for applying high performance polymers to graphite fiber tow, which could potentially circumvent many of the environmental and processing problems prominent in melt or solution prepregging. The method, however, requires the matrix resin to be in the form of small particles dispersed in a stable aqueous suspension.[74,75] This section focuses on the development of a high performance stabilizer which can be used for suspending poly(ether ether ketone) (PEEK) particles in water (forming stable colloids), thereby facilitating the development of processes for aqueous dispersion prepregging.

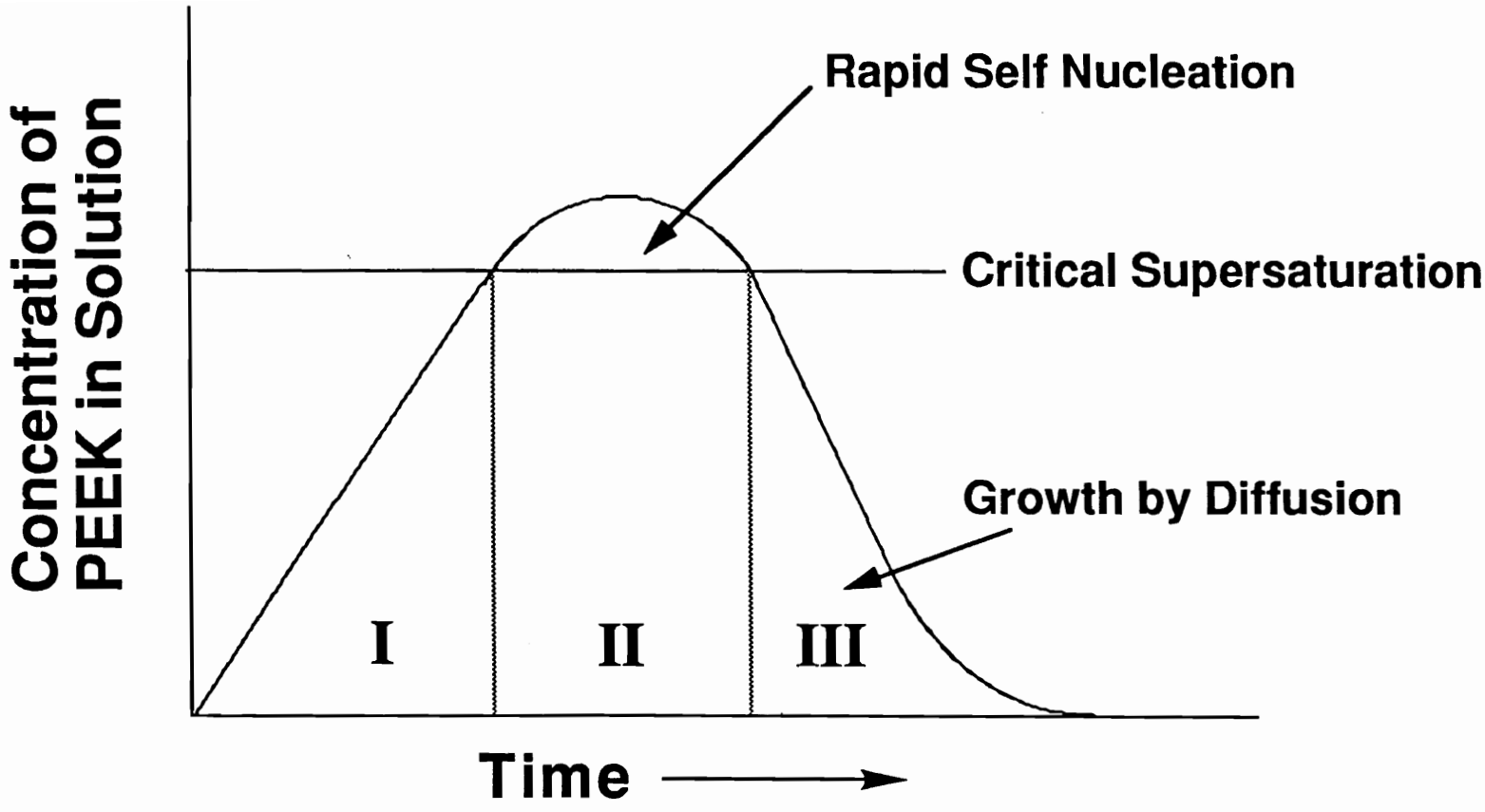

Figure 4.25: The Nucleation Rate of Poly(ether ether ketone)

Homopolymerization of 4,4'-difluoro(N-benzohydroxylidene aniline) and hydroquinone, as well as the copolymerization of these monomers with 4,4'-difluorobenzophenone has been discussed. The hydrolysis of these soluble materials to the semicrystalline, insoluble poly(arylene ether), PEEK, in the form of submicron size particles has also been examined. Suspensions of these particles in water were demonstrated, but the suspending agents used were poly(amide acid)s at basic pHs, and these materials are not chemically stable under such conditions.[75] Because of the elevated use temperatures in the targeted applications of the final composites prepared from these resins, thermo-oxidative stability of all components involved is also a desirable property. It has also been shown that the miscibility of the stabilizer with the matrix resin is beneficial for good interfacial adhesion which translates into good composite properties.[131]

This section discusses the development of a high performance stabilizer which can be used for suspending PEEK particles in water (forming stable colloids), thereby facilitating the development of processes for aqueous dispersion prepregging. The stabilizer is a copolymer formed from 4,4'-difluoro-(N-benzohydroxylidene aniline), 2,6-dichloropyridine and hydroquinone according to the scheme outlined in Figure 4.26. This copolymer forms self stabilizing particles upon hydrolysis (Figure 4.27). Alternatively, it can be adsorbed onto PEEK particles from 1-methyl-2-pyrrolidinone (NMP) and subsequently acid hydrolyzed to a poly((pyridine ether) - co - (ether ether ketone)) copolymer where the pyridine units have been protonated. In this latter process, the copolymer containing the protonated pyridine units forms an electrostatic stabilizer on the surface of the PEEK particles. It is also believed

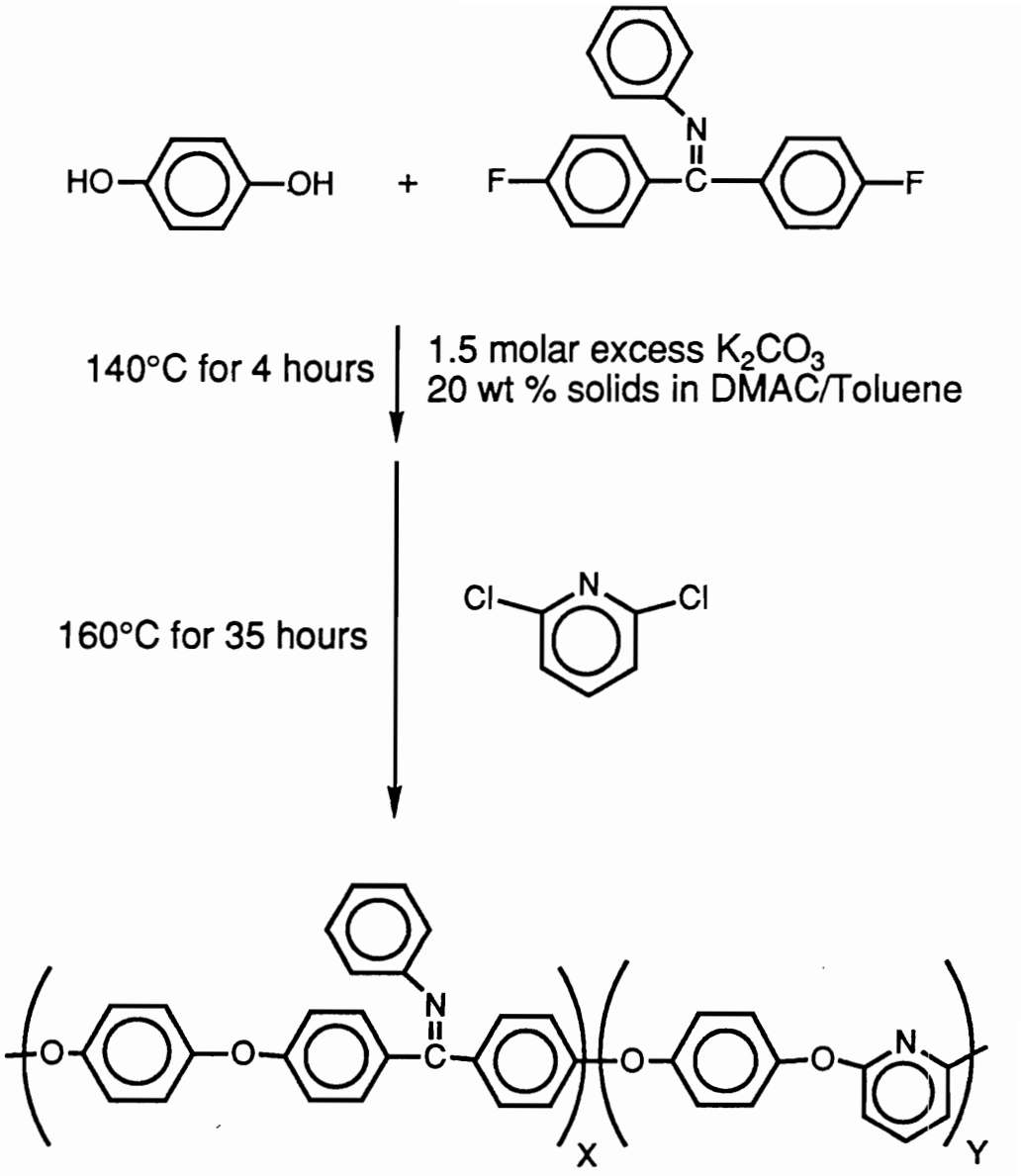

Figure 4.26: Synthesis of Poly((pyridine ether) - co - (ether ether ketimine))

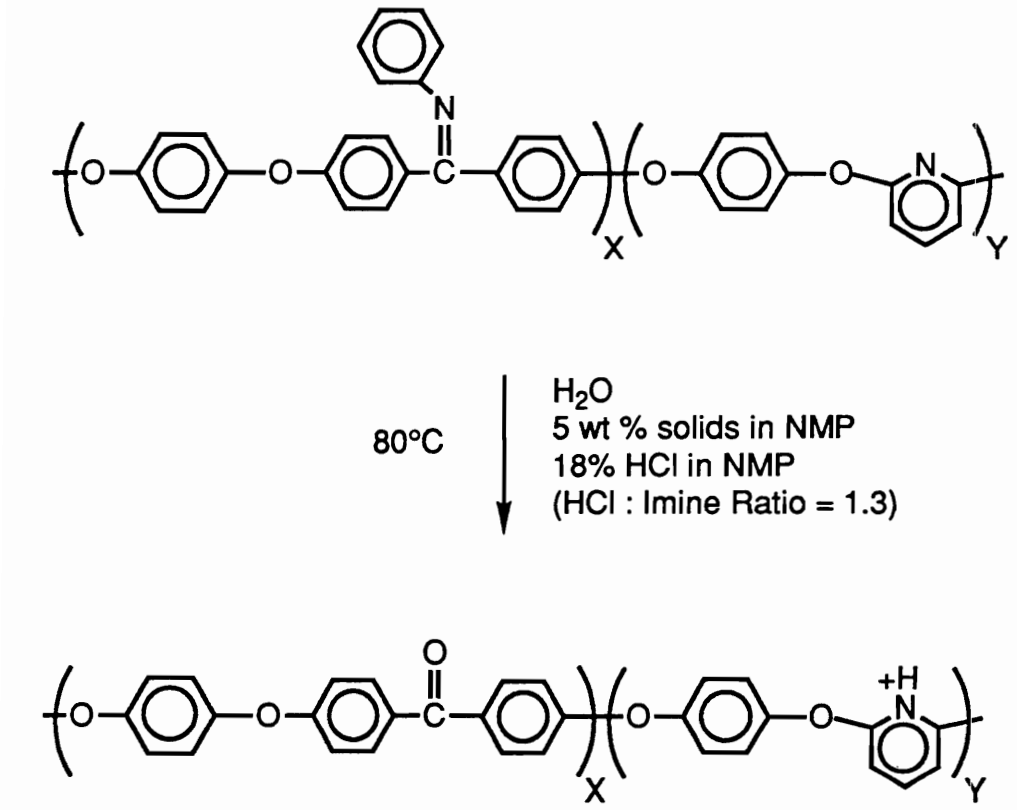

Figure 2.27: Hydrolysis of Poly((pyridine ether) - co - (ether ether ketimine)) to Poly((pyridine ether) - co - (ether ether ketone))

that pyridine units might exhibit specific interactions with the carbon fiber and therefore provide a good interface between the matrix and the fiber.[132]

Nucleophilic aromatic substitution reaction conditions for incorporating pyridine units into the polyarylene ether ketimine backbone structure, using 2,6-dichloropyridine as the comonomer, have been established. Conversion of the ketimine to the ketone with concurrent pyridine protonation produces a material which functions as a high performance stabilizer for PEEK in water. Dynamic thermal gravimetric analyses of these stabilizers, in air, indicate that significant weight loss does not occur until well above 500°C. This suggests that these materials may be stable to consolidation temperatures of high-performance polymer matrix composites.

4.3.2 Synthesis of Poly((pyridine ether) - co - (ether ether ketimine)):

A series of poly(ether ether ketone)s with controlled, varied levels of 2,6-dichloropyridine incorporated as a comonomer have been synthesized. Nucleophilic aromatic substitution polymerizations using dichloropyridine have been reported previously, but only low molecular weight materials were obtained.[133-135] In this case, the first attempts at the synthesis of poly((pyridine ether) -co- (ether ether ketimine)) with systematically varied molar ratios of pyridine to ketimine (10/90, 20/80, and 30/70) also provided only moderate molecular weight polymers (≈ 10,000 g/mole) as determined by GPC (Figure 4.28, Table 4.4). For this reason a modified synthesis procedure (see experimental) was monitored using gel permeation chromatography. The increase in molecular weight as a function of reaction time was evaluated for aliquots taken from a poly((ether pyridine) - co - (ether ether ketimine))

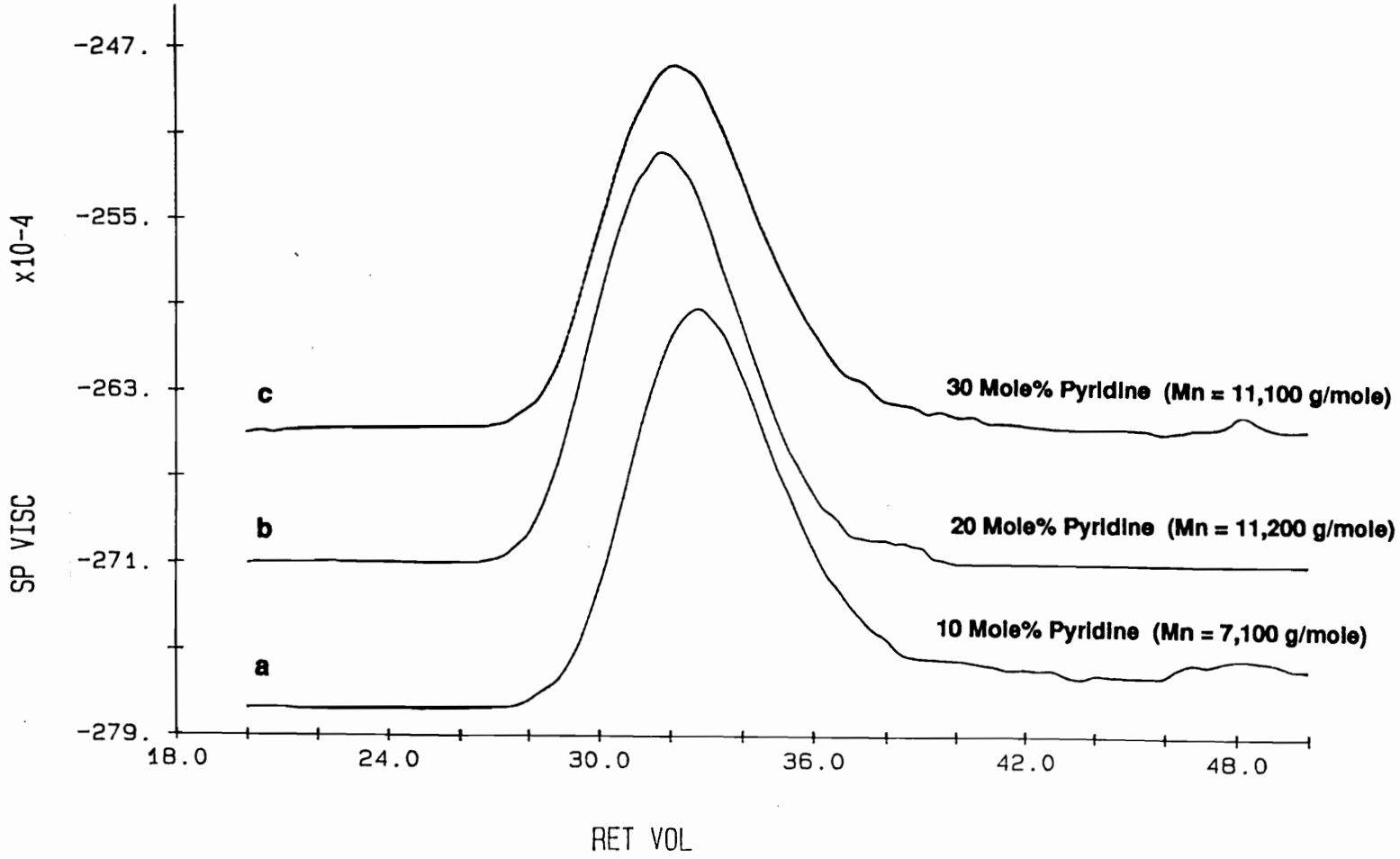

Figure 4.28 Gel permeation chromatography of poly((pyridine ether) - co - (ether ether ketimine)) copolymers; Reaction time = 17 h.; theoretical molecular weight = 22,000 amu. (a) 10 Mole% pyridine. (b) 20 Mole% pyridine. (c) 30 Mole% pyridine: solvent = NMP, flow rate of 1 ml/min. with universal calibration.

polymerization containing 20 mole % pyridine (Figure 4.29). This experiment indicated that, compared to many poly(arylene ether) polymerizations which react by nucleophilic aromatic substitution mechanisms, 2,6-dichloropyridine requires relatively long reaction times (≈ 35 hours at 160°C) for high, or controlled molecular weights to be achieved. Table 4.4 outlines a comparison of targeted and experimental number average molecular weights for a series of pyridine containing polymers prepared using the 35 h reaction time vs. 16 h. The molecular weights reported in this table were calculated using a universal calibration method with a combination of concentration and viscosity GPC detectors as described in the Experimental section. Controlled molecular weight (DP = 66 and 40) poly((pyridine ether) - co - (ether ether ketimine)) copolymers with 20 mole % pyridine were synthesized using the extended reaction time, and essentially the expected molecular weights were obtained (Figure 4.30).

Table 4.4: Molecular Weight Analysis of Poly((pyridine ether) - co - (ether ether ketimine)) Copolymers

Mole % Pyridine	Reaction Time (hrs)	<Mn> Theor.	<Mn> by GPC*	<Mw> by GPC*
10	16	22,000	7,100	14,300
20	16	22,000	11,200	22,700
30	16	22,000	11,100	22,300
20	35	Uncontrolled	34,900	65,700
20	35	22,000	19,500	38,800
20	35	13,000	11,700	22,600

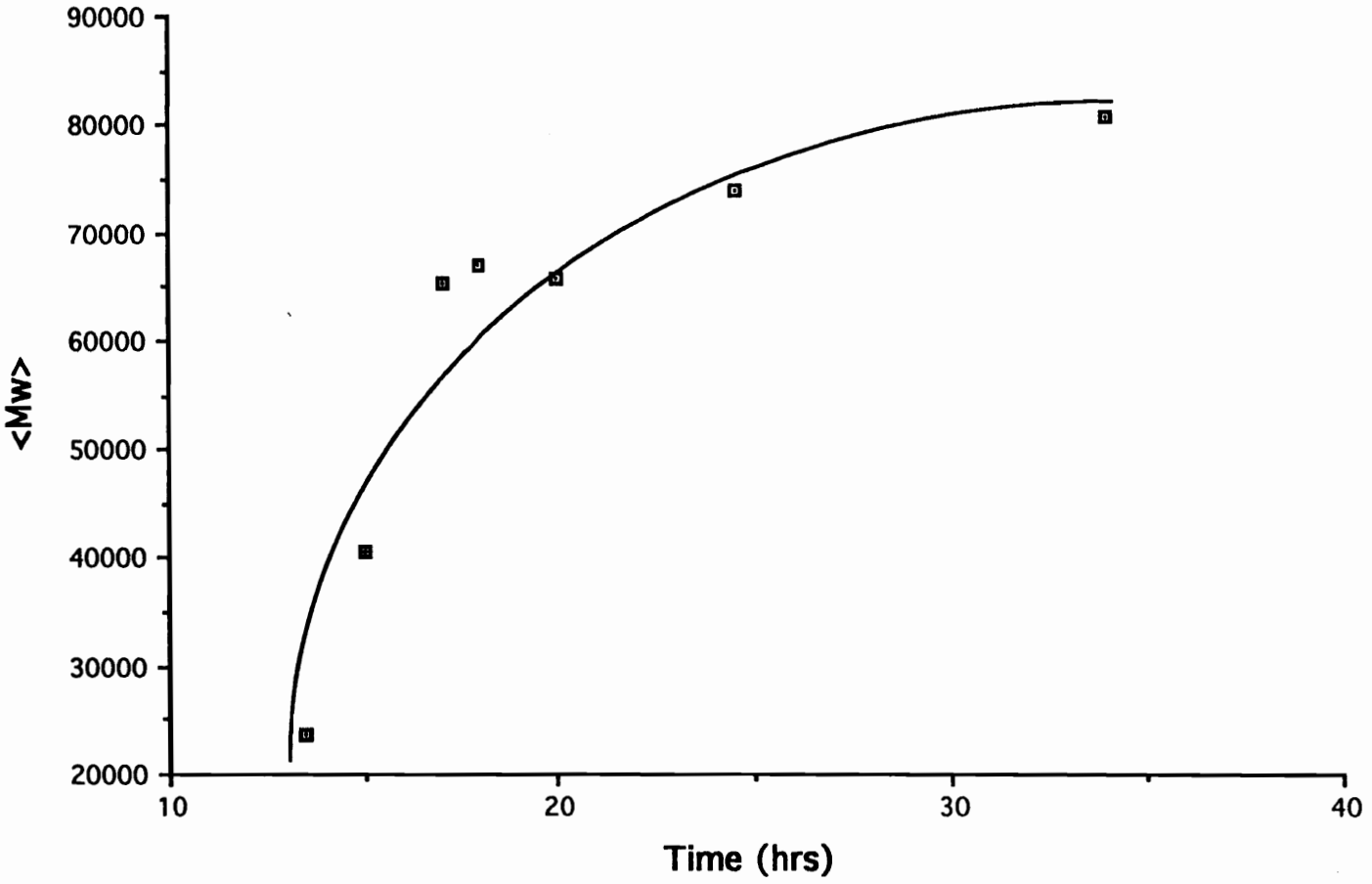

Figure 4.29: Dependence of weight average molecular weight on reaction time for the synthesis of poly((pyridine ether) - co - (ether ether ketimine)) with 20 mole% pyridine (determined by GPC with polystyrene standards).

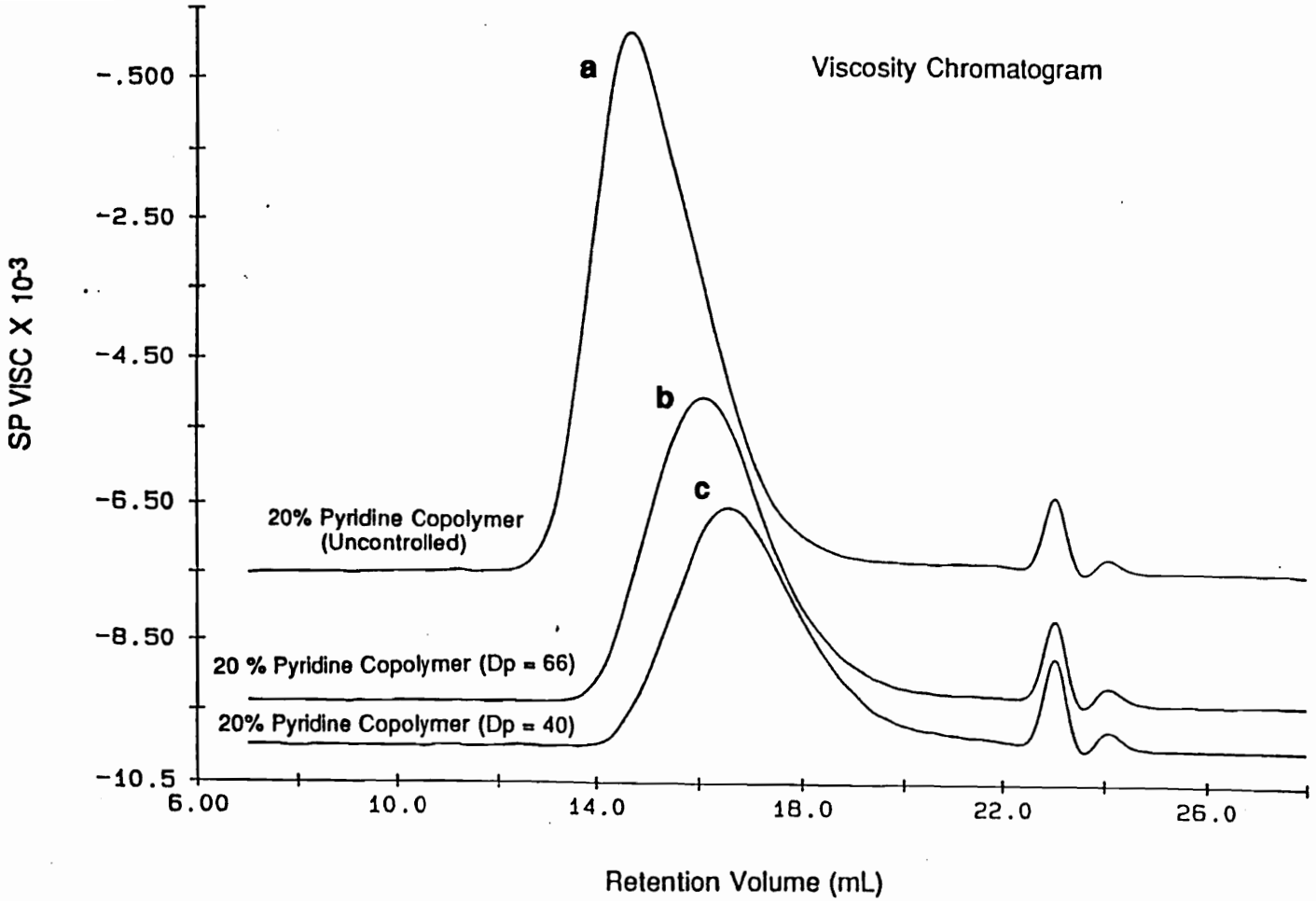

Figure 4.30: Gel permeation chromatography of poly((pyridine ether) - co - (ether ether ketimine)) copolymers; Reaction time = 35 h. (a) Uncontrolled molecular weight. (b) Controlled molecular weight (Dp = 66). (c) Controlled molecular weight (Dp = 40): solvent = NMP, flow rate of 1 ml/min. with universal calibration.

Proton NMR chemical shifts for protons ortho to a pyridine nitrogen (δ 8.6 ppm) as compared to those ortho to the sulfone on diphenylsulfone (δ 7.95 ppm) suggest that the pyridine nitrogen should be more strongly activating toward nucleophilic aromatic substitution than a sulfone group.[126,127] This suggests that 2,6-dichloropyridine should undergo nucleophilic aromatic substitution under less stringent conditions than 4,4'-dichlorodiphenylsulfone. However, the opposite of what was expected was observed. This can be understood by examining the reaction intermediates. After the first chloro group has been substituted with an ether on 2,6-dichloropyridine, a prominent resonance form exists that deactivates the pyridine ring from nucleophilic aromatic substitution of the second chlorine (Figure 4.31). Therefore, although substitution of the first chlorine on 2,6-dichloropyridine should be fast, substitution of the remaining chlorine may be correspondingly slow. In fact, as the ^{1}H NMR analysis originally suggested the first chlorine is substituted quite readily, even water will displace it. This adds another challenge in the quantitative nucleophilic aromatic substitution of 2,6-dichloropyridine, in that the system needs to be 100% dehydrated before the monomer is introduced into the reaction medium.

Another interesting point was discovered about the polymerization of 2,6-dichloropyridine from the GPC analysis shown in Figure 4.30. At high elution volumes, another relatively low intensity peak occurred indicating a low molecular weight side product in the polymer. Upon vacuum drying the purified polymer a white crystalline material sublimed out of the material, which is believed to be responsible for the peak in the GPC. It was hypothesized that this material was the cyclic dimer of 2,6-dichloropyridine and hydroquinone

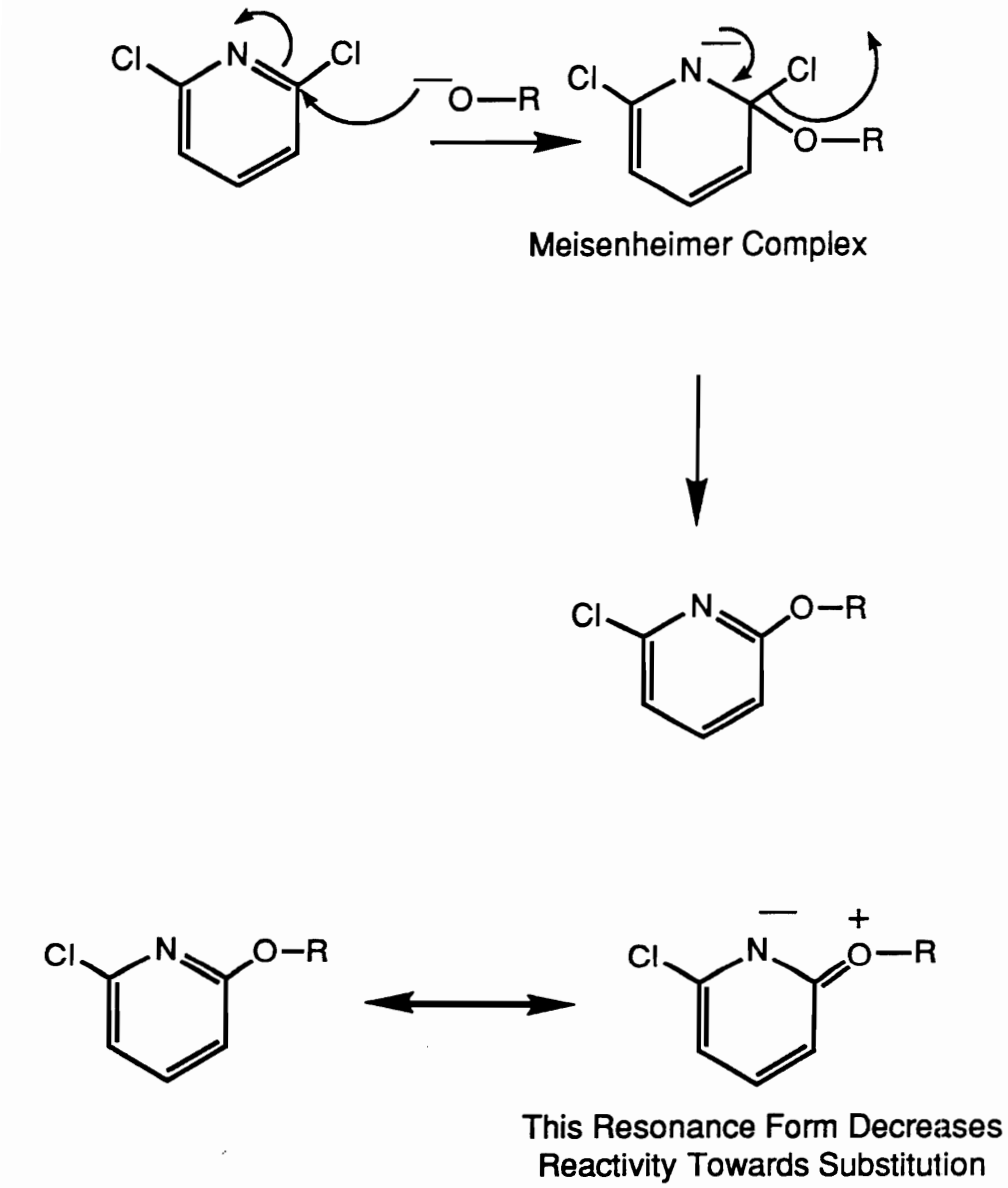

Figure 4.31: Substitution of 2,6-Dichloropyridine

(Figure 4.32). This dimer would have a molecular formula of $C_{22}H_{14}N_2O_4$ with a formula weight of 370 g mole^{-1}. The dimer would also have only 3 types of protons due to its symmetry. The ^1H NMR in $CDCl_3$ [7.68 (2H, t), 6.82 (8H, s), 6.61 (4H, d)] (Figure 4.33), and the mass spectral analysis (Figure 4.34) confirmed this low molecular weight impurity to be the cyclic dimer, as anticipated. Although this cyclic dimer is of academic interest it should not interfere with the polymer synthesis as it uses up two equivalents of activated halides as well as phenolate groups. Also, as long as the dimer is removed from the polymer during purification it should not affect any of the physical properties obtained.

With an understanding of the peculiarities of 2,6-dichloropyridine, a series of copolymers were prepared using 4,4'-difluoro(N-benzohydroxylidene aniline) (the ketimine), 2,6-dichloropyridine and hydroquinone were synthesized with systematically varied molar ratios of pyridine to ketimine (10/90, 20/80, and 30/70). All were shown to be amorphous by DSC (Table 4.5) even though the homopolymerization of 2,6-dichloropyridine and hydroquinone results in a semicrystalline polymer with Tg = 100°C and Tm = 272°C[133]. A typical DSC thermogram of a 20 mole% pyridine copolymer is shown in Figure 4.35. Thermal gravimetric analysis showed that these polymers were quite thermally stable (Table 4.5) A typical curve is shown for a 20 mole % pyridine copolymer (Figure 4.36). These amorphous materials are soluble in a variety of solvents including dipolar aprotic solvents (NMP, DMAc, DMSO), chloroform, and toluene, and a typical ^1H NMR in $CDCl_3$ of a 20 mole% pyridine copolymer is shown in Figure 4.37.

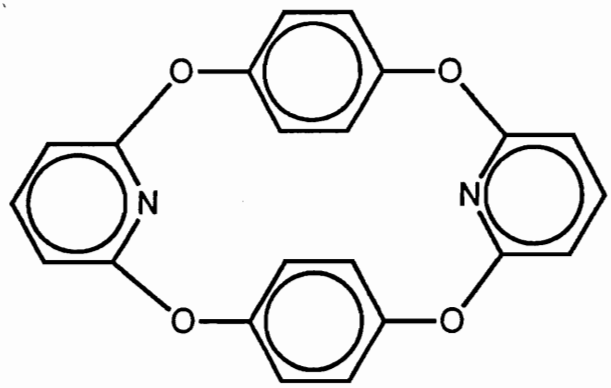

Figure 4.32: Cyclic Dimer Derived From 2,6-Dichloropyridine and Hydroquinone

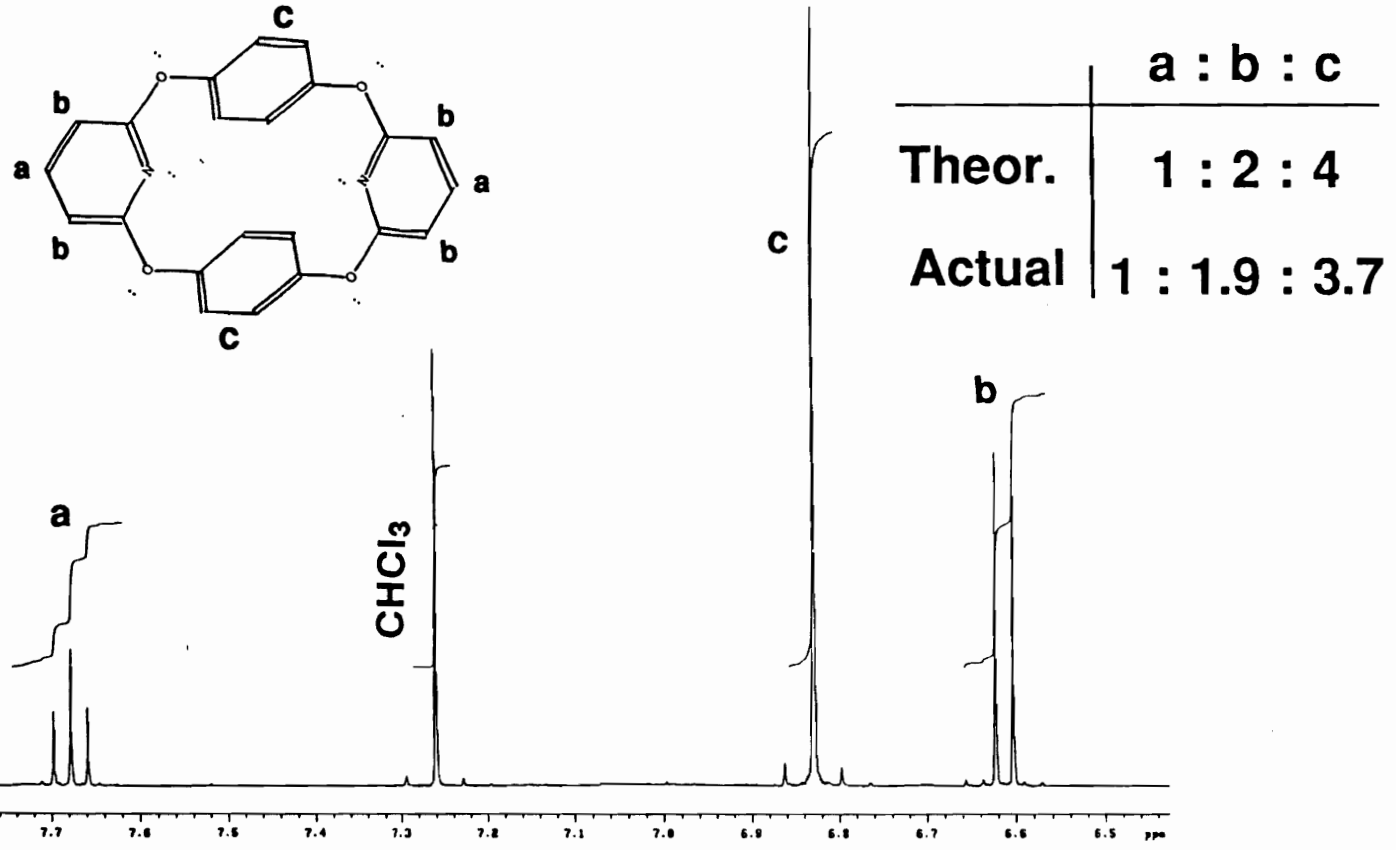

Figure 4.33: ^{1}H NMR of the Cyclic Dimer of 2,6-Dichlorpyridine and Hydroquinone

$C_{22}H_{14}N_2O_4$ FW = 370

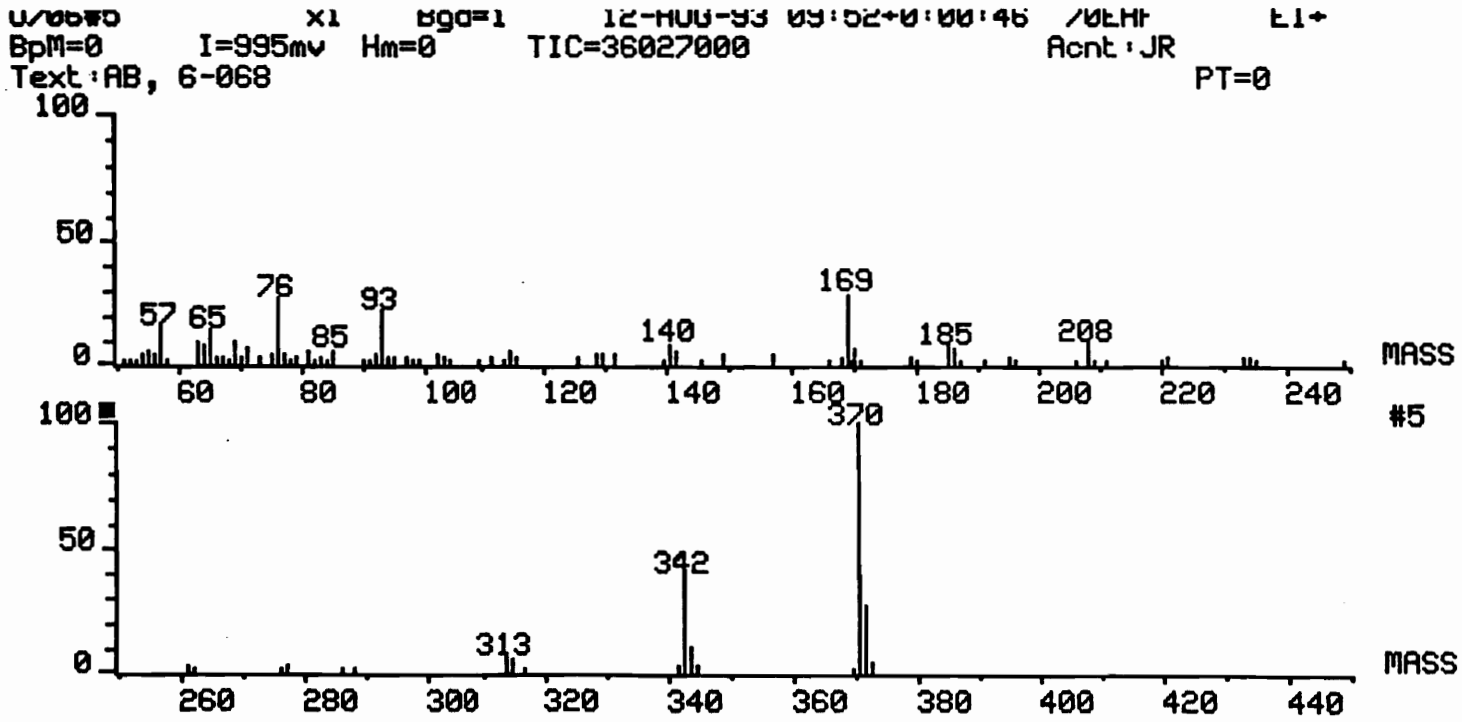

Figure 4.34: Mass Spectral Analysis of the Cyclic Dimer of 2,6 - Dichloropyridine and Hydroquinone

Table 4.5: Thermal Analysis of Poly((pyridine ether) - co - (ether ether ketimine))

Mole % Pyridine	<Mn> (GPC)	Tg (°C)	5% wt loss (°C) (nitrogen)
10	7,100	143	522
20	11,200	144	509
30	11,100	135	488
20	34,900	154	502
20	19,500	145	—

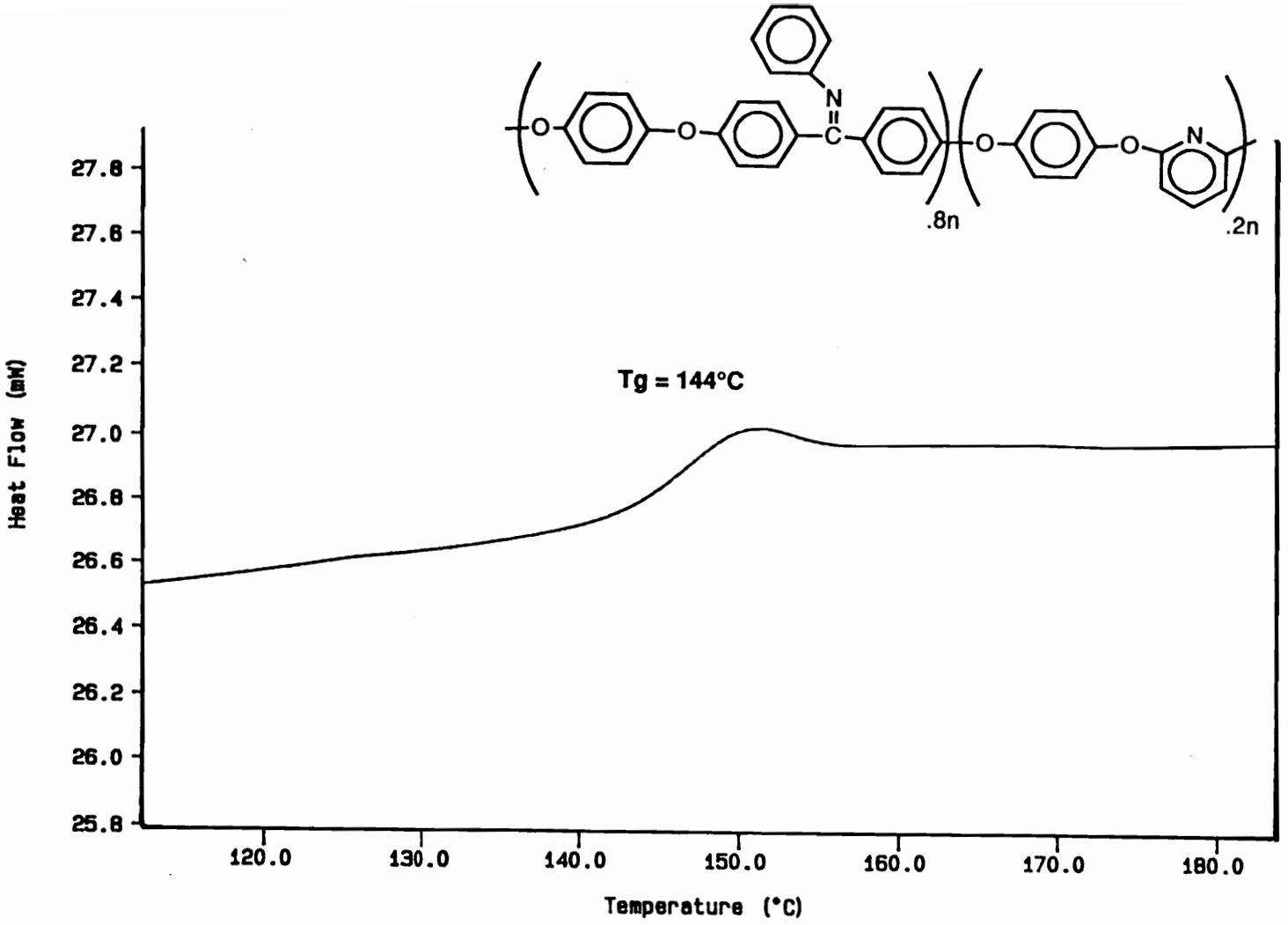

Figure 4.35: Differential Scanning Calorimetry of poly((pyridine ether) - co - (ether ether ketimine)) Containing 20 Mole% Pyridine; Heating Rate of 10 °C per minute

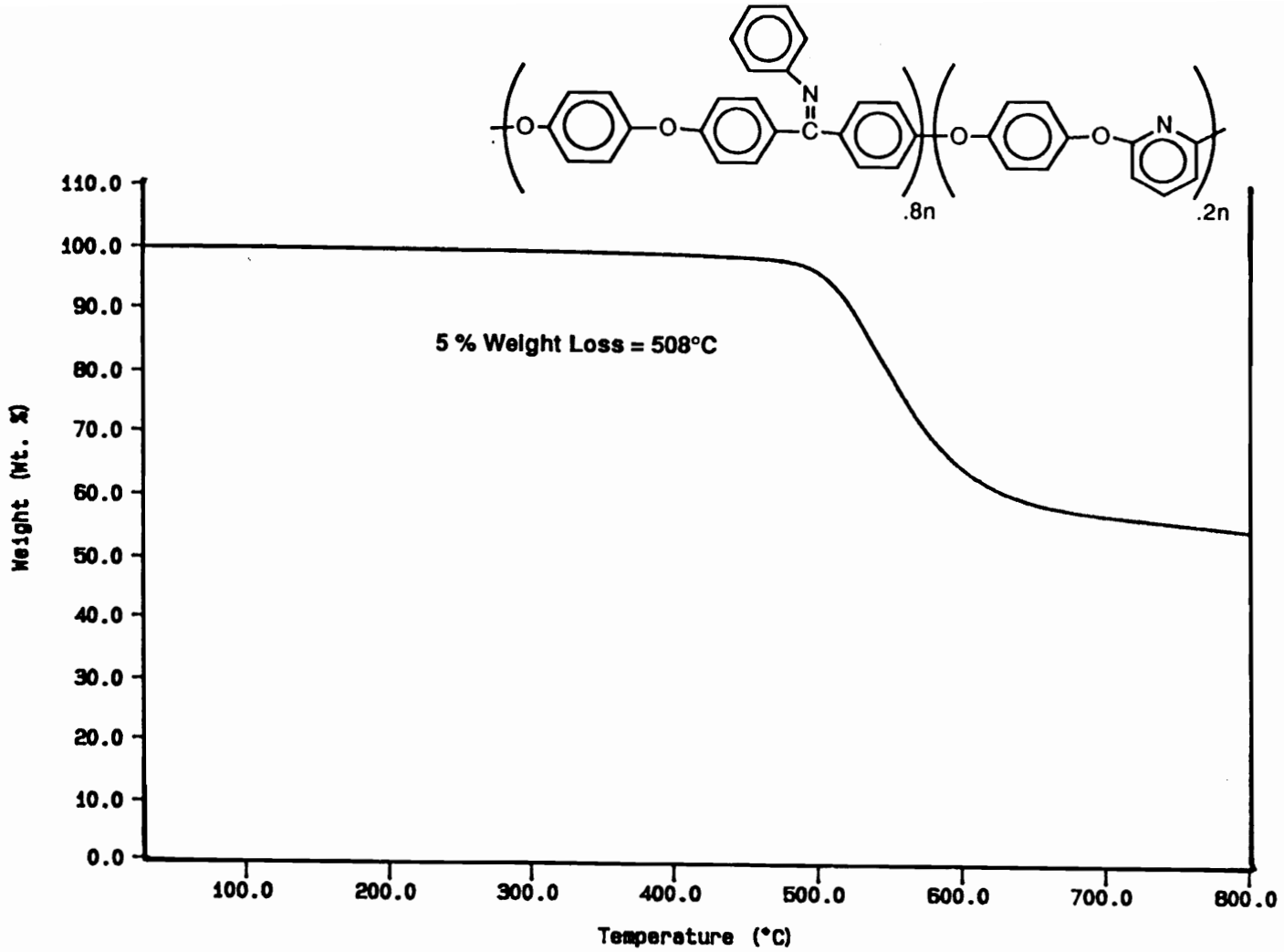

Figure 4.36: Thermal Gravimetric Analysis of poly((pyridine ether) - co - (ether ether ketimine)) Containing 20 Mole% Pyridine: Heating Rate of 10°C per minute. in a Nitrogen Atmosphere

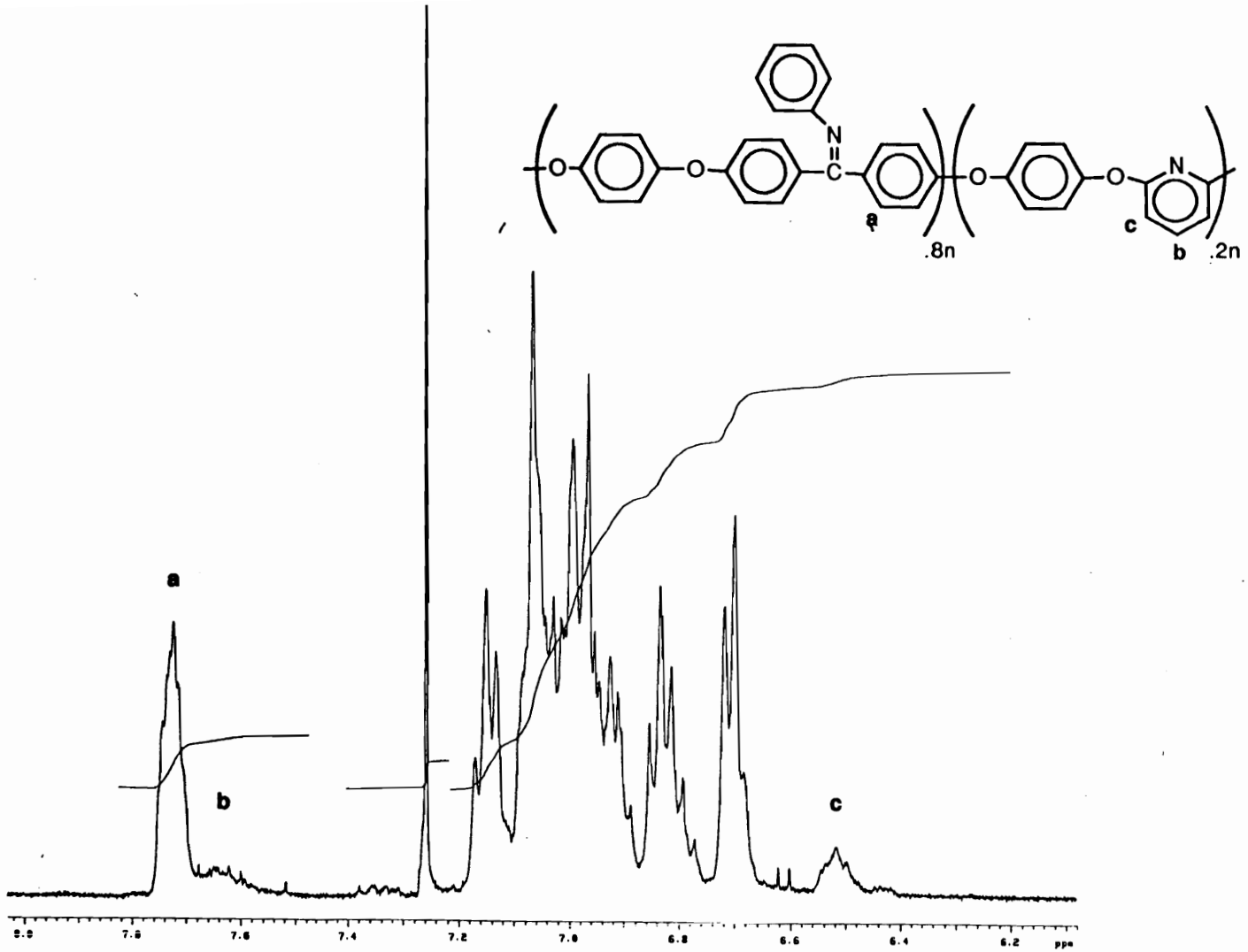

Figure 4.37: ^{1}H NMR of Poly((pyridine ether) - co - (ether ether ketimine)) Containing 20 Mole% Pyridine in $CDCL_3$

4.3.3 Hydrolysis of Poly((pyridine ether) - co - (ether ether ketimine)):

Once the copolymers had been synthesized, they were hydrolyzed from the ketimine to the ketone as previously discussed . Upon conversion to the ketone, the copolymers crystallized rapidly from solution in the form of fine particles. This hydrolysis procedure also protonates the pyridine moiety in the backbone and provides electrostatic stabilization to the particles when dispersed in water (Table 4.6). These particles were investigated both with an additional stabilizer (LaRC TPI Polyamic acid) and without. It was determined through particle size analysis that these particles were completely self stabilizing, as their size and distribution was identical in both cases. Interestingly, the smallest particles were formed from the polymer with the 20/80 pyridine to ketimine ratio (the middle composition), and are shown by SEM in Figure 4.38. It is hypothesized that this may be attributable to a combination of two opposing effects; increasing rates of crystallization with less pyridine units (note that 0% pyridine would be PEEK), but increased electrostatic stabilization with more pyridine. It seems that 20% pyridine is the best balance of these two factors.

Table 4.6: Particle Size Analysis of Hydrolyzed Copolymers

Mole % Pyridine	Median Diameter With no Stabilizer (μm)	Median Diameter With LaRC TPI PAA (μm)
0	flocculates	0.3
10	10.5	10.6
20	1.8	1.4
30	11.0	9.1

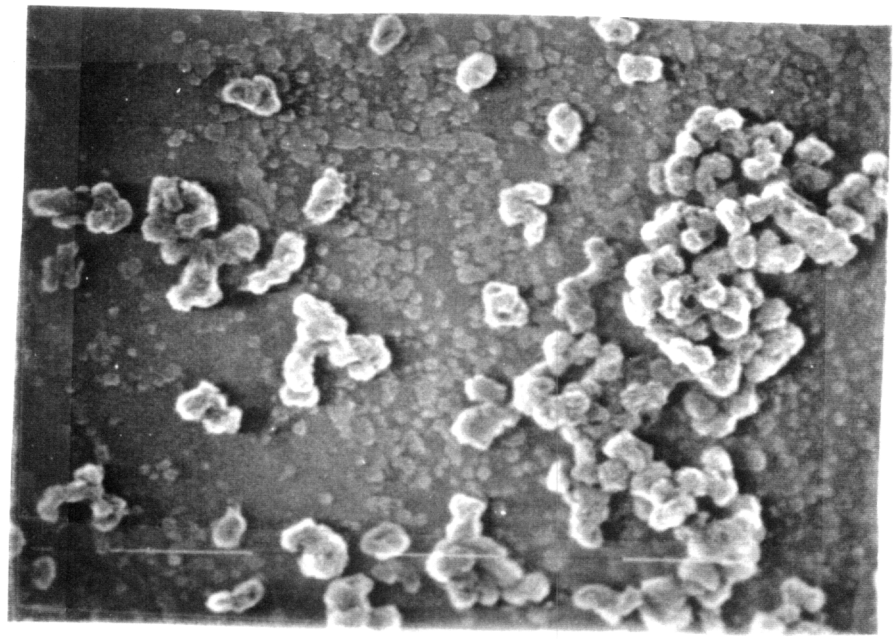

A

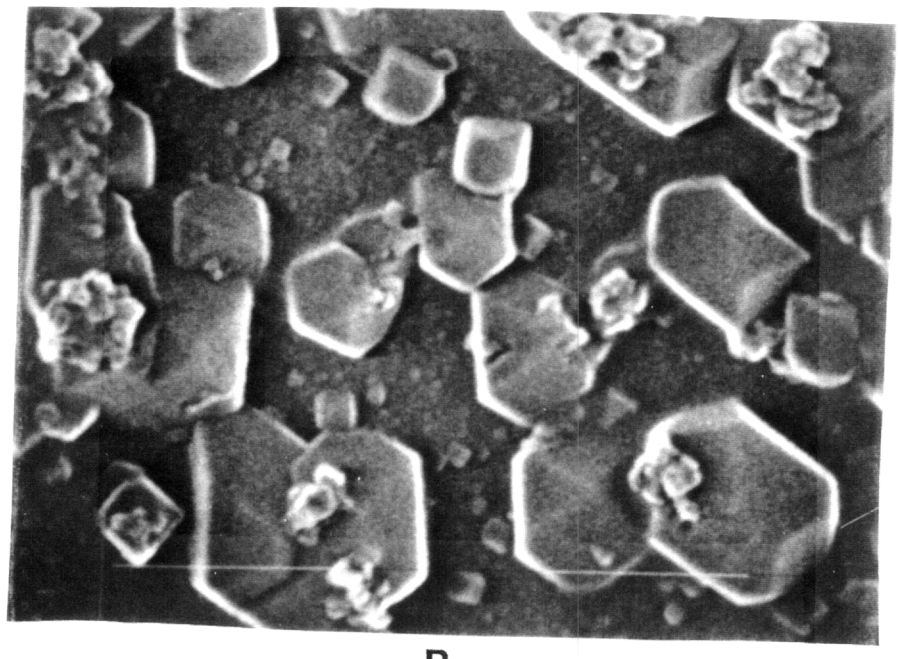

B

Figure 4.38: Scanning electron micrographs of poly((pyridine ether) - co - (ether ether ketimine)) containing 20 mole% pyridine: (A) Magnification = 3,200 with a 5 μm marker. (B) Magnification = 50,000 with a 0.5 μm marker.

Thermal properties of the poly((pyridine ether) - co - (ether ether ketone)) materials were probed using differential scanning calorimetry and thermal gravimetric analysis (Table 4.7). Importantly, even with significant levels of pyridine incorporated into the poly(arylene ether ketone) backbone, the polymers readily crystallized, and melting points remained high. An exemplary DSC scan for a 20 mole % pyridine copolymer is shown in Figure 4.39. This scan was obtained by heating at 10°C per minute after heating the sample to 350°C for three minutes and then quench cooling in the DSC at 200°C per minute. The Tg can be seen (127 °C) as well as the crystallization exotherm (≈ 160 °C) followed by the melting endotherm (316 °C). Additionally, significant weight loss was not apparent by dynamic TGA until temperatures in excess of 500°C were reached, Figure 4.40 shows a typical TGA scan for a 20 mole% pyridine copolymer run at 10°C per minute in an air atmosphere. These results are extremely significant, because as discussed in the introduction the stabilizer requirements are such that their thermal stability should be similar to PEEK. Another requirement of the stabilizer is that it be miscible with the matrix resin (PEEK). This was examined using the highest pyridine containing copolymer (30 mole %) by utilizing DSC. When the DSC was used to examine the glass transition temperature of a 50:50 blend of the 30 mole% pyridine copolymer with PEEK only one Tg was found, and it was an average of the individual values (Figure 4.41). This provides the evidence that the stabilizer is not only thermally stable, but also miscible with PEEK.

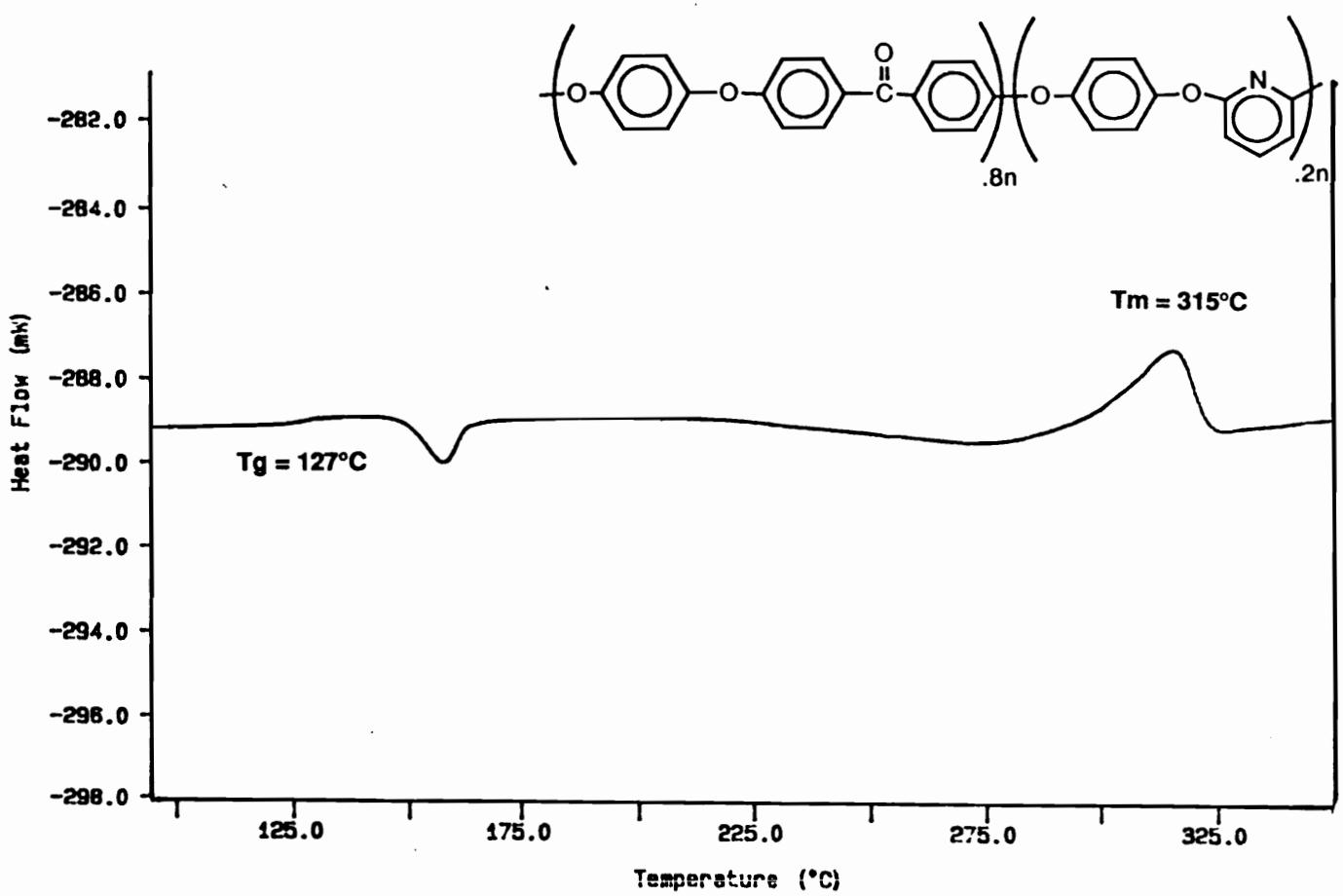

Figure 4.39: Differential Scanning Calorimetry of Poly((pyridine ether) - co - (ether ether ketone)) Containing 20 Mole% Pyridine: Heating Rate of 10°C per minute

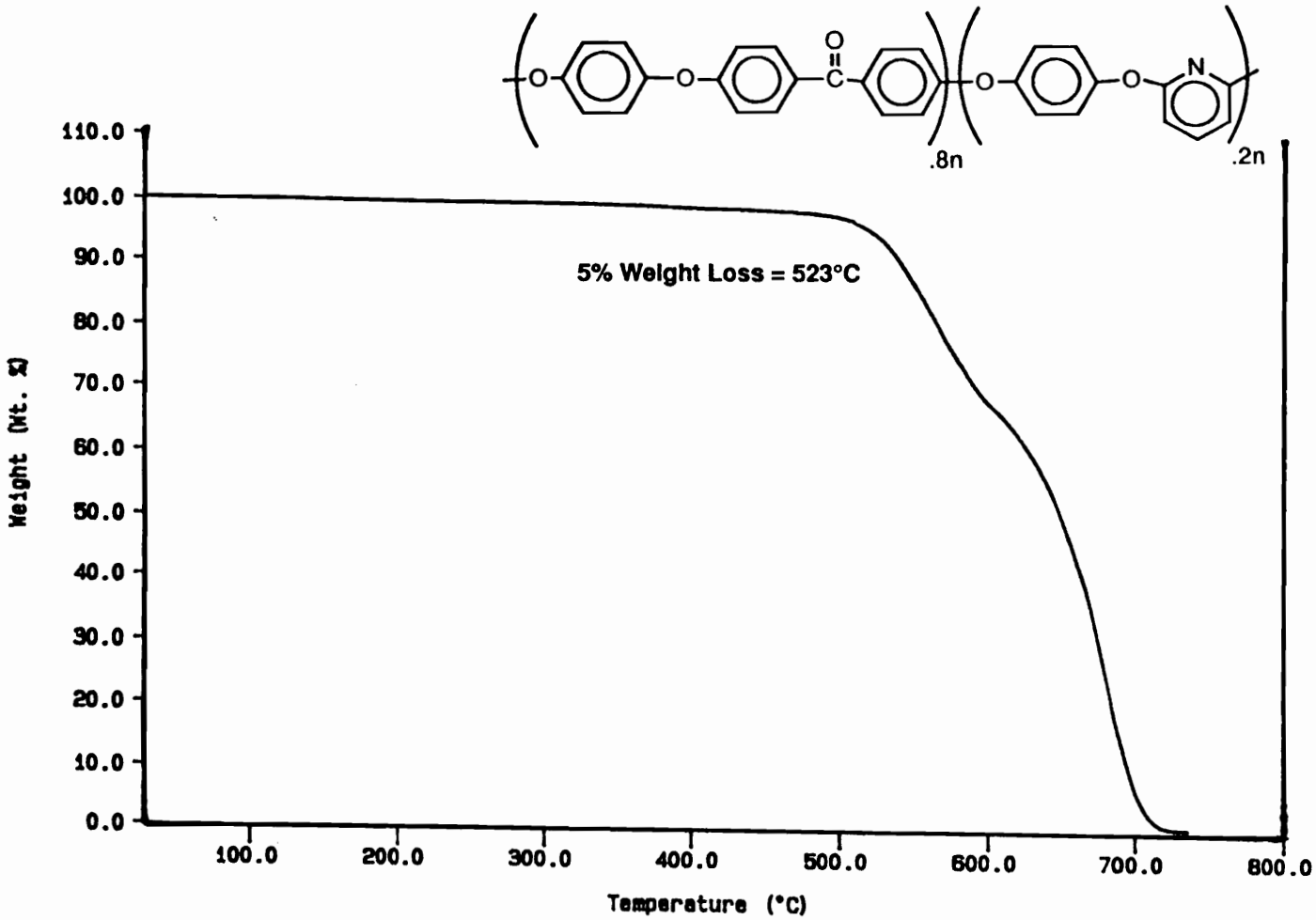

Figure 4.40: Thermal Gravimetric Analysis of Poly((pyridine ether) - co - (ether ether ketone)) Containing 20 Mole% Pyridine: Heating Rate of 10°C per minute Under a Air Purge

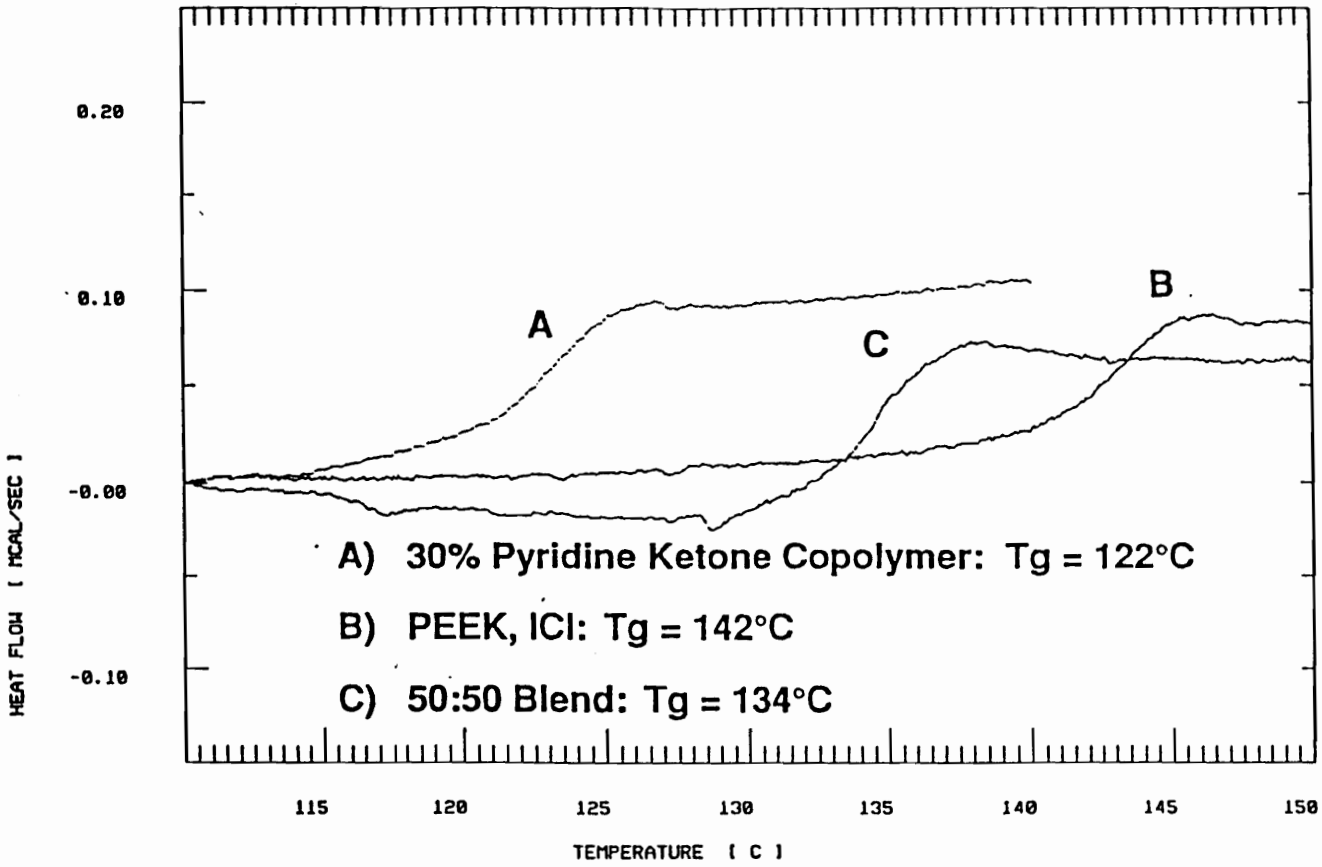

Figure 4.41: Differential Scanning Calorimetry Analysis to Determine the Miscibility of Poly((pyridine ether) - co - (ether ether ketone)) Containing 30 Mole% Pyridine with Poly(ether ether ketone)

Table 4.7: Thermal Analysis of Poly((pyridine ether) - co - (ether ether ketone))

Mole % Pyridine	Tg (°C)[a]	Tm(°C)[a]	5% wt loss (°C)[b]
0	143	335	574
10	126	330	543
20	127	316	526
30	121	300	523

a Determined from second heat at a rate of 10°C/min.
b Determined in air with a heating rate of 10°C/min.

4.3.4 Stabilization of Poly(ether ether ketone) particles:

One major interest in these polymers is their applicability as suspension stabilizers for preformed PEEK particles. Aqueous suspensions were prepared using a range of PEEK particle sizes (0.3, 15, 100 μm). This was done by preparing a solution of poly((pyridine ether) - co - (ether ether ketimine)) containing 20 mole% pyridine in NMP and adding the preformed PEEK particles. The ratio of stabilizer to PEEK particles was 10/90 by weight. This suspension was stirred for 24 hours to allow the stabilizer to adsorb onto the particle surfaces, then the copolymer stabilizer was acid hydrolyzed as done previously. After hydrolysis these particles were washed extensively with deionized water as described in the experimental section. After washing these particles were placed in deionized water (< 1 wt%) and sonicated, these particles formed a stable suspension. The larger PEEK particles (15 and 100 μm) settled out in a few hours, however upon agitation were easily re-suspended. The smallest PEEK particles (0.3 μm) formed a suspension that was stable for 3-5 days, but did eventually flocculate. The quality of the

suspension was also assessed by examining the particle size using the Shimadzu particle size analyzer. If the measured size was equivalent to the predetermined value (0.3, 15, or 100 μm) then a good suspension was assumed. For comparison, the same procedure was followed in the absence of the pyridine copolymer, and only flocculation occurred (Table 4.8).

Table 4.8: Particle Size Data for PEEK Particles

Predetermined Particle Size (μm)	Stabilizer	Measured Median Diameter (μm)
0.3	none	flocculates
0.3	LaRC TPI PAA	0.3
0.3	30% Pyridine Copolymer	1.1
15	30% Pyridine Copolymer	14.8
100	30% Pyridine Copolymer	100.5

After determining that poly((pyridine ether) - co - (ether ether ketone)) was thermally stable, miscible with PEEK, and an effective electrostatic stabilizer it was examined for feasibility in aqueous dispersion prepregging. For this model study three suspensions were made, one stabilized with poly((pyridine ether) - co - (ether ether ketone)), one with LaRC TPI PAA, and one with no stabilizer at all. Into each of these suspensions was dipped a short segment of carbon fiber tow, pulled out and allowed to dry. These tows were then qualitatively evaluated to see if the PEEK particles were binding to the fiber, and how well were they distributed. A photograph of all three samples is shown in Figure (4.42). In the absence of a stabilizer, the particles did not stick effectively to the fiber tow. The particles suspended with LaRC TPI PAA were

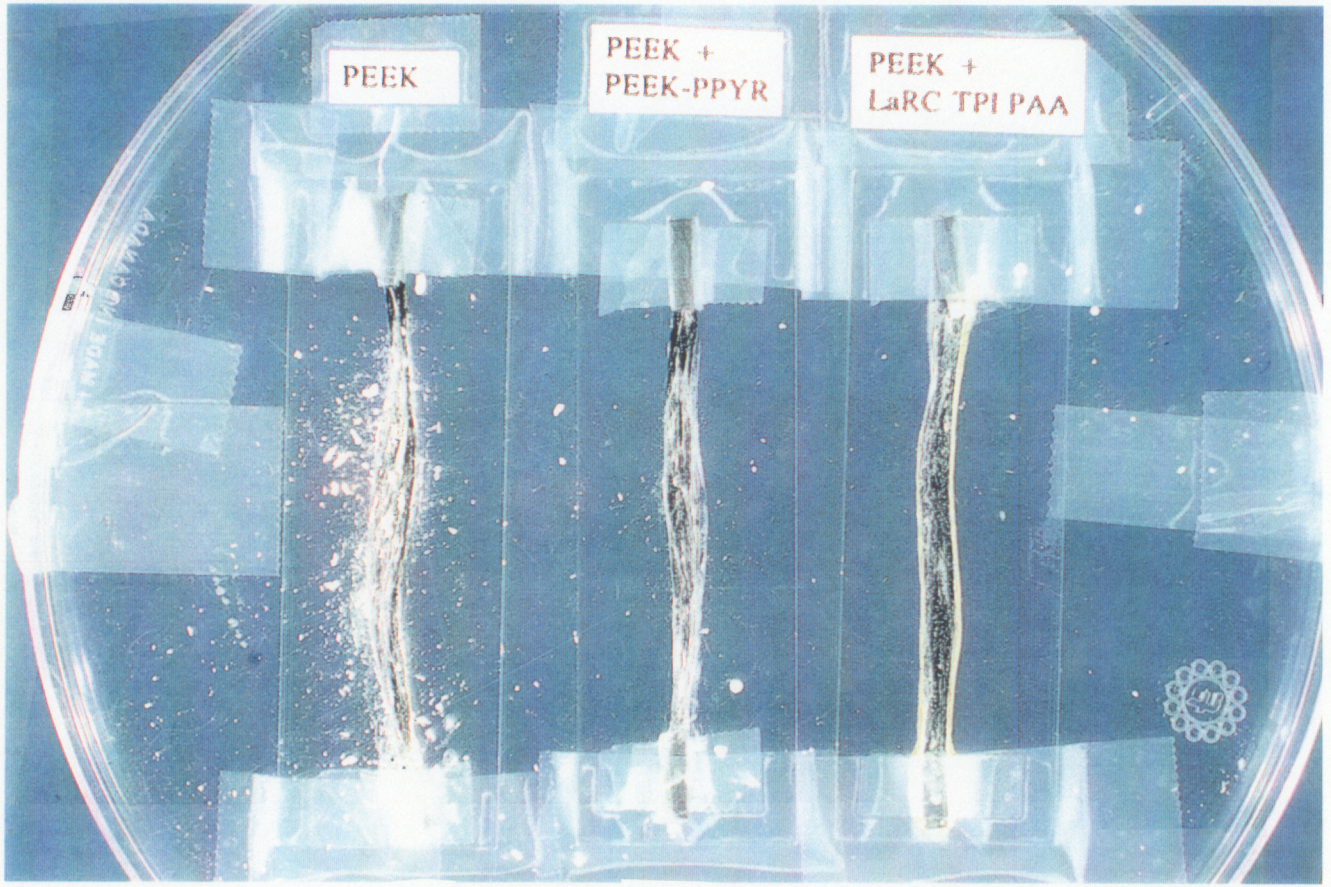

Figure 4.42: Photograph of Model Prepregs Comparing Stabilizers; A) 15 µm PEEK Particles with no Stabilizer, B) 15 µm PEEK Particles with Poly((pyridine ether) - co - (ether ether ketone)) Containing 20 Mole % Pyridine, C) 15 µm PEEK Particles with LaRC TPI PAA

bound to the fiber, however they were not actually evenly distributed but rather caked onto the fiber tow. This is because the ammonium salt of LaRC TPI PAA is water soluble and upon drying creates a film that covers the particles and holds them onto the graphite fiber. The poly((pyridine ether) - co - (ether ether ketone)) stabilized particles did bind to the fiber, not quite as effectively as with LaRC TPI PAA, but with a more even distribution. In contrast to LaRC TPI PAA, the poly((pyridine ether) - co - (ether ether ketone)) polymer is not water soluble and does not form a "binding film", but rather relies on specific interactions between the stabilizer and the carbon fiber to adhere the particles onto the fiber surface. These samples were also examined by ESEM (Figure 4.43) and again this showed that, although the LaRC TPI PAA stabilized sample had a large amount of particles on the fiber, they were in extremely large aggregates. These large aggregates should not have the beneficial processing advantages of being in the form of small particles. The ESEM confirms also that the poly((pyridine ether) - co - (ether ether ketone)) stabilized sample had individual particles binding to the fiber in a more even distribution.

Once the feasibility of using poly((pyridine ether) - co - (ether ether ketone)) as a stabilizer for aqueous dispersion prepregging was established the next step was to form prepregs utilizing this methodology. For these experiments a suspension of 15 μm PEEK particles was prepared using 5 wt% poly((pyridine ether) - co - (ether ether ketimine)) with 20 mole % pyridine in NMP. This suspension was treated with the acid hydrolysis procedure, washed thoroughly and then suspended in water. The suspension was then prepregged by Mr. Alvaro Ibarra-Gonzalez in the Chemical Engineering Department as part of his Master's Degree.[136] Upon consolidation

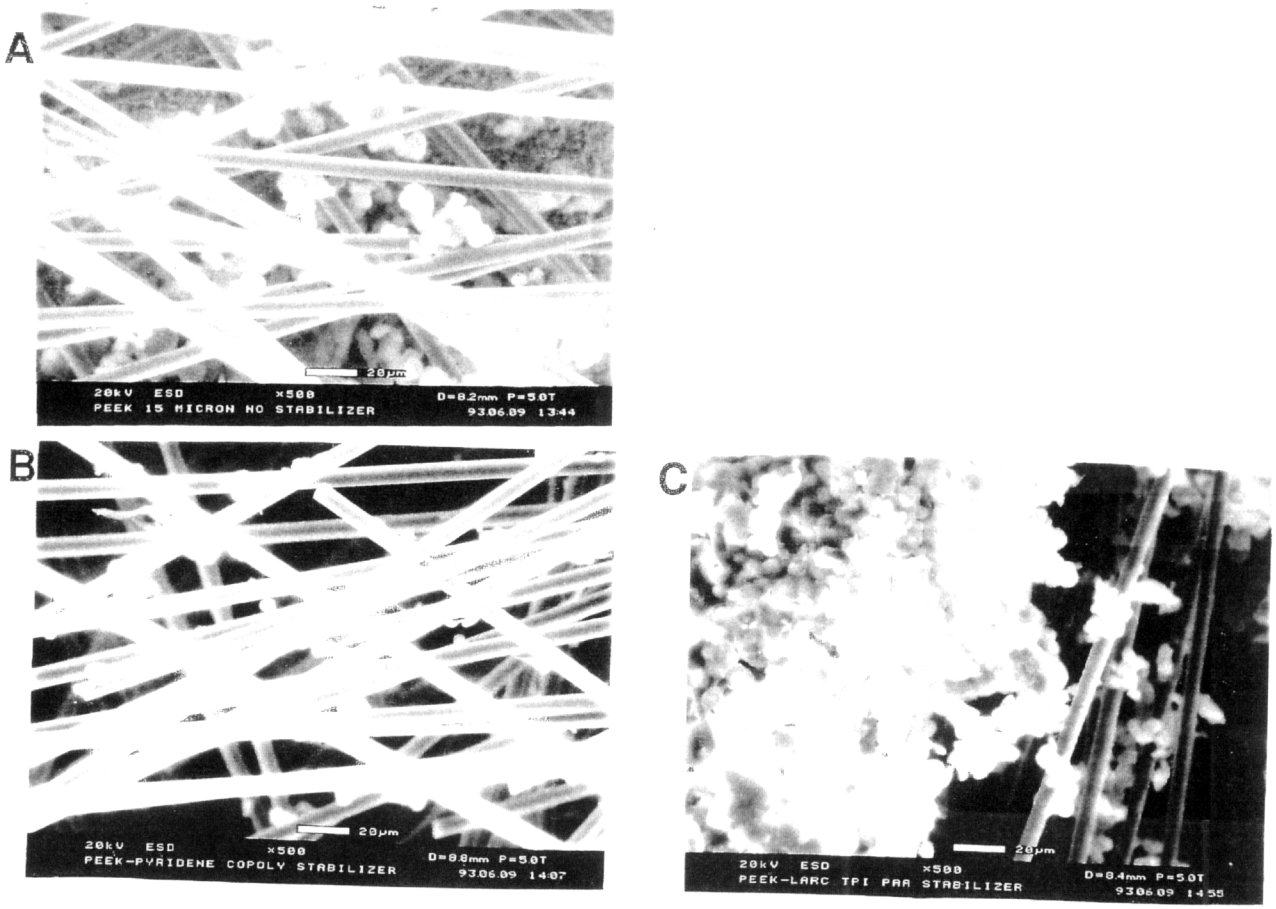

Figure 4.43: ESEM Analysis of Model Prepregs Comparing Stabilizers; A) 15 µm PEEK Particles with no Stabilizer, B) 15 µm PEEK Particles with Poly((pyridine ether) - co - (ether ether ketone)) Containing 20 Mole% Pyridine, C) 15 µm PEEK Particles with LaRC TPI PAA

Mr. Gonzalez noted by optical microscopy that the composites contained a significant void fraction (Figure 4.44). This was theorized as being due to a high melt viscosity under the processing conditions, which was confirmed by a melt rheology study comparing the stabilized particles to pure PEEK particles at 370°C (Figure 4.45). This data indicates that the stabilized particles do indeed have a higher melt viscosity than PEEK at 370°C. Also compared is LaRC TPI PAA stabilized particles. These particles also have a higher melt viscosity than neat PEEK, however it is low enough for effective consolidation. The high melt viscosity of the pyridine stabilized particles is believed to be due to the fact that the poly((pyridine ether) - co - (ether ether ketone)) stabilizer is an ionomer, since the pyridine moieties are protonated. This results in physical crosslinking and therefore a higher viscosity. This suspension was made using 5 wt% stabilizer, and therefore it is reasonable to anticipate that if the concentration of the stabilizer is minimized, the viscosity can be reduced to an acceptable and processable value. Therefore a series of suspensions were made with systematically varied weight concentrations (0.5, 1, 2.5 wt %) of poly((pyridine ether) - co - (ether ether ketone)). These suspensions were evaluated using the Shimadzu particle size analyzer and their distributions are reported in Figure 4.46. The maximum particle size in these suspensions was previously determined to be 20 μm, and therefore if any particles are measured as larger than 20 μm, this must be due to aggregation. The suspension prepared with only 0.5 wt% stabilizer did show significant amounts of aggregation However, with only 1 wt% stabilizer these aggregates were not present. It is therefore proposed that using 1 wt% poly((pyridine ether) - co - (ether ether ketone))

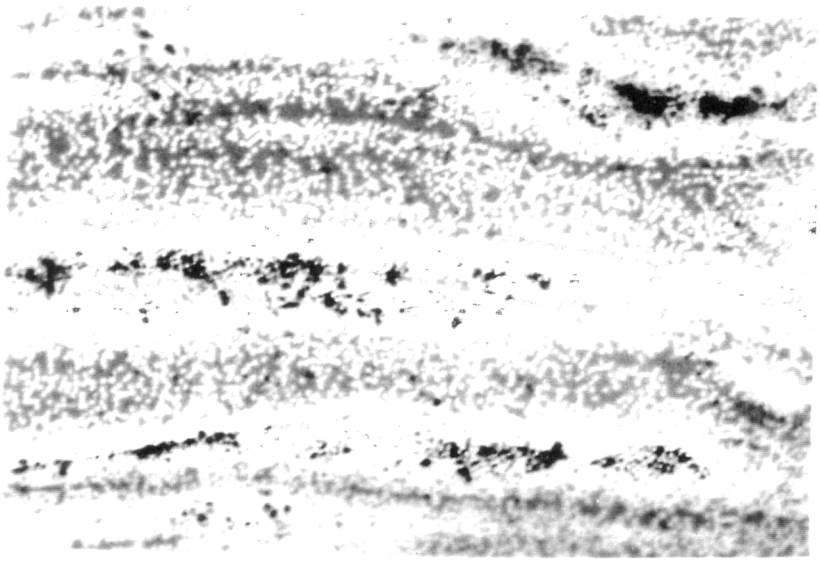

A

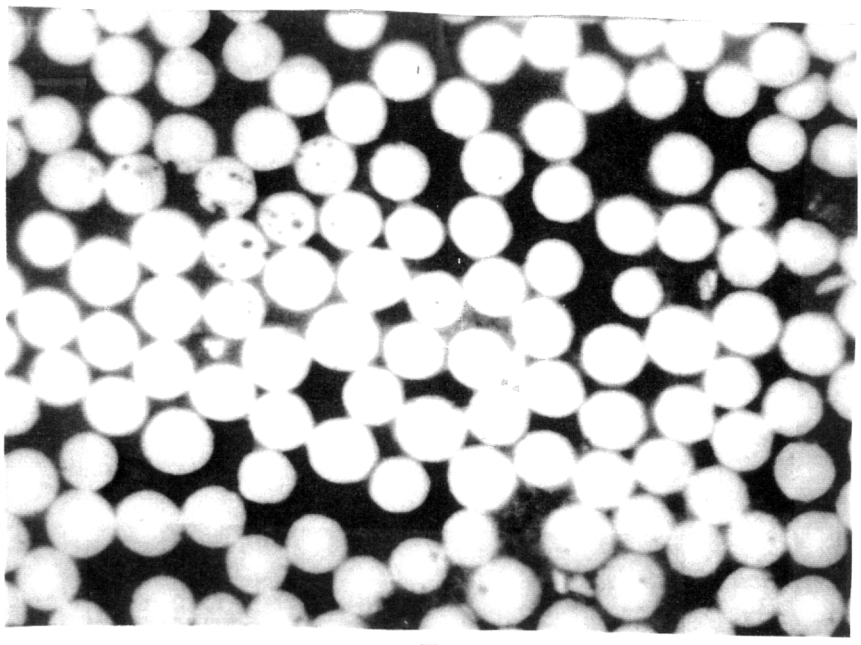

B

Figure 4.44: Optical micrographs of composites made by aqueous suspension prepregging utilizing 5 wt % poly((pyridine ether) - co - (ether ether ketimine)) containing 20 mole% pyridine as a stabilizer: (A) Magnification = 100. (B) Magnification = 1,000. The scale is represented by the average fiber diameter of 7 μm.

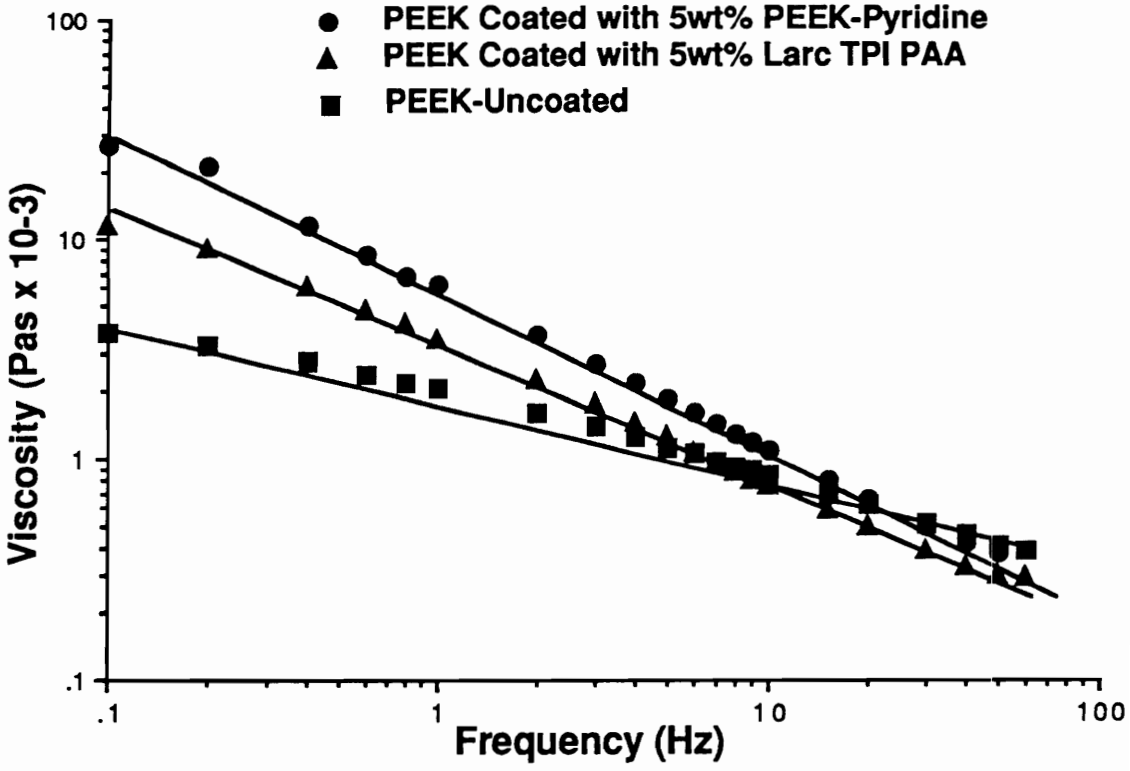

Figure 4.45: Melt Viscosity of Stabilized PEEK Particles at 370°C as a Function of Frequency

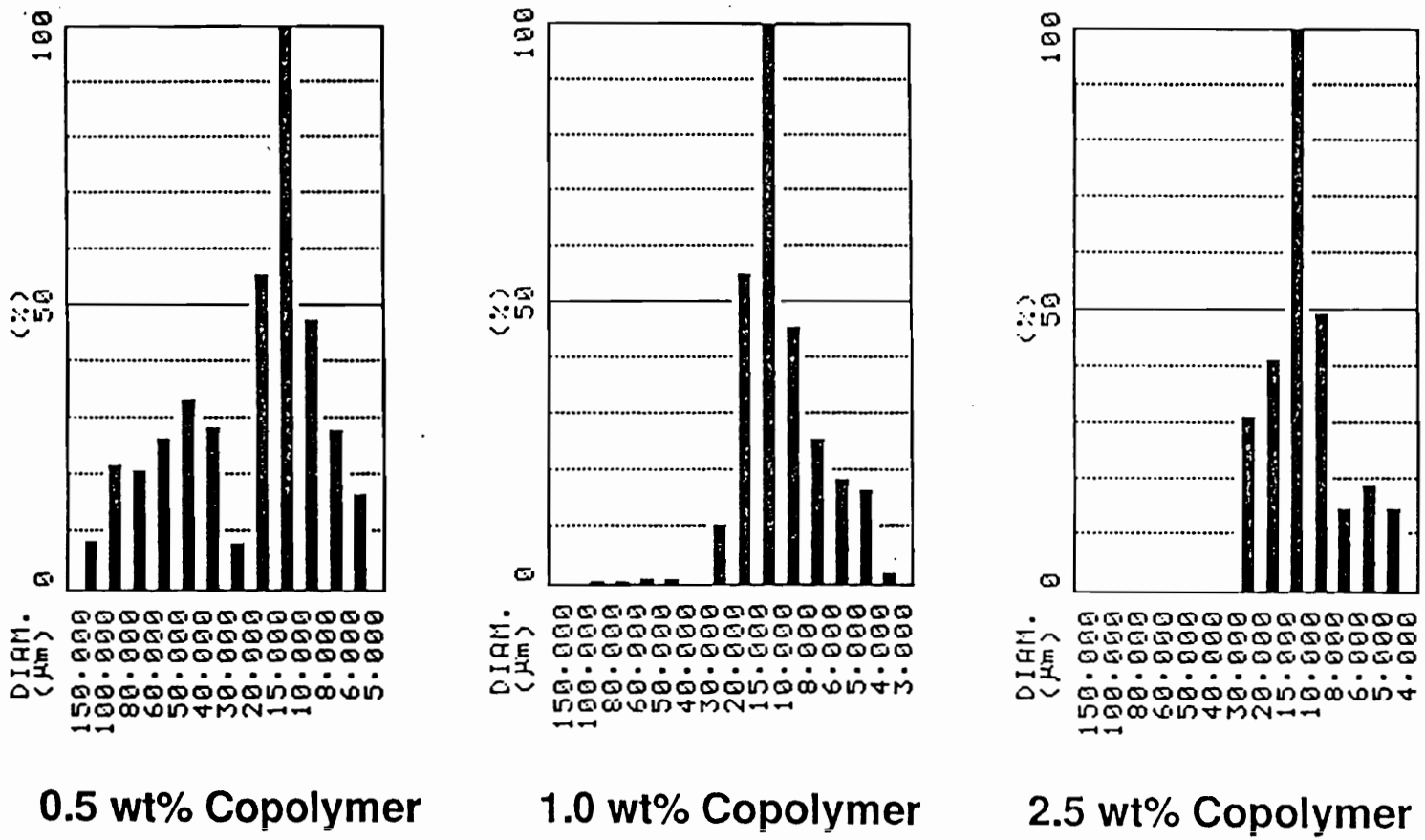

Figure 4.46: Particle Size Distribution Analysis of 15 µm PEEK Particles as a Function of Wt % Poly((pyridine ether) - co - (ether ether ketone)) Stabilizer Containing 20 Mole% Pyridine

should be an effective stabilizer for aqueous suspension prepregging, and allow for consolidation of the final composite.

4.4 Sintering Poly(ether ether ketone) Powders

4.4.1 Introduction:

Poly(ether ether ketone) (PEEK) is a high performance semicrystalline thermoplastic with a glass transition temperature of 143°C. The Tm is often quoted as 334°C but the equilibrium melting point is significantly higher (384°C).[106] Due to its high thermal transitions PEEK requires high temperatures for processing, at least 370 - 400°C. It has been determined that under the recommended processing conditions PEEK undergoes branching and eventually crosslinks, as previously discussed. An alternative to melt processing PEEK is to apply the powder metallurgy technique of sintering. This involves cold (room temperature) compaction of the polymeric powder, followed by pressure free sintering of the resultant green body. This procedure is not new for polymeric powders, as discussed in the Literature Review. In polymer powder sintering studies a particle size of less than 100 μm was required and a free sintering temperature above the polymer glass transition temperature, or the melt temperature for the semicrystalline polymers, was necessary. These polymer sintering temperatures relative to the material transition temperatures are high compared to temperatures normally employed for metal and ceramic sintering. Ceramic sintering is conducted at temperatures less than the absolute melting point of the material. However, particle sizes reported in polymeric powder sintering are large compared to the submicron particles often

used for ceramics and metals.[97] Since sintering occurs due to a reduction of surface free energy, smaller particles (larger surface area) have larger driving forces for sintering. Thus the relatively high temperatures required for polymeric systems could be explained by the large particles used thus far. It should also be noted that organic materials in general have lower surface free energies than metals, and this also lowers the driving force for sintering. The previous sections discussed a process for preparing submicron PEEK particles, and the focus of this section is on the free sintering of these particles with emphasis on the effects of particle size, sintering temperature and compaction pressure. The data is evaluated using the two particle model developed by Frenkel[103], derived in the Literature Review,

$$\frac{X^2}{a} = \frac{3}{2}\frac{\gamma}{K}t \qquad (4.1)$$

where γ is the surface free energy, t is time, and K is a measure of mobility in a power law fluid (4.2).

$$\sigma = K(\dot{\varepsilon}_s)^n \qquad (4.2)$$

Equation (4.1) can be used qualitatively to predict the effect of material parameters such as particle size, surface free energy and melt viscosity on sintering rate (i.e., the time required for X/a = 1). This equation has been verified for sintering glass[105] and poly(methylmethacrylate) spheres[104]. The crack healing theory developed by Wool[116-118] , which is based on the reptation theory of de Gennes[121] and Doi and Edwards[123] will also be discussed.

4.4.2 Dilatometry Sintering Studies:

Preliminary studies were conducted on 15 μm diameter PEEK particles to evaluate the behavior of PEEK particles under free sintering conditions. These particles were first cold pressed as described in the experimental section, forming a green body with sufficient strength to withstand normal handling. This green body was heated in a dilatometer at 3°C/min., and the change in sample length with temperature was recorded. A slight downward curvature in the thermal expansion curve just above Tg resulted (Figure 4.47), indicating that densification had begun. Under these conditions, densification began to take place at a significant rate at ≈ 313°C. It is interesting to note that 313°C is above the onset of melting (303°C) as determined by DSC at 1°C/min. but still substantially below the peak melting temperature of 345°C (Figure 4.48). A melt processed control sample (prepared by heating a cold pressed sample above the melt (380°C) under low pressure for 30 min.), experiencing identical conditions, showed no downward curvature or densification (Figure 4.49). Careful examination of the sintered sample revealed that heating was not uniform. Thus, the heating rate for further studies was decreased to 0.5°C/min. which provided uniform samples.

A series of samples (particles of 120, 93.7, 59.7, 42.6, 34.8, 15, and 0.30 μm median diameter) were compacted at 100 MPa and sintered to determine the effect of particle size on densification (see Table 4.9 and Figure 4.50). Sintering conditions involved a heating rate of 0.5°C/min. to 313°C, then holding at 313°C for 300 min. (313°C represents the onset of significant densification in the dynamic studies). A particle size of 15 μm or less was

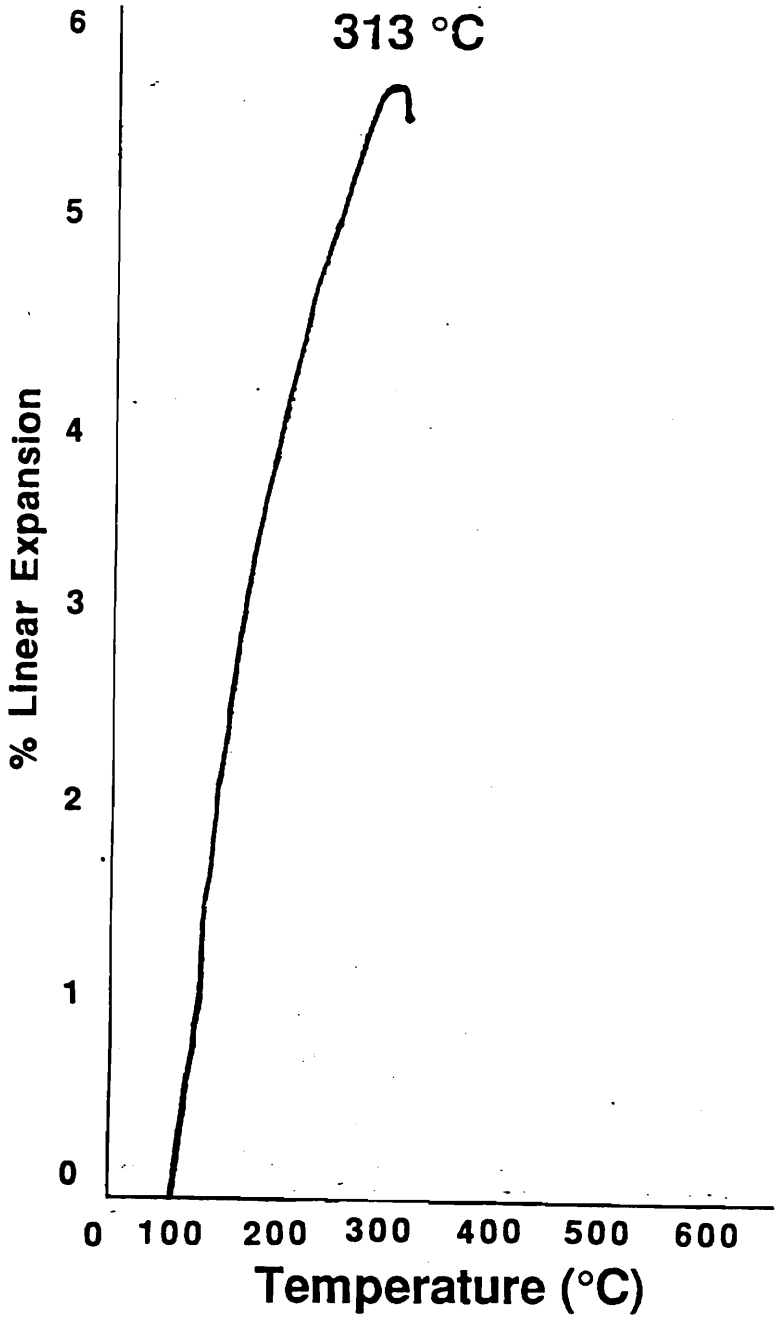

Figure 4.47: Dynamic Dilatometry Results of 15 µm PEEK Particles Compacted at 100 MPa with a Heating Rate of 3°C per minute

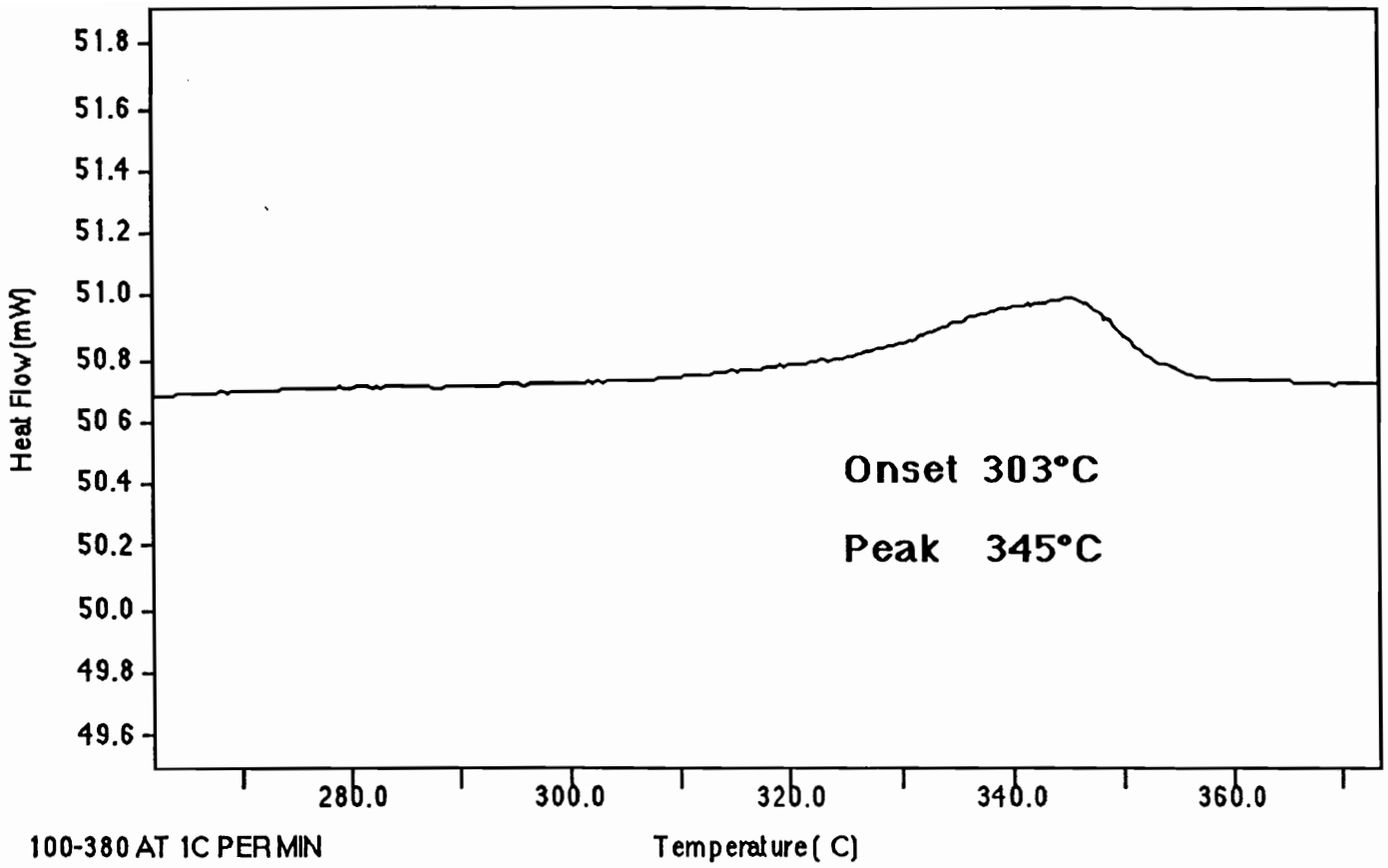

Figure 4.48: Differential Scanning Calorimetry of 15 µm PEEK Particles, First Heat at 1°C per Minute

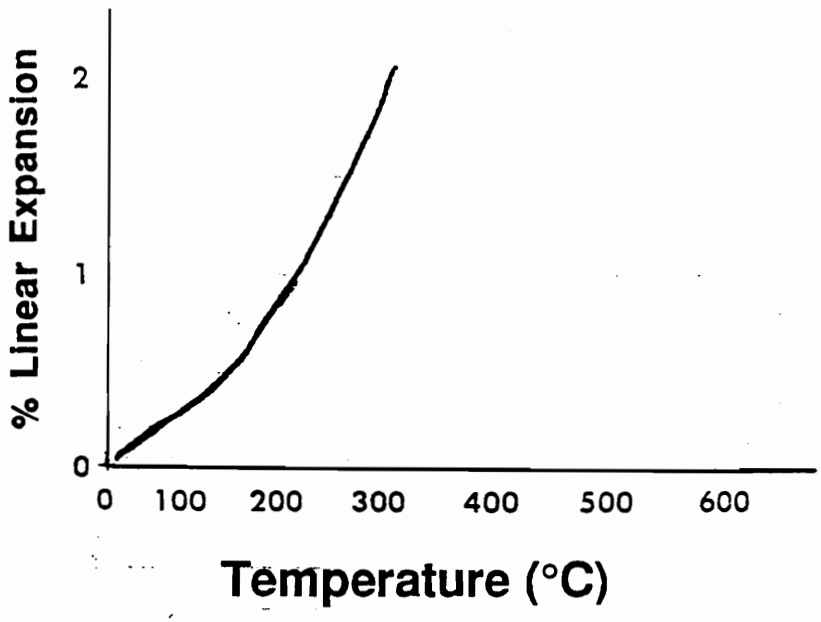

Figure 4.49: Dynamic Dilatometry Results of Melt Processed PEEK Control; Heating rate of 0.5°C per minute and Held at 313°C for 60 minutes

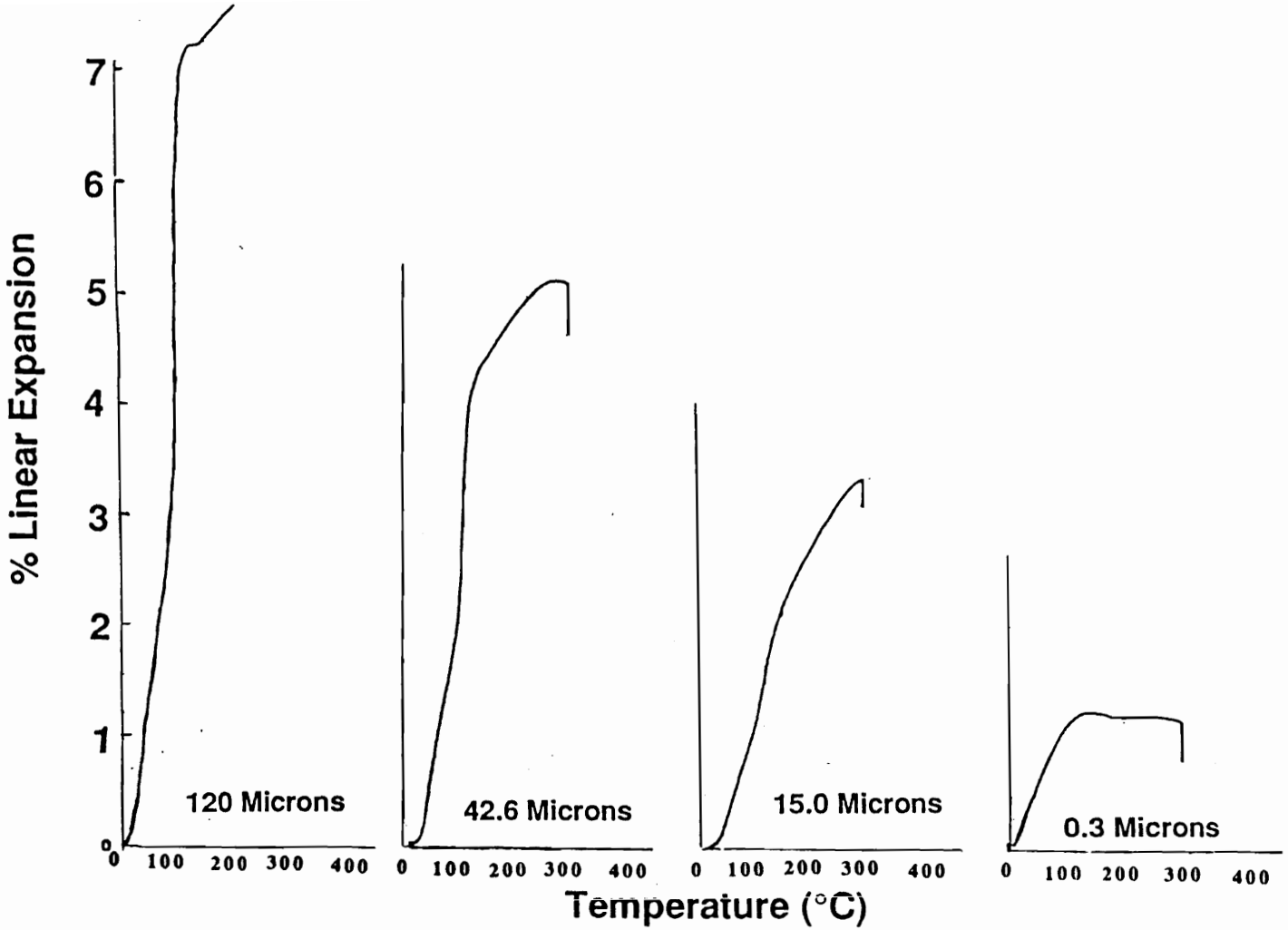

Figure 4.50: Dilatometry Results Showing the Effect of Particle Size on the Densification of PEEK Powders (Compact Pressure = 100 MPa, Heating Rate = 0.5°C/min., Held at 313°C for 300 min.)

required for densification of the green bodies under these conditions. A significant difference in sintering rates at low temperatures using submicron particles is evident (Figure 4.50). The 0.3 μm particles began densifying at a significant rate just above Tg, but did not sinter to the bulk density of PEEK (1.3 g/cm^3) under these conditions. Since degree of crystallinity can affect density and also mobility of the polymer chains, it is important to note that both the 15 and 0.3 μm particles had essentially identical degrees of crystallinity (≈ 30%) as determined by DSC (Figure 4.51) and WAXS (Figure 4.52). Since the driving force for sintering is reduction of surface free energy, smaller particles have a stronger driving force to sinter due to their relatively higher surface area.

Table 4.9: Effect of Particle Size on Densification

Particle Size (μm)	Green Density (g/mL)	Sintered Density (g/mL)	% Change
120	1.10	0.97	-11.8
93.7	1.10	1.01	-8.18
59.7	1.10	1.03	-6.36
42.6	1.07	1.04	-2.80
34.8	1.06	1.03	-2.83
15.0	1.08	1.10	+1.85
0.3	1.10	1.13	+2.73

The effect of sintering temperature was investigated using the 15 μm particles using a compaction pressure of 100 MPa and a heating rate of 0.5°C/minute. All samples were held at the sintering temperature (250, 280, 300, 307, or 313°C) for 300 min. (Table 4.10).

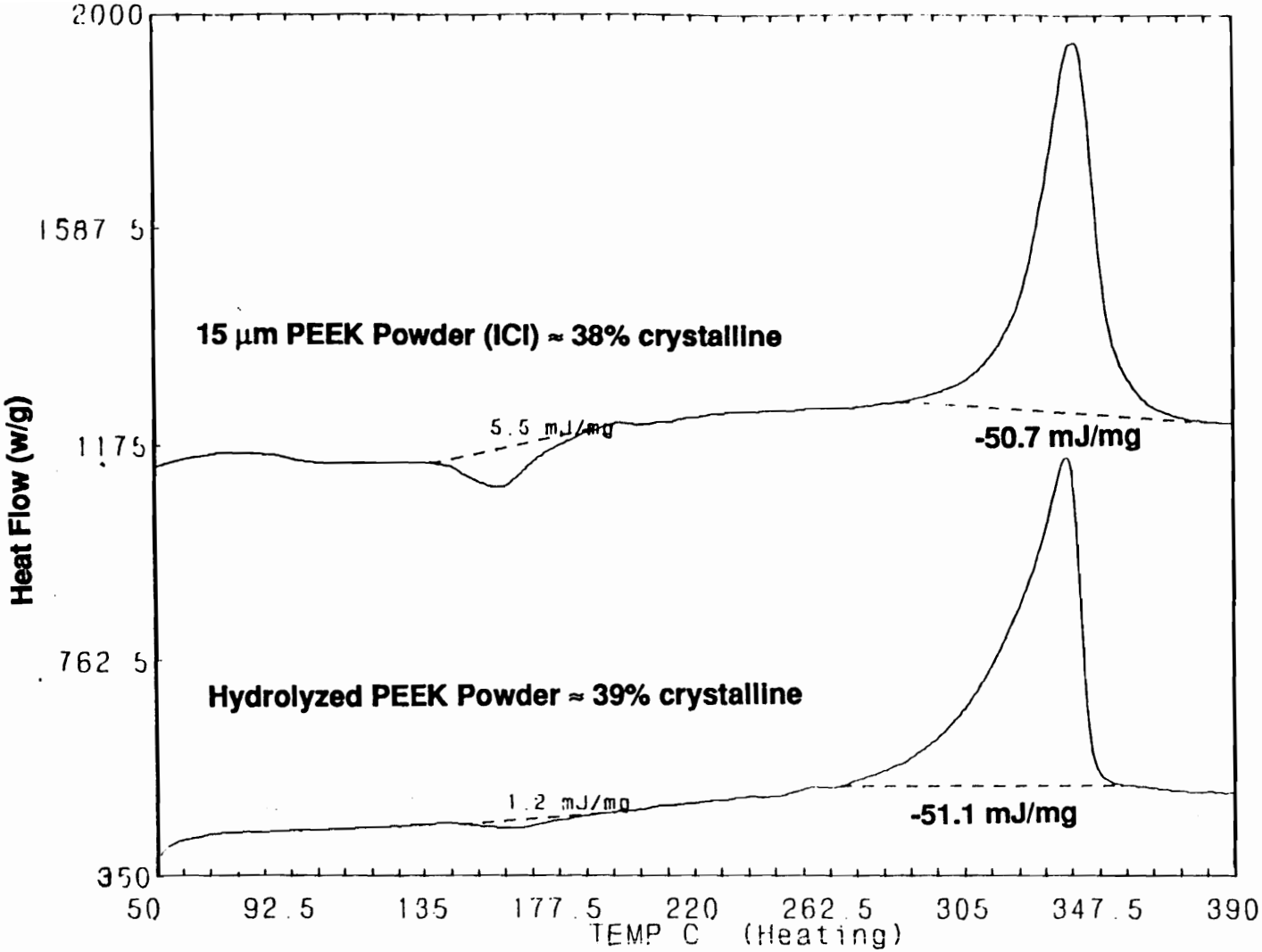

Figure 4.51: Differential Scanning Calorimetry Analysis to Compare the % Crystallinity Between 15 µm PEEK Particles Provided by ICI and 0.3 µm PEEK Particles Synthsized From PEEKt Hydrolysis; Heating Rate of 20°C per minute

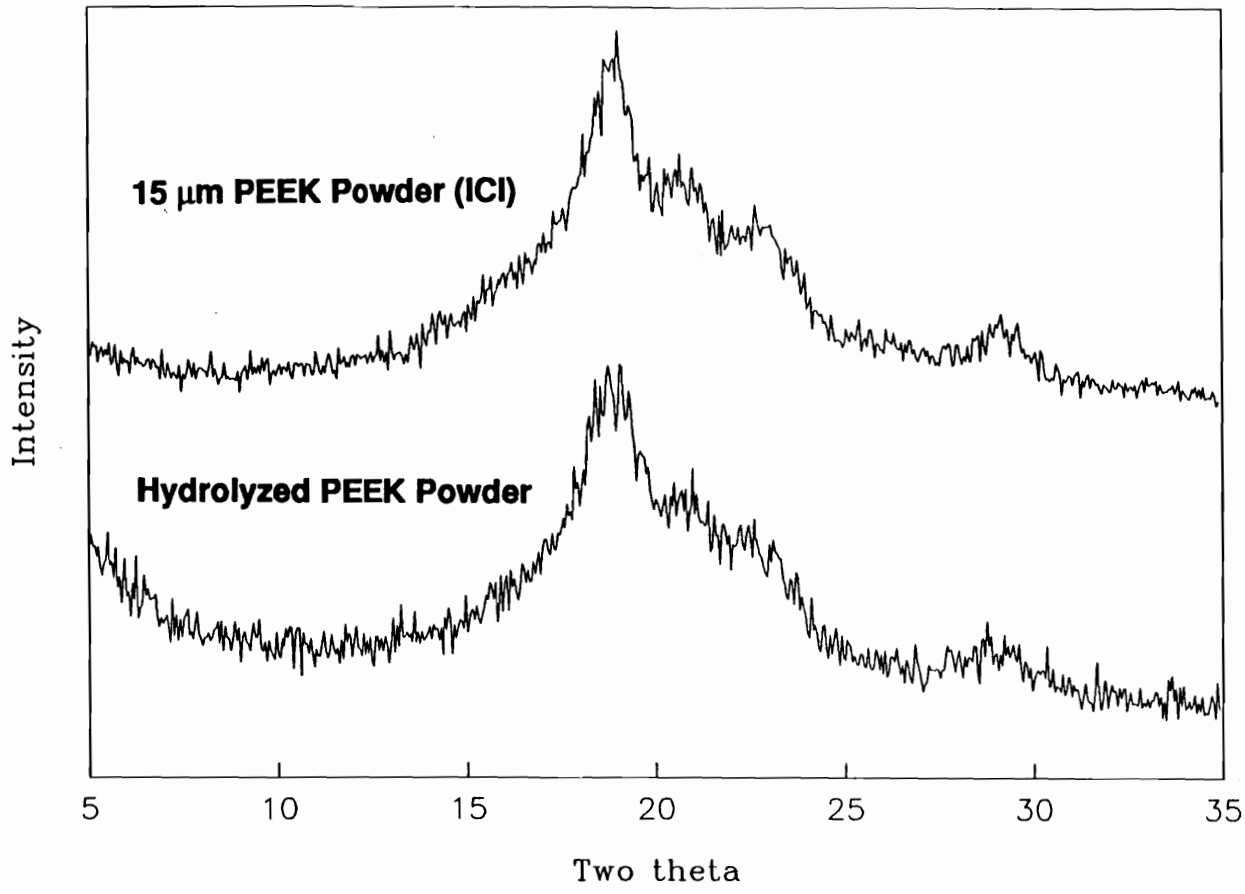

Figure 4.52: WAXS Analysis to Compare the % Crystallinity Between 15 µm PEEK Particles Provided by ICI and 0.3 µm PEEK Particles Synthsized From PEEKt Hydrolysis

Table 4.10: The Effect of Temperature on Densification

Temp. (°C)	Green Density (g/mL)	Final Density (g/mL)	% Change
250	1.00	0.97	-3.2
280	1.04	1.03	-1.0
300	1.03	1.03	0.0
307	1.07	1.08	+0.9
313	1.08	1.10	+1.85

Under these conditions, 15 μm particles required a temperature of greater than 300°C for densification. Again it is noteworthy that this is slightly above the onset of melting. This suggests that at least for 15 μm and larger diameter particles, some of the crystals must melt to provide enough mobility for sintering to occur.

Compact pressures from 33 MPa to 333 MPa were investigated (Table 4.11) using 15 μm powders. A heating profile of 0.5°C/min. to 313°C and then held for 300 minutes was employed. With the exception of the first and last entries in Table 4.11, as the compaction pressure was increased, the % change

Table 4.11: Effect of Compact Pressure on Densification

Compact Pressure (MPa)	Green Density (g/mL)	Final Density (g/mL)	% Change
33	0.83	0.85	+1.6
50	0.90	0.93	+3.3
100	1.08	1.10	+1.85
150	1.11	1.13	+1.80
200	1.14	1.12	-1.80
333	1.22	1.22	0.0

in density decreased. This is reasonable since higher compact pressures result in denser green bodies and therefore allow less room for change. Also a higher compact pressure forces the particles closer together resulting in an increased frictional force reducing the particle mobility.[97] However, as compact pressure was increased, the final density increased as well except for the samples compacted at 200 and 333 MPa.

The driving force for sintering can also be described as a pressure excess. The pressure inside a spherical droplet exceeds that of its surroundings by ΔP. This pressure excess is dependent on the radius of curvature, and therefore the pore diameter (d) as expressed by the following equation[97]:

$$\Delta P = \frac{4\gamma_{LV} Cos\theta}{d} \qquad (4.3)$$

where γ_{LV} is the liquid-vapor surface energy and θ is the liquid - solid contact angle. As pore diameter decreases, ΔP increases. With the lowest compaction pressure we believe the pores were not small enough (the particles were not pressed close enough together) to create a large ΔP and therefore less sintering resulted. The highest compaction pressure, 333 MPa, resulted in a green density of 1.22 g/mL. By contrast, we believe this is so compact that no change in density could occur due to the large frictional force between particles reducing their mobility. This prevented even the swelling which was evident in the sample compressed at 200 MPa. Swelling is caused by the expansion of internal pores upon heating being greater than densification due to sintering.

The sample compressed at 333 MPa had very low porosity as indicated by the high green density.

An attempt was made to view the sintering process directly in the ESEM utilizing a hot stage. This allowed one to heat the cold pressed samples up while viewing in real time on the ESEM. Utilizing this procedure resulted in several complications, however. The first of which was that the electron-beam in the ESEM caused crosslinking of the PEEK sample at elevated temperatures, and therefore the sintering could not be viewed continuously. This was solved by heating the sample in the ESEM and only focusing the electron beam for seconds to take pictures as a function of time. This process did allow the viewing of the sintering of 15 μm PEEK particles at 313°C as a function of time (Figure 4.53). However, when compared to results from a similar experiment where the sample was heated in a convection oven at 313°C for the same period of time (one hour) (Figure 4.54) very different results were obtained. In the convection oven essentially no sintering took place under these conditions, however, in the ESEM almost complete sintering occurred. It is believed that the electron-beam first causes chain cleavage at low exposure times to the radiation, followed by crosslinking if the exposure is continued. For this reason the experiment in the ESEM was probably breaking up the PEEK chain allowing for faster sintering.[137] After learning the hazards of sintering in the ESEM, other studies were conducted by viewing samples in the ESEM at room temperature which had previously sintered in a convection oven.

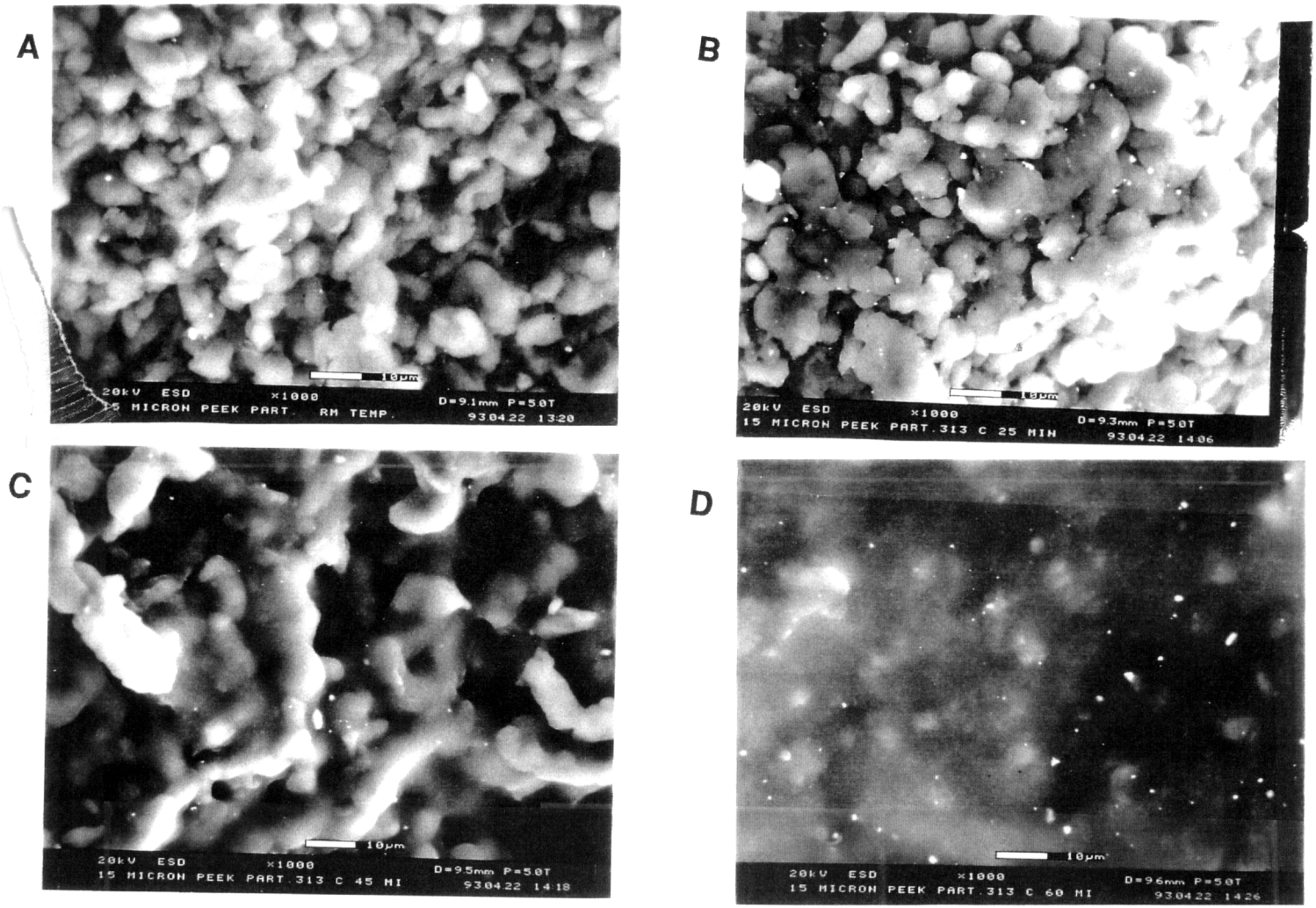

Figure 4.53: The Sintering of 15 µm PEEK Particles in the ESEM; A) Room Temperature, B) 313°C 25 min., C) 313°C 45 min., D) 313°C 60 min. All Photgraphs are at 1000 X Magnification with a 10 µm Marker Displayed

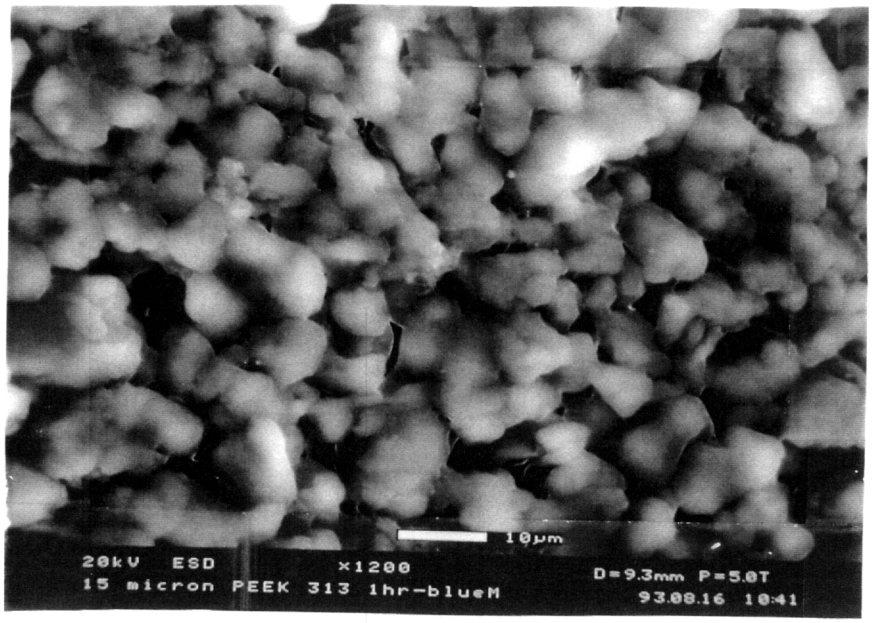

A

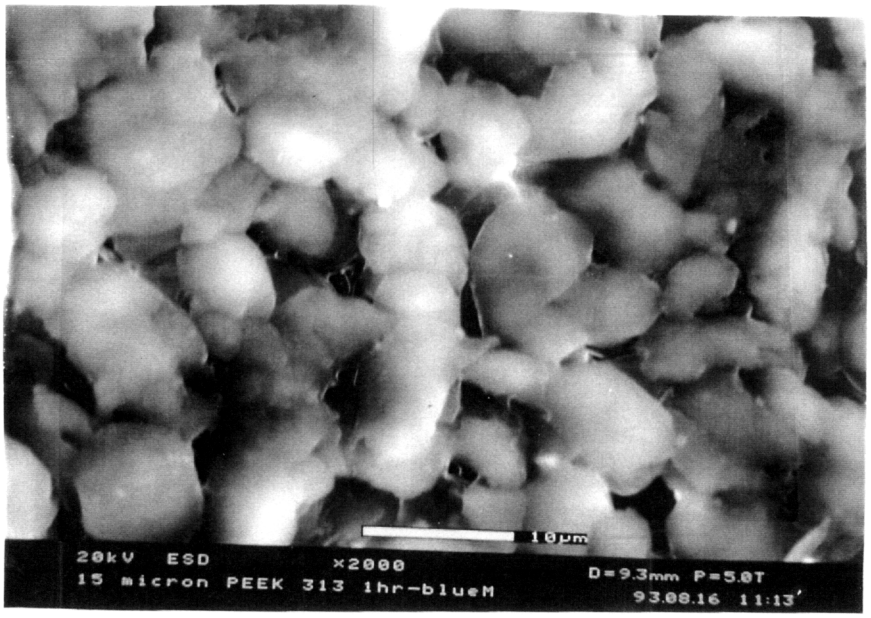

B

Figure 4.54: ESEM Photomicrographs of Presintered (313°C, 60 min.) 15 µm PEEK Particles; A) 1200 X Magnification (10 Mm Marker), B) 2000 X Magnification (10 µm Marker)

4.4.3 Development of Mechanical Integrity by Sintering:

The development of mechanical properties, namely yield strength, and density were examined as a function of sintering time, temperature and particle size. The 15 μm particle samples were prepared as described in the experimental section and sintered as a function of time and temperature (Table 4.12). For this study, temperatures within the melting range of PEEK were investigated in hopes of achieving densities equivalent to bulk PEEK in reasonable time periods.

Table 4.12: Development of Mechanical Integrity During Sintering for 15 μm PEEK Particles

Sintering Temp. (°C)	Time (min.)	Yield Stress (MPa)	%Strain break	Density (g/mL)
Control*	—	100	50	1.3
380	12	101	34	1.29
360	30	100	187	1.31
360	20	98	28	1.29
360	15	83**	4.4	1.27
350	30	87**	4.2	—
350	15	80**	7.1	1.3

* Values obtained from Nguyen, et al.[73]
** These Samples Underwent Brittle Failure

At 380°C, without applied external pressure, mechanical properties comparable to melt processed PEEK result within 12 minutes. When the temperature is lowered to 360°C, 20 min. are required to reach equivalent properties, and at 350°C, even 30 min. was not sufficient to obtain a ductile material. It is interesting to note that although sintering at 350°C for 30 min. did not provide

the desired mechanical integrity, the density achieved was essentially that of bulk PEEK. This is believed to result from slow diffusion on the molecular level across the grain boundary between particles in contact. Frenkel's theory addresses the relative time required to achieve intimate contact between the particles, thus minimizing the surface free energy. It does not treat polymer diffusion across the grain boundaries, which is required to reach good mechanical properties. ESEM can also be used to examine the changing morphology of the sintering samples. For example, the grain boundary disappears in a 15 μm PEEK particle sample being sintered at 360°C as a function of time (Figure 4.55). The disappearance of the grain boundary, incidentally, also correlates very well to the development of bulk mechanical properties, providing support to the explanation that molecular diffusion across the grain boundary is required for good mechanical integrity.

The effect of particle size was examined by comparing 120, 15, and 0.3 μm diameter particles compacted at 100 MPa and then sintered at either 380 or 360°C for systematically varied times (Table 4.13). Entries 2 through 5 in Table 4.13 comparing the 120 μm particles to the 15 μm particles illustrate the beneficial effect of smaller particle size under sintering conditions. Under both sets of conditions, the 15 μm particles exhibited yield strengths essentially equivalent to the control whereas the samples prepared from 120 μm particles were so brittle that they could not be tested (they failed while cutting out the dogbones). A comparison of 15 μm to 0.3 μm particles, however, did not exhibit the expected trend. This was attributed to sample preparation, and not to a consequence of particle size. The submicron PEEK particles were prepared via

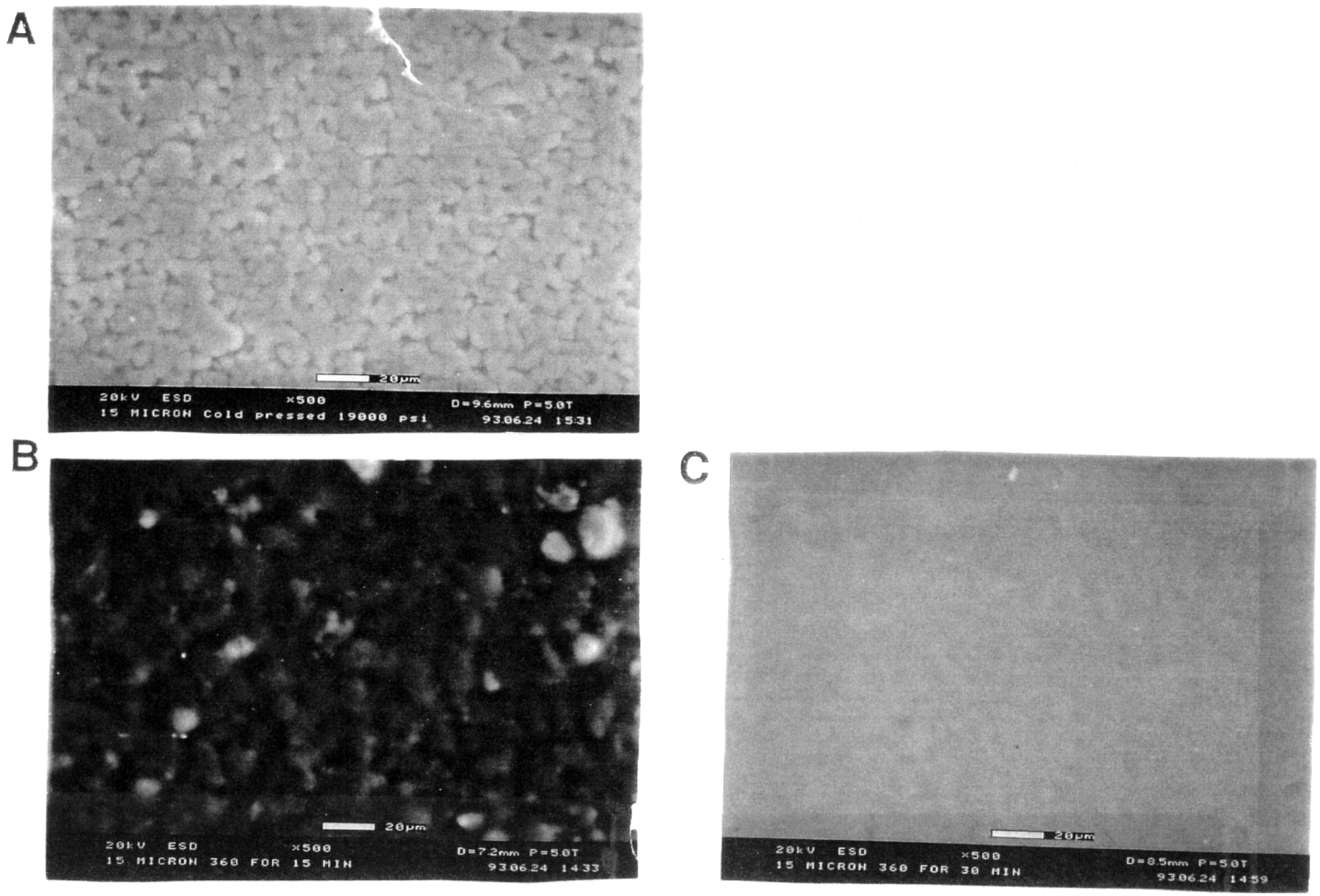

Figure 4.55: ESEM Photographs of 15 µm PEEK Particles Sintered at 360°C: A = 0 min., B = 15 min., C = 30 min.: All Photographs Display a 20 µm Marker

a hydrolysis reaction, and the particles crystallized out of solution, as previously discussed. They were washed with water and dried. The drying process results in formation of loose aggregates comprised of small primary particles. Although dilatometry experiments on these same particles indicated rather dramatic densification, we believe that defects caused by aggregation result in poor mechanical properties. The grain boundaries caused by the aggregates could be seen by the naked eye in these samples.

Table 4.13: Effect of Particle Size on Development of Mechanical Integrity

Particle Diameter (μm)	Processing Conditions	Yield Stress (MPa)	% Strain at break	Density (g/mL)
—	Control[73]	100	50	1.3
15	380°C, 12 min.	101	35	1.29
120	380°C, 12 min.	Brittle*	—	1.26
15	360°C, 30 min.	100	187	1.31
120	360°C, 30 min.	Brittle*	—	—
15	360°C, 20 min.	98	28	1.29
0.3	360°C, 20 min.	67**	8.7	1.21

* Sample was brittle, broke before testing
** Sample underwent brittle failure

Ongoing research within our laboratory is focused on preparing green bodies from submicron PEEK using a process known as pressure casting, a common practice in the ceramics industry. This involves forming the sample from a concentrated stable suspension, thus preventing aggregation. Preliminary experiments exploring this procedure were conducted using the

submicron PEEK particles. Qualitatively, pressure cast samples sintered for 15 min. at 360°C resulted in "creasable" films. The 15 μm particles sintered under identical conditions resulted in a very brittle films. Thus it is believed that the 0.3 μm particles do indeed sinter faster, as one would expect.

Frenkel's equation, as discussed in the introduction, can be used to analyze the effect of particle size on sintering. If one defines a sintering parameter[108] (δ) as the neck radius divided by the particle radius (δ = X/a), then equation (4.1) can be re-written as

$$\delta^2 = \frac{3}{2}\frac{\gamma}{K}\frac{t}{a} \qquad (4.4)$$

A graph of δ^2 vs. t/a should yield a straight line with a slope of 3γ/2K. Using the method described in the experimental section, ESEM photomicrographs were taken of the samples prepared from 15 μm particles as a function of time at 350°C (Figure 4.56). The sintering parameter (δ), a, and time were obtained from these photographs. A plot of δ^2 vs. t/a indeed resulted in a straight line with a slope of 9.28 e -10 m/s (Figure 4.57). Equation 4.4 also indicates that the resulting line should have a zero intercept. Figure 4.57, however, shows the intercept is actually 0.0897. This is hypothesized to be a measure of the amount of intimate contact, or neck growth, resulting from the cold compaction.

The surface free energy (γ) for PEEK was measured as described in the experimental section and a value of 4.77e-2 J/m^2 was obtained. Using this value for γ, K is calculated to be 7.71e7 Kg m^{-1} s^{-1}. K could be interpreted as a melt viscosity, because if the exponent n in equation 2 [$\sigma = K(\dot{\varepsilon}_s)^n$] is equal to

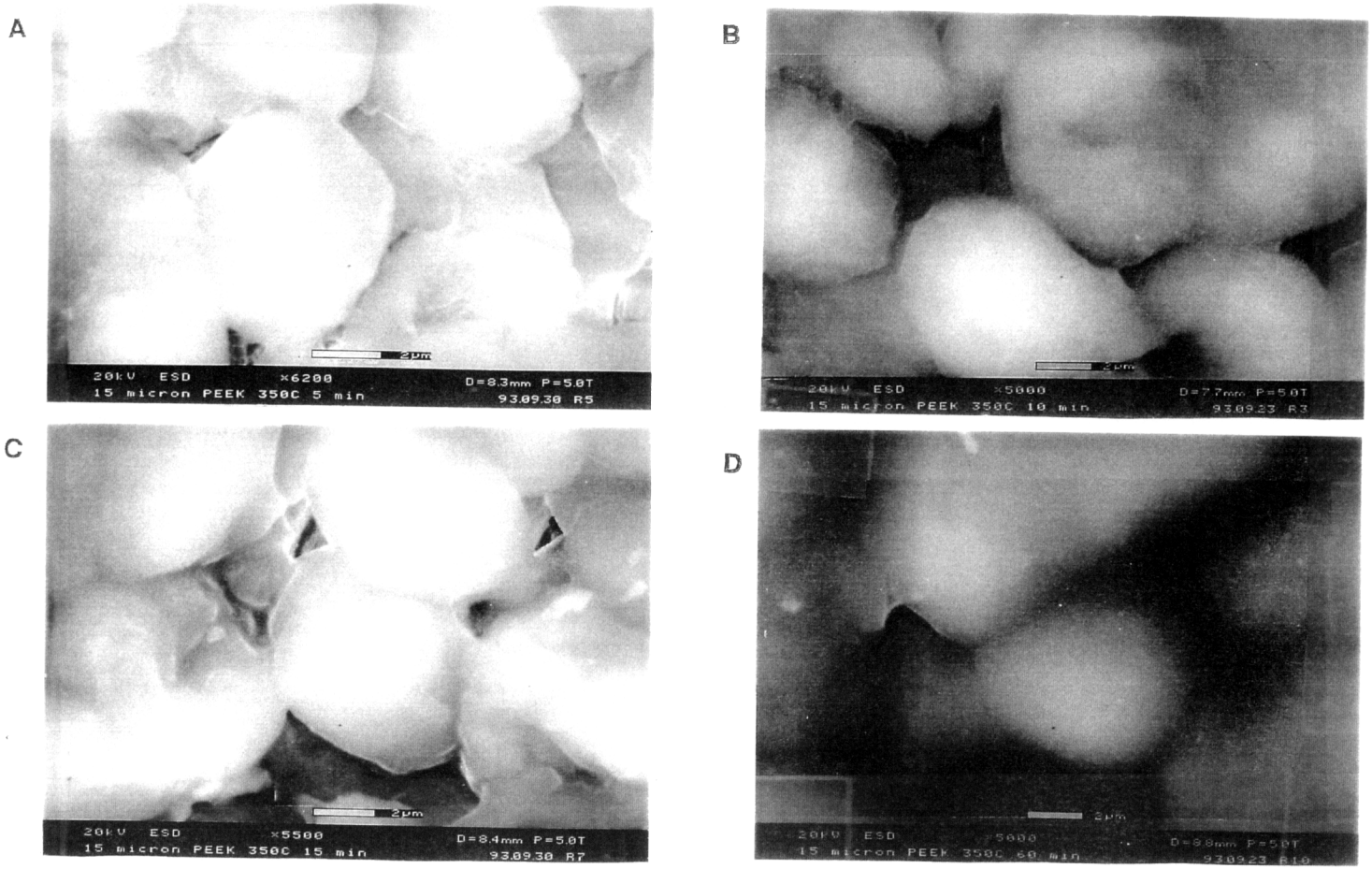

Figure 4.56: ESEM Photographs of 15 μm PEEK Particles Sintered at 350°C: A = 5 min., B = 10 min., C = 15 min., D = 60 min.: All Photographs Display a 2 μm Marker

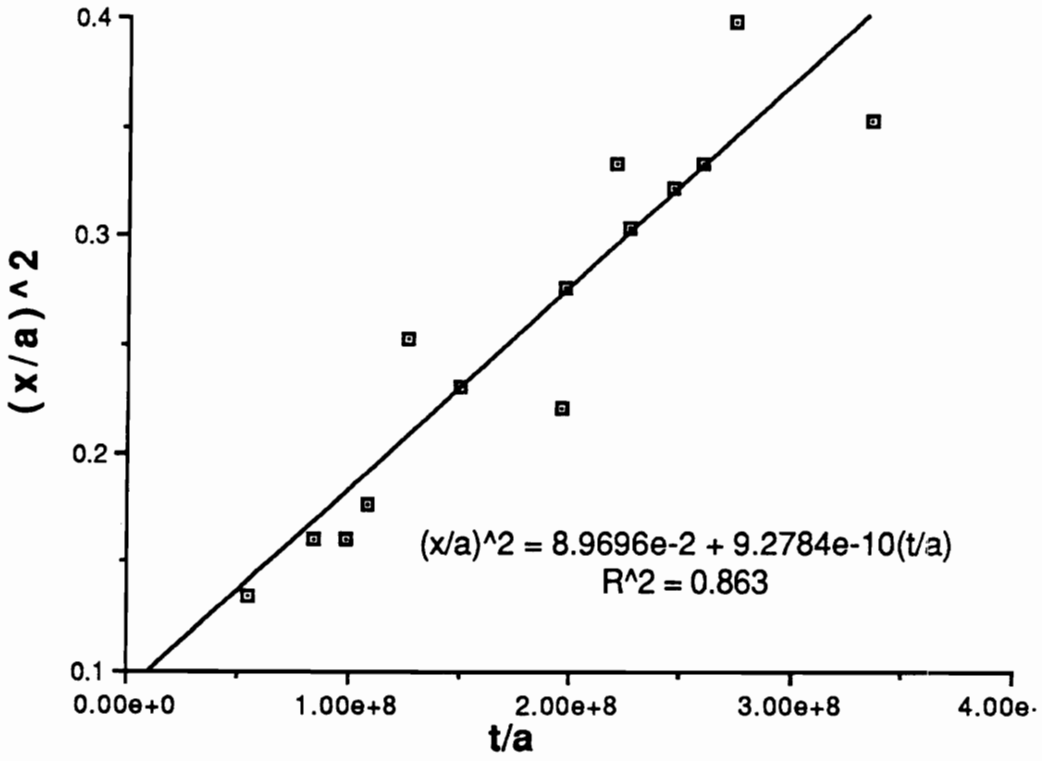

Figure 4.57: Graphic Analysis of the Sintering Parameter (δ = x/a) With Time for 15 µm PEEK Particles

one, then K becomes η. The value calculated for K is quite high relative to typical melt viscosities for high molecular weight thermoplastics. However, this is actually as one would expect considering the temperature (350°C) was essentially at the melting point for PEEK.

Since the slope from Figure 4.57 should be independent of particle size, rearrangement of equation (4.4) to

$$\frac{\delta^2 a}{\frac{3}{2}\frac{\gamma}{K}} = t \qquad (4.5)$$

allows one to compare the sintering rates as particle size changes. By defining complete sintering as the point where δ is equal to one and substituting 9.28e-10 m/s for $3\gamma/2K$, sintering times as a function of particle radius have been calculated. Using this analysis, one can predict that 0.3 μm particles should sinter 50 times faster than the 15 μm particles at 350°C. However, the reader should again be cautioned that this analysis only takes into consideration the time required to reach intimate contact, which does not in general include the time required to reach bulk mechanical integrity.

The crack healing theory developed by Wool et al.[116-118] examines scaling laws relating the development of mechanical properties to processing time and molecular weight. This theory is based on the minor chain model of reptation[121-123] and is divided into five separate stages; surface rearrangement, surface approach, wetting, diffusion, and randomization. The first three stages are required to achieve complete wetting (i.e. intimate contact), which can be modeled by Frenkel's theory for obtaining intimate contact between two particles. The remaining two stages are based entirely on

reptation, and should be independent of particle size. Wool has assumed instantaneous intimate contact, then followed the development of mechanical integrity by diffusion[116], as well as time dependent wetting. The sintering processes discussed herein apparently include time dependent wetting, where a portion of the diffusion occurs before complete wetting is achieved. Approximately 80% of PEEK's ultimate mechanical integrity has already developed by the time complete intimate contact is reached when sintered at 360°C. After this point the development of mechanical strength can be modeled using Wool's scaling laws. This theory predicts that the tensile strength (σ) should increase with time to the 1/4 power (4.6).

$$R(\sigma,t) = R_0 + k\frac{t^{1/4}}{\sigma_\infty} \qquad (4.6)$$

where

$$R_o = \frac{\sigma_o}{\sigma_\infty} \qquad (4.7)$$

and

$$R = \frac{\sigma(t)}{\sigma_\infty} \qquad (4.8)$$

the subscripts o and ∞ indicate zero and infinite time respectively, and k is a constant that is dependent on temperature, pressure and molecular weight. A graphical analysis of this scaling law can be analyzed by plotting the $\log(R-R_o)$ vs. log t. A slope of 1/4 should be obtained. Preliminary studies of this relationship do indeed correlate to this prediction. For example if 15 μm particles are sintered at 360°C for times of 15, 20 and 30 minutes tensile strengths of 83, 98 and 100 MPa, respectively, are obtained. Analyzing these by equation (4.6) provide a slope of 0.254 with a correlation coefficient of 0.752

(Figure 4.58). It was difficult to get more than the three data points shown here for this analysis because the samples had to be sufficiently sintered to have enough mechanical integrity to cut the dogbone shaped sample. Because of this an alternate method, meso-indentation, was examined. This method avoided the need to cut out a dogbone, and tested the sample directly in its sintered disk shape, as described in the Experimental section. A preliminary study of this method was performed utilizing the 15 μm particles sintered for 15, 25 and 30 minutes at 360°C (Table 4.14). These values were analyzed according to Wool's scaling laws as previously. However, the graph obtained had a slope of 0.401 instead of the expected 0.25 (Figure 4.59). Wool's scaling law was developed for uniaxial tension, however, and it is believed that the slope was not as expected because the meso-indentation measurements are in compression. The meso-indentation technique did not provide the desired analysis, and therefore the experimentation was discontinued. However, meso-indentation does provide a method of obtaining relative mechanical properties as a function of sintering time, and could therefore be potentially useful for other applications.

Table 4.14: Meso-Indentation Analysis of Sintered 15 μm PEEK Powders

Temperature (°C)	Time (min.)	$<\sigma_y>$ (MPa)	%ε
360	30	59.97	3.64
360	25	57.76	3.72
360	15	45.84	3.44

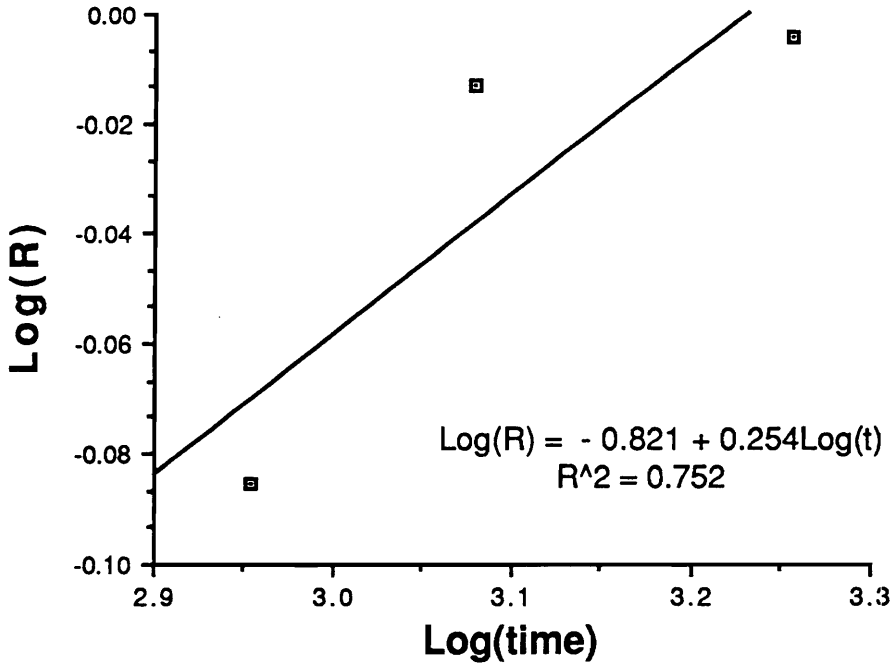

Figure 4.58: Graphic Analysis of Wool's Scaling Law for 15 μm PEEK Particles at 360°C

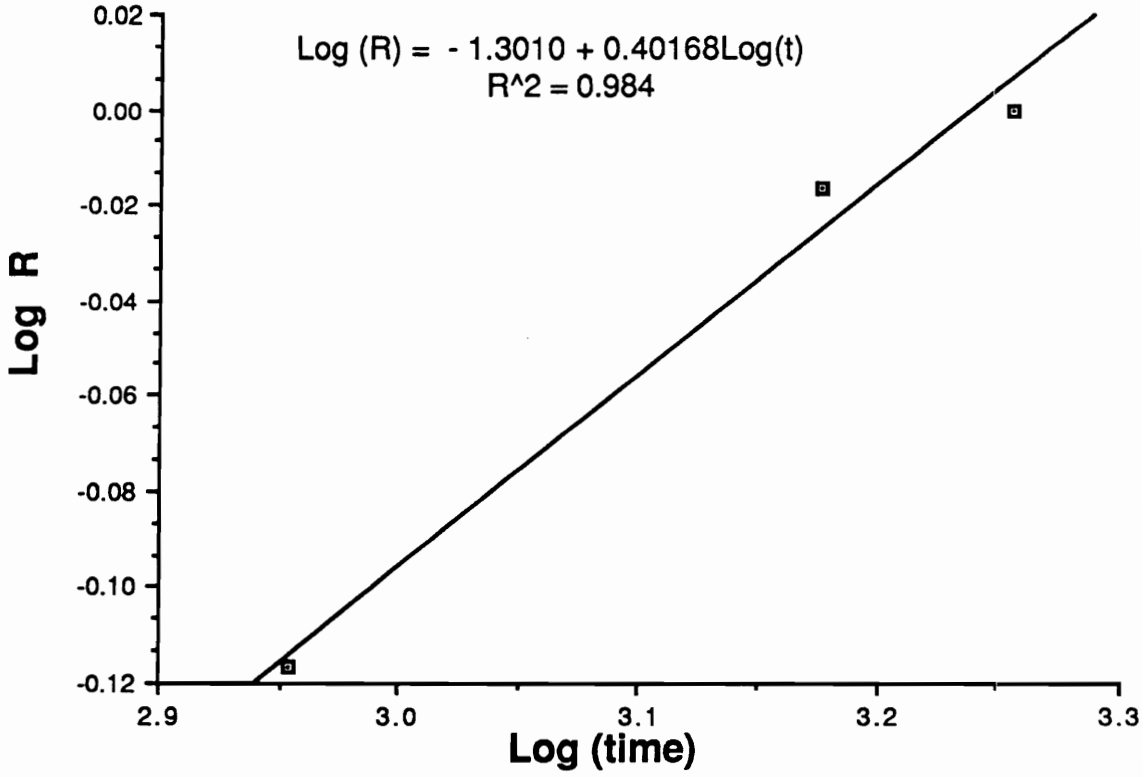

Figure 4.59: Graphic Analysis of Wool's Scaling Law for 15 μm PEEK Particles at 360°C Utilizing Meso-Indentation Data

Chapter 5 - Conclusions

The 4,4'-difluoro (N-benzohydroxylidene aniline) monomer was synthesized and fully characterized by NMR techniques. The copolymer of 50% 4,4'-difluoro (N-benzohydroxylidene aniline) and 50% 4,4'-difluorobenzophenone with hydroquinone is semicrystalline with a Tm of 228°C. Due to its relatively low melting point, compared to PEEK, this copolymer dissolves in NMP at high temperatures (>200°C) and remains in solution upon cooling to room temperature. Methods have been established to hydrolyze the ketimine polymers to insoluble, semicrystalline PEEK. This very rapid process causes the polymer to crystallize from solution, forming small particles. If hydrolysis is faster than nucleation, then essentially all of the ketimine is converted to ketone before nucleation occurs. This results in the formation of the maximum number of nuclei and therefore the smallest particle size. Therefore the size of the particles is dependent on the temperature, acid concentration, water concentration, solvent concentration, and copolymer composition. Careful control of these five parameters to achieve rapid hydrolysis can produce submicron PEEK particles.

A high performance electrostatic stabilizer was developed by incorporating 2,6-dichloropyridine as a comonomer into poly(ether ether ketimine). The 'dual' reactivity of 2,6-dichloropyridine has been recognized, whereas the first chloro substitution on 2,6-dichloropyridine is quite facile and the second chloro substitution is very slow. With this understanding conditions have been established for synthesis of high molecular weight poly((pyridine ether) - co - (ether ether ketimine)) copolymers. These copolymers, upon hydrolysis, form self stabilizing particles with the size of the particle dependent

upon the amount of pyridine used. The hydrolysis conditions convert the ketimine bond back to a ketone and simultaneously protonates the pyridine nitrogen. This allows these copolymers to be used as electrostatic stabilizers for aqueous suspensions of preformed PEEK particles. The resulting poly((pyridine ether) - co - (ether ether ketone)) stabilizers are miscible with PEEK as well as thermo-oxidatively stable and thus the objectives have been met. This stabilizer has been shown to aid in aqueous suspension prepregging of PEEK particles. However an increase in viscosity is believed to hinder final consolidation of the graphite composite. This increase in viscosity is believed to be due to the protonated form of poly((pyridine ether) - co - (ether ether ketone)) forming physical crosslinks similar to other ionomers. Additional research will be necessary to better define the rheological parameters of these composites.

The effect of particle size on sintering PEEK powders has been investigated. As expected, smaller particles result in pronounced densification, and the most dramatic difference clearly resulted using submicron PEEK particles. Effects of temperature and compact pressure were also examined and trends much like those observed for ceramic sintering resulted. As sintering temperature was lowered, the samples did not densify. A temperature of 300°C was required for the 15 μm particles before densification started, which correlates well with the onset of melting. As compact pressure was increased, the general trend was that densification decreased. The effect of particle size on the sintering time and temperature required to achieve good mechanical properties was also examined, and again the benefical effect of a smaller particle size was illustrated. The sintered 15 μm particles exhibited yield strengths essentially equivalent to the control whereas the samples

prepared under indentical conditions from 120 μm particles were so brittle that they could not be tested. Sintering was also examined in light of the two particle model first derived by Frenkel, and a resonable fit was obtained. This theory allowed us to compare the relative sintering rate as a function of particle size, and therfore it was concluded that the submicron particles should reach intimate contact 50 times faster than the 15 μm particles at 350°C. Unfortunately, we have not yet been able to measure this directly because the submicron particles were too small to view with good resolution using the ESEM. The faster sintering rate does not necessarily correlate to mechanical properties, since this requires interdiffusion across the grain boundaries. This process, modeled by Wool, is independent of particle size. However, it can be used to examine the development of mechanical strength after intimate contact is reached. Preliminary studies indicate that this system does indeed follow the scaling laws developed by Wool.

References:

1. M. J. Jurek and J. E. McGrath, *Polymer*, **1989**, 30, 1552.

2. P. M. Hergenrother, B. J. Jensen and S. J. Havens, *Polymer*, **1988**, 30, 358.

3. T. E. Attwood, P. C. Dawson, J. L. Freeman, L. R. J. Hoy, J. B. Rose and P. A. Staniland, *Polymer*, **1981**, 22, 1096.

4. R. N. Johnson, A. G. Farnham, R. A. Clendinning, W. F. Hale and C. N. Merriam, *J. Polymer Sci. A-1*, **1967**, 5, 2375.

5. W. F. Hale, A. G. Farnham, R. N. Johnson and R. A. Clendinning, *J. Polymer Sci. A-1*, **1967**, 5, 2399.

6. R. N. Johnson and A. G. Farnham, *J. Polymer Sci. A-1*, **1967**, 5, 2415.

7. W. H. Bonner (DuPont), US Patent, 3,065,205 (1962).

8. I. Goodman, J. E. McIntyre and W. Russell, Br. Patent, 971,227 (1964).

9. T. E. Attwood, P. C. Dawson, J. L. Freeman, L. R. J. Hoy, J. B. Rose and P. A. Staniland, *Am. Chem. Soc. Polym. Prepr.*, **1979**, 20(1), 191.

10. J. I. Kroschwitz, ed., High Performance Polymers and Composites, John Wiley and Sons, NY, 1991.

11. Imperial Chemical Industries Ltd., German Patent, 2,635,101 (1977).

12. Imperial Chemical Industries Ltd., German Patent, 2,733,905 (1978).

13. B. Gerd and C. Claus (BASF - A-G), German Patent, 2,749,645 (1978).

14. R. Viswanathan, B. C. Johnson and J. E. McGrath, *Polymer*, **1984**, 25, 1827.

15. F. A. Carey and R. J. Sundberg, Advanced Organic Chemistry Part A: Structure and Mechanisms, Plenum Press, NY, 1990.

16. T. E. Attwood, A. B. Newton and J. B. Rose, *Br. Polym. J.*, **1972**, 4, 391.

17. M. S. Reisch, Chemical and Engineering News, August 30, 1993, 24.

18. Y. Lee and R. S. Porter, *Macromolecules*, **1988**, 21, 2770.

19. N. T. Wakelyn, *Polym. Commun.*, **1984**, 25, 306.

20. D. J. Blundell and J. D'Mello, *Polymer*, **1991**, 32(2), 304.

21. P. Aoller, T. Kehl, H. W. Starkweather, Jr. and G. A. Jones, *J. Polymer Sci.: Part B: Polymer Physics*, **1989**, 27, 993.

22. A. Jonas, R. Legras and J. Issi, *Polymer*, **1991**, 32(18), 3364.

23. H. Colquhoun, C. O'Mahoney and D. Williams, *Polymer*, **1993**, 34(1), 218.

24. Y. Lee, R. Porter and J. S. Lin, *Macromolecules*, **1989**, 22, 1756.

25. Y. Lee and R. Porter, *Macromolecules*, **1987**, 20, 1336.

26. V. Velikov and H. Marand, *Am. Chem. Soc. Polym. Prepr.*, **1993**, 34(2), 835.

27. D. J. Blundell, *Polymer*, **1987**, 28, 2248.

28. D. J. Blundell and B. N. Osborn, *Polymer*, **1983**, 24, 953.

29. ICI Americas, Inc., U. S. Patent, 4,263,458 (1982).

30. J. Rose and P. Staniland (ICI Ameicas, Inc.) U. S. Patent 4,320,224 (1982).

31. D. Kelsey, L. Robeson, R. Clendinning and S. Blackwell, *Macromolecules*, **1987**, 20, 1204.

32. J. Devaux, D. Delimoy, D. Daust, R. Legras, J. Mercier, C. Strazielle and E. Nield, *Polymer*, **1985**, 26, 1994.

33. M. Bishop, F. Karasz, P. Russo and K. Langley, *Macromolecules*, **1985**, 18, 86.

34. J. Devaux, D. Daust, R. Legras, J. Dereppe and E. Nield, *Polymer*, **1989**, 30, 162.

35. A. Jonas, R. Legras and J. Devaux, *Macromolecules*, **1992**, 25, 5841.

36. A. Jonas and R. Legras, *Polymer*, **1991**, 32, 15.

37. D. K. Mohanty, T. S. Lin, T. C. Ward and J. E. McGrath, *Int. SAMPE Tech. Conf.*, **1986**, 31, 945.

38. D. K. Mohanty, R. C.Lowery, G. D. Lyle,and J. E. McGrath, *Int. SAMPE Tech. Conf.*, **1987**, 32, 408.

39. D. K. Mohanty, J.S. Senger, C. D. Smith and J. E. McGrath, *Int. SAMPE Tech. Conf.*, **1988**, 33, 970.

40. K. R. Lyon, D. K. Mohanty, G. D. Lyle, T. Glass, H. Marand, A. Prasad and J. E. McGrath, *Int. SAMPE Tech. Conf.*, **1991**, 36, 417.

41. J. Roovers, J. Cooney and P. Toporowski, *Macromolecules*, **1990**, 23, 1611.

42. V. Velikov, J. Vivirito and H. Marand, *Macromolecules*, **1994**, Submitted.

43. D. W. Holty, *Chem Tech*, **1993**, June, 40.

44. C. A. Arnold, P. M. Hergenrother and J. E. McGrath, Composite Applications: The Role of Matrix, Fiber and and Interface, T. L. Vigo and B. J. Kinzig, eds., VCH Publishers, NY, 1993, 3-30.

45. J. E. McGrath, *Polymer* , **1993,** 34(4), 675.

46. P. M. Hergenrother and M. E. Rogalski, *Am. Chem. Soc. Polym. Prepr.*, **1992**, 33(1), 354.

47. P. M.Hergenrother, Gordon Research Conference on Composites, Ventura, CA, January, 1994.

48. I. Chang, *Int. SAMPE Tech. Conf.*, **1992**, 37, 1276.

49. J. M. Kenny, A.Trivisano, M. E. Frigone and L. Nicolais, *Am. Chem. Soc. PMSE Proc.*, **1990**, 63, 790.

50. D. E. Kranbuel, S. M. Hart and A. Loos, *Mat. Res. Soc. Symp. Proc.*, **1993**, 305, 231.

51. D. Sohn, N. Sung, *Am. Chem. Soc. PMSE Proc.*, **1990**, 63, 517.

52. X. Wang and J. K. Gillham, *Am. Chem. Soc. PMSE Proc.*, **1990**, 63, 505.

53. C. J. deBakker, N. A. St. John and G. A. George, *Polymer*, **1993**, 34(4), 716.

54. B. A. Osinski, *Polymer*, **1993**, 34(4), 752.

55. G. W. Meyer, S. Jayaraman, Y. J. Lee, G. D. Lyle, T. E. Glass and J. E. McGrath, *Mat. Res. Soc. Symp. Proc.*, **1993**, 305, 3.

56. V. Altstadt, D. Gerth, M. Stangle and H.Recker, *Polymer*, **1993**, 34(4), 907.

57. R. Don, J. Gillespie, Jr., and C. Lambing, *Polym.Eng. Sci.*, **1992**, 32(9), 620.

58. R. Don, L. Bastien, T. B. Jakobsen and J. W. Gillespie, Jr., *SAMPE Journal*, **1990**, Jan./Feb., 59.

59. J. Jakobsen, R. Don and J. Gillespie, Jr., *Polym. Eng. Sci.*, **1989**, 29, 23.

60. J. L. Hedrick, I. Yilgor, G. L. Wilkes and J. E. McGrath, *Polym. Bull.*, **1985**, 13, 201.

61. J. L. Hedrick, I. Yilgor, G. L. Wilkes and J. E. McGrath, *Int. SAMPE Tech. Conf.*, **1985**, 30, 947.

62. J. L. Hedrick, M. J. Jurek, I. Yilgor, and J. E. McGrath, *Am. Chem. Soc. Polym. Prepr.*, **1985**, 26(2), 293.

63. J. A. Cecere and J. E. McGrath, *Int. SAMPE Tech. Conf.*, **1986**, 31, 583.

64. J. C. Hedrick, J. L. Hedrick, J. A. Cecere, S. C. Liptak and J. E. McGrath, *Am. Chem. Soc. PMSE Proc.,* **1990**, 63, 190.

65. P. T. McGrail and S. D. Jenkins, *Polymer*, **1993**, 34(4), 677.

66. R. Bauer, *Am. Chem. Soc. PMSE Proc.* **1990**, 63, 672.

67. J. Manson, T. Schneider and J. Seferis, *Polymer Composites*, **1990**, 11(2), 114.

68. W. Lawerence, J. Seferis and J. Gillespie, Jr., *Polymer Composites*, **1992**, 13(2), 86.

69. R. Lusignea, K. Blizard and L. Rubin, *Mat. Res. Symp. Proc.*, **1993**, 305, 247.

70. J. Manson and J. Seferis, *J. Comp. Mater.*, **1992**, 26(3), 405.

71. M. Nardin, E. M. Asloun, F. Muller and J. Schultz, *Polymers for Advanced Technologies*, **1991**, 2, 161.

72. Y. Lee and R. S. Porter, *Polym. Eng. Sci.*, **1986**, 26(9), 633.

73. H. Nguyen and H. Ishida, *Polymer Composites*, **1987**, 8(2), 57.

74. D. Hirt, J. Marchello and R. Baucom, *Int. SAMPE Tech. Conf.*, **1990**, 22, 360.

75. T. Towell, D. Hirt and N. Johnston, *Int. SAMPE Tech. Conf.*, **1990**, 22, 1156.

76. R. Cochran and R. Pipes, *Int. SAMPE Tech. Conf.*, **1991**, 23, 1169.

77. R. M. Davis, A. Texier, T. H. Yu, K. Lyon, A. Gungor, J. E. McGrath and J. S. Riffle, *Am. Chem. Soc. Polym. Prepr.*, **1992**, 33(1), 416.

78. A. Texier, R. M. Davis, K. R. Lyon, A. Gungor, J. E. McGrath, H. Marand and J. S. Riffle, *Polymer*, **1993**, 34(4), 896.

79. T. Lin, K. W. Stickney, M. Rogers, J. S. Riffle, H. Marand, J. E. McGrath, T. H. Yu, R. M. Davis, *Polymer*, **1993**, 34(4), 772.

80. R. H. Ottewill, *J. of Colloid & Interface Science*, **1977**, 58(2), 357.

81. D. H. Everett, Basic Principles of Colloid Science, Royal Society of Chemistry, London, 1992.

82. D. J. Shaw, Introduction to Colloid and Surface Chemistry, 3rd ed., Butterworths, London, 1986.

83. J. Th. G. Overbeek, *J. of Colloid & Interface Science*, **1977**, 58(2), 408.

84. D. H. Napper, Polymeric Stabilization of Colloidal Dispersions, Academic Press, NY, 1983.

85. F. Th. Hesselink, A. Vrij and J. Th. G. Overbeek, *J. of Phys. Chem.*, **1971**, 75(14), 2094.

86. D. H. Napper, *J. of Colloid & Interface Science*, **1977**, 58(2), 390.

87. J. Lyklema and G. J. Fleer, *Colloids & Surfaces*, **1987**, 25, 357.

88. O. V. Borisov, *Am. Chem. Soc. Polym. Prepr.*, **1993**, 34(1), 934.

89. S. Barany and A. Baron, *Am. Chem. Soc. Polym. Prepr.*, **1993**, 34(1), 945.

90. M. A. C. Stuart, T. Cosgrove and B. Vincent, *Advan. in Colloid Interface Sci.*, **1986**, 24, 143.

91. G. J. Fleer and J. M. H. M. Scheutjens, *J. of Colloid & Interface Science*, **1986**, 111(2), 504.

92. J. Lyklema, *Advan. in Colloid Interface Sci.*, **1968**, 2, 65.

93. A. L. Loeb, J. Th. G. Overbeek and P. H. Wiersema, The Electrical Double Layer Around a Spherical Particle, The M.I.T. Press, Cambridge, MA, 1961.

94. P. Pincus, *Macromolecules*, 1991, 24, 2912.

95. V. A.Hackley and S. G. Malghan, *Am. Chem. Soc. Polym. Prepr.*, **1993**, 34(1), 1024.

96. S. Somiya and Y. Moriyoshi, eds., Sintering: Key Papers, Elsevier Applied Science, NY, 1990.

97. R. M. German, Liquid Phase Sintering, Plenum Press, NY, 1985.

98. H. E. Exner, E. Arzt, Physical Metallurgy, 3rd ed., R. W. Cahn and P. Haasan (eds.), Elsevier Science Publishers, Amsterdam, 1983, 1885.

99. W. D. Kingery, *Transactions of the VIIth International Ceramic Congress, London, 1960, Institute on Ceramics*, Stoke-on-Trent, 1960, 461.

100. J. E. Burke, Ceramic Fabrication Processes, W. D. Kingery, ed., M.I.T. Press, Cambridge MA, 1958, 120.

101. W. D. Kingery and M. Berg, *J. Appl. Phys.*, **1955**, 26(10), 1205.

102. F. V. Lenel, Sintering: Key Papers, S. Somiya and Y. Moriyoshi (eds.), Elsevier Applied Science, NY, 1990, 543.

103. J. Frenkel, *J. Phys. USSR*, **1945**, 9, 385.

104. G. C. Kuczynski, B. Neuville and H. P. Toner, *J. Appl. Poly. Sci.*, **1970**, 14, 2069.

105. G. C. Kuczynski, *J. Appl. Phys.*, **1949**, 20, 1160.

106. H. Chen and R. S. Porter, *Polym. Eng. Sci.*, **1992**, 32(24), 1870.

107. E. R. Baumgaertner and F. Park, U. S. Patent, 3,847,888, 1974.

108. R. W. Truss, K. S. Han, J. F. Wallace and P. H. Geil, *Polym. Eng. Sci.*, **1980**, 20(11), 747.

109. G. W. Halldin and I. L. Kamel, *Polm. Eng. Sci.*, **1977**, 17(1), 21.

110. G. S. Jayaraman, J. F. Wallace, P. H. Geil and E. Baer, *Polym. Eng. Sci.*, **1976**, 16(8), 529.

111. J. L. Throne, *Advan. Polym. Tech.*, **1989**, 9(4), 281.

112. D. M. Bigg and M. M. Epstein, Science and Technology of Polymer Processing: Proceedings of the International Conference on Polymer Processing, M.I.T. Press, Cambridge, MA, 1979.

113. K. W. Rausch, Jr. and W. J. Farrissey, *Soc. of Plastics Engineers Annual Tech. Conf.*, 1976, 34, 644.

114. H. E. Exner, *Powder Metallurgy*, **1980**, 4, 203.

115. Y. Wang, L. Li, J. Feng, M. A. Winnik, H. Yan, T. North and Z. Wang, *Am. Chem. Soc. Polym. Prepr.*, **1992**, 33(1), 843.

116. R. P. Wool, B. L. Yuan and O. J. McGarel, *Polym Eng. Sci.*, **1989**, 29(19), 1340.

117. H. Zhang and R. P. Wool, *Macromolecules*, **1989**, 22, 3021.

118. R. P. Wool and Y. H. Kim, *Macromolecules*, **1983**, 16, 1115.

119. K. L. Foster and R. P. Wool, *Macromolecules*, **1991**, 24, 1397.

120. R. P. Wool and K. M. O'Connor, *J. Appl. Phys.*, **1981**, 52(10), 5953.

121. P. G. de Gennes, *J. Chem. Phys.*, **1971**, 55(2), 572.

122. P. G. de Gennes, *J. Phys. France*, **1989**, 50, 2551.

123. M. Doi and S. F. Edwards, *J. Chem. Soc., Faraday Trans.*, **1978**, 2, 1789.

124. T. Provder, ed.; Particle Size Distribution: Assessment and Characterization: ACS Symp. Series no. 332, American Chemical Society, Washington, DC, 1987.

125. D. K. Owens and R. C. Wendt, *J. Appl. Poly. Sci.*, **1969**, 13, 1741.

126. J. L. Hedrick and J. W. Labadie, *Macromolecules*, **1990**, 23, 1561.

127. J. L. Hedrick, *Polymer*, **1992**, 33, 1399.

128. A. Jonas and R. Legras, *Polymer*, **1991**, 32, 1102.

129. R. J. Abraham and I. S. Haworth, *Polymer*, **1991**, 32, 121.

130. D. W. Van Krevelen, Properties of Polymers: Their Correlation with Chemical Structure: Their Numerical Estimation and Prediction From Additive Group Contributions, 3rd ed., Elsevier Scientific, NY, 1990.

131. A. Texier, M. S. Thesis, Department of Chemical Engineering, Virginia Polytechnic Institute and State University, 1991.

132. M. Nardin, E. M. Asloun and J. Schultz, J. *Surf. Interface Anal.*, **1991**, 17, 485.

133. H. R. Kricheldorf, G. Schwarz, and J. Erxleben, *Makromol. Chem.*, **1988**, 189, 2255.

134. H. R. Kricheldorf and P. Jahnke, *Polym. Bull.*, **1991**, 27, 135.

135. H. R. Kricheldorf and P. Janhke, *Makromol. Chem.*, **1990**, 191, 2027.

136. A. Ibarra-Gonzalez, Masters Thesis, Department of Chemical Engineering, Virginia Polytechnic Institute and State University, 1993.

137. G. L. Wilkes, Personal Communication, 1993.

Vita

The author was born in Los Angeles, California on November 15th, 1968. He grew up in central Pennsylvania where he graduated from Penns Valley Area High School in 1986 and enrolled at Virginia Polytechnic Institute and State University. In 1990 he graduated Summa Cum Laude with a Bachelor of Science in Chemistry with a Polymer Option. After a summer of research at ARCO Chemical Company he entered a Ph.D. program at Virginia Polytechnic Institute and State University under the advisement of Dr. Judy S. Riffle where he obtained his Doctoral degree in Polymer Chemistry in 1994. As a graduate student he presented papers in regional and national meetings in polymer chemistry, and coauthored eight publications and a patent.

On August 8, 1992 he married Mary Heather Woodard at Blacksburg, Virginia. Heather, also a graduate student in Chemistry at Virginia Tech, obtained her Doctoral degree in Polymer Chemistry in 1994. Together, on June 13th they joined Eastman Chemical Company in Kingsport, TN as Advanced Research Chemists.